Optimising high speed coating processes.

Eckermann, Jurgen

Swansea University
Prifysgol Abertawe

Optimising High Speed Coating Processes

A thesis presented

By

Jürgen Eckermann

Submitted to the University of Wales

In fulfilment of the programm Doctor of Engineering

Swansea University

2012

Abstract

The coil coating process of strip steel is a continuous and highly automated process in which the aim is to apply a paint layer of uniform thickness onto metal sheet at high operational speed. However, the performance of the coil coating process has been limited due to the occurrence of coating defects, such as ribbing and fat edges, which leads ultimately to a reduction in the operational speed of coating. Therefore, in order to enhance coating productivity, the complex flow behaviour of commercial paints needs to be fully understood. Consequently, the main objective of this work was to obtain rheological parameters for the commercial paints using rotational Rheometers, Capillary Break-up Rheometer and Capillary Extrusion Rheometer to allow the characterisation of the complex flow behaviour. This research project was tailored over its course to generate a solid knowledge foundation of the rheological properties of polyester resin based paints prior to the defining of different experimental procedures so as to guarantee the reproducibility of the data measured with various Rheometers. Once these rheological characteristics were fully understood for one paint, the project was moved forward by selecting other commercially available paints which were similarly analysed to allow a comparison of the various rheological behaviours.

One key finding was that the commercial paints behaved in either a Newtonian or a Non Newtonian fashion. The Non Newtonian paints possessed a high internal microstructure which was reflected in the degree of elasticity exhibited, whereas the Newtonian paint did not seem to exhibit any elasticity. Furthermore, a mutual, ideal operability window for the Capillary Break up Rheometer could be derived from data which was systematically collected by varying the input parameters including opening time, stretch profile and Hencky strain. Capillary Extrusion Rheometer provided extensional and shear information at very high strain rates. At the end, a steady state flow curve for both shear and extensional viscosity could be determined for a strain rate range of 10^{-1} to 5×10^{4}, which is unique for the polyester resin based paints analysed in this work.

Declaration and Statements

DECLARATION

This work has not previously been accepted in substance for any degree and is not being concurrently submitted in candidature for any degree

Signed ..... (candidate)

Date 10th October 2012

STATEMENT 1

This thesis is the result of my own investigation, except where otherwise stated. Where correction services have been used, the extent and nature of the correction is clearly marked in a footnote(s).

Other sources are acknowledged by footnotes giving explicit refrences. A bibliography is appended.

Signed: ..... (candidate)

Date 10th October 2012

STATEMENT 2

I hereby give consent for my thesis, if accepted, to be available for photocopying and for inter-library loan, and for the title and summary to be made available to outside organisations.

Signed.. ..... (candidate)

Date 10th October 2012

Contents

DEDICATION

To my mother and my daughter who gave me the determination and energy to finish this thesis for them.

Acknowledgments

This thesis is especially dedicated to my daughter Ffion and my mother Lieselotte who will always be important in my life. My daughter has given me happiness, strength and purpose in writing this thesis in the very difficult years 2010, 2011 and 2012. Her unconditional love has given me the strength to focus my aim to fight for her. Especially thanks goes to my mother, (15th October 2008 †) who taught me that you need to look forward even in the worse situations. You both have given me the determination to finish this thesis. Thanks for your belief in me.

My heartfelt thanks for all the professional, technical financial, emotional and moral support in this hard time goes to family, friends, supervisors and work colleagues. I owe an enormous debt of emotional and moral support to my brother Sascha and my work colleague Ian who became a very close friend and advisor during my research year. Without them I would not have been able to finish this thesis.

I owe an enormous debt of gratitude to my supervisor Dr. Rob English and my friend Tom Dobbie who showed a lot of patience in teaching me the world of Rheology which was very strange for a Mechanical / Material and Design Engineer like myself. They have been a source of inspiration in my research. Thanks to Saumil with whom I had a lot of useful discussions about Rheology and Helen for her help in understanding some chemical processes. Immense thanks to the International Badminton Team who cheered me up during my writing-up phase.

Furthermore, I would like to express my gratitude to the Swansea University team, especially to my supervisor Prof. Dave Worsley and Beverley Williams. In addition, further thanks go to all the EngD-students who supported me during my 4 year course. Especially thanks to Sara and her husband Jonathan for the hospitality in their house. Also I am grateful for the support from Chris, Ian, Dyfyr, Adam and Joel during my learning phase in passing my modules. These pleasant memories from staying in Swansea and the Netherlands were only possible because of your friendly and great personalities.

The financial sponsorships of EPSRC, Tata/Corus and BASF are gratefully acknowledged. Especially thanks go to the industrial supervisors Dr. Jonathan Elvins, Joel Rousseau and John Crinson (Tata/Corus), Graham Swanston and Paul Davies (BASF). They provided me with some gratifying and interesting work experiences in the coil and paint industries.

My thanks for their supports also go to Ben, Dave, Dawn, Jennifer, Mauro, Shahid, Yatish and the rest of my current work colleagues and friends from the Astute.

But last and not least, I would like to thanks Ronald, Rosemarie and Toni, Erika, Angela, Rita, Beate, Brigitte and Heinrich, Sonja's family, Manfred's family for their support and help from the years 2006 until now.

Jürgen Eckermann

List of tables

List of figures

List of symbols

Greek alphabet

α	Degree of Deformation [°]
α_c	Angle of the cone [°]
δ	Phase angle [°]
$\dot{\gamma}$	Shear rate [s^{-1}]
$\dot{\gamma}_a$	Apparent shear rate [s^{-1}]
γ_e	Strain due delay elastic response
γ_i	Initial strain
$\dot{\gamma}_{true}$	True shear rate [s^{-1}]
δt_0	Opening / strike timescale [ms]
$\dot{\gamma}_w$	Shear rate after Weissenberger Rabinowitch correction [s^{-1}]
γ_0	Strain amplitude
Δl	Extended length [m]
ΔP	Total pressure drop [Pa]
ΔP_{cap}	Capillary die pressure drop [Pa]
ΔP_{corr}	Pressure drop correction [Pa]
ΔP_e	Excess pressure drop of the die [Pa]
ΔP_{en}	Entrance pressure [Pa]
ΔP_{exit}	Exit pressure drop [Pa]

ε	Extensional strain
$\dot{\varepsilon}$	Extension rate [s^{-1}]
$\dot{\varepsilon}_{axi}$	Strain rate in axisymmetric contraction [s^{-1}]
ε_f	Actual hencky strain
ε_{max}	Maxiamal measurable hencky strain
$\dot{\varepsilon}_{pl}$	Strain rate in a planar contraction [s^{-1}]
ε_t	True hencky strain
η	Viscosity [Pa.s]
η_a	Apparent extensional viscosity [Pa.s]
η_e	Extensional viscosity [Pa.s]
η_E	Extensional Viscosity [Pa.s]
$\eta_{e,0}$	Initial viscosity [Pa.s]
η_{EB}	Biaxial extensional viscosity [Pa.s]
η_{EP}	Planar extensional viscosity [Pa.s]
η_{EU}	Uniaxial extensional viscosity [Pa.s]
η_s	Viscosity of Newtonian fluid [Pa.s]
η_0	Zero shear viscosity [Pa.s]
$\eta_{\infty,0}$	Viscosity at equilibrium stage [Pa.s]
η'	Dynamic viscosity [Pa.s]
λ	Longest relaxation time
λc	Characteristic time
Λf	Final aspect ratio

λ_{ret}	Retardation time [ms]
Λ_0	Initial aspect ratio
Π	Pi
ρ	Density [Kg/m^3]
σ	Stress [N/m^2]
$\sigma_{A,u}$	apparent wall shear stress [Pa]
σ_{O1}	First overshoot stress [Pa]
σ_{O2}	Second overshoot stress [Pa]
σ_s	Surface tension [mN/m]
σ_y	Apparent yield stress [N/m^2]
σ_{xx}, σ_{yy}, σ_{zz}	Normal stress [Pa]
σ_w	True shear stress [Pa]
σ_0	Stress amplitude [N/m^2]
τ_E	Tensile stress [Pa]
τ_{xy}, τ_{xz}, τ_{yz},	Shear stress [Pa]
ψ_1	First normal stress coefficient [$Pa.s^2$]
ψ_2	Second normal stress coefficient [$Pa.s^2$]
ω	Angular frequency [s^{-1}]
ϕ	Elastocapillary number

Latin alphabet

A	Area
Bo	Bond number
Ca	Capillary number
d	Diameter [mm]
D	Filament diameter [mm]
De	Deborah number
d_{mid}	Filament diameter [mm]
d_o	Initial diameter [mm]
d_1	Diameter at t0 [mm]
d_2	Diameter at next phase [mm]
El	Elasticity number
Eu	Euler Number
F	Force [N]
F_z	Tensile Force [N]
G	Elastic Modulus [Pa]
G_s	Shear Modulus [Pa]
G_1	Elastic moduli for immediate elastic response [Pa]
G_2	Elastic moduli for delayed elastic response [Pa]
G'	Storage modulus [Pa]
G''	Loss modulus [Pa]
G*	Complex modulus [Pa]

h	Height [m]
h_f	Final height [mm]
H_R	Half nip gap [mm]
h_0	Initial height [mm]
k	Consistency
L	Die length [mm]
l_{cap}	Capillary length [mm]
Lo	Initial length [mm]
L_{max}	Maximum stable length [mm]
l_0	Original length [m]
l_1	Total extended length [m]
M	Torque [Nm]
n	Power law index
N_1	Primary normal stress different [Pa]
N_2	Second normal stress differences [Pa]
Oh	Ohnesorge number
Q	Volumetric flow rate [mm^3/min]
r	Dimensional constant
R	Radius of the die [mm]
Re	Reynolds number
R_0	Initial Radius [mm]
R_1	Radius after stretching at t_0 [mm]
t	Time [s]

tc	Relaxation time of the fluid
tp	Characteristic time of the experiment [ms]
t_r	Rayleigh time or Inertial time
t_v	Viscous break up time [ms]
t_λ	Time constant [s]
U	Roll Speed [mm/min]
U_B	Biaxial extensional flow
U_P	Planar extensional flow
U_u	Uniaxial extensional flow
v	Capillary velocity
v_{raw}	Raw average velocity [mm/s]
v_{slip}	Slip velocity [mm/s]
v_{true}	True velocity [mm/s]
V	Velocity [m/s]
Vc	Characteristic velocity
V_0	Initial Volume [m^3]
W	Deformation distance [m]
We	Weissenberger number
X	Correction factor

1 Introduction

All industry sectors in Europe are facing increased competition due to the current economic climate and only companies with new ideas and improvements are able to survive in such difficult times. For the manufacturing sector, one way to remain successful is to increase productivity and quality whilst simultaneously decreasing the costs associated with wastage due to defects. Considering the coil coating manufacturing processes such as tension leveller, hot water rinses and coating, all or some of these could be optimised which could lead to a better quality of final product and subsequently reduce the likelihood of defect products. For this thesis, research efforts were concentrated on the coating process in particular determining the rheological behaviour of the paints (Dockey 2009 and Friedersdorf 2009).

Shoff (2005) reflects the view of how important the science of rheology is in boosting the economic benefits for the coating industry, which had a turnover of nearly 270 million tonnes worldwide in 2009.

Furthermore, the quality control for paint could be revolutionised by a better understanding of the flow behaviour of paints. New rheological devices which have been developed within the last two decades, for example, the capillary break up rheometer and the capillary extrusion rheometer make it possible to measure the extensional viscosity at very high strain rates which provide a better rheological understanding of the samples (DRRheology 2011 and Cambridge Polymer Group 2011).

This thesis focuses on both rotational and extensional viscosities in order to obtain a general understanding of how polyester resin based paints behave under the influence of shearing or stretching. A rotational rheometer was used to obtain rheological behaviour subject to a pure shear rate. Additionally, two techniques were employed to measure the extensional viscosity of paint under different extensional rate ranges. The first technique used a capillary break up extensional rheometer (extentional rate $< 10^2 s^{-1}$) and the second technique used a capillary extrusion rheometer (extentional rate $> 10^2 s^{-1}$)

1.1 Motivation

This long term research project has been divided into several major milestones in order to achieve the ambitious goal of improving the roll coating process through rheological control; with motivation for the optimisation of the roll coating process driven by the factors of quality and productivity improvement.

One of the major milestones of this project was the generation of fundamental rheological data which were attained by repeatable methods. The outcome of the research project is hoped to be an increase of production speed and quality performance which currently are held back by process instabilities caused by air entrainment, ribbing or other flow instability defects. At present, roll coating can achieve a speed of up to 120 m/min without the presence of flow instabilities, depending on the properties of the paint used. Therefore, the motivation is to enhance production speed (>120m/min) whilst still producing uniform stable films. The economic benefits of such improvements are axiomatic and will make a significant contribution to the future competitiveness and profitability of Tata/Corus' Colorcoat operation. It would also be beneficial in terms of sales price to the construction industry (e.g. roofing sheets and wall cladding systems), for domestic appliances (e.g. wash machines and ovens) and manufactured goods (e.g. lighting and office furniture) as well as for automotive (e.g. car doors and car bonnets).

Currently, the coil coating process is more of an art form rather than a science particularly in terms of process control and quality optimisation, which depend on the experience of operators to make the correct decisions regarding set up. The incentive of the sponsors is to enhance knowledge about the behaviour of paints and move a step closer to making coil coating a more scientific process in terms of understanding.

1.2 Achievements

Generally, the rheological characterisations for polyester resin based paints were successfully undertaken which was necessary for continuing the whole research project. A failure would have meant that the project would have come to a halt and new research activities would have not been able to carry out. With this new knowledge and derived experimental procedures, it was possible to provide trustworthy rheological data which were the basis of further research activities.

To reach this successful outcome, several smaller milestones were required. The first milestone was to provide steady state flow procedures for stress and strain controlled rheometry whose results were identical.

Once suitable experimental procedures for the rotational experimental works were successfully established, four commercial polyester resin based paints were used to highlight the rheological differences and therefore the second milestone of comparing each paints was finally achieved. The results allowed yield stress and Newtonian behaviours to be assigned to the samples. The rheological classification of the commercial paints was one of the project aims which was also successfully completed.

A significant achievement was to obtain an ideal operation window for the Capillary Break up Rheometer for polyester resin based paints which was the third milestone. There is now the opportunity for comparing paints in the field of filament thinning. Additional information about the evolution of filaments and the occurrence of defects such as recoiling were captured by a high speed camera and which helped to increase the understanding of the behaviour of commercial paints.

During the fourth milestone phase, further successful rheological parametric characterisation was attained by using capillary extrusion rheometer with different die geometries and piston speeds. This instrument mimicked more realistically the flow behaviour between the rolls.

A steady state flow curve could be provided, utilising the different rheometers, for a shear rate between 10^{-1} and 5×10^{4} s^{-1}, which is unique for polyester resin based paint pigmented with dark red analysed in this work. This type of flow map for this

commercial paint has not been published previously to the best of the author's knowledge.

1.3 Thesis structure

- Preface : provides Abstract, Declaration, Statements, Table of contents, Dedication, Acknowledgements, List of tables, List of figures, List of symbols
- Chapter 1: outlines the introduction, motivation and achievements.
- Chapter 2: describes the coil coating line and includes a section on the coating process and additional information is given about the product defects and how this is driven by surface tension and viscosity.
- Chapter 3: provides general information about the chemistry, components and inner structure of commercial paints
- Chapter 4: aims to provide an understanding of the general concepts of the science of rheology in particular the aspect of the extensional and rotational effects.
- Chapter 5: informs the reader about the principles of operation for the different extrusion rheometers and especially focuses especially on the capillary break up rheometer used in this study and the scientific background.
- Chapter 6: Provides an understanding about the contraction flow phenomena and details about the capillary extrusion rheometer.
- Chapter 7: summaries the test equipments which were used in the research and may be considered as a reference chapter. Additional test parameters for each experimental procedure were included.
- Chapter 8: describes the development of shear rheometry methodologies. It discusses the obstacles of measuring rheological parameters and gives solutions to overcome these problems.

- Chapter 9: focuses on the rheological characterisation of commercial paints analysed in this study by using the capillary break up rheometer. A description of the systematic methodology used is described, in particular the changing of the set up parameters in order to obtain the ideal operational window.

- Chapter 10: deals with the analysis of the raw data from a paint measured with a Capillary extrusion rheometer to provide a paint map with all the data obtained along with locations of the experimental instrument used.

- Chapter 11: outlines the conclusions from the thesis.

- Chapter 12: suggests the future research work.

1.4 Bibliography

Cambridge Polymer Group, Cambridge Polymer Group's Instruments, Available: http://www.campoly.com/caber.html, Access: 26 November 2011

Dockey J. (2009, January 11). Retrieved August 12, 2012 from Innovation Solution: Coil coaters provide prompt delivery, cost savings, sustainability and quality control: http://www.metalconstructionnews.com/articles/products/paints,-coatings-and-finishes/innovative-solutions-coil-coaters-provide-prompt-delivery,-cost-savings,-sustainability-and-quality-control.aspx

DRRheology P9000 Ltd., DrRheology - on demand technical resources, Available: http://www.drrheology.com/, Access: 26 November 2011

2 Industrial background

2.1 Coil coating of strip steel

The coil coating of strip steel is a continuous and highly automated process in which the aim is to apply a uniform thickness paint layer onto a metal sheet (Weinstein and Ruschak 2004). A coil coating line represents a capital investment of several million pounds and involves a number of distinct operations which apply organic or inorganic coatings onto up to 30 tonnes coil of metal. Typical operations are cleaning and treating the surface, applying and curing the coating layers (e.g. primer, top coat) and rewinding. Each coating run can process up to 1.6 km length of metal. The width capabilities start from 100 mm and go to 1900 mm for steel and 2700 mm for aluminium. The gauge capabilities vary from 0.15 mm to 2.5 mm. Production capacities of around 4550 tonnes of steel or 2750 tonnes of aluminium per week are possible. (Vayeda and Wang 2007, Froehlich 1998, Graziano 2000, Drufke 2006, Meuthen and Jandel 2007). The majority of coil coating lines use liquid paints based on organic solvents and as a consequence, harmful volatile organic compounds (VOC) will be released during the drying process in which the solvent evaporates. This requires VOC control equipment (such as solvent destruction systems extracting solvent laden air into chamber where it is converted into carbon dioxide and water through heating and burning the solvent laden air) in order to remove the harmful materials. A completely different set up is used with water based liquid paint. In this case, the coil coating lines are equipped with infrared ovens instead of incinerators to remove the water and the level of VOC emissions is almost zero in this case. Some coil coating lines can even be used for powder coating (Vayeda and Wang 2007, Froehlich 1998 and Drufke 2006).

The major advantage of pre-painted metal is that manufacturing plants are fully in compliance with the environmental regulations because it has an integrated facility to treat the VOC. In respect to the commercial side, the manufacturing cost for producing this product is relatively cheaper in comparison to other techniques such as a manual spraying process (Froehlich 1998 and Graziano 2000). In addition to the painting capability, modern coil coating lines can also laminate directly onto the

metal substrate on either or both sides. The capabilities of printing and embossing are available to produce multicolour designs or wood grain appearances (Graziano 2000 and Drufke 2006).

2.2 Processes in coil coating line

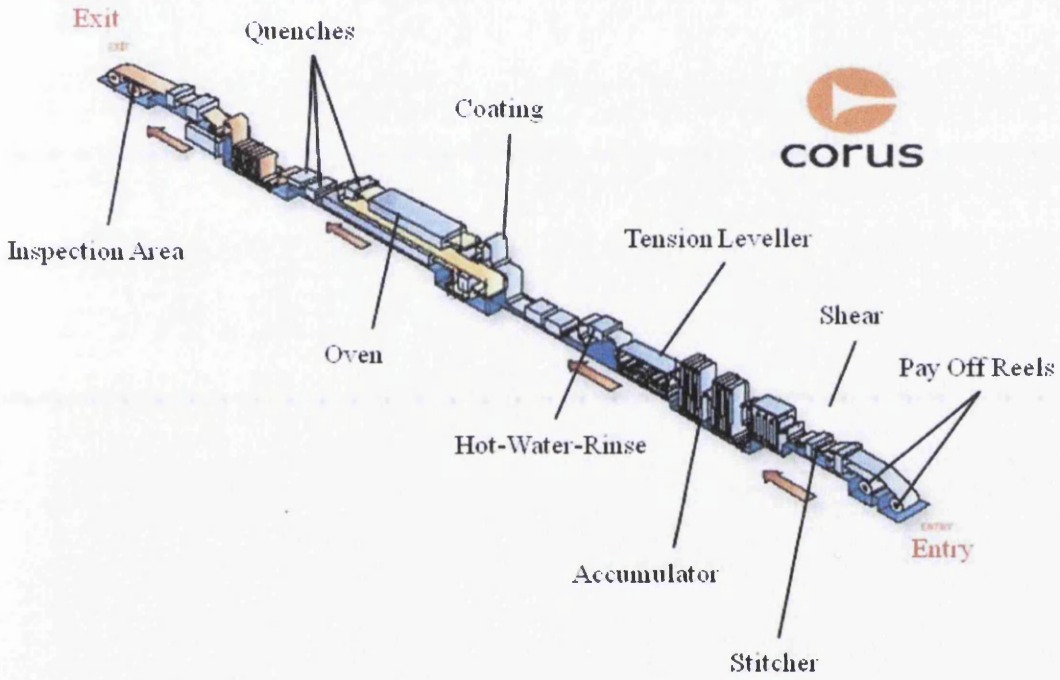

Figure 2-1: Illustration of the coating line with the different process stages

Before the material is fed into the coil coating line, the steel is coated with a metallic layer which provides sacrificial corrosion protection. Substrates such as Galfan (95 % zinc, 5% aluminium) (Woldman and Frick 2000) and Gavalume or Zincalume (55% aluminium, 43.4% zinc, 1.6% silicon) (Cleary 1985) are typically used in the coil coating process. A metallic layer produced by hot dip galvanising normally has a zinc content of around 99.7% and an aluminium content of around 0.3%.

The first process in the coil coating line takes place in the pay off reel, where the metal coil is unwound and fed into the line. To guarantee a continuous automated process, a new strip will be stitched or welded to the previous material just before the stock runs out. Each new roll undergoes a quality control check whose purpose is to detect any damage that may have occurred during the transport before use.

Additionally, the width and gauge will be manually measured (Froehlich 1998) to confirm the correct dimensions requested by the customer. Afterwards, the adhesion of the paint to the metal will be enhanced by pre-cleaning the surface with alkali which helps remove any contamination and detritus (Vayeda 2007 and Goodwin 1984). The remaining strong alkali will be removed under a shower of water with temperature of around 50° C in the hot water rinse section.

The necessary time for the stitching process between the new and previous substrates, without stopping the whole coil coating process, can be gained from the storage section, labelled accumulator, which is the next process after the cleaning process (Froehlich 1998). Normally, the flatness of the strip needs to be improved which can be achieved by the tension leveller (Wilshire 2006). A final cleaning process follows using hot water to rinse the remaining alkali and impurities away.

Now, the strip is ready for receiving a pre treatment layer resulting in enhanced adhesion and corrosion protection. Afterwards, primer or topcoat layers are applied in the coating section. Many coil coating lines have the capability to apply primer and topcoat on both sides using two separated coating sections with two different oven sections (Froehlich 1998). In the curing oven, the substrate is heated up to Peak Metal Temperature (PMT) or curing temperature. Consequently, the wet paint changes its aggregate condition from liquid into solid through evaporation of solvent and hardening of the polymer via cross linking of the polymer chains. Correct curing conditions are important to obtain a coating layer which has sufficient adhesion to the substrate, hardness, flexibility and strength. An incinerator is also included in the oven to burn off the solvent emissions.

It is envisaged that the conventional curing will be replaced by radiation curing using electrode arc systems to produce ultraviolet light or electron beams to harden a solvent free coating film within seconds (Graziano 2000, Abbasian 2004, Glöckner et al. 2008).

After curing, the coating is cooled down in the quench section (Froehlich 1998). Finally, the semi-finished product is ready for the quality control examination in the inspection area. The standard inspections include checking the gloss level and determining the colour level by visual or electronic methods. In addition, the

adhesion and flexibility of the coating will be measured for example according to cross cut test (ASTM D3359-07) and Erichsen (Froehlich 1998).

2.2.1 Types of roll coating

The outcome of this research presents an understanding of fluid behaviour in the coating section where rheology plays an important role in production performance, therefore, a short introduction in roll coating is essential.

There are two types of roll coating, namely direct roll coating and reverse roll coating. The advantage of direct roll coating is that the wet film thickness can be controlled more accurately than in reverse roll coating. Another advantage of direct roll coating is that the applicator roll has a longer life expectance compared to that in a reverse roll coating system since the total friction force is smaller. However, reverse roll coating also has distinct advantages, for example the surface finish is better and a higher line speed performance can be achieved (Graziano 2000 and Wicks et al. 2007).

2.2.2 Direct roll coating

In this process, the direction of movement of the substrate is in the same direction as the rotation of the applicator roll. The journey of the paint begins under the effect of adhesion and viscous lifting (Chong et al. 2007) from the pick-up roll via feed to the applicator roll from which the paint will be applied to the substrate. The gap between the feed and applicator rolls and the viscosity of the paint determine the applied film thickness. The applicator rolls are normally made of metal covered with a polyurethane elastomer, whose flexibility allows compensation for the variation in the thickness of the substrate. The direct roll coating process is ideal for metal sheet and can be found in the can coating and metal decorating industries (Graziano 2000 and Wicks et al. 2007).

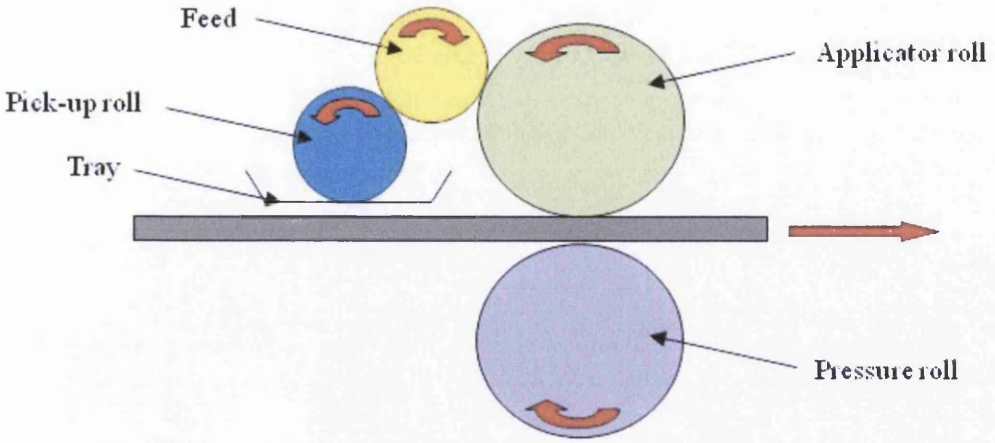

Figure 2-2: Schematic diagram of a direct roll coater (adapted from Wicks et al. 2007)

2.2.3 Reverse roll coating

In this case, the substrate's movement is in the opposite direction to that of the applicator roll's direction of rotation. The wet film thickness is controlled by the gap between the pick up and application rolls and/or the rate of the rotation of the coating application roll (or pick-up roll) to the line speed of the substrate. The reverse roll coating technique is used, for example in painting, printing and embossing (Graziano 2000).

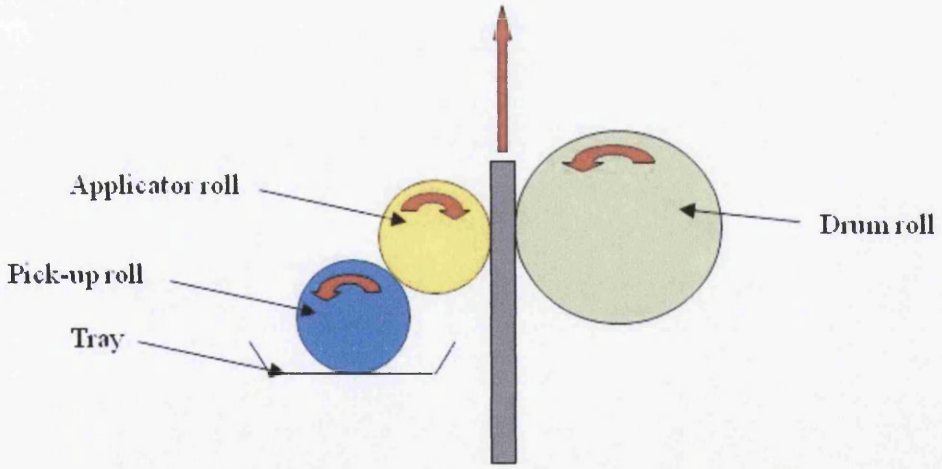

Figure 2-3: Schematic work principle of a reverse coating process – 2 Roll (adapted from Cohu and Magnin 1995)

Before the industrial paint is pumped into the tray, the paint needs to be stirred to achieve a homogenous mixture. The pick-up roll, which is partly immersed in paint,

transfers the complex fluid to the application roll covered with elastomer layer through a nip.

2.3 Pre – finished steel products

Pre finished steel possesses several layers which can be seen below.

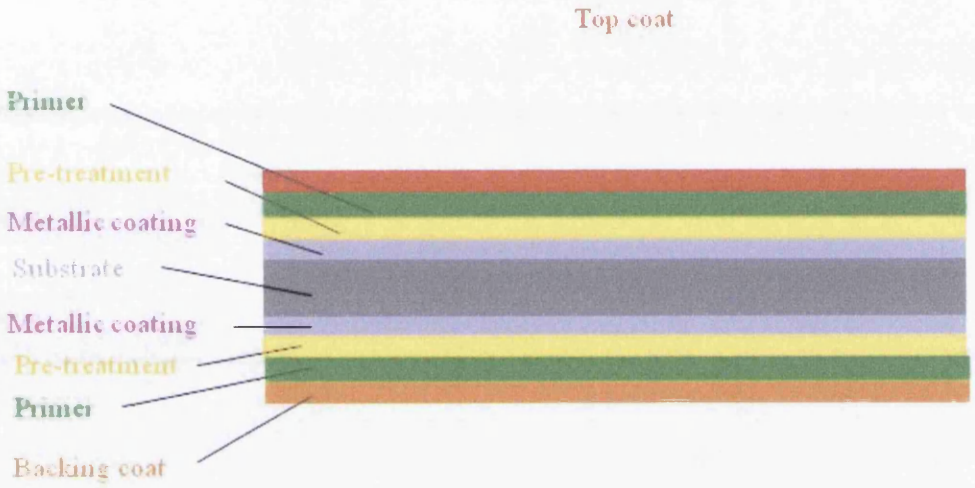

Figure 2-4: Pre finished product with various types of layers

The layers comprise:

- **Metallic coated steel substrate**

  The main component of pre-finished steel is the steel itself. The steel gets its required mechanical properties by further treatments according to national and international standards (Corus Group 2007).

- **Pre-treatment**

  Pre-treatment chemically changes the surface of the substrate through passivation leading to an improvement in adhesion of the applied paint and corrosion resistance. This is also known as surface activation.

- **Primer**

  The primer is the first paint layer to be applied and the main component is either epoxy or polyester resin (Goldschmidt and Streitberger 2003). The primer is used to impart a better corrosion protection to the substrate (Nanetti 2006). Additionally, it enhances the adhesion between the metal and the top coat (Arimes 1994). A primer is especially suitable for metals intended for use in moist or wet environments.

- **Top-coat**

  Finally, the top coat is applied which typically contains one of the four following systems, PVC-Plastisol, Polyester melamine, Polyester isocyanate and Polyvinylidene Difluoride (Corus Group 2007). The dry film thickness of all except of plastisol is around 15 to 40 μm. A dry film made of plastisol can achieve a thickness of up to 300 μm (Goldschmidt and Streitberger 2003) but is normally between 100 and 200 μm. All samples examined in this research are used as top coats.

- **Back coating**

  Back coats provide good adhesion and corrosion protection. Since the back coat is not fully exposed to the environment, the film thickness is much smaller than the top coat (Corus Group 2007) with a typical thickness of 8 to 10 μm (Goldschmidt and Streitberger 2003).

2.4 Product defects

The majority of defects can be immediately detected after application or after the curing process when the film has dried. Unfortunately, a correction is not possible at this stage and the presence of defects increases the scrap cost accordingly. Some common fluid instabilities or defects driven, for example by surface tension or viscosity are frequently observed in coating flow (Gutoff and Cohen 1995, Abbasian 2004 and Schoff 2004). Many investigations of flow instabilities or defects

(Koschmieder and Biggerstaff 1986, Roper et al. 1999, Gostling 2001, Lopez and Rosen 2002, Ryntz and Yaneff 2003 Rouseau 2006, Schatz et al. 2008 and Lécuyer et al. 2009) have been conducted both experimentally and numerically. Despite these research efforts, there are still unexplained phenomena and flow processes in this area such as the effect of viscoelasticity on the coating flow, flow dynamics in multilayer coating and product enhancement without defects. Some common defects are mentioned below (Lee et al 2010).

2.4.1 Convection or Bénard cells

The appearance of small hexagonal shapes on the surface is an unwanted effect driven by surface tension gradient (Schatz et al. 2008). These shapes are known as convection cells or Bénard Cells. In the past, the explanation for this defect was that the difference in temperature of the paint layer between the top surface of the hot substrate and the paint – air interface results in a density gradient. As a consequence, a layer of convection or Bénard cells are able to be formed in the layer (Koschmieder and Biggerstaff 1986). A more recent investigation shows that low viscosity and pigment flocculation promote the occurrence of the convection or Bénard cells (Ryntz and Yaneff 2003). Research by Gutoff and Cohn (2006) outlines methods to counter convection cell formation by either applying a thinner layer, using paint with a higher viscosity or increasing the drying time by adding lower volatility solvent or surfactants (e.g. fluorinated surfactants).

2.4.2 Fat edges or Picture framing

An accumulation of paint at the edge of a layer is described as fat edges or picture framing. In this area around the edge, surface tension is higher due to the higher concentration of dissolved solids which leads to a flow stream of paint from lower surface tension area to the higher surface tension area. Reducing surface tension with surfactant prevents a flow towards the edge (Gutoff and Cohen 2006).

2.4.3 Ribbing

Above a critical operation speed, the meniscus profile undergoes a periodical instability leading to an uneven coated film. As a result, a sinusoidal pattern in the direction of coating can be detected on the surface which is classified as ribbing (Gostling 2001, Lopez and Rosen 2002 and Rouseau 2006). Currently, Newtonian and viscoelastic liquids have been used to investigate the ribbing instability in rigid and deformable forward roll coating processes. Parameters such as capillary number (see equation 5.7, in this case roll speed is used for the characteristic velocity) or roll speed, coating gap, hardness of the complaint cover and viscosity all play an important role in the onset of ribbing. For example, an increase in capillary number, increasing hardness of the compliant roll and decreasing the coating gap will reduce the wavelength in Newtonian and viscoelastic liquids and, consequently, a reduction or even avoidance of ribbing altogether (Lee et al. 2010 and Chong et al. 2007).

2.5 Bibliography

Abbasion, A. (2005). Study on different platform of paint's solvents and the effect of surfactant (on them). *Process in Organic Coatings , 49*, 229-235.

Arimes, T. (1994). *HVAC and Chemical Resistance Handbook for the Engineer and Achitect.* BCT.

Ascanio, G., Carreau, P. J., & Tanguy, P. A. (2006). High-Speed roll coating with complex rheology fluids. *Experiments in Fluids , 40*, 1-14.

Basto, A. C., Ferreira, M. G., & Simoes, A. M. (2005). Comparative electrochemical studies of zinc and zinc phosphate as corrosion inhibitors for zinc. *Progress in Organic Coatings , 52*, 339-350.

Bosma, M., Brinkhuis, R., Coopmans, J., & Reuvers, B. (2006). The role of sag control agents in optimizing the sag/leveling balance and a new powerful tool to study. *Progress in Organic Coating , 55*, 97-104.

Chong, Y. H., Gaskell, P. H., & Kapur, N. (2007). Coating with deformable rolls:An experimental investigation of the ribbing instability. *Chemical Engineering Science , 62*, 4138-4145.

Clapp, T. C., Umbreit, T. H., Meeker, R. J., Kosson, D. S., Gray, D., & Gallo, M. A. (1991). Bioavailability of lead and chromium from encapsulated pigment materials. *Bulletin of Enviromental Contamination and Toxicology , 46*, 271-275.

Clearly, H. J. (1985). The microstructure and corrosion resistance of 55% Al-Zn coatings on sheet steel . *Corrosion Microstructure and Metallography* , 103-113.

Cohu, O., & Magnin, A. (1995). Rheometry of paints with regards to roll coating process. *Journal of Rheology , 39*, 767-785.

Coyle, D. J. (1992). *Roll coating, in Modern Coating and Drying Technology.* New York: Wiley -VCH.

Coyle, D. J. (1984). The fluid mechanics of roll coating: Steady flows, stability and rheology. University of Minnesota.

Dalager, N. A., Mason, T. J., Fraumeni, J. F., Hoover, R., & Payne, W. W. (1980). Cancer mortality among workers exposed to zinc chromate paints. *Journal of Occupational Medicine , 22*, 25-29.

Deligny, P., Tuck, N., & Oldering, P. K. (2000). *Resins for Surface Coating: Alkyds and Polyesters* (2n Edition ed., Vol. 2nd Volume). London: John Wiley and Sons.

Duarte, R. G., Bastos, A. C., & Ferreira, M. G. (2005). A comparative study between Cr(VI)- containing and Cr-free films for coil coating systems. *Progress in Organic Coating , 52*, 320-327.

Durfke, R. (2006). An Introduction to Coil Coating, Finishing process leads to constantt quality and appearance in metal parts. *Metal Finishing , 4* (1), 35-37.

Froehlich, R. W. (1998). Coil Coating 101. *Metal Finishing , 96* (11), 46-49.

Glass, J. E. (1978). Dynamics of roll spatter and tracking. 2. Formulation effects in experimental paints. *Journal of Coating Technology , 50*, 61-68.

Glass, J. E. (1978). Dynamics of roll spatter and tracking. 3. Importance of extensional viscosity. *Journal of Coating Technology , 50*, 56-71.

Glass, J. E. (1978). Dynamics of roll spatter and tracking. 1. Commercial latex trade paints. *Journal of Coating Technology , 50*, 53-60.

Gloeckner, P., Jung, T., Struck, S., & Studer, K. (2008). *Radiation curing for coating and printing inks: Technical basic and applications.* Hannover: Vincentz Network.

Goldshmidt, A., & Streitberger, H.-J. (2003). *BASF Handbook on basic of coating Technology.* Hannover: Vincentz Network.

Goodwin, F. (1984). *Galfan galvalising alloy technolgy* (2nd Edition ed.). International Lead and Zinc Research Organisation.

Gostling, M. J. (2001). Stability of rigid and deformable roll coating flows. *PHD Thesis* . Unversity of Leeds: Department of Physics and Astronomy.

Graziano, F. (2000). Coil and sheet coating. *Metal Finishing , 98*, 175-176.

Corus Group. (2007, April 20). Retrieved May 10, 2008, from Product development: http://corusconstruction.com/en/products and services/roofs/colorcoat/durability/product development

Gustoff, E. B. (2006). *Coating and drying defects.* New Jersey: Wiley and Sons.

Koschmieder, E. L., & Biggerstaff, M. I. (1986). Onset of surface tension driven Bernard convection. *Journal of Fluid Mechanics , 167*, 49-64.

LaPuma, P. T., Fox, J. M., & Kimmel, E. (2001). Chromate concentration bias in primer paint particles. *Regulatory Toxicology and Pharmacology , 3*, 343-349.

Lecuyer, H. A., Mmbaga, J. P., Hayes, R. E., & Tanguy, P. A. (2009). Modelling of forward roll coating flows with a deformable roll: Application to Non-Newtonian inudstrial coating formulations. *Computer and Chemical Engineering , 33*, 1427-1437.

Lee, J. H., Han, S. K., Lee, J. S., Jung, H. W., & Hyun, J. C. (2010). Ribbing instability in rigid and deformable forward roll coating flows. *Korea-Australia Rheology Journal , 22* (1), 75-80.

Lopez, F. V., & Rosen, M. (2002). Rheological effects in roll coating of paints. *Latin American Applied Research , 32* (3), 247-252.

Meuthen, B., & Jandel, A. S. (2008). *Coil coating* (2nd Edition ed.). Wiesbaden: Vievweg and Sohn.

Nanetti, P. (2006). *Coating from A to Z.* Hannover: Vincentz Network.

Roper, J. A., Salminen, P., Urscheler, R., & Bousfield, D. W. (1999). Studies of orange peel formation in high speed film coating. *TAPPI Journal , 82*, 231.

Ryntz, R. A., & Yaneff, P. V. (2003). *Coating of polymers and plastics.* New York: Marcel Dekker.

Saatweber, D., & Vogt-Birnbrich, B. (1996). Microgel in organic coating. *Progress in Organic Coating* , 33-41.

Schatz, M. F., VanHook, S. J., Cormick, W. D., Swift, J. B., & Swinny, H. L. (2008). Onset of surface-tension driven Benard convection. Austin, Texas: Centre for Nonlinear Dynamics and Department of Physics, The University of Texas at Austin.

Soules, D. A., Fernardo, R. H., & Glass, J. E. (1988). Dynamics uniaxial extensional viscosity (DUEV) effects in roll application. 1. Rib and web growth commercial coating. *Journal of Rheology , 32*, 181-198.

Vayeda, R., & Wang, J. (2007). Adhesion of coating to sheet metal under plastic deformation. *International Journal of Adhesion , 27*, 480-492.

Weinsten, S. J., & Ruschak, K. J. (2004). Coating flows. *Annual Review of Fluids Mechanics , 36*, 29-53.

Wicks, Z. W., Jones, F. N., & Wicks, D. A. (2007). *Organic coating science and technology* (3rd Edition ed.). New Jersey: Wiley-Interscience.

Wilshire, B. (2006). *Processing of uncoated sheet steels.* Swansea: Material Research Centre, School of Engineering.

Woldman, N. E., & Frick, J. P. (2000). *Woldman's engineering alloys.* ASM International, Technology and Engineering.

3 A concise introduction to commercial paint

By looking around in our environment, colourful coated metals stand out as a beautiful appearance (instead of having the typical dull metal colour) and their existence can be attributed to the variation of available paint systems. Furthermore, the coating layers protect the metal from the aggressive atmospheric environment. Without the protection, the metal slowly starts to corrode and simultaneously loses its mechanical and chemical properties. Paint can be applied to the object either in a simple way by using a paint brush for instance or in a more sophisticated way by using automatic machine, whose technique is used in the coil coating process for example. Paint itself can be considered as a semi-finished product (Turner 1997). So before directly entering into the science of paint, the first few subchapters are dedicated to the main components in the paint which are polymers.

3.1 A brief introduction to polymer science

As outlined in the previous chapter, the main component of paint is the polymer (also known as the macromolecule). Polymer is characterised by its large relative size and consists of chemically bound smaller similar molecules or repeat units called monomers. Its skeletal structures can be linear or non linear such as branched or networked (also called cross linked). A linear structure is the simplest arrangement which has a chain with two ends. Branched polymers are more complex in nature due to small branches connected to the main chain. The connection points are named as branch points or junction points. In contrast to the before mentioned two dimensional structures, network polymers have a three- dimensional construction and each chain is linked to the other chain in this structure which is called cross-linked (Steven 1990, Speer et al 1994 and Young and Lovell 1997).

a) Linear b) Branched c) Network

Figure 3-1: Pictorial representations of different types of polymer structures (Young and Lovell 1997)

3.2 The classification of polymers in different aspects

Many further classifications of polymers exist but only a few should be mentioned for sake of simplicity. One way to classify polymers is to consider the repeatability of monomers in the chain. In this group, a polymer formed by identical monomers is coined as homopolymer. An example is polyethylene (PE) which is made out of many single ethylene monomers and its polymerisation is illustrated in Figure 3-2. A copolymer consists of at least two or more varieties of monomer whose occurrence can be random, block or alternate in the chain. An example is fluorinated ethylene propylene (FEP) which consists of tetrafluoroethylene and hexafluoropropylene depicted in Figure 3-3 (Young and Lovell 1997).

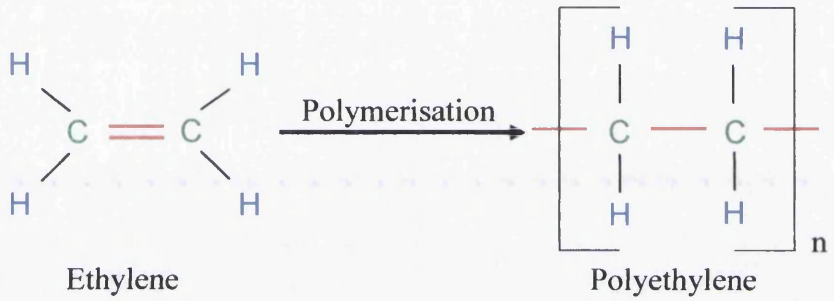

Figure 3-2: Polymerisation of Polyethylene due to the break up of the weak double bond

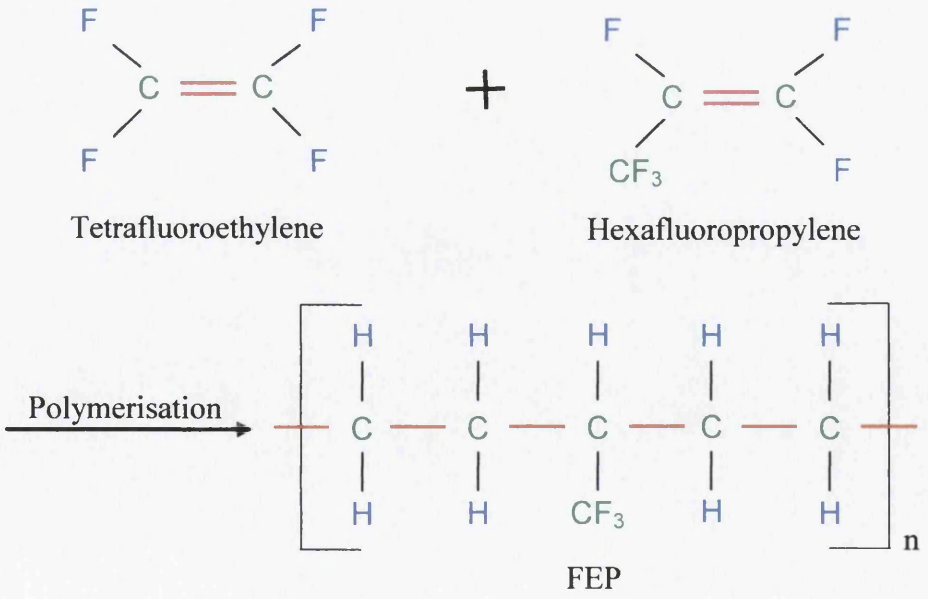

Figure 3-3: Copolymer FEP made out of two different monomers due to break up of the weak double bond

Alternatively, polymers can be classified into thermoplastic, thermoset and elastomer by considering the properties. Thermoplastic polymer consists of linear or branched molecules and comprises polymers which can be melted or resolidified by increasing or decreasing the temperature. Another type is the thermoset polymer which has a network structure with a high degree of crosslinking. As a result of the connections, thermoset polymer possesses very rigid and brittle properties. They do not melt when heated but decompose irreversibly at high temperature. Most of them do not dissolve or swell in solvents (Fischer 1990). Last but not the least, an elastomer consists of crosslinked rubbery polymers. As a result of their low crosslinking density, they are good at stretching and recovering after release of the stress. Due to its structure, it will not dissolve but it will swell in some solvents (Speer et al. 1994, Young and Lovell 1997).

In terms of polymerisation process, polymer can be grouped into condensation and addition polymerisation. A polymer formed with a release of small molecules as a by - product is known as a condensation polymer (e.g. polyester). The exact opposite is the type of addition polymer. In this case, an addition reaction forms the chain without the lost of any by-products (Nicholson 1994).

The final classification mentioned in this chapter considers the compounds of the polymer. A natural polymer consists of proteins, nucleic acids, cellulose (polysaccharides) or rubber (polyisoprene) whereas synthetic polymers are made of organic compounds derived from mineral oil such as nylon, poly- (hexamethylene adipadime), Dacron, poly- (ethylene terephalate) and so on (Speer et al. 1994).

3.3 Introduction to commercial paint

Paint can be considered as a complex fluid that possessing two different systems namely a dispersion phase also called internal phase and dispersion medium or continuous phase (resin or resin solution) (Oldring 2000). Additional to the polymer or binder (resin), solvent (carrier), pigment (colourant) and additive (e.g. flow agents, dispersants) are needed to manufacture a commercial paint. To obtain a heterogeneous blend, a special order for mixing the materials together needs to be

followed. By not considering the order of the mixing, lumps in the paint can occur (Turner 1997).

3.3.1 Binders/ resins

The bulk of a paint is made of binder which occurs as a solid aggregate condition and only by using appropriate type of solvents can the resin be dissolved. The main tasks of binders are firstly to hold the pigments together and secondly to provide the adhesion necessary to stay on the substrate. In addition, it has a strong influence on gloss level, durability, flexibility and toughness. Generally binder is made of a tough amorphous polymeric material. Paint can be classified by the main binder (e.g. alkyds, epoxy and polyester). Only the properties and chemical reactions of polyester will be briefly explained and illustrated in this chapter since paints based on polyester resins were used in our investigation. Polyester resin possesses good flexibility, good resistance against heat, stains and detergents. Furthermore, they give gloss coating as well as low permeability to gases and solvents (Scheirs and Long 2003). Polyesters can be made in linear, branched or cross-linked structures. The samples which will be used and analysed for this project fall into cross-linked polyester category. However, there are two types of cross-linked polyester namely saturated and unsaturated. The unsaturated polyesters are mostly used for producing fibres and composites whereas saturated cross-linked polyester resin find their application in paint manufacture.

A direct esterification describes the chemical reaction between an alcohol and an acid, which forms an ester as a reaction product. This method is normally chosen for producing polyester resins used for making paints (Hall 1989). A good example of polyester resin formation is the reaction of terephthalic acid with ethylene glycol (alcohol) (Weiss 1997).

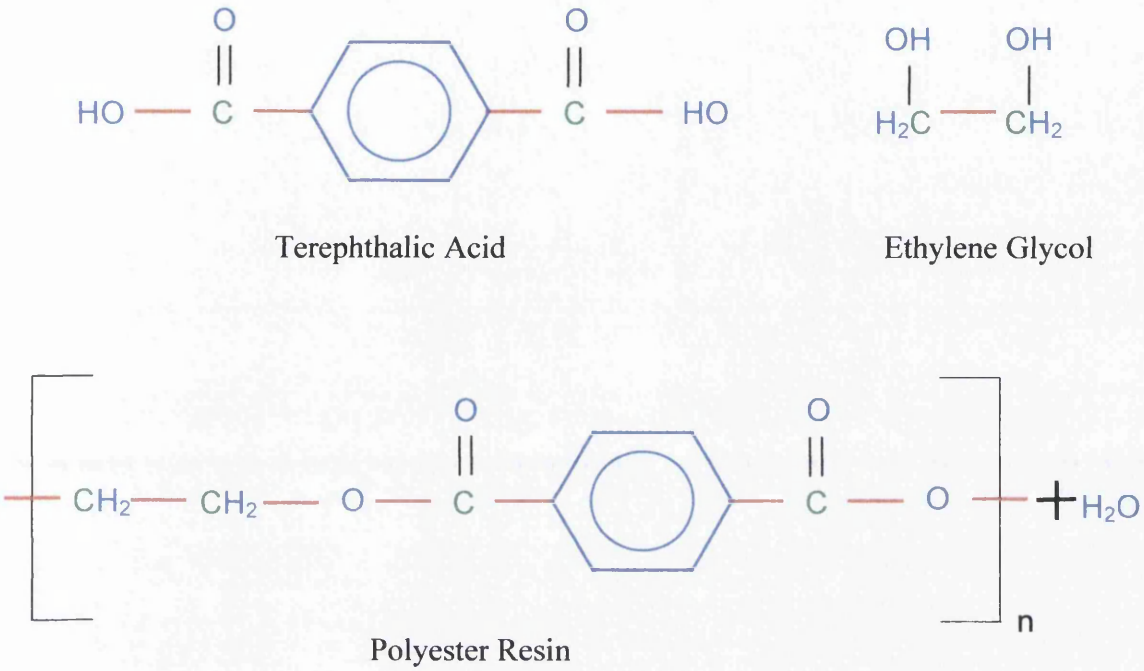

Figure 3-4: Illustrates the requirement of chemical compounds to obtain polyester resin (adapted from Weiss 1997)

3.3.2 The task of solvent in paint and its occurrence

The main reason for using solvents is to liquefy the materials used for paints and under this liquefied condition, the paint can be coated over the substrate (McKeen 2006). After the paint is on the product surface, the solvent is no longer needed and therefore will be removed by heating up the paint in an oven. In the coil coating industry, a high evaporation rate of solvent is desirable so that a fast dried paint film can be achieved (e.g. through oven drying or air drying) (Stoye and Freitag 2001). The common solvent groups are aliphatic hydrocarbons, aromatic hydrocarbons, esters, ketones, ethers and ether-alcohols, nitroparaffins and chlorinated paraffins (Koleske 1995). Some solvents are listed in the table below with data about the chemical formula, viscosity, boiling point and flash point and general information about the groups (Turner 1997).

3.3.3 Types of additives and their purpose

Additives impart particular properties to the paint (e.g. UV stability) and an amount between 0.01 and 1% is normally added to improve and change the properties of the paint (e.g. wet film or dried film which can affect flexibility, colour, fastness, gloss, solvent resistance, graffiti resistance, conductivity etc.) (Stoye and Freitag 1998).

Plasticisers and surfactants are some of the important additives used. An improved flexibility can be achieved by the inclusion of plasticiser molecules into the polymer matrix, which due to dipolar effects provides separation of the polymers chains making them less tangled and allowing them to move more easily. More than 300 different types of plasticisers are available on the market and a typical plasticiser family is the phthalates, which give the PVC flexibility and durability. The surfactant reduces the surface tension resulting in an improved wetting of surface by the paint (Koleske 1995 and Patrick 2005). Flow additives improve the spreading of the paint with the result of an enhanced surface quality. Furthermore, the presence of surface defects can also be solved by using the appropriate type of flow additive which depends heavily on the resin (Turner 1997). The smallest size which can be achieved by the milling process ranges between 0.1 to 2 μm (Stoye and Freitag 2001).

3.3.4 Brief insight into pigments

Pigments are commonly used to give the paint the required colour and the amount of pigment in paint depends on the type of colour and its colour strength. Furthermore, pigments may strengthen the paint film or provide a better adhesion of the film. Even increasing the corrosion resistance of metallic substrates or lowering the gloss level is possible by using the right sort of pigments (Turner 1997). The smallest particle size which is possible ranges from 0.1 to 2 μm (Stoye and Freitag 2001).

3.4 The principle of a network structure occurring within paint

Disperse systems are thermodynamically unstable, therefore the pigments move around and start to build up in clusters (Müller and Poth 2006). Poor dispersion techniques can be the reason for the production of clusters. A certain degree of network structure (e.g. flocculation) imparts elasticity to the paint which is desirable in some circumstances and furthermore it can prevent sagging and cratering (McKay 1994). In contrast, a large number of clusters may settle to the bottom of the paint and resulting in paint defects (Talbert 2007). Kaluza (1980) also reported that flocculation may increase the rate of sedimentation and reduce the gloss level. Flowability is impaired and the occurrence of the yield stress is accrued (Kaluza 1980). Excessive flocculation prevents flowing and levelling and may cause streaks and blotches (McKay 1994). The structure of flocculation can be broken down into primary structures like agglomerates and then further into primary particles. It is important to stabilise this state as most clumps are dispersed during the milling process for short while (Balfour 1995). The degree of dispersion strongly influences the properties of the final coating layer such as colour strength, opacity and gloss. Sang et al. (2001) also noticed a change in gloss level between two different inks made of two dissimilar red pigments. The reason seems to be the variation of the degree of dispersion which naturally occurs for each pigment. The aim is to have a stable well dispersed state which can be gained by using dispersing agent (Liphard and Rybinski 1991).

Pigment models have been proposed based on the various structural units of particles occurring in a dispersed medium (Honigmann and Stabenow 1962). Figure 3-5 illustrates the types of pigment particles. The smallest units are called primary particles. Due to strong interaction forces such as electrostatic or Van de Waals, the primary particles in a dispersed medium start to attract each other forming clusters specifically aggregates or agglomerates. Agglomerates are made up of single loose primary particles connected over a low contact area whereas aggregates consist of rigidly joined together particles, which are connected over large area of contact. (Hunter 1989, Goldschmidt 2003). A small formation of an opened aggregate is named a floc and occurs in a concentrated suspension (Nelson 1988 and Parfit 1981),

further growth leads to a three dimensional network structure called a flocculation (Everett 1988).

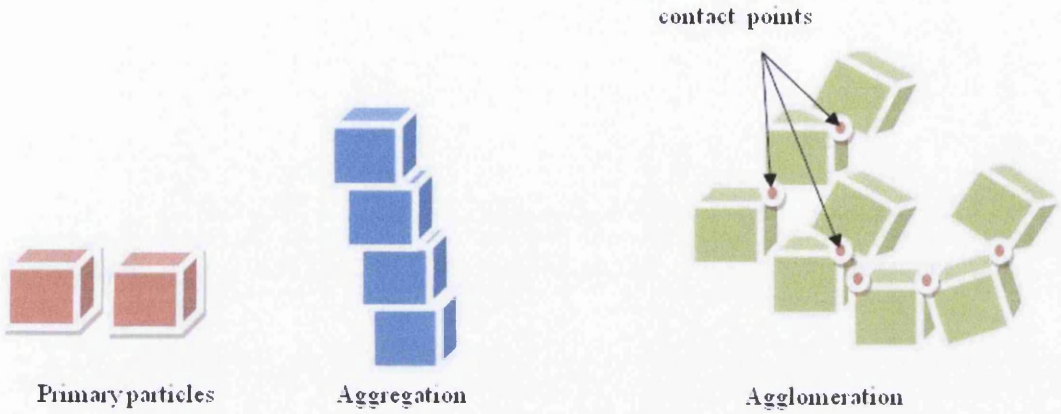

Figure 3-5: Schematic illustration of various types of network occurring in paints

Kaluza (1980) provided two features to distinguish the flocculates from the agglomerates. The first feature is the presence of cavities which are filled with components of the dispersion medium in a flocculated structure whereas an agglomerated structure possesses atmosphere in the core instead of fluids. The second feature focuses on the stability. The agglomeration structure is more stable than the one for the flocculation and flocculation breaks down under the action of very low forces.

3.5 Bibliography

Balfour, J., & Huchette, D. (1995). Paint and Ink International 8.

Bower, D. I. (2002). *An introduction to polymer physics.* Cambridge: Cambridge University Press.

Breuker, M. (1993). Rheological problems in the paint industry. *Applied Rheology, 48* .

Christie, R. M. (1993). *Pigments structures and synthetic procedures,* (5th Edition ed.). Basingstoke: Oil & Colour Chemists' Association.

Fischer, U. (1990). *Fachkunde Metall* (15th Edition ed.). Düsseldorf: Europa-Lehrmittel.

Honigmann, B., & Stabenow, J. (1965). VIth FATIPEC Congress., (p. 89).

Hunter, R. J. (1987). *Foundation of Colloid Science* (Vol. I). Oxford: Clarendon Press.

Kaluza, U. (1980). *Flocculation which factors influence it? Part 1, Pigment and Resin Technology.*

Kheirandish, S., Gubaydullin, I., Wohlleben, W., & Willenbacher, N. (2008). Shear and elongational flow behavior of acrylic thickener solutions, Part I: Effect of intermolecular aggregation. *Rheologica Acta , 47*, 999–1013.

Koleske, J. V. (1995). *Paint and coating testing manual* (4th Edition ed.). Ann Arbor: Garden-Sward

Liphard, M., Rybinski, W., & Schieferstein, L. (1991). *Farbe and Lack.* Hannove: Vinzenyz Network.

López, F. V., & Rosen, M. (2002). Rheological effects in roll coating paints. *Latin American applied Research , 32*, 247-252.

McKay, R. B. (1994). *Technological applications of dispersions.* New York: Marcel Dekker.

McKeen, L. W. (2006). *Fluorinated coatings and finishes handbook.* Norwich: William Andrew.

Müller, B. (2009). *Additive kompakt, Farb und Lack* (3rd Edition, ed.). Hannover: Vincentz Network.

Müller, B., & Poth, U. (2006). *Coatings formulation: an international textbook.* Honnover: Vincentz.

Nelson, R. D. (1988). *Dispersing Powders in Liquids.* Amsterdam: Elseveir.

Nicholson, J. W. (1984). *The chemistry of polymers.* Cambridge: The Royal Society of Chemistry.

Oldring, P. T., Deligny, P., & Tu. (2000). *Resin for Surface Coating: Alkyds & polyesters,* (2nd Edition ed., Vol. II). London: John Wiley and Sons.

Osterhold, M. (2000). Rheological methods for charterising modern paint systems. *Process in Organic Coating , 40*, 131-137.

Sang, T. V., Bhaskar, V. V., & Ronald, R. A. (2001). Comparison of methods to assess pigment dispersion. *Journal of Coating Technology , 73*, 923.

Speer, J., Kromm, J., & Maisel, J. (1994). *Chemistry* (5th Edition ed.). McGraw-Hill.

Stevens, M. P. (1990). *Polymer Chemistry An Introduction* (2nd Edition ed.). Oxford: University Press.

Stoye D., D., & Freitag, W. (2001). *Paints, Coating and Solvents* (2nd Edition ed.). Germany: Wiley-VCH Verlag.

Talbert, R. (2007). *Paint technology handbook.* CRC Press.

Turner, G. P. (1997). *Paint Chemistry, and Principle of Paint Technology* (3rd Edition ed.). London: Chapman and Hall.

Weiss, K. D. (1997). Paint and Coatings: A Mature Industry In Transition. *Progress in Polymer Science , 22*, 203-245.

Young, R. J., & Lovell, P. A. (1997). *Introduction to polymer* (2nd Edition ed.). Chapman & Hall London.

4 Introduction to rheology

The Researcher Professor Bingham invented the term Rheology, defined as

"The study of the deformation and flow of matter." (Barnes 2000)

Many scientific disciplines and industry sectors (e.g. agriculture, chemistry, industry, oil industry) are involved in Rheology research for their products. For example, Geller and Goodrum (2000) used rheological method (e.g. to provide flow curves) to answer the question whether diesel can be replaced with traditional vegetable oils in terms of its rheological properties. The conclusion was that one of the tested vegetable oil (Captex 355) was more likely to be able to replace diesel fuel in respect to the rheological properties such as flow resistance. The scientist Newton (c.1700) introduced the term viscosity for describing the degree of the flow resistance of a material subjected to an applied stress. The root of the flow resistance is the internal friction within the microstructure of the material. More detailed information about the theories and experimental works of rheology have been well explained in the books by Barnes et al. (1994), Barnes (2000) and Whorlow (1992).

4.1 Mathematical rheological relationships

Basically, a force, F, acting on an area of a body, A, causes a stress, σ, and if the resulting stress is beyond a critical stress level, the material starts to flow. There are two main types of forces which can be applied to the body namely extensional force (vertically away from the body) or a shear force (tangentially or parallel to the surface) which helps to provide useful information about either the extensional or shear rheology (Barnes 2000).

The displacement of a body is the response to the action of a force and is described as strain. In Figure 4-1, a distortion of a cube is depicted to illustrate the principle of shear deformation. The ratio of distance, W, along the force direction and the height, h, between the two force directions provides the dimensionless value of the shear strain where tan α indicates the degree of deformation.

$$\tan\alpha = \gamma = \frac{W}{h}$$ Equation 4-1

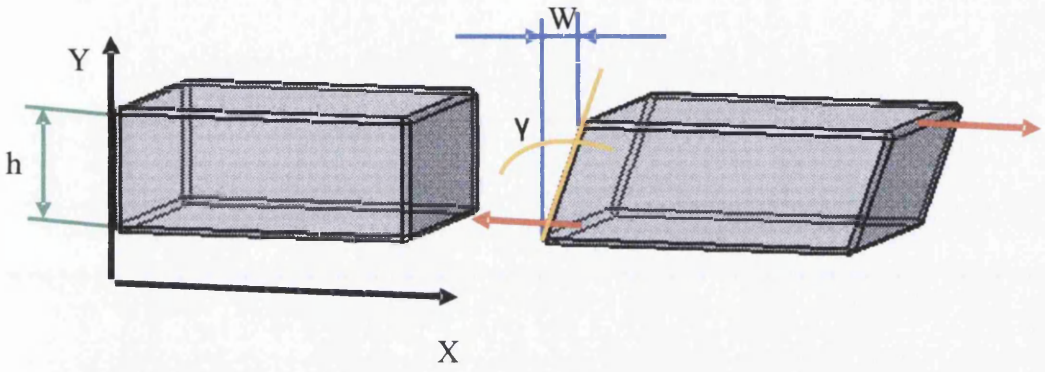

Figure 4-1: Schematic models for explaining the shear rate definition

By considering the time during which the deformation takes place, the physical parameter, velocity, *V*, comes into play and shear strain is converted into strain rate, $\dot{\gamma}$, with the unit of s^{-1}

Strain is converted into strain rate with respect to change in time (Barnes 1994).

Strain → Strain rate

$$\gamma = \frac{W}{h}$$ Equation 4-2

$$V = \frac{dW}{dt}$$ Equation 4-3

$$\dot{\gamma} = \frac{d\gamma}{dt} = \frac{V}{h}$$ Equation 4-4

4.2 Differences between perfect, viscous and viscoelastic behaviour

A material can exhibit perfect elastic (solid like) behaviour or perfect viscous (fluid like) behaviour, which are the classical extremes of the material behaviours. A

combination of elastic and viscous can also be found which is called as viscoelastic behaviour. Depending on the time scale, viscoelastic material can sometimes behave more elastic or more viscous (Malkin et al. 2006).

4.2.1 Characteristic feature for a perfect elastic solid behaviour

A perfectly elastic solid obeys Hooke's Law which means that the applied stress is proportional to the strain. After releasing the stress, the stretched body returns back to its original shape. This implies that the deformation is reversible and any energy during the deformation is stored elastically by the structure. (i.e. no energy loss). Figure 4-2 illustrates an example of the response of a perfect elastic solid. As can be seen, the solid directly responds to the applied stress, σ_1, in the form of a deformation. When the stress, σ_2, is reduced, a proportional reduction of the deformation occurs immediately. Such a relationship between stress, σ, and the resulting strain, γ, is described by the Hooke's Law equation as: (Barnes 2000)

$$\sigma = G\gamma \qquad \text{Equation 4-5}$$

Whereby the rigidity modulus, G, is a proportional constant which describes the stiffness of the material.

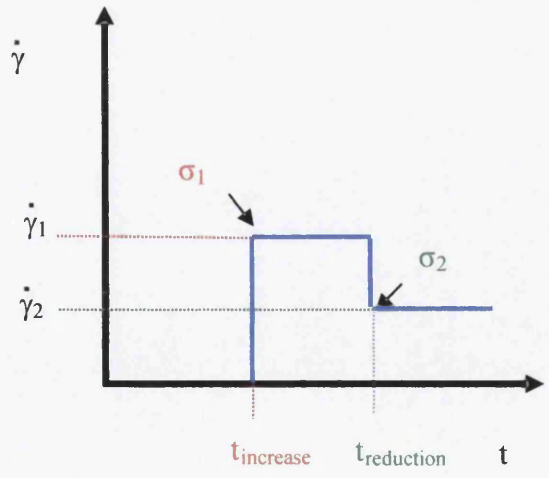

Figure 4-2: Strain responses of shear stresses σ_1 and σ_2 for a perfect elastic material (Elley 1995)

4.2.2 Characteristic feature for a viscous behaviour

A proportional relationship between applied force (shear stress) and rate of deformation (shear rate) portrays perfect Newtonian behaviour. For instance, water, air and gasoline behave as ideal Newtonian fluids and exhibit a constant viscosity which is independent of shear rates (Barnes 1994 and 2000). Figure 4-3 shows the response of a perfect viscous fluid. When stress, σ_1, is applied, the material starts to flow continuously. By removing the stress ($\sigma_2 = 0$) at t_{off}, the deformation in the fluid remains because all the energy is lost as heat.

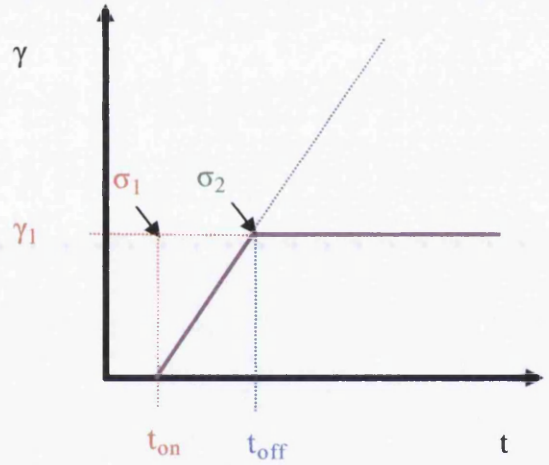

Figure 4-3: The strain responses of shear stresses σ_1 and σ_2 for an perfect viscous material (Elley 1995)

The behaviour of a perfect Newtonian fluid can be described by the constitutive equations:

$$\sigma = \eta \dot{\gamma} \qquad \text{Equation 4-6}$$

where η is the viscosity with a SI Unit of Pa.s

It is important to point out, that the normal stress differences do not exist in a pure fluid like material (i.e. $N_1 = 0$ and $N_2 = 0$).

At this stage of knowledge, a simple shear flow also called viscometric flow, can be fully described by considering the viscosity (see equation 4.11) and the elasticity of the fluid (see equations 4.4 and 4.5).

4.2.3 Characteristic features for a viscoelastic behaviour

Last but not least, viscoelastic materials exhibit both viscous and elastic properties depending on the time scale of an experiment. In a fast experiment, the time scales are short so that the materials microstructure may not have enough time to rearrange in response to an applied stress and the material appears to have an elastic response. However, when the time scales are long enough for the microstructure to rearrange then the material appears viscous (Barnes 2000).

When a stress, σ_1, is applied to a viscoelastic material at time, t_{on}, the response regarding shear rate is not immediate. It will take a certain time, t_x, until an equilibrium is established at a certain shear strain value, γ_1,. By reducing the stress, σ_1, to 0, the strain, γ_1, will go back to a certain strain, γ_2, but not to 0 because some energy is lost as heat through the viscous contingent (Barnes 2000).

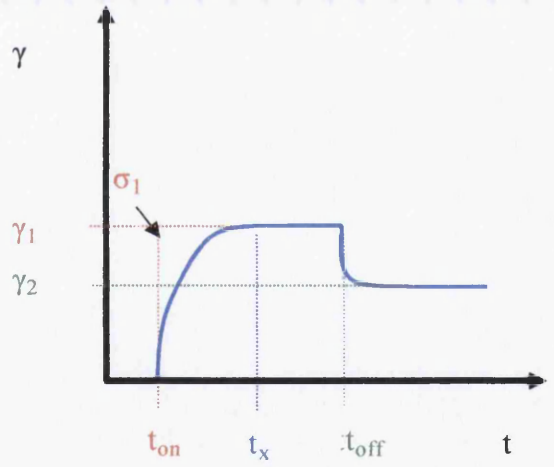

Figure 4-4: Schematic graph to show the response of a viscoelastic material subjected to stresses (Elley 1995)

4.3 Non- Newtonian fluid

With regards to a non-Newtonian fluid, the rate of shear does not have a proportional relationship to the stress $\sigma = \eta(\dot{\gamma})\dot{\gamma}$. Furthermore, non –Newtonian fluids such as paints and polymer solutions normally generate normal stress differences ($N_1 = \sigma_{xx} - \sigma_{yy}$ and $N_2 = \sigma_{yy} - \sigma_{zz}$) under flow condition. Additionally, the viscosity will not

change at a constant shear rate over a long time scale. By applying a wide spectrum of shear rate the following conditions may occur at such type of fluids:

- Shear - thinning or pseudoplastic
- Shear - thickening or dilatant

A more complex fluid such as plastisol can have both shear thinning and shear thickening behaviour depending on the shear rate applied. At low shear rate (<10 s^{-1}), plastisol exhibits shear thinning and at intermediate shear rate (from 10 s^{-1} to 100 s^{-1}), shear thickening occurs (Barroso 2007).

4.3.1 Shear thinning

For a shear thinning fluid, the viscosity decreases with increasing shear rate normally between the lower and upper Newtonian regimes. The constant viscosity exhibited in the lower Newtonian region is often called infinite shear viscosity whereas the upper Newtonian regime is known as zero-shear viscosity. The power law describes the viscosity decreasing linearly on a log / log plot against shear rate or stress and can be expressed mathematically as: (Chhabra and Richardson 2008 and Barnes 2000)

$$\sigma = k\gamma^n \qquad \text{Equation 4-7}$$

where k is the flow consistency index and n is power law index

4.3.2 Shear thickening

In contrast to shear thinning, shear thickening behaviour describes a material whose viscosity increases with the shear rate, attributed to the reorganisation of the microstructure. At a lower shear rate, the viscosity is almost proportional to the shear rate. Generally, the dilatant material has a closely packed structure and possesses a small volume in the resting condition. By applying higher shear rates, the volume

will increase through the induced deformation on the system. The liquid molecules between the particles will be forced to move out of their position. Consequently, the friction between the particles increases. A good example is wet sand. By applying stress on the wet sand, the sand particles will be moved closer together and even come into contact. This causes the water between the sand particles to be pushed out and the friction between the sand particles increases (Shay 1995).

4.3.3 Comparison between the time independent Newtonian and Non-Newtonian fluids

The following graph helps to visually demonstrate the differences between a Newtonian fluid and Non – Newtonian fluids.

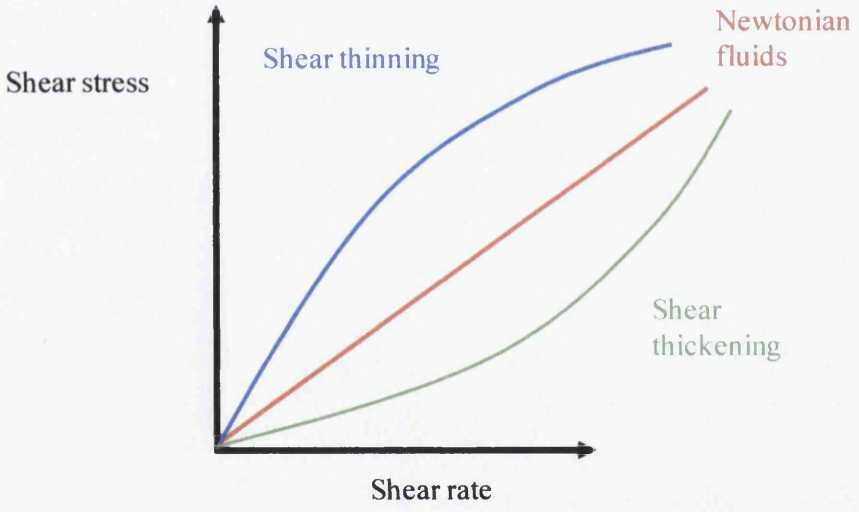

Figure 4-5: Comparison of time independent fluids (Mezger 2006)

4.3.4 Time dependent viscosity

Viscosity can increase or even decrease at a constant applied strain rate during the period of time until the fluid reaches an equilibrium. The reason is that it takes time to totally rebuild the microstructure after the removal or reduction of shear rate through Brownian motion (Barnes 2000).

The reduction of the viscosity over time at a constant shear rate is known as Thixotropy (Mewis and Wagner 2009). This type of behaviour can be encountered for example in the paint and food industry. A classical example from the food industry is Ketchup (Eley et al. 1995). On the contrary, a mixture of cornstarch and water behaves with rheopecty.

Barnes (2000) considered two cases of responses in form of viscosity changes caused by suddenly applying the shear rate from lower shear rate to higher shear rate and by immediately reducing the shear rate from high level to a lower level. The first case means that the structure from the lower shear rate cannot react on the sudden higher induced shear rate. The consequence is that the viscosity (the resistance to flow) remains and causes a higher stress in the system. An overshoot or peak stress occurs as a result. Now the structure or flocculation starts to break, an activity is known as relaxation. In the second case, a build-up of structure occurs when the strain rate is reduced from a higher level to a lower level and is governed by flow and Brownian-motion induced collision.

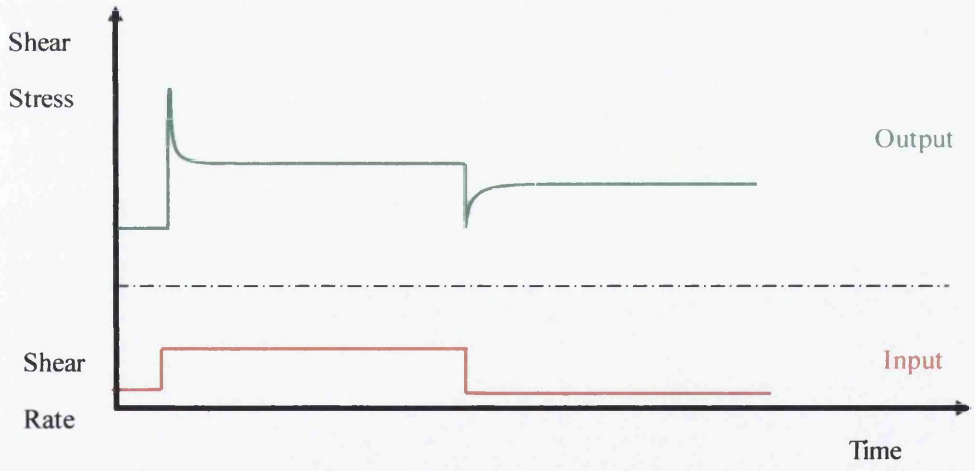

Figure 4-6: Thixotropic behaviour illustrated by inducing high and low shear rate adapted from Barnes (2000).

4.4 Rheological Models

The Newtonian model (see equation 4.11) and the Power Law model (see equation 4.12) assume that the flow always starts at zero stress whereas the Bingham Plastic

model and Herschel- Bulkley mode include an apparent yield stress which must be exceeded before any flow can be detected (Rao 2007 and Chhabra et al. 2008).

Bingham Plastic model	Herschel-Bulkley model
$\sigma = \sigma_y + K\dot{\gamma}$	$\sigma = \sigma_y + B\dot{\gamma}^{m-1}$
Equation 4-8	Equation 4-9

K, B, σ_y and m are the abbreviations for Bingham viscosity (also called plastic viscosity), Herschel-Bulkley viscosity coefficient, yield stress and shear rate index respectively.

The occurrences of the yield stresses are strongly dependent upon the applied shear rate range selected. Barnes (1999) went a step further and reported that a true yield stress can actually be found in very few materials. Some previous statements about apparent yield stress free materials need to be revised with new improving technology which would allow yield stress to be detected at lower shear rates.

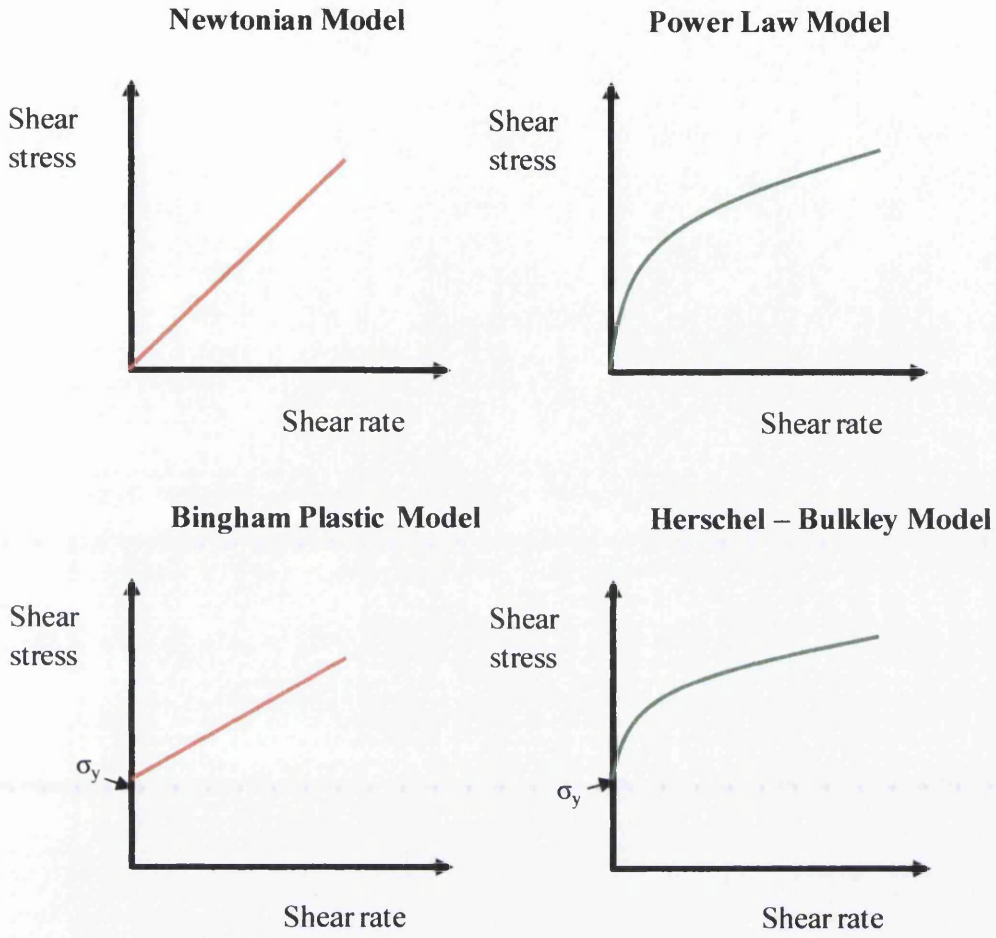

Figure 4-7: Comparing the different empirical models as a function of shear rate

4.4.1 Experimental procedure performed by rotational rheometer

Various procedures are available to obtain different rheological parameters from the samples. From the huge bulk of procedures, only the flow, creep and dynamic oscillatory test procedures need to be explained because these methods were used for this research.

4.4.1.1 Flow procedure

The flow tests use input variables such as strain, shear rate, stress rate and time to determine the viscosity, elasticity and normal stress (Barnes 2000). To obtain a flow curve, a wide spectrum of shear rate or shear stress within a specific time is step

wisely applied on the sample. The subsequent curve depicted on a viscosity versus strain rate or stress rate graph is called steady state flow curve when the measurement of the viscosity occurs in equilibrium. A step strain procedure applies a sudden strain rate on the sample to highlight the degree of the elasticity of the material and the level of viscosity. The microstructure needs time to change from one state to the other. When the imposed strain rate is faster than the time scale of rearrangement of the microstructure, an overshoot occurs. Additionally, this type of test is used to determine time dependent (e.g. thixotropy) behaviour (Barnes 1997). Recently published research used this type of procedure with lubricating grease (Moreono et. al. 2010) and with molten LDPE suspensions containing fibres (Keshtkar 2010).

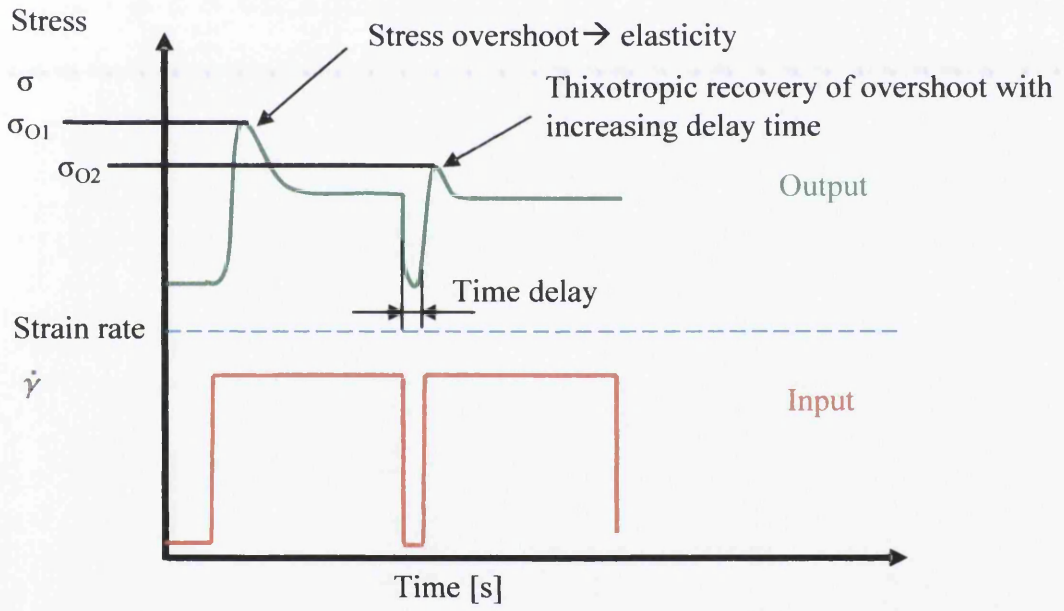

Figure 4-8: Example of how stress overshoot dictates the degree of elasticity and thixotropy behaviour.

4.4.1.2 Creep test

In this type of transient experiment, a stress is quickly applied on the material and kept constant for a long period of time. It is important to control the temperature since viscoelastic materials are strongly temperature dependent. The result is

displayed as a deformation γ to time t graph. The main reason for using a creep test is to gain information about the steady state rate which is used to add missing values at very low shear rate or shear stress on the flow curve. A characteristic deformation – time graph divided into three phases namely immediate elastic response, delayed elastic response and steady – state viscous response can be seen for a viscoelastic fluid in Figure 4-11 (Barnes 2000).

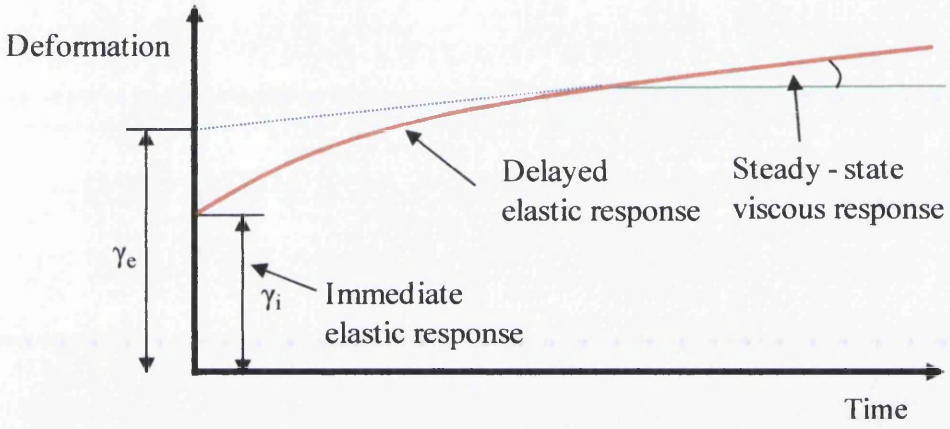

Figure 4-9: A classical creep curve with three distinctive response zones

At the first stage, the viscoelastic material responds directly to the applied stress. In the next phase, the deformation rate does not follow the input factor character and it becomes slower and slower. This second phase is called the delayed elastic phase. In the last phase, the steady – state viscous response, the deformation rate is very slow. It is said the material has achieved its steady flow at this point (Barnes 2000).

4.4.1.3 Oscillatory test

The main objective of the oscillatory test is to probe the microstructure of complex materials by quantifying both viscous and elastic like properties at different time scales. Thereby, stress or strain will be applied to the sample in a sine shaped form which varies harmonically in time (see equation 4.17). The value of the applied stress or strain is chosen in the linear viscoelastic regime where strain or stress is constant

over a constant frequency range in which the microstructural "linkages" are not destroyed due to the low deformation.

$$\sigma=\sigma_0 \cos(\omega t) \text{ and } \gamma=\gamma_0 \cos(\omega t-\delta) \qquad \text{Equation 4-10}$$

Where the stress amplitude is expressed as σ_0, the angular frequency ω (= $2\pi n$ (n = frequency of the oscillation)), the resulting strain amplitude γ_0 and phase angle δ.

If the liquid-like-material is totally viscous then the phase-shift difference between the stress and the strain has a value of 90°. In the case of a solid like material (elastic), the input signal and output signal are in phase with each other. (i.e. $\delta = 0$). Generally, most materials exhibit viscoelastic behaviour, therefore the phase shift displacement usually is between 0° and 90° i.e. between solid and liquid like.

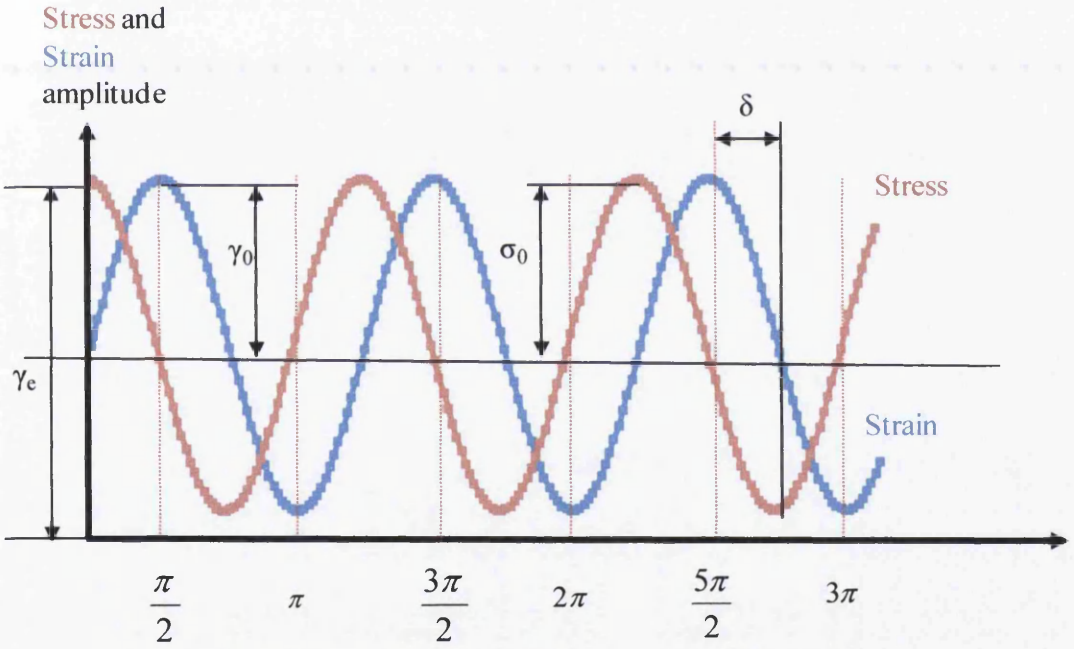

Figure 4-10: Definition of stress and strain amplitudes

The two parameters storage modulus G' and loss modulus G'' help to describe the viscoelastic behaviour of the system. G' represents elastic storage of energy and indicates how well a solid-like material is structured. If a material is predominantly elastic or well structured, then value of the storage modulus is much higher than the loss modulus. The degradation of its structures will cause G' to decrease. Storage modulus is also called elastic or rigidity modulus. A high loss modulus G'' can be

found in a liquid like material and presents the loss of energy or viscous dissipation (Rao 1999). Moduli are expressed in Pascals. Both mathematical relationships for storage modulus *G'* and loss modulus *G''* are defined as:

$$G' = \frac{\sigma_0 \cos\delta}{\gamma_0} \qquad \text{Equation 4-11}$$

$$G'' = \frac{\sigma_0 \sin\delta}{\gamma_0} \qquad \text{Equation 4-12}$$

Where σ_0 is used for the applied stress in wave shape, and γ_0 is the resultant strain

Delta δ describes the phase-shift difference between the input and output and can be expressed mathematically as:

$$\tan\delta = \frac{G''}{G'} = \frac{\frac{\sigma_0 \sin\delta}{\gamma_0}}{\frac{\sigma_0 \cos\delta}{\gamma_0}} \qquad \text{Equation 4-13}$$

The loss tangent, *tan* δ, for liquid like behaviors (G''>> G') approaches infinity whereas the loss tangent of solid like materials (G'' << G') tends towards zero.

The sum of the elastic modulus, *G'*, and loss modulus, *G''*, provides the complex modulus, *G**,

$$G^* = G' + iG'' \qquad \text{Equation 4-14}$$

The dynamic viscosity can be calculated from the equation:

$$\eta' = \frac{G''}{\omega} = \frac{\sigma_0}{\omega\gamma}\sin\delta \qquad \text{Equation 4-15}$$

given that, ω is the frequency in s^{-1} (Barnes 2000 and Mezger 2006)

4.5 Extensional parameters

4.5.1 Extensional strain

The extensional strain, ε, for a body is the ratio of the difference between original length, l_0, and final length, l_1, (corresponding to extended length, Δl), and original length, l_0, i.e.: (Barnes 2000).

$$\Delta l = l_0 - l_1 \qquad \text{Equation 4-16}$$

$$\varepsilon = \frac{\Delta l}{l_0} \qquad \text{Equation 4-17}$$

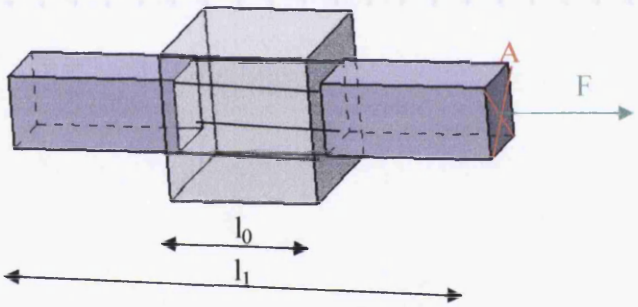

Figure 4-11: An illustration of extensional expansion

4.5.2 Extension rate

Similar to the strain rate, the time will be involved so that elongation strain, ε, will be converted into extension rate $\dot{\varepsilon}$ (Barnes 2000).

Elongation strain → Extension rate

$$\varepsilon = \frac{\Delta l}{L_0} \qquad V = \frac{\Delta l}{dt} \qquad \dot{\varepsilon} = \frac{d\varepsilon}{dt}$$

Equation 4-18 Equation 4-19 Equation 4-20

4.5.3 Extensional viscosity

Extensional flows are more common than shear flows in the practical environment because materials such as polymers are more likely to get stretched or elongated in their manufacturing process, for example blow molding and film extrusion (Barnes 2000 and Cogswell 1994).

An extensional viscosity is defined as the resistance to flow which is generated by elongating or stretching the fluid. Therefore, extensional viscosity can also be called elongational or tensile viscosity (Barnes 2000 and Eley 1995).

To date, the existing test devices are unable to generate an extensional steady state flow. As a consequence, the term transient extensional viscosity as a function of t as well as $\dot{\varepsilon}$, ($\eta_e(t, \dot{\varepsilon})$) describes this situation in the best way (see chapter 6 for more information about extensional viscosity).

The journey of a drop through the extensional and shear flows highlights the difference between them both. Figure 4-12 shows a drop in an extensional flow environment. The drop starts to stretch and deform before it goes into the smaller tube until it has achieved the maximum deformation. At the end of the tube, the drop starts to expand to its original size again, provided that no deformation energy has been lost. In contrast to the drop in an extensional flow environment, the degree of deformation in a shear flow environment is small (Barnes 2000).

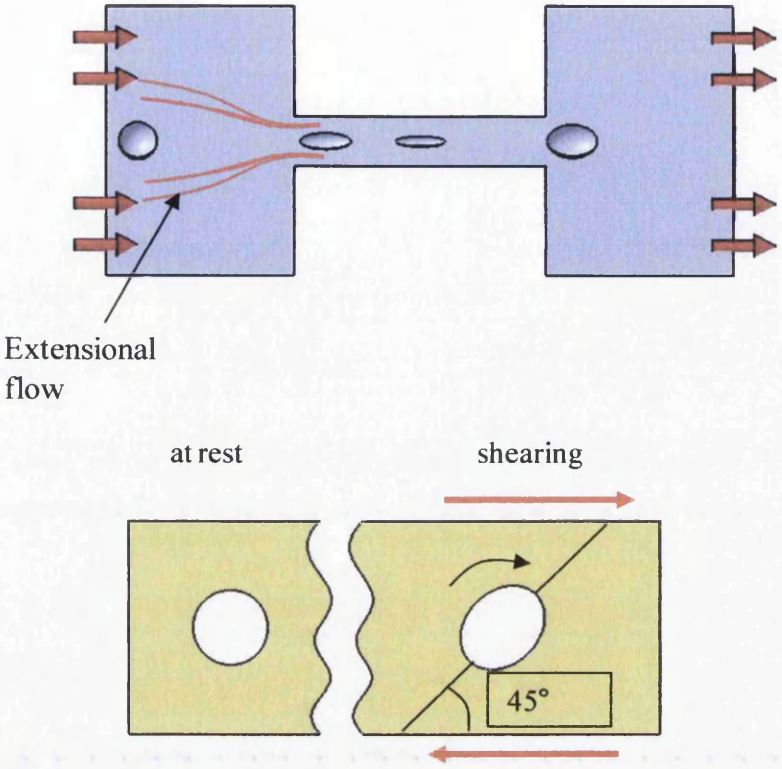

Figure 4-12: Illustration of the differences in behaviour of a drop under extensional and shear influence.

4.5.4 Type of extensional viscosity behaviours

The extensional viscosity can behave in two different manners:

- Tension - thickening
- Tension - thinning

A material with a tension thickening behaviour increases its extensional viscosity when the extensional rate increases, whereas, a material with tension thinning behaviour decreases its viscosity with increasing extension rate (Barnes 2000).

4.5.5 Types of extension flows

Uniaxial, biaxial and planar flows are the basic types of extension flows which are explained below:

- Uniaxial

  In a uniaxial extension, a force is applied in one direction away from the centre leading to a reduction in the sizes in the other two directions.

- Biaxial

  Similar to the uniaxial extension, the applied force compresses the material in one direction causing an increase in the sizes of the other two directions. Radial tensile stress is produced during biaxial extension.

- Planar

  During a planar extension, the width will always be constant while length is stretched and the height decreases as a consequence.

  (Barnes 2000)

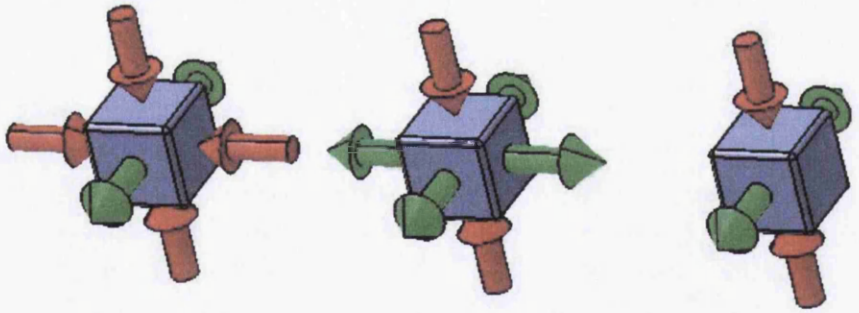

Uniaxial	Biaxial	Planar
e.g. thread pulling	e.g. balloon inflation	e.g. cylinder inflation

Figure 4-13: Visualizing various types of extension flows

At small strains, the following relationships between extensional and shear viscosities for Newtonian fluids have been developed and proposed: (Dealy 1994, Walters 1975 and Petrie, 1979):

$$\eta_{EU}=3\eta \quad \text{Equation 4-21}$$

$$\eta_{EB}=6\,\eta \quad \text{Equation 4-22}$$

$$\eta_{EP}=4\eta \quad \text{Equation 4-23}$$

Trout (1906) discovered a proportional relationship between extensional viscosity and shear viscosity for Newtonian fluids $\eta_{EU} = 3\eta$. Some recent investigations show that the Trouton ratio can even achieve a value of 12 for a low solids concentration suspension (Della Valle et al. 2000) and even higher Trouton ratio ranging from 30 to 60 has been detected for kaolin suspensions (O'Brien and MacKay 2002). From this point of view, the trout's number of 3 is not valid for all material. However, if the trouton ration is known for a specific material then only a shear viscosity is needed to mathematically determine the extensional viscosity.

4.6 Rheometer

A rheometer is a device which can measure viscosity and viscoelastic properties over a wide range of shear rate and shear stress. In contrast, a viscometer is an instrument which can only collect data of viscosity over a limited shear rate range. Rotational instruments can be classified into controlled stress and controlled strain rheometers (see section 5.3 for information about extensional rheometers). It is very important to choose the correct geometries for experiments which are carried out with a rotational rheometer. There are many geometries available such as cone and plate, parallel plate and concentric cylinder (also known as cup and bob, or couette). The double concentric cylinder is ideal for fluids with a very low viscosity. Cup and bob is normally used when the sample has a low viscosity whereas parallel plate or cone plate find applications for samples with higher viscosity. Only parallel plate and cone plate are able to measure the normal stress caused by the normal force acting on the plates. (TA Instrument 2003).

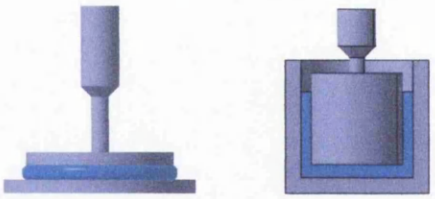

Parallel Plate

Double Concentric

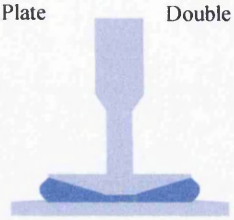

Cone Plate

Figure 4-14: Comparison of the differences between Parallel plate, Double concentric and Cone plate

A brief summary of the advantages, disadvantages and suitable materials for each geometry is listed in the Table 4-1.

Geometries	Suitable materials	Advantages	Disadvantages	Comments
Cone and plate	single-phase homogeneous samples or samples submicron particles	suitable for measuring normal stress, ideal for viscoelastic measurement, stress is uniform across the cone	only for low shear rate	bigger particles move in the truncated area (gap between plate and cone) and cause a jam.
Parallel plate	samples with bigger particles	no truncated gap for particles to become jammed	stress is not uniform across the entire	set up the gap 10 x the largest particle size
concentric cylinder (or cup and bob or couette)	Using for samples with lower viscosity	measuring for low viscosity, can apply high shear rate	can not be used for measuring normal stress	ideal for measuring low viscosity

Table 4-1: Advantages and Disadvantages of the geometries (TA Instrument 2003)

For this research project, a cone and plate geometry has been used and therefore an explanation of the mathematical relationships for this geometry only will be given.

$$\dot{\gamma}=F_{\dot{\gamma}}\omega \qquad \text{Equation 4-24}$$

$$F_{\dot{\gamma}}=\frac{1}{\tan\alpha} \qquad \text{Equation 4-25}$$

$$\sigma=F_{\sigma}M \qquad \text{Equation 4-26}$$

$$F_{\sigma}=\frac{3}{2\pi R^3} \qquad \text{Equation 4-27}$$

The angle of the cone is expressed as α and M is the torque. ω represents the angle velocity.

4.6.1 Slip

One of the main disadvantages of cone and plate geometries with a smooth surface is that slip effects may give erroneous results. A roughened or serrated surface on the geometry prevents any slip during the experiment. Another approach to detect any possible slip effect is by comparing flow curve data using different size geometries. An agreement of the data indicates a slip free condition. The attachment of sandpaper on parallel plate is another possible way to reduce slip (Sofou et al. 2008). Under slip conditions, the measured viscosity tends to be smaller than the viscosity measured with the same geometry without slip effect. (Barnes 2000, Rides 2005). The occurrence of slip the effect is common with complex fluid such as mayonnaise (Ma and Barbosa Canovas 1995) or vaseline (Chang et al. 2003).

There are two circumstances leading to slip in polymer flow.

4.6.1.1 Particle depletion

Depletion describes the reduced local concentration of particles by migration in a filled material close to a moving surface. As a consequence of such particle migration, a lubrication layer may be created which leads to the well known slip effect. Regarding the paint, a solvent and resin – a rich (fluid rich) layer acting as a lubricator is created on an adjacent wall, leaving the bulk of particles less sheared.

4.6.1.2 Loss of adhesion

A slip effect may arise by polymers losing adhesion to the wall.

4.7 Bibliography

Armelina, E., Martia, M., Rudeb, E., Labandab, J., Llorensb, J., & Alemana, C. (2006). A simple model to describe the thixotropic behavior of paints. *Progress in Organic Coatings , 57* (3), 229-235.

Ascanio, G., Carreau, P. J., & Tanguy, P. A. (2006). High-speed roll coating with complex rheology fluids,. *Experiments in Fluids , 40*, 1-14.

Ascanio, G., Carreau, P. J., Fuente, E. B., & Tanguy, P. A. (2002). Orifice Flowmeter for measuring extensional rheological properties. *The Canadian Journal of Chemical Engineering , 80*, 1189-1196.

Bagley, E. B. (1957). End correction in capillary flow of polyethylene. *Journal of Physics , 28* (5), 624-627.

Balfour, J., & Huchette, D. (1995). Paint and Ink International 8.

Barnes, H. A. (2000). *A Handbook of Elementary Rheology, Aberystwyth.* Instittution of Non-Newtonian Fluid Mechanics University of Wales.

Barnes, H. A. (1997). Thixotropy – a review. *Journal of Non Newtonian Fluid Mechanics , 70*, 1-33.

Barnes, H. A., & Bell, D. (2003). Controlled-stress rotational rheometry: A historical review. *Korea-Australia Rheology Journal , 15* (4), 187-196.

Barnes, H. A., Hulton, J. F., & Walters, K. (1994). *An Introduction to Rheology.* Amsterdam:: Elsevier Science B.V.

Barroso, E. G., Duarte, F. M., Couto, M., & Maia, J. M. (2007). A rheological study of the ageing of emulsion and micro suspension-based PVC plastisols. *Journal of Applied Polymer Sciene , 109* (1), 664-673.

Bower, D. I. (2002). *An introduction to polymer physics.* Cambridge: Cambridge University Press.

Breuker, M. (1993). Rheological problems in the paint industry. *Applied Rheology, 48* .

Brock, Groteklaes, & Mischke. (2000). *European Coating Handbook.* Hannover: Vincentz Verlag.

Buxbaum, G., & Pfaff, G. (2005). *Industrial Inorganic Pigments* (3rd Edition ed.). Weinheim: Wiley VCH-Verlag.

Chang, G. S., Koo, J. S., & Song, K. W. (2003). Wall slip of vaseline in steady shear rheometry. *Korea-Australia Rheology Journal , 15*, 55-61.

Cheremisinoff, N. P. (1998). *Advanced Polymer Processing Operations.* New Jersey: Noyes.

Chhabra, R. P., & Richardson, J. F. (2008). *Non-Newtonian flow and applied rheology.* Oxford: Butterworth-Heinemann.

Christie, R. M. (1993). *Pigments structures and synthetic procedures,* (5th Edition ed.). Basingstoke: Oil & Colour Chemists' Association.

Christopher, H. (1989). *Polymer Materials* (2nd Edition ed.). Basingstoke: Macmillan Education Ltd.

Cogswell, F. N. (1994). *Polymer Melt Rheology.* Cambridge: Woodhead Publishing Limited.

Cross, M. M. (1965). Rheology of non-Newtonian fluids: A new flow equation fo pseudoplastic systems. *Journal of Colloid Science , 20*, 417 – 437.

Dealy, J. M. (1994). Official nomenclature for material functions describing the response to a viscoelastic fluid to various shearing and extensional deformations. *Journal of Rheology , 38*, 179-191.

Della, V. D., Tanguy, P. A., & Carreau, P. J. (2000). Characterization of the extensional properties of complex fluids using an orifice flowmeter. *Journal of Non Newtonian Fluid Mechanics , 94*, 350.

Eley, R. R., & Koleske, J. V. (1995). *Paint and Coating testing manual: Chapter 33 – Rheology and Viscometry* (14th Edition ed.). Philadelphia: Gardner-Sward Handbook.

Evans, D. F., & Wennerström, H. (1999). *The Colloidal Domain* (2nd Edition ed.). New York: Wiley-VCH.

Everett, D. H. (1998). *Basic Principles of Colloid Science.* Letchworth: The Royal Society of Chemistry.

Fischer, U. (1990). *Fachkunde Metall* (15th Edition ed.). Düsseldorf: Europa-Lehrmittel.

Geller, D. P., & Goodrum, J. W. (2000). Rheology of Vegetable Oil Analogs and Triglycerides. *JAOCS , 77*, 111-114.

Goodwin, J. W., & Huges, R. W. (2008). *Rheology for chemists: an introduction.* Cambridge: Royal Society of Chemistry.

Gutoff, E. B., & Cohen, E. D. (2006). *Coating and drying defects* (2nd Edition ed.). New Jersey: John Wiley and Sons.

Hatzikiriakos, S. G. (1994). The onset of wall slip and shaskin melt fracture in capillary flow. *Polymer Engineering Science , 34* (19), 1441-1449.

Hatzikiriakos, S. G., & Deal, J. M. (1992). Wall slip of molten highdensity polyethylenes II. Capillary rheometer studies. *Journal of Rheology , 36*, 703-707.

Honigmann, B., & Stabenow, J. (1965). VIth FATIPEC Congress., (p. 89).

Hunter, R. J. (1987). *Foundation of Colloid Science* (Vol. I). Oxford: Clarendon Press.

Kaluza, U. (1980). *Flocculation which factors influence it? Part 1, Pigment and Resin Technology.*

Kesktkar, M., Heuzey, M. C., & Carreau, P. J. (2010). Rheology of LDPE-Based Semiflexible Fiber Susoensions. *Polymer Composites , 31*, 1474-1468.

Kheirandish, S., Gubaydullin, I., Wohlleben, W., & Willenbacher, N. (2008). Shear and elongational flow behavior of acrylic thickener solutions, Part I: Effect of intermolecular aggregation. *Rheologica Acta , 47*, 999–1013.

Koleske, J. V. (1995). *Paint and coating testing manual* (4th Edition ed.). Ann Arbor: Garden-Sward.

Labanda, J., & Llorens, J. (2006). A structural model of thixotropy of colloidal dispersion. *Rheologica Acta , 45*, 305-314.

Larson, R. G. (1999). *The structure and rheology of complex fluids.* Oxford: Oxford University Press.

Laun, H. M. (2004). Capillary rheometer for polymer melts revisited. *Rheologica Acta , 43*, 509-528.

Laun, H. M., & Schluch, H. (1899). Transient elongational viscosity and drawability of polymer melts. *Journal of Rheology , 33*, 119-176.

Liang, J.-Z. (2007). Die swell behaviour during the short tube flow of rubber compounds. *Journal of Applied Polymer Science , 104*, 70-74.

Liphard, M., Rybinski, W., & Schieferstein, L. (1991). *Farbe and Lack.* Hannove: Vinzenyz Network.

Long, T. L., & Schiers, J. (2003). *Modern Polyesters:Chemistry and Technology of Polyesters and Copolyesters.* Chichester: John Wiley & Sons, Wiley Series In Polymer Science.

López, F. V., & Rosen, M. (2002). Rheological effects in roll coating paints. *Latin American applied Research , 32*, 247-252.

Ltd, T. I. (2003). *AR 2000 Rheometer Operator's Manual.*

Ma, L., & Barbosa-Canovas, G. V. (1995). Rheological characterization of mayonnaise. Part I : Slippage at different oil and xanthan gum concentrations. *Journal of Food Engineering , 25*, 397.

Malkin, A. A., Malkin, A. Y., & Isayev, A. I. (2006). *Rheology:Concept, Methods and Application.* Toronto: Chem Tech Publishing.

McKay, R. B. (1994). *Technological applications of dispersions.* New York: Marcel Dekker.

McKeen, L. W. (2006). *Fluorinated coatings and finishes handbook.* Norwich: William Andrew.

Meier-Westhues, U. (2007). *Polyurethanes:coatings, adhesives and sealants,.* Hannover: Vincents Network.

Metzger, T. C. (2006). *The Rheology Handbook: For users of rotational and oscillatory rheometers* (2nd revised Edition ed.). Hannover: Vincentz.

Mirsaeedghazi, H., Emam-Djojem, Z., & Mousavi, S. M. (2008). Rheometric Measurment of Dough Rheological Characteristics and Factors Affeting It. *International Journal of Agriculture and Biology , 10*, 112-119.

Møller, P. C., Mewis, J., & Bonn, D. (2006). *Yield stress and thixotropy: on the difficulty of measuring yield stresses in practice* (Vol. II).

Moreno, B., Franco, J. M., Valencia, C., & Gallegos, C. (2010). Rheology of lubricating greases modified with reactive NCO-terminated polymeric additives. *Journal of Applied Polymer Science , 118*, 693-704.

Müller, B. (2009). *Additive kompakt, Farb und Lack* (3rd Edition, ed.). Hannover: Vincentz Network.

Müller, B., & Poth, U. (2006). *Coatings formulation: an international textbook.* Honnover: Vincentz.

Nelson, R. D. (1988). *Dispersing Powders in Liquids.* Amsterdam: Elseveir.

Nicholson, J. W. (1984). *The chemistry of polymers.* Cambridge: The Royal Society of Chemistry.

Nigen, S., & Walters, K. (2002). Viscoelastic contraction flows: comparison of axisymmetric and planar configurations. *Journal of Non-Newtonian Fluid Mechanics , 102*, 343-359.

O'Brien, V. T., & MacKay, M. E. (2002). Shear and elongation flow properties of kaolin suspensions. *Journal of Rheology , 46*, 557.

Oldering, P. T., Deligny, P., & Tu. (2000). *Resin for Surface Coating: Alkyds & polyesters,* (2nd Edition ed., Vol. II). London: John Wiley and Sons.

Osterhold, M. (2000). Rheological methods for charterising modern paint systems. *Process in Organic Coating , 40*, 131-137.

Petrie, C. J. (1979). *Extensional Flows.* London: Pittman.

Rao, M. A. (2007). *Rheology of Fluid and Semisolid Foods.* New York: Springer Science Business Meda.

Rosato, D. V., & Rosato, M. V. (2004). *Plastic Product Material & Process Selection Handbook.* Oxford: Elsevier Advanced Technology.

Sang, T. V., Bhaskar, V. V., & Ronald, R. A. (2001). Comparison of methods to assess pigment dispersion. *Journal of Coating Technology , 73*, 923.

Schramm, G. (1994). *A Practical Approach to Rheology and Rheometry.* Karlsruhe: Gebrueder HAAKE Gmbh.

Shaw, M. T. (1896). An alternative analysis of capillary rheometer Data. *SPE Technical Papers , 32*, 707-710.

Shay, G. D., & Kolesky, J. V. (1995). *Paint and coating testing manual: Chapter 30 - Thickeners and Rheology Modifiers* (14th Editon ed.). Philadelphia: Gardner-Sward Handbook.

Snabre, P., & Mills, P. (1999). Rheology of concentrated suspension of viscoelastic particles. *Colloids and surfaces , 152*, 79-88.

Sofou, S., Muliawan, E. B., Hatzikiriakos, S. G., & Mitsoulis, E. (2008). Rheological characterization and constitutive modelling of bread dough. *Rheologica Acta , 47*, 369-381.

Speer, J., Kromm, J., & Maisel, J. (1994). *Chemistry* (5th Edition ed.). McGraw-Hill.

Stevens, M. P. (1990). *Polymer Chemistry An Introduction* (2nd Edition ed.). Oxford: University Press.

Stoye D., D., & Freitag, W. (2001). *Paints, Coating and Solvents* (2nd Edition ed.). Germany: Wiley-VCH Verlag.

Streitberger, H. J., & Dössel, K. F. (2008). *Automotive Paints and Coatings* (2nd Edition ed.). Weinheim: Wiley-VCH.

Talbert, R. (2007). *Paint technology handbook.* CRC Press.

Trouton, F. T. (1906). On the coefficient of viscous traction and its relationto that of viscosity. *77*, p. 426. Proceedings of Royal Society London A.

Turner, G. P. (1997). *Paint Chemistry, and Principle of Paint Technology* (3rd Edition ed.). London: Chapman and Hall.

Walter, K. (1992). Recent Development in Rheometry. *Proceedings XIth International, Conferernce on Rheology*, (pp. 16-23).

Walters, K. (1975). *Rheometry.* London: Chapman and Hall.

Weiss, K. D. (1997). Paint and Coatings: A Mature Industry In Transition. *Progress in Polymer Science , 22*, 203-245.

Weldon, D. G. (2009). *Failure Analysis of Paints and Coatings* (1st Edition ed.). Chister: John Willey and Sons.

Whorlow, R. W. (1992). *Rheological Techniques.* Ellis Horwood.

Wicks, Z. W., Jones, F. N., Pappas, S. P., & Wicks, D. A. (2007). *Organic Coatings* (3rd Edition ed.). John Wiley & Sons.

Willenbacher, N., Hanciogullari, H., & Wagner, H. G. (1997). High shear rheology of paper coating colors-more than just viscosity. *Chemical Enginneering and Technolgy , 20*, 557-563.

Young, R. J., & Lovell, P. A. (1997). *Introduction to polymer* (2nd Edition ed.). Chapman & Hall London.

5 Introduction to capillary rheometry

Within less than one second, paint stored in a feeding pan will be transported from the pickup roll via a feed roll, over an applicator roll to the substrate (see Figure 2-2 and Figure 2-3). During this very short industrial process, extensional flow combined with shear flow can be encountered in the coil coating process. Additionally, a thin liquid filament or thread is generated between the rolls which will be elongated and finally breaks (see Figure 5-1). A capillary Break-up Rheometer seems to be one of the commercial test devices that can closely simulate the complex free surface flow which is generated during the coil coating process.

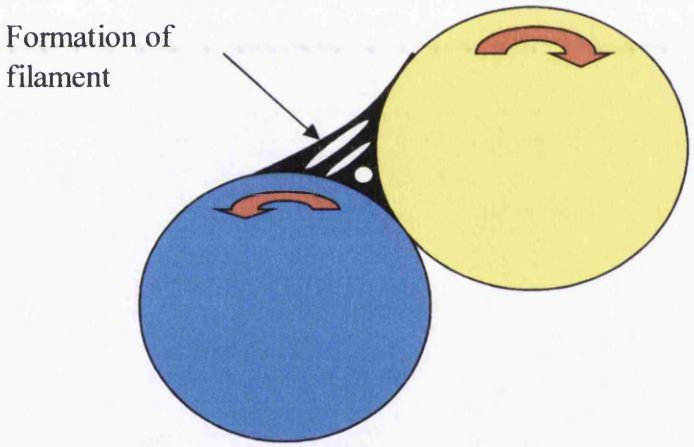

Figure 5-1: Illustrates schematic the formation of filament between two rolls

5.1 Historical development of extensional rheometers

A number of stretching devices were developed to obtain estimated extensional viscosities of fluids in the late 1980s and early 1990s. One of the devices is the falling cylinder device introduced by Matta and Tytus (1990) which generates an almost pure extensional flow. A small amount of fluid sample is inserted between two plates. Subsequently, the bottom plate moves downwards in free fall with a nearly constant force or acceleration due to gravity. The filament break up process is

captured by a high speed camera to allow the determination of the liquid deformation rate and filament stress from which the extensional viscosity can be deduced.

A similar concept to the falling device is the Capillary Break-up Rheometer which was first described by Bazilevsky (Bazilevsky et al. 1990a) (fully described in chapter 5.3.3). Capillary breakup rheometry has previously been employed for the characterisation of polymer solutions, wormlike micelle solutions and immiscible polymer blends (Miller et al. 2009 and Bhardwaj et al 2007).

A similar technique to the capillary break up rheometer is the filament stretching extensional rheometer also known as FiSER. In this case, one of the end plates moves at exponential velocity upwards or downwards and the measured parameters are the force on the plate and the midfilament diameter. Sridhar and co-workers were the first to introduce the first filament stretching device which allows an exponential separation of the plates (Sridhar et al. 1991b, Tirtaatmadja and Sridhar 1993). Similar styles of devices have been subsequently designed (Berg et al. 1994, Spiegelberg et al. 1996 and Jain et al. 1997).

Furthermore, devices have been constructed to create contraction and converging flow, stagnation- point flow (created by opposed Jet devices or four roll mills) and spinning flow to extract the apparent extensional viscosity (see methods in chapter 5.3). The drawbacks of these methods are the unknown deformation history which is mixed with the extensional flow and the fact that they do not allow the measurement of the extensional stress until the achievement of the steady state (Gupta and Sridhar 1988; 89: James and Walters 1994).

Currently, commercially available extensional rheometers such as Rheotens (Fiber spinning) from Göttfert, CaBER (Capillary breakup) from ThermoFisher, Sentmanat extensional rheometer (Constant length) from Xpansion Instruments and FiSER (Filament stretching) from Cambridge Polymer Group are on the market and are mainly employed to obtain extensional rheological parameters (see chapter 5.3).

5.2 Experimental challenges in measuring the extensional viscosity

Considerable progress in measuring the extensional viscosity of complex fluids such as polymer solution with low viscosity, elastic fluids ($\eta_s < 1$ Pas), inks, emulsions and polymer melts have been made by improving instruments or optimising procedures over the last two decades (Bazilevsky et al. 1990a , Willenbacher et al 1999, Rodd et al. 2004, Sentmanat 2005 and Niedzwiedz et al 2009). To theoretically determine extensional viscosity from the measured data at the end, good approximations are needed by using for example correction factors (described in chapter 5.8.7) or correcting the raw data (e.g Bagley correction see chapter 6.6.1). However, there are still challenges to create extensional flow which might never be overcome. One of the challenges is to generate a pure extensional flow during the experiment. Currently, all extensional rheological devices generate a flow which has both extensional and shear components because of the nature of solid-fluid interface. (McKinley 2001). Another challenge is the measurement of samples with low viscosity which may cause problems, for example due to the inertial effects leading to oscillation of the liquid bridge during filament thinning or the bead on string effect (Rodd et al 2004). Last but not the least, the insufficient test time or residence time may only allow the sample to achieve an unsteady state during the uniaxial extensional flow. However, it is common to have a transient flow in the industrial process. Therefore, the steady extensional viscosity, η_E, may not need to be considered to understand or improve the process where the rheological data from the transient flow is sufficient (Bird 1982, Laun and Schuch 1988). Previously, the assumption was made that steady state was achieved at the Hencky strain of 5 to 6. Further studies provided evidence that steady state was not achieved when applying a Hencky strain of 7 (Meissner et al. 1981, Meissner 1985). Especially, a large number of melting polymers may cause problems in obtaining steady extensional viscosities (Bird et al. 1987 (a)).

5.3 Types of extensional rheometer

Extensional rheometers can be classified into constant length or constant volume devices, filament stretching devices and capillary devices and even by range of viscosity. Materials with viscosities higher than 1000 Pas can be measured with length device. A filament stretching extensional rheometer is ideal for measuring materials with viscosities in the range between 1 and 1000 Pas. Capillary rheometry can be used for obtaining low extensional viscosity within the range of 0.01 – 1 Pas. (Tropea at al. 2007). Some examples of extensional rheometers are schematically depicted below and explained in the following subchapter.

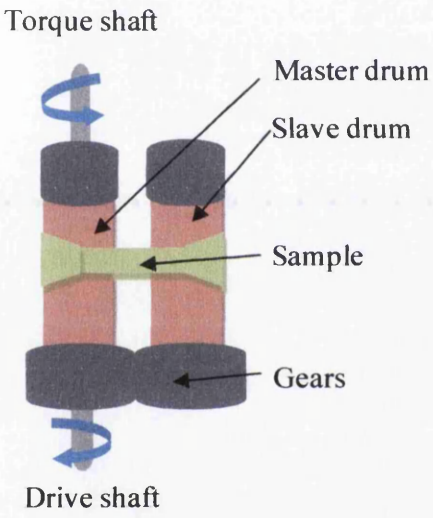

a) Filament stretching
Constant length

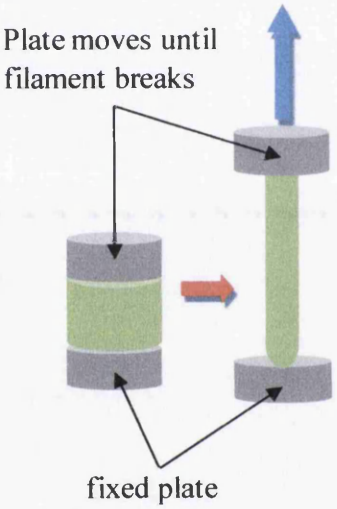

b) Filament stretching
Constant volume

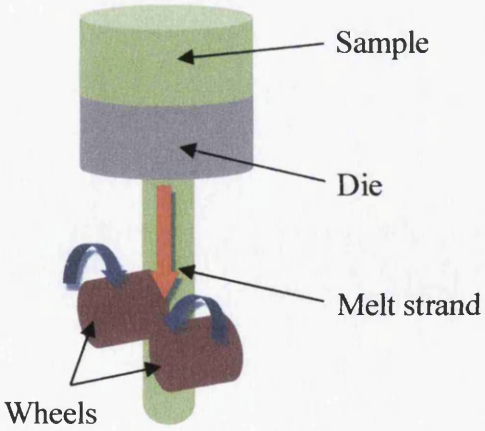

c) Fibre spinning

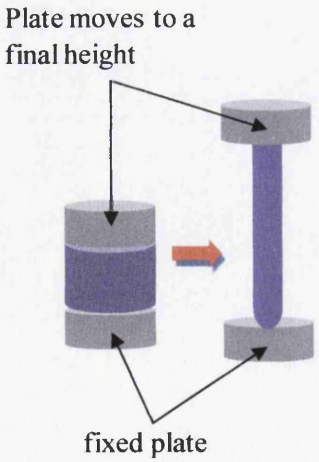

d) Capillary break up

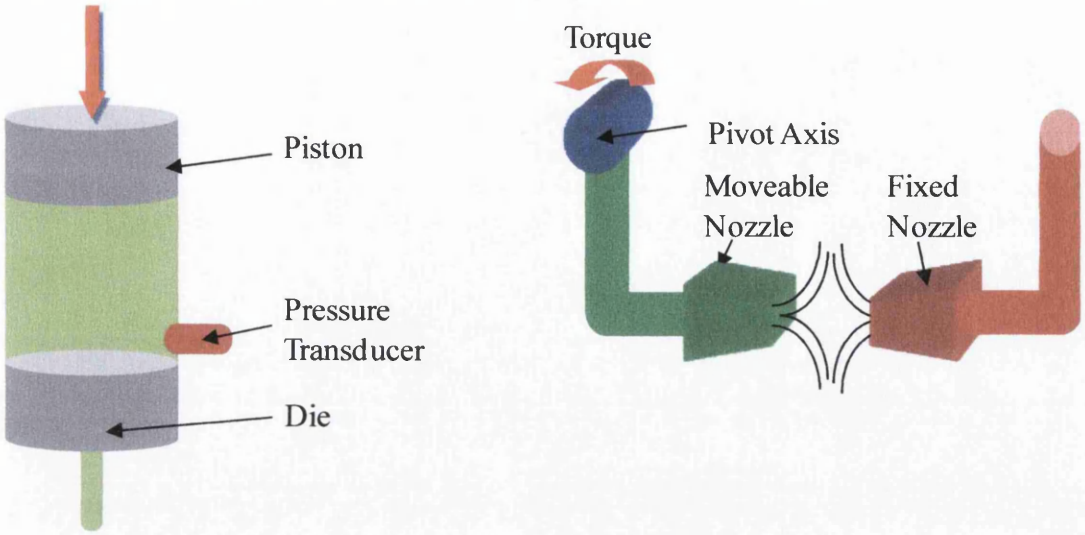

e) Entrance Flow f) Opposed jet

Figure 5-2: Schematic diagrams of various extensional methods

Device	Type of Flow	Shear viscosity range	Limitations
Filament stretching, constant volume, medium viscosity	uniaxial extension, constant strain rate	1 -1000	Sample gripping, limited to medium to high viscosity elastic instability
Filament stretching, constant length, high viscosity	uniaxial extension, constant strain rate	>1000	limited to low strain rates, temperature control
Fibre spinning	uniaxial extension	>1	Low strain, non uniform strain rates, pre-shear history
Capillary breakup rheometry	uniaxial extension	0.01-10	Inertia and surface tension dominate at low end of viscosity, variable strain rate
Entrance flows	uniaxial extension	>1	Variable strain rate, mixed with shear
Opposed jet	Uniaxial extension	0.01-1	Variable strain rates and strain histories, some shear
Tubeless siphon	Uniaxial extension	1-1000	Pre-shear history, variable strain rate, low achievable strain rates

Table 5-1: List of devices, application ranges and limitations (adapted from Tropea et al. (2007))

5.3.1 Filament stretching

The filament stretching devices can be divided into constant length and constant volume (see Figure 5-2 a and b). The constant length principle is exhibited by the Sentmanat Extensional Rheometer (SER) and is ideal for samples with viscosity higher than 1000 Pas. The device uses two drums namely the master and slave drum on which a sample film is clamped. By applying a rotational rate on the master drum, both drums connected through an intermeshing gear start to move and commence to stretch the sample. The stress which is derived from the cross sectional area of the sample, the applied torque measured on the master drum and extensional deformation will be used to calculate the extensional viscosity (Sentmanat 2004).
While the Sentmanat Extensional Rheometer has two drums at a fix position, the Filament Stretching Extensional Rheometer (FiSER) exponentially moves the plates apart and measures the force on one of the plates and the diameter of the filament. This device belongs to the group called filament stretching with a constant volume. It can measure viscosity between 1 and 1000 Pas. The previous version of the FiSER devised by Matta and Tytus (1990) used a constant force to separate two plates. For fluid with a viscosity of less than 1 Pas, the resolution of the force transducer measuring the tensile force from a sample might find its limitation. A desirable shear free homogeneous transient extensional flow can almost be obtained by the filament stretching extensional rheometer developed in recent years. (Sridhar et al. 1991, Tirtaatmadja and Sridhar 1993, Anna and McKinley 2001, McKinley and Sridhar 2002)

Trevor et al. (2006) compared the data obtained by Filament Stretching Extensional Rheometer (FiSER) with the data measured by wind up extensional rheometer (SER) noting a very good agreement in the strain range from 0.7 and 1.9.

5.3.2 Fibre spinning

This type of flow (depicted in Figure 5-2 c) can be generated for example by the Rheotens instrument manufactured by the company Göttfert, which is ideal for samples with viscosity higher than 100 Pas. The melted polymer is confined in a

container and is extruded downwards through an extruder die. As a result, a vertical melt strand is generated which is drawn at a constant extension rate by two counter rotating wheels on which a force transducer is mounted. Finally, the resulting tensile stress within the strand will be plotted as a function of time or velocity of the rollers (Muke et al. 2001 and Göttfert 2002).

5.3.3 Capillary break up

For a very dilute or semi dilute fluid with a shear viscosity between 0.01 and 10 Pa.s. , rheological data can be measured by Capillary break up Rheometer (CaBER). The sample is positioned between two plates; at least one of them moves apart from the other to a fixed position, forcing a capillary flow within the fluid (illustrated in Figure 5-2.d). More details about the concept can be read in section 5.4. The manufacturer Thermo Fisher offers Capillary break up instruments for commercial and scientific research. It is a compact and robust device, suitable for daily use on the shop floor or in the laboratory. The simple design of the device provides the possibilities for easy modification. Another positive factor attributed to the CaBER instrument is that the operation is very simple and the result can be obtained in a very short time without lengthy data processing. In additional, loss of volatile solvent, occurrence of phase separation or chemical change will not take place at very short experimental time. The determination of extensional rheology can be obtained for fluids with lower concentration and low viscosity. (Anna and McKinley 2001, Clasen et al. 2006, Rodd el al. 2005 and Yesilata et al. 2006).

5.3.4 Entrance flow

The DrRheologyP9000 instrument creates an entrance flow (demonstrated in Figure 5-2 e) by extruding the sample through a die whereby the pressure drop is measured with a pressure transducer. With well-defined approximate formula, the extensional viscosity can be determined from the parameter piston speed and the pressure drop. A more detailed explanation can be found in the whole of chapter 6.

5.3.5 Opposed jet

The commercially available device which measured extensional viscosity for fluids with viscosity from 0.01 Pas to 1 Pas in an opposed jet flow (see Figure 5-2.f) was the RFX instrument built by Rheometric Scientific. The tested sample is drawn or pushed through nozzles at a fixed volumetric flow rate. The torque rebalance transducer on the moveable nozzle measures the resulting torque from which ultimately the extensional viscosity can be calculated (Hermansky and Boger 1995 and Eastman et al. 2000).

5.4 Differences between Newtonian and non – Newtonian fluid during filament thinning

The thinning process of Newtonian fluids is qualitatively different compared to that takes place in a viscoelastic fluid, which will be mentioned and explained in the following subchapter. A more detailed theory about the prediction of transient midfilament for both Newtonian and viscoelastic filaments as well as a comparison between theory and experiment was published by several authors such as Entov (1999), Entov and Hinch (1997), Eggers (1997), Kolte and Szabo (1999) Tripathi and McKinley (2000) and Anna and McKinley (2001).

5.4.1 Newtonian fluid

The simplest filament thinning process occurs for a Newtonian fluid. After stretching a sample with Newtonian fluid behaviour, viscocapillary drainage occurs between the top fluid reservoir and bottom reservoir until filament breakup. (McKinley and Tripathi 2000). A distinctive feature of a Newtonian fluid during filament thinning is that the midfilament linearly decays with a constant capillary velocity, $v_{cap} \sim \sigma/\eta_s$, when the inertia effect does not influence the process. Consequently, the apparent viscosity is constant during evolution of the filament decay. The filament has an inhomogeneous axial profile which is typical for a Newtonian fluid. Its profile is

shaped concavely which means that the diameter of the filament close to the plate is much greater than at the diameter between the plates (McKinley 2005 and McKinley and Tripathi 2000). Furthermore, the minimum diameter is located just above the midplane due to the gravitational effect (Anna and McKinley 2001). In Figure 5-3, a sequence of images shows the evolution of a Newtonian liquid film over time.

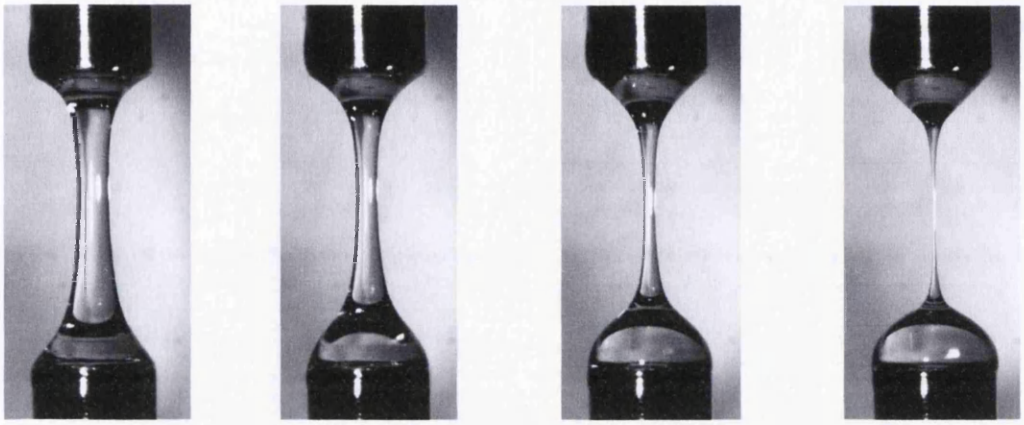

$t_0 = 0ms$ $t_1 = 140ms$ $t_2 = 280ms$ $t_3 = 420ms$

Figure 5-3: Illustrates a sequence of images captured by high speed camera showing some stages of the filament decay of a Newtonian silicon oil (Vadodaria 2011)

5.4.2 Viscoelastic fluid

The inhomogeneous axial profile of the filament thinning of a viscoelastic fluid resembles that of the Newtonian profile at the beginning since the Newtonian solvent dominates at small strains (Yao and McKinley 1998). However, this initial profile starts to change into an axially uniform cylindrical filament which is linked to two almost hemispherical fluid reservoirs close to the endplates (Anna and McKinley 2001). Filament thinning with a uniform cylindrical shape was especially observed for weakly viscous elastic fluids, for example dilute and semi dilute polymer solutions (Kheirandish et al. 2008, Oliveira et al. 2006 and Stelter et al. 2000).

Another distinctive feature is the more complex filament thinning process which consists of three regimes instead of one occurring for a Newtonian fluid. The first regime is called the initial viscous stage, followed by second regime named as the elastic or intermediate stage and the third regime described as final viscous stage. In the viscous stage, pure viscous stress in a dilute polymer solution is dominated by the

solvent viscosity when the ratio of early time (opening time) and longest relaxation time is much smaller than 1. However, the elastic stress starts to grow whereas the viscous stress decreases during the filament thinning to a point where both stresses and capillary stress are equal. A smooth crossover to the elastic capillary balance occurs where extensional rate, $\dot{\varepsilon} = \frac{2}{3\lambda_E}$, remains constant until the polymer is fully stretched. The Weissenberg number,$W_i = \dot{\varepsilon}\lambda_E$, is 2/3 accordingly (Entov and Hintch 1997). In this elastic stage, the diameter of the filament exponentially decays and the relaxation time of the polymer can be obtained by a model fit. (Stelter et al. 2000, Dontula et al. 1997 and Liang and Mackley 1994, Entov and Hinch 1997). Note, inertial, viscous and gravitational forces are considered negligible in their analysis.

Clasen et al. (2004) analysed a series of polystyrene solutions with different concentrations and noticed that the influence of elastic effects in a uniaxial flow driven by surface tension is noticeable when elastocapillary number (see equation 5.13) is bigger than 1. The lifetime is increased by additional resistance of elastic stresses within the thread against the surface tension (Rodd et al. 2004). Anna and McKinely (2001) reported a dramatic enhancement of life time when the polymer molecular weight increases. After reaching the extensibility of the individual polymer coils, the extensional strain rate rapidly diverges infinity. During this phase, the elastic stress is not able to grow due to the fully stretched polymer and therefore it cannot resist the increased capillary pressure. As a result, the midpoint diameter rapidly decreases until the filament breaks because the remaining viscous force cannot counteract against the growing capillary force. In this phase, the behaviour of the fluids can be described as very viscous anisotropic Newtonian fluids whose viscosity can be considered as a steady state extensional viscosity η_∞ (Stelter et al. 2000, Bazilevsky et al. 1997 and Entov and Hinch 1997). Samples can break up before the upper plate reaches the final height because the material is not viscous enough for the experimental condition (Rodd et. al. 2004). A classical filament thinning process was captured by a high speed camera and can be seen in Figure 5-4.

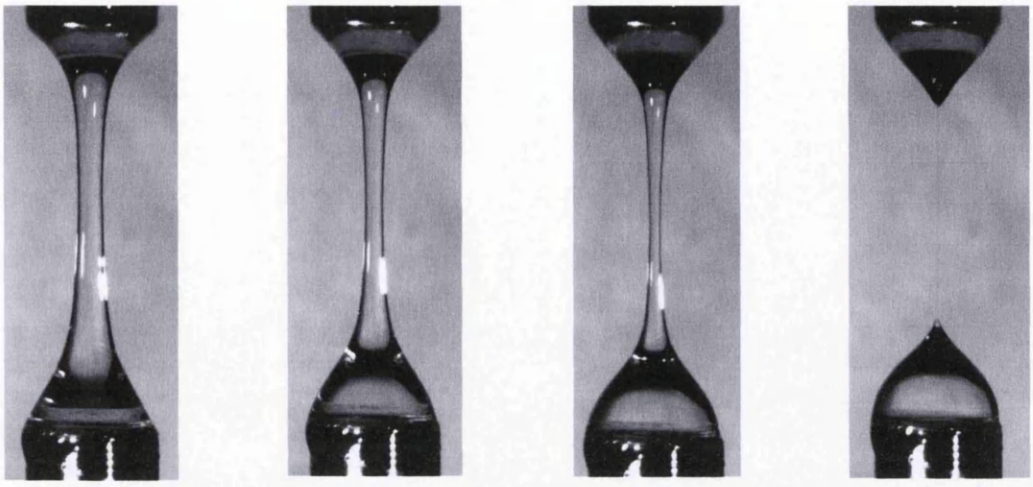

Figure 5-4: Axisymmetric thinning of a viscoelastic solution of polysaccharide in water (Vadodaria 2011)

5.5 Generic model for the force balance

A generic model has been developed to describe the filament thinning in a mathematical way. Szabo (1997) provided a successful force balance, which was used in an international study conducted by Anna et al (2001) using a filament stretching device (see section 5.3.1). The following formula used in the international study for determining the viscoelastic tensile stresses is valid for a filament stretching extensional rheometer. The force transducer for measuring the tensile force is located on the stationary bottom plate (Szabo 1997, Anna et al. 2001).

$$\langle \tau_{zz}-\tau_{rr}\rangle=\left(\frac{F_p}{\pi D_{mid}^2/4}\right)+\frac{1}{2}\frac{\rho g V_0}{\left(\pi D_{mid}^2/4\right)}-\frac{\sigma_s}{D_{mid}/2}+\frac{1}{2}\frac{\rho V_0 \ddot{L}_p}{\left(\pi D_{mid}^2/4\right)} \qquad \text{Equation 5-1}$$

Whereas tensile stress difference is written as $\langle \tau_{zz}-\tau_{rr}\rangle$, the volume of the fluid sample is calculated as $V_0=\pi L_0(\frac{D}{2})^2$ with length, L_0 and diameter, D , σ_s and ρ are accordingly surface tension and density. F_p is the force for stretching the filament and D_{mid} is the midfilament diameter. The acceleration of the plate along the L-direction is expressed as $\ddot{L}_p$. The inertia effect is defined with the last term on the right side of the formula and influences only 1% of the whole process which can be neglected. Furthermore, a uniform shape hints that the inertia effect has a low

influence during the filament thinning (Szabo 1997). Renardy (1995) provided a generic model as stated below. As can be seen the inertia effects have been removed from the Equation 5.1.

$$3\eta_s\left(-\frac{2}{D_{mid}}\frac{dD_{mid}}{dt}\right)=3\eta_s\dot{\epsilon}=\frac{4F_z}{\pi D_{mid}^2}-[\tau_{zz}-\tau_{rr}]-\frac{2\sigma_s}{D_{mid}} \qquad \text{Equation 5-2}$$

Viscous stress = Tensile stress- Elastic / Non-Newtonian Stress – Capillary Pressure

The formulation describing the balance of forces employs the surface tension, σ_s, the tensile force, F_z which is applied on the column end, the Newtonian viscosity of the solvent, η_s, and the total stress normal differences in a non-Newtonian fluid, $[\tau_{zz} - \tau_{rr}]$.

In terms of capillary break-up thinning where the tensile force will not be applied, equation 5-2 can be reduced further by removing the tensile stress.

$$3\eta_s\left(-\frac{2}{D_{mid}}\frac{dD_{mid}}{dt}\right)=3\eta_s\dot{\epsilon}=-[\tau_{zz}-\tau_{rr}]-\frac{2\sigma_s}{D_{mid}} \qquad \text{Equation 5-3}$$

In this case, the tensile stress comes from the polymer while it gets stretched to its finite extensibility. For a classic Newtonian fluid which does not exhibit an elastic effect, the generic model for a self selected force balance will be shortened again to

$$3\eta_s\left(-\frac{2}{D_{mid}}\frac{dD_{mid}}{dt}\right)\sim\frac{2\sigma_s}{D_{mid}} \qquad \text{Equation 5-4}$$

Viscous stress ~ Capillary Pressure

5.6 Mathematical determination of apparent extensional viscosity

The Capillary break-up rheometer measures the midfilament diameter, D_{mid}, from which the extensional viscosity is determined with the known surface tension of the fluid, σ_s, which is mathematically expressed in equation 5.5 (Anna et al. 2001):

$$\eta_{E,\,app}=\frac{2\sigma_s/D_{mid}(t)}{\left(-\frac{2}{D_{mid}(t)}\frac{dD_{mid}(t)}{dt}\right)}=\frac{\sigma_s}{\frac{dD_{mid}(t)}{dt}} \qquad \text{Equation 5-5}$$

For Newtonian fluid, the term, $D_{mid}(t)/dt$ remains constant until breakage because the midfilament diameter linearly decays over time and the surface tension maintances constant.

5.6.1 Calculation of strain rate

The terms in the brackets from equation 5.5 describes the extensional strain rate, $\dot{\varepsilon}$, and is expressed in the following simplified way (Anna et al. 2001):

$$\dot{\epsilon} = -\frac{2}{D_{mid}(t)}\frac{dD_{mid}(t)}{dt} \qquad \text{Equation 5-6}$$

5.7 Description of capillary thinning using dimensionless variables

The use of various appropriate dimensionless ratios of forces/timescales simplifies the description of the behaviour of non-Newtonian and Newtonian fluids in a free surface flow. Furthermore, it provides an unambiguous terminology for describing the physical effect of flow behaviour and also gives a simple way for comparing different samples with different material properties. By combining the classical dimensional numbers, the number of variables will be significantly reduced. McKinley (2005) illustrates an operating window for visco-elastic-inertia-capillary thinning and breakup based on dimensionless numbers as seen in Figure 5-5.

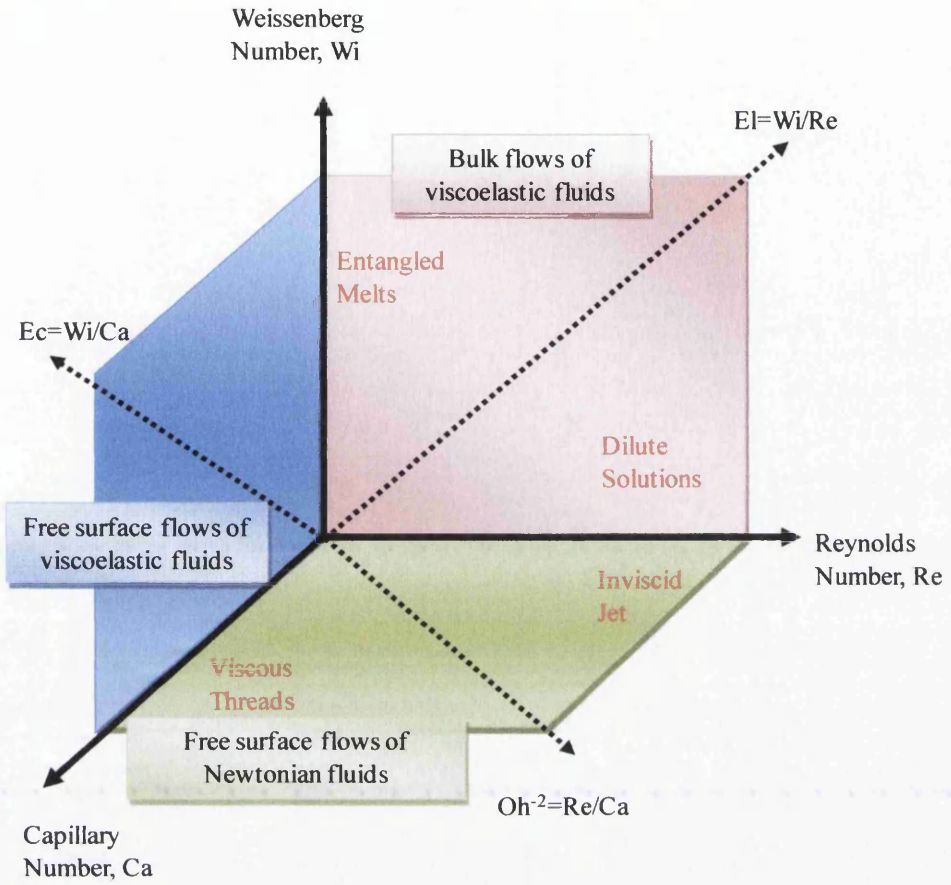

Figure 5-5: Illustrates an operation window for fluids undergoing filament thinning and breakup created by the classical dimensionless numbers; capillary number, Reynolds number and Weissenberg number (adapted from McKinley 2005)

5.7.1 Dependence of dimensionless Numbers on process kinematics

Initially, consider three dimensionless numbers, the Capillary number, Reynolds number and Weissenberg number which vary with different process speeds and depend on the type of material. Two of the three numbers are always involved in one of the flows mentioned in Figure 5-5. The capillary number, *Ca*, describes the relationship between viscous force and surface tension which acts across an interface (e.g. liquid/gas or immiscible liquid A / immiscible liquid B). By using the characteristic velocity, V_c, and capillary velocity, υ = *zero shear viscosity,* (η_0) / *surface tension* (σ_s), capillary number can be expressed as following:

$$Ca = \frac{V_c}{\upsilon} = \frac{\eta_0 V_c}{\sigma_s} = \frac{\text{viscous force}}{\text{surface tension}} \qquad \text{Equation 5-7}$$

Filament thinning is driven by surface tension and the viscous force acts to balance capillary force to stabilise the shape. The degree of the stability of a fluid filament during stretching is given by the magnitude of the capillary number. A capillary number less than 1 indicates that the viscous stress cannot withstand the effects of the surface tension. As a result, the filament thread is unstable and is prone to the formation of a liquid drops (McKinley 2005). As can be seen in Figure 5-5, the dimensionless number capillary number allows description of the free surface flows of viscoelstic fluids and Newtonian fluids.

The magnitude of Reynolds number provides information regarding whether the flow is dominated by inertial or viscous stress. It can mathematically be formulated as:

$$\mathrm{Re}=\frac{\rho V_c l}{\eta}=\frac{\text{density}\times\text{characteristic velocity}\times\text{length}}{\text{viscosity}} \qquad \text{Equation 5-8}$$

In the case of filament thinning, the diameter of the filament is used as the characteristic length, l,. Furthermore the magnitudes of the characteristic velocity, V_c, the density, ρ, and viscosity, η, influence the Reynolds number . The higher the viscosity of the fluid the smaller the Reynolds number will be under the same condition. Bulk flows of viscoelastic fluids and free surface flows of Netwonian fluids can be characterised by the Reynolds number.

A further dimensionless number considered in this group is the Weissenberg number which describes the ratio of the longest relaxation time, λ, the characteristic velocisty, V_c, and length scale, l,

$$\mathrm{Wi}=\frac{\lambda V_c}{l}=\dot{\gamma}\lambda \qquad \text{Equation 5-9}$$

The ratio of elastic stress and viscous stress plays an important role in describing free surface flows of viscoelastic fluids and bulk flows of viscoelastic fluids (McKinley 2005).

5.7.2 Independence of dimensionless Numbers on process kinematics

A number of characteristic ratios / dimensionless groups that are not a function of the characteristic velocity for the process, includes the Ohnesorge number, Deborah number, Elasticity number, Elastocapillary number and Bond number.

The first dimensionless number mentioned here is the Ohnesorge number and is defined as the ratio of viscous time scale, t_v (see equation 5.21), and Rayleigh time scale, t_r (see equation 5.23):

$$Oh \equiv \frac{t_v}{t_r} \qquad \text{Equation 5-10}$$

The dimensionless Ohnesorge number relates to Reynolds number and Capillary number as

$$Oh^{-2} = \frac{\rho \upsilon R_0}{\eta_0} = \frac{Re}{Ca} \qquad \text{Equation 5-11}$$

and describes the slope in Capillary and Reynolds number plane of the Cartesian coordinate system (McKinley 2005).

The ratio of Weissenberg number and Reynolds number provides the Elasticity number which can be written as

$$El = \frac{Wi}{Re} = \frac{\eta_0 \lambda}{\rho l^2} \qquad \text{Equation 5-12}$$

and corresponds to the magnitude of the linear slope in the plane for bulk flows of viscoelastic fluids. An indication of the degree of elastic or viscous effects is given by the ratio of the two dimensionless numbers Deborah and Ohnesorge also denoted as the elastocapillary number and the corresponding equation can be seen below.

$$Ec = \frac{De}{Oh} = \frac{\lambda \sigma_s}{\eta_0 R_0} = \frac{\text{elastic force}}{\text{viscous force}} \qquad \text{Equation 5-13}$$

After investigation of solutions of polystyrene in styrene oligomers at different concentrations, it was concluded that the dominance of the elastic effect in flow is noticeable when Ec > 1 (Clasen et al. 2004). Ec is an additional value to characterise fluids which is assigned to the free surface flows of viscoelastic fluids.

The dimensionless Deborah number considers the time of the deformation process in rheology and therefore it is the ratio of the relaxation time of the fluid, t_c, and the characteristic time of the experiment, t_p . For a given experimental time, a solid like material has a higher Deborah than a liquid-like material. Accordingly, the fluid appears more fluid when the Deborah number is getting smaller (Spiegelberg et al. 1996). The equation below uses the characteristic relaxation time, λ_c, the density, ρ, initial radius, R_0, and the surface tension, σ_s, to calculate the Deborah number.

$$De=\frac{tc}{tp}=\frac{\lambda_c}{\sqrt{\frac{\rho R_0^3}{\sigma_s}}} \qquad \text{Equation 5-14}$$

Rodd et al (2004) suggested that the Deborah number needed to be around 1 to allow measurement of the relaxation time of dilute and semi-dilute solution of polyethylene oxide (PEO) with Capillary Break-up Extensional rheometry.

The ratio of gravitational body force to surface tension force is expressed by the dimensionless Bond number, Bo,. It is a useful dimensional number in the CaBER experiment providing information about the "quality" of the cylindrical shape of the filament between the plates at the beginning. A dominant gravitational force causes sagging and draining of the filament. However, the desired cylindrical shape of the filament can be achieved when the surface tension, σ_s, dominates the gravitational force, g,.

$$Bo=\frac{\Delta\rho g R_0^2(t)}{\sigma_s} \qquad \text{Equation 5-15}$$

Where $\Delta\rho$ is calculated from differences of the density of the bridge and ambient medium (Mahajan et.al. 1999).

Plateau (1863) realised that a liquid bridge of $V_0=\pi R_0^2 L_0$ can have the maximum stable length of $L_{max}=2\pi R_0$ when B_0 is zero.

A smaller diameter of the plate can help to reduce the Bond number and accordingly the gravitational effect.

5.8 Experimental consideration

In the evolution of midfilament diameter, the process of filament decay depends strongly on length scale, time scale and dimensional parameters.

5.8.1 Length scales

The length scales comprise of the aspect ratios and capillary length and they depend on the set up parameter of the experiments.

5.8.2 Aspect ratios

Aspect ratio describes the geometrical relationship between the height and diameter. There are two aspect ratios namely the initial and the final aspect ratio. The initial aspect ratio, Λ_0, is expressed in terms of initial height, h_0, and cylindrical plate diameter, D_0, similarly the final aspect ratio, Λ_f, is expressed in terms of D_0 and final height, h_f,

$$\Lambda_0 = \frac{h_0}{D_0} \qquad \text{Equation 5-16}$$

$$\Lambda_f = \frac{h_f}{D_0} \qquad \text{Equation 5-17}$$

The ideal value of the initial aspect ratio is $0.5 \leq \Lambda_0 \leq 1$ which has been determined from numerical simulations for filament stretching rheometry (Yao and McKinley 1998). When the initial aspect ratio is $\Lambda_0 \ll 1$, reverse squeeze flow within a fluid occurs during the separation time of the plates. Consequently, the initial filament radius is smaller after cessation of stretching and thus radial stress is higher (Yao and McKinley 1998). It is clear that the break up time of the filament will be shorter accordingly. By increasing the initial aspect ratio, the axisymmetric filament of a self similar shape goes closer to the endplates (McKinley and Sridhar 2002). Problems such as sagging and bulging of the liquid occur at very high initial aspect ratios attributed to the effect of gravity.

5.8.3 Timescale

The whole process from separation of the plate until the filament break-up goes through several characteristic timescale zones. For a viscoelastic fluid, the timescales include the opening, the polymeric relaxation, the viscous break-up and finally the Rayleigh time. In contrast, for a viscous fluid, the polymeric relaxation time scale is practically zero due to fact that it does not behave elastically.

5.8.4 The opening / strike timescale

The first timescale in the capillary break-up procedure covers the separation of the plates. In our case, the Capillary break up rheometer allows an opening time or strike time of, $\delta t_0 \geq 0.02$s (20ms). To guarantee that the filament will not break before the upper plate reaches the end position, viscous break-up time, t_v, (see equation 5.21) must be longer than the opening timescale, δt_0,. During this opening time, only the background solvent viscosity generates the viscous stress in the filament (Entov and Hinch 1997).

5.8.5 Polymeric relaxation time

An exponential filament thinning of a viscoelastic fluid can be detected before the final stage occurs. This relaxation stage is mathematically described as (Clasen et al. 2004):

$$\frac{R_{mid}(t)}{R_1} = \left(\frac{GR_1}{2\sigma}\right)^{\frac{1}{3}} e^{-\frac{t}{3\lambda_c}} \qquad \text{Equation 5-18}$$

The characteristic relaxation time and elastic modulus are abbreviated to λ_c and G respectively. R_1 is the radius at time $t_0 + \delta t_0$ and may be determined by the lubrication solution for a viscous Newtonian fluid as $R_1 \sim R_0 (L_f / L_0)^{-3/4}$ (Spiegelberg et al. 1996). The strain rate self selected by the material has the relationship of $W_i = \dot{\varepsilon}\lambda_c = 2/3$ which is constant in this phase (Kheirandish et al. 2008).

Anna and McKinley (2001) and Stelter et al. (2000) carried out some experiments on different polymeric solutions to obtain information about the relaxation time. The experimental conclusion was that the characteristic relaxation time, λ_c, of a modelled elastic fluid (semi dilute PIB/PB Boger) closely agreed with the longest relaxation time, λ, obtained at crossover point in the frequency sweep ($\lambda_c \sim \lambda$). A discrepancy between these parameters seems to occur which is perhaps due to the effect of radial inhomogeneity influenced by the aspect ratio (Kolte and Szabo 1999). By choosing the optimal aspect ratio, the longest relaxation time from Rouse/Zimm for an ideal elastic fluid can be measured. Furthermore, the steady relaxation time can be extracted from the exponential decrease of radius (Anna and McKinley 2001).

5.8.6 The viscous break up time

Throughout the final phase of filament thinning, the elongated polymer chain maintained its finite extensibility condition and therefore additional resistance from the polymer against the capillary stress cannot be given anymore. The only source of resistance is given by the viscous stress now which is noticeable through the linear decay of the filament until rupture over the time (Entov and Hinch 1997). McKinley and Tripathi (2000) constructed a formula which describes the evolution of the midpoint radius when the effect of gravity is neglected ($R_{mid} << l_{cap}$).

$$R_{mid}(t)=R_0-\frac{(2X-1)}{6}\frac{\sigma_s}{\eta_s}t=\frac{(2X-1)}{6}\frac{\sigma_s}{\eta_s}(t-t_c) \qquad \text{Equation 5-19}$$

σ/η_s is the capillary velocity which has the unit [m/s] and the correction factor X for very simple Newtonian fluids is used. The critical time of the break-up event is denoted as t_c.

The following equation is valid for determination of viscous break up time.

$$t_v=\frac{6}{(2x-1)}\frac{\eta_s R_0}{\sigma_s} \qquad \text{Equation 5-20}$$

The previous assumption was that the value for X equals 1 (Bazileski et al 1990, Liang and Mackley 1994, Kolte and Szabo 1999) but the correction factor of 0.7127 introduced by Papageorgiou (1995) has been widely accepted for an inertia free

viscous filament (McKinley and Tripathi 2000). Using the X value from Papageorgiou, equation 5.19 can be rewritten as:

$$R_{mid}(t)=R_0-\frac{\sigma_s}{14.1\eta_s}t=R_0-\frac{R_0}{t_v}t=R_0-0.0709\upsilon_{cap}t \qquad \text{Equation 5-21}$$

Where t_v is the viscous break-up time as formulated in 5.21. The capillary velocity, v_{cap}, provides information about the rate of thinning in a viscous fluid. η_s is the viscosity and finally the surface tension is denoted as σ_s.

Eggers (1993 and 1997) mathematically formulated the pinching of an axisymmetric fluid by considering capillary, viscous and inertia stress. As a result, the process which occurred within a jet or during the dripping of a faucet obeys the following relationship $R_{mid} = 0.0304\ (\sigma_s/\eta_s)(t_c-t)$. A different description of evolution of midfilament radius for a Newtonian fluid is the equation; $R_{mid} = (\sigma_s/6\eta_s)(t_c-t)$ which has been derived from the balance between capillary, elastic and viscous stresses (Entov and Hinch 1997). Whereas, Papageorgiou (1995) has considered only the balance between capillary and viscous stress during the thinning (see equation 5 22).

5.8.7 The Inertial or Rayleigh time

The Rayleigh time scale in which the inertia capillary thinning occurs, is formulated as: (Rayleigh 1879)

$$t_R=\sqrt{\frac{\rho R_0^3}{\sigma_s}} \qquad \text{Equation 5-22}$$

A low number for t_R means that the evolution of the necking and rupture process takes place very rapidly.

5.9 Operability diagrams for Caber

Rodd et al (2004) provided a two dimensional operability diagram comprising a relaxation time axis and a viscosity axis (see Figure 5-6). The development of this diagram is based on a natural time scale, which includes viscous flow time, elastic

stress growth time and inertial oscillation time. Additionally, it was possible to specify the minimum requirements of relaxation time of 1 ms and viscosity of 70mPas. However, these values vary with different aspect ratios. When the aspect ratio is outside of the suggested range of 0.5 to 1, inertial oscillations of the liquid bridge or 'bead on string' phenomena are more likely to appear.

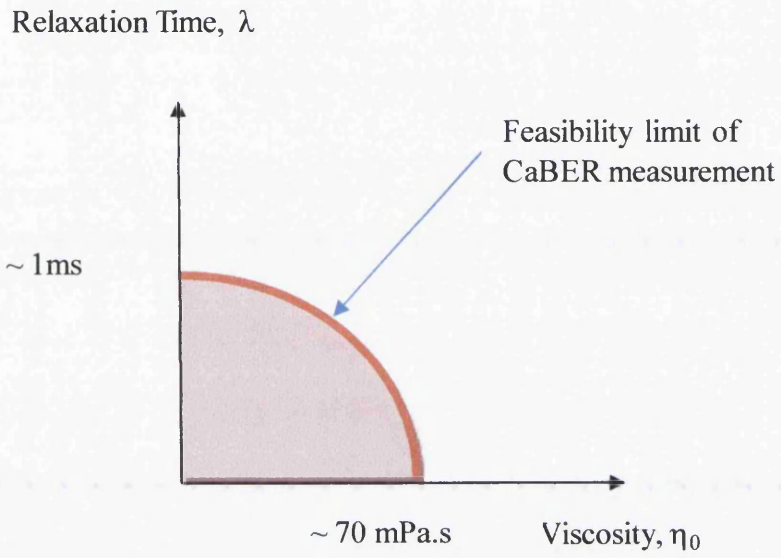

Figure 5-6: Schematic graph for an 'operability diagram' for capillary break-up

5.10 Problems with low viscosity samples

The 'beads on string' morphology is one of the complex shapes that appears more likely for viscoelastic fluids with low viscosity due to the inertial effect (Li and Fontelos 2003 and Rodd et. al. 2004). Another drawback is that low viscosity fluids break before the final gap has been achieved and therefore monitoring of the filament decay is not possible. This implies that the viscous time scale, t_v, is smaller than the opening time of the plate, δt, (Rodd et al. 2004).

5.11 Bibliography

Anna, S. L., & McKinley, G. H. (2001). Elasto capillary Thinning and Breakup of Model Elastic Liquids. *Journal of Rheology , 45* (1), 115-138.

Anna, S., McKinley, G. H., Nguyen, D. A., Sridhar, T., & Muller, S. J. (2002). An interlaboratory comparison of measurements from filament-stretching rheometers using common test fluids. *Journal of Rheology , 45*, 82-115.

Bazilevky, A. V., Entov, V. M., Lerner, M. M., & Rozhk, A. N. (1997). Failure of polymer solution filaments. *Polymer Science Series A , 39*, 316-324.

Bazilevsky, A. V., Entov, V. M., & Rozhkov, A. N. (2001). Breakup of an oldroyd liquid bridge as a method for testing the rheological properties of polymer solutions. *Polymer Science , 43*, 716-726.

Bazilvesky, A. V., Entov, V. M., & Rozhkov, A. N. (1990). Liquid Filament Microrheometer and Some of its Application. *Third European Rheology Conference* (pp. 41-43). Elsevier Applied, D.R. Oliver (ed.).

Berg, S., Kröger, R., & Rath, H. J. (1994). Measurement of Extensional Viscosity by Stretching Large Liquid Bridges in Microgravity. *Journal of Non-Newtonian Fluid Mechanics , 55*, 307-319.

Bhardwaj, A., Miller, E., & Rothstein, J. P. (2007a). Filament stretching and capillary breakup extensional rheometry measurements of viscoelastic wormlike micelle solutions. *Journal of Rheology , 51*, 693–719.

Bird, B. R., Armstrong, C., Hassager, O., & Curtiss, C. (1987). *Dynamics of Polymeric Liquids: Kinetic Theory* (Vol. 2). New York: Jone Wiley & Sons.

Bird, R. B. (1982). Polymer kinetic theories and elongational flows. *Chemical Engineering Communications , 16*, 175-187.

Birks, A. M., & Bagley, E. B. (1960). Flow of polyethylene into a capillary. *Journal of Applied Physics , 31*, 556-561.

Black, W. B., & Graham, M. D. (1999). Effect of wall slip on the stability of viscoelastic plane shear flow. *Physics of Fluids , 11*, 1749.

Blyler, L. L., & Hart, A. C. (1970). Capillary flow instability of ethylene polymer melts. *Polymer Engineering and Science , 10*, 193-203.

Boger, D. V., & Binnington, R. J. (1990). Circular Entry Flows of Fluid M1. *Journal of Non-Newtonian Fluid Mech. , 35*, 339–360.

Clasen, C., Eggers, J., Fontelos, M. A., & McKinley, G. H. (2006). The beads-on-string structure of viscoelastic threads. *Journal of Fluid Mechanics , 556*, 283-308.

Clasen, C., Plog, J. P., Kulicke, W. M., Owens, M., Macosko, C., Scriven, L. E., et al. (2006). How dilute are dilute solutions in extensional flows? *Journal of Rheology , 50*, 849–881.

Clasen, C., Verani, M., Plog, J. P., McKinley, G. H., & Kulicke, W. M. (2004). Effects of Polymer Concentration and Molecular Weight on the Dynamic of Visco-Elastic-Capillary Breakup. *Proceeding of the XIVth International Congress on Rheology.* Seoul.

Dontula, P., Pasquali, M., Scriven, L. E., & Macosko, C. W. (1997). Can extensional viscosity be measured with opposed nozzle devices? *Rheologica Acta , 36*, 429 – 448.

Eggers, J. (1997). Nonlinear dynamics and breakup of free surface flows. *Review of Modern Physics , 69*, 865-929.

Eggers, J. (1993). Universal pinching of 3d axisymmetric free-surface flow. *Physical Review Letters , 71*, 3458-3460.

Entov, V. M. (1999). Polymer solutions elongational flow: suspension of extensible rods model. *Journal of Non- Newtonian Fluid Mechanics , 82*, 167-188.

Entov, V. M., & Hinch, E. J. (1997). Effect of a Spectrum of Relaxation Times on the Capillary Thinning of a Filament of Elastic Liquid. *Journal of Non Newtonain Fluid Mechanics , 72* (1), 31-54.

Göttfert. (2002). The New Tensile Tester for Polymer Melts. Rheotens 71.97:.

Hermansky, C. G., & Boger, D. V. (1995). Opposing – Jet Viscometry of Fluids with Viscosity Approaching That of Water. *Journal of Non-Newtonian Fluid Mechanics , 56*, 1-14.

Kheirandish, S., Gubaydullin, I., Wohlleben, W., & Willenbacher, N. (2008). Shear and elongational flow behavior of acrylic thickener solutions, Part I: Effect of intermolecular aggregation. *Rheologica Acta , 47*, 999–1013.

Kheirandish, S., Guybaidullin, I., & Willenbacher, N. (2009). Shear and elongational flow behavior of acrylic thickener solutions, Part II: effect of gel content. *Rheologica Acta , 48*, 397–407.

Kheirandish, S., Guybaidullin, I., Wohlleben, W., & Willenbacher, N. (2008). Shear and elongational flow behaviour of acrylic thickener solutions Part I: Effect of intermolecular aggregation. *Rheologica Acta , 47*, 999-1013.

Kheirandish, S., Guybaidullin, I., Wohlleben, W., & Willenbacher, N. (2009). Shear and elongational flow behaviour of acrylic thickener solutions, Part II: effect of gel content. *Rheologica Acta , 48*, 397-407.

Kolte, M. I., & Szabo, P. (1999). Capillary thinning of polymeric filaments. *Journal of Rheology , 43*, 609-625.

Laun, H. M. (2004). Capillary rheometer for polymer melts revisited. *Rheologica Acta , 43*, 509-528.

Laun, H. M., & Schluch, H. (1899). Transient elongational viscosity and drawability of polymer melts. *Journal of Rheology , 33*, 119-176.

Li, J., & Fontelos, M. A. (2003). Drop Dynamic on the Beads-on-String Structure for Viscoelastic Jets: A Numerical Study. *Physics of Fluids , 15*, 922-937.

Liang, R. F., & Mackley, M. R. (1994). Rheological characterisation of the time and strain dependence of polyisobytlene solution. *Journal of Non-Newtonian Fluid Mechanics , 52*, 387-404.

Mahajan, M. P., Tsige, M., Taylor, P. L., & Rosenblatt, C. (1999). Stability of liquid crystalline bridge. *Physics of Fluid , 11*, 491-493.

Matta, J. J., & Tytus, R. P. (1990). Liquid stretching using a falling cylinder. *Journal of Non-Newtonian Fluid Mechanics , 35*, 215-229.

McKinley, G. H. (2000). Decades of Filament Stretching Rheometer. *Processing of the 13th International Congress on Rheology,* (pp. 15-22). Cambridge: DM Binding et al. (Eds.).

McKinley, G. H. (2005). *Dimensionless groups for understanding free surface flows of complex fluids.* SOR Rheology Bulletin.

McKinley, G. H. (2005). Visco-elastic-capillary thinning and break-up of complex fluids. *Rheol. Rev.* , 1-48.

McKinley, G. H., & Sridhar, T. (2002). Filament-Stretching Rheometry of complex Fluids. *Annual Review of Fluid Mechanics , 34*, 375-415.

McKinley, G. H., & Tripathi, A. (2000). How to Extract the Newtonian Viscosity from Capillary Breakup Measurements in a Filament Rheometer. *Journal of Rheology , 44* (3), 653-671.

McKinley, G. H., Anna, S. L., Tripathi, A., & Yao, M. (1999). Extensional rheometry of polymeric fluids and the uniaxial elongation of viscoelastic filaments,. *15th Annual Meeting of the International Polymer Processing Society.*

McKinley, G., & Sridhar, T. (2002). Filament-Stretching Rheometry of Complex Fluids. *Annual Review of Fluid Mechanics , 34*, 375-415.

Meissner, J. (1985). Experimental aspects in polymer melt elongational rheometry. *Chemical Engineering Communications , 2*, 159-180.

Meissner, J., Raible, T., & Stephenson, S. E. (1981). Rotary clamp in uniaxial and biaxial extensional rheometry of polymer melts. *Journal of Rheology , 2*, 1-28.

Miller, E., Clasen, C., & Rothstein, J. P. (2009). The effect of step-stretch parameters on capillary break up extensional rheology (CaBER) measurements. *Rheologica Acta , 48* (6), 1435-1528.

Miller, J. C. (1963). Swelling behaviour in extrusion. *Polymer Engineering and Science , 3*, 134-137.

Niedzwiedz, K., Arnold O., Willenbacher N. & Brummer R. (2009). How to characterize yield stress fluids with capillary breakup extensional rheometry (CaBER), *Applied Rheology, 19, 41969 -1 - 41969-10*

Oliveira, M. S., Yeh, R., & McKinley, G. (2006). Extensional Rheology and Formation of Beads-on-a-String Structures in Polymer Solutions. *Journal of Non-Newtonian Fluid Mechanics , 137*, 137–148.

Papageorgio, D. T. (1995). On the breakup of viscous liquid threads. *Physics of Fluids , 7*, 1529-1544.

Plateau, J.A.F.(1863). Experimental and theoretical researches on the figures of equilibrium of a liquid mass withdrawn from the action of gravity, *Annual Report Smithsonian Institution*

Rayleigh, L. (1879). On the Instability of Jets. *Proceedings of the London Mathematical Society, 10*, pp. 4-13.

Renardy, M. (1995). A numerical study of the asymptotic evolution and breakup of Newtonian and viscoelastic jets. *Journal of Non-Newtonian Fluid Mechanics , 59*, 267-282.

Renardy, M. (2001). Self-similar breakup of Giesekus. *Journal of Non-Newtonian Fluid Mechanics , 97*, 261–293.

Renardy, M. (2002). Similarity solution for jet breakup for various models of viscoelastic fluids. *Journal of Non-Newtonian Fluid Mechanics , 104*, 65–74.

Renardy, M. (1994). Some comments on the surface-tension driven break up (0r the lack of it) of viscoelastic jets. *Journal of Non-Newtonian Fluid Mechanics , 54*, 97-107.

Rodd, L. E., Cooper-White, J. J., Boger, D. V., & McKinley, G. H. (2007). Role of the elasticity number in the entry flow of dilute polymer solutions in micro-fabricated contraction geometries. *Journal of Non-Newtonian Fluid Mechanics , 143*, 170-191.

Rodd, L. E., Scott, T. P., Boger, D. V., Cooper-White, J., & Mckinley, G. H. (2005). The inertio-elastic planar entry flow of low-viscosity elastic fluids in microfabricated geometries. *Journal of Non-Newtonian Fluid Mechanics , 129*, 1–22.

Rodd, L. E., Scott, T. P., Cooper-White, J. J., & McKinley, G. H. (2004). Capillary Break-Up Rheomtry of low viscosity elastic fluids. Department of Chemical and Biomolecular Engineering, Australia: The University of Melborne.

Sentmanat, M. L. (2004). Miniature universal testing platform: from extensional melt rheology to solid-state deformation behaviour. *Rheologica Acta , 43*, 657-669.

Sentmanat, M. L., Wang, B. N., & McKinley, G. H. (2005). Measuring the Transient Extensional Rheology of Polyethylene Melts Using the SER Universal Testing Platform. *Journal of Rheology , 49*, 585- 606.

Spiegelberg, S. H., & McKingley, G. H. (1996). Stress relaxation and elastic decohesion of viscoelastic polymer solutions in extensional flow. *Journal of Non-Newtonian Fluid Mechanics , 67*, 49-76.

Spiegelberg, S. H., Ables, D. C., & McKingley, G. H. (1996). The role of end-effects on measurements of extensional viscosity in filament stretching rheometers. *Journal of Non-Newtonian Fluid Mechanics , 64* (2-3), 229-267.

Sridhar, T. V., Tirtaatmadja, D. A., Nguyen, D. A., & Gupta, R. K. (1991b). Measurement of extensional viscosity of polymer solutions. *Journal of Non-Newtonian Fluid Mechanics , 40*, 271-280.

Stelter, M., Brenn, G., Yarin, A. L., Singh, R. P., & Durst, F. (2000). Validation an dApplication of a Novel Elongational Device for Polymer Solutions. *Journal of Rheology , 44*, 595-616.

Szabo, P. (1997). Transient filament stretching rheometer I: force balance analysis. *Rheologica Acta , 36,* 277-284.

Trevor, S. K., McKinley, G. H., & Padmanabhan, M. (2006). Linear to Non-linear Rheology of Wheat Flour Dough. *Applied Rheology , 16* (5), 265-274.

Tropea, T., Yarin, A., & Foss, J. (2007). *Experimental Fluid Mechanics.* Berlin: Springer-Verlag.

Willenbacher, N. (2004). Elongational Viscosity of Aqueous Thickener Solutions from Capillary Breakup Elongational Rheometry. *Proceedings of 14th International Congress on Rheology.* Seoul.

Willenbacher, N., Hanciogullari, H., & Wagner, H. G. (1997). High Shear Rheology of Paper Coating Colors – More Than Just Viscosity,. *Chemical Engineering Technology , 20*, 557 – 563.

Yao, M., & McKingley, G. H. (1998). Numerical simulation of extensional deformation of viscoelastic liquid bridges in filament stretching devices. *Journal of Non-Newtonian Fluid Mechanics , 74* (1-3), 47-88.

Yao, M., McKinley, G. H., & Debbaut, B. (1998). Extensional deformation, stress relaxation and necking failure of viscoelastic filaments. *Journal of Non-Newtonian Fluid Mechanics , 79*, 469-501.

6 The concept of an induced capillary extrusion flow

6.1 Introduction to contraction flow method

A capillary extrusion flow is generated when a fluid suddenly flows from an initial tube into a smaller tube causing a dominated extensional deformation in the convergence of the streamlines and a shear deformation which dominates at the wall along the contraction (Binding 1988 and Binding and Walters 1988). During this process, the pressures in the initial tube experience a drop at the entrance of the smaller tube (see Figure 6-1). This incident of the pressure drop is used to determine the transient extensional viscosity for various materials including polymer with high viscosity (Laun and Schuch 1989) and polymers solutions with low viscosity (Binding and Walters 1988)

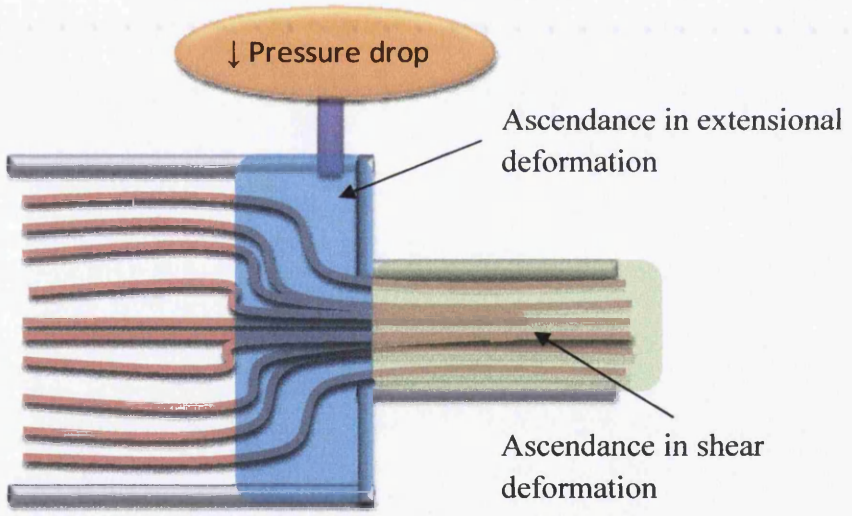

Figure 6-1: Schematic diagram showing flow streamlines and two distinctive locations which are dominated by either extensional deformation or shear deformation. Extensional deformation dominates in the blue area whereas a pure shear deformation occurs on the wall of the green area.

In the previous chapter, it was mentioned that the stretching method from a capillary break up rheometer can only apply an extension rate around 10 s^{-1}, whereas in the nip of the coil coating roller, an extension rate above 10^5 s^{-1} will be achieved. In this respect, the contraction flow method can achieve a high extensional rate, which helps to more closely simulate the coil coating flow. Furthermore, a capillary extrusion

rheometer can simulate the pressure gradient in the fluid that paint experiences when it passes through the converging and diverging geometry between the roll cylinders (see Figure 5-1). Moreover, both extensional and shear deformations take place in the coil coating process which the capillary extrusion rheometer can also mimic. Thus, these complex flow behaviours can only be understood when the full range of rheological properties can be obtained from different rheometers. (Ascanio et al. 2006, O'Brien & MacKay 2002). One of the other advantages of this confined contraction flow method is that it is already widely accepted in the study of behaviour of complex fluids such as paint, polymer melts, ink and melting of high density polyethylenes (Dealy 1982 and Ferry 1980, Hatzikiriakos and Dealy 1991, Willenbacher 1997 and Laun 2004).

6.2 Capillary rheometers principles

The common type of a capillary extrusion rheometer consists of a piston, a barrel wall, a heater, a pressure transducer and a capillary die (also named as a capillary) as can be seen in Figure 6-2. The material is located in a confined bore from where the sample will be extruded through the smaller capillary die by the action of the piston. A shear rate (flow rate) is maintained constant by keeping the piston speed constant. Due to the dissipation of the energy in the material, a pressure drop occurs during the flow which can be measured by a transducer located just above the upper die face (Fuller et al 1987) (see Figure 6-3). By knowing the excess pressure drop, ΔP, and the volumetric flow rate derived from the piston speed and the size of the bore, it is possible to determine extensional rate, $\dot{\varepsilon}$, by applying an analysis method such as those proposed by Binding (1988, 1991 and 1993) and Cogswell (1972).

These methods were built up with assumptions such as isothermal flow, no slip boundary, pressure independency of the viscosity and incompressible (isochoric) flow (see sections 6.11.1 and 6.11.2 for more details). However, in most cases, the collected raw data may need to undergo both shear and stress corrections due to the slip effect caused by wall depletion (explanation of wall depletion see section 4.6.1) (Cogswell 1972) and excess pressure drop in front of the entrance to the capillary

(Bagley 1957) to obtain the true shear viscosity and extensional viscosity (see more details in section 6.5). Dissipation of heat, compressibility and pressure dependence of viscosity may also need to be separated from the raw data. For example, the shear and elongational viscosity of some polymers such as HDPE, LDPE, LLDPE, PP, PC, PMMA and PS are strongly affected by pressure (Sedláček 2004).

Nearly 40 years ago, Cogswell (1972) suggested that the length to diameter ratio (L/D) needs to be in the range from 20 to 50 to obtain a fully developed flow in order to reduce any unwanted effects. In the case of a L/D ratio of less than 20, flow may not be fully developed. Using L/D ratio above 50 may cause two unwanted effects during the experiments. Firstly, the pressure acting on the sample will be increased which may affect the viscosity of sample. Secondly, a high pressure drop across a die increases the temperature in the material due to dissipative heating. Both the elevated pressure and dissipative heating are strongly coupled (Denn 1981 and Hay et al. 1999).

These effects were also detected during the work from Hatzikiriakos and Dealer (1992), and Laun and Schuch (1990). If the Nahme number ($Na=\frac{\text{zero shear viscosity * thermal coefficient * velocity characteristic of the flow}}{\text{fluid thermal conductivity * absolute Temperature}}$) is below 1 then viscous heating can be neglected (Winter 1997). Rides and Allen (2001) conducted some experiments with thermoplastic material and observed the effect of low length to diameter ratio on the shear viscosity. The conclusion was that shear viscosity derived from the low length to diameter ratios (L/D = 0.25) is almost the same as those with higher length to diameter ratios (L/D = 30).

The effect of die geometry was investigated by Sombatsompop et al. (1997) who used rubber. One of the findings was that the central velocity of flow is smaller when using a die than without. By using different die diameters and constant die length, the flow pattern is generally the same (Sombatsompop et al. 1997). More studies with various materials are needed to provide a better understanding of the effect of dies. For very low length to diameter ratio, reasonable test results are guaranteed by using dies with a radius between 0.25mm and 2mm (Cogswell 1972). However, this is material dependent. For rubber materials for an example, die diameters of 1.75, 6 and 8 mm have been used for an extrusion capillary experiment (Sombatsompop 1997).

A small die radius (< 0.25mm for paint) would extremely enhance the pressure in the systems which leads to a tremendous increase in temperature or may cause pressure related structural changes. From the practical point of view, dies with radii smaller than 0.25 mm are not ideal for pigmented systems due to susceptibility of blockages. But when using a bigger radius (>2 mm for fluid with low viscosity) the end result may suffer more noise due to the lower pressure drop (i.e. noise has more influence on the end result). Using dies with different diameters allows detection of slip effects in the system.

During the entire procedure, both extensional and shear deformation can be encountered in the capillary extrusion rheometer (Ramamurthy and McAdam1980).

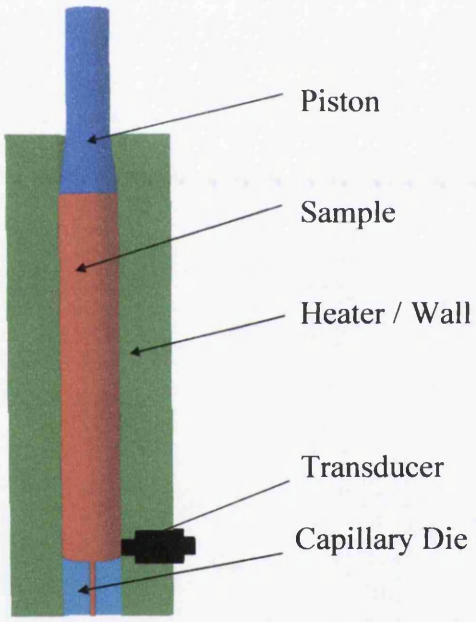

Figure 6-2: Sectional cut view of a capillary extrusion rheometer

6.3 Advantages and disadvantages of capillary extrusion rheometer

A capillary extrusion rheometer can give useful information about extensional viscosity at high shear rates of around 10^5 s^{-1}, which is a huge advantage for understanding industrial processes such as roll coating and extrusion /injection moulding. Furthermore, it nearly mimics the flow in the nip between the rolls of the coil coating process. The execution of the whole test is user-friendly and therefore

test preparation consists only of loading the bores with the samples. The concept of a capillary extrusion rheometer is regulated according to the ISO 11443 which indicates high standard.

A disadvantage of capillary extrusion rheometer is its limitations of measurement of fluids with viscosity lower than 1 Pas. This fluid with low viscosity will flow by gravity through the traditional vertical capillary die without any driving force coming from the piston. Furthermore, low-pressures are generated by samples with low viscosity, which is difficult to measure due to the limitations of the pressure transducer.

6.4 Dimensionless Numbers for describing the fluid dynamics of the contraction flow

The most commonly used dimensionless numbers for describing the flow behaviour occurring in a capillary extrusion rheometer are the elasticity number, *El*, Euler number, *Eu*, and the Reynolds number, *Re*. All of these have been used for comparison of samples (Ascanio et al. 2002 and Della Vale 2000).

6.4.1 Elasticity number

The elasticity number expresses the ratio of elastic to inertial stresses or the ratio of the Weissenberger number (see Equation 5.9) to the Reynolds number (see Equation 6.3).

$$El=\frac{Wi}{Re}=\frac{\lambda\eta}{\varrho l^2} \qquad \text{Equation 6-1}$$

From Equation 6.1, it can be seen that the elastic number is only a function of fluid properties and geometry. Whereas process kinematics do not have any influence on it.

6.4.2 Euler Number

Generally, the Euler number describes the ratio of pressure forces to inertial forces and it is:

$$Eu=\frac{\Delta P}{\rho v^2} \qquad \text{Equation 6-2}$$

Where v stand for the velocity of fluid which occurs in the orifice

6.4.3 Reynolds Number for convergent flow

The Reynolds number is the ratio of inertial to viscous forces and can be expressed in terms of the capillary rheometer with the variables density, ρ, velocity, $v=Q/\pi R_d^2$, inner diameter of the die, d_d, and zero shear viscosity, η_0, as.

$$Re=\frac{\rho v d_d}{\eta_0}=\frac{\text{density} \times \text{velocity x diameter}}{\text{viscosity}} \qquad \text{Equation 6-3}$$

When the Reynolds number is greater than 100, the inertial forces need to be considered due to the increased pressure drop in the capillary extrusion rheometer (see Equation 6.8) (Ascanio et al. 2006).

6.4.4 Determination of Deborah number for capillary extrusion rheometer

The Deborah number is the ratio of characteristic relaxation time of the fluid, λ, and characteristic flow time, T,. A high Deborah number indicates that the material behaves like a solid whereas a low Deborah number designates a viscous like material. The inverse of the deformation rate just before the onset of the contraction region determines the characteristic flow time. (Rothstein and McKinley 1999).

6.5 Pressure drops in the capillary extrusion rheometer

The total pressure drop, ΔP, is one of the important factors to determine the extensional viscosity. The magnitude of the pressure drop is measured above the die and it is the sum of the pressure drops which occur before the entry, ΔP_e, within the capillary die, ΔP_{cap}, and at the exit of the die, ΔP_{exit},. ΔP_e is used to push the material from the reservoir to the capillary die. The loss of energy over the capillary is represented by the value of ΔP_{cap}. Equation 6.4 describes the mathematical relationship and Figure 6-3 schematically illustrates the split of the total pressure drop (Mitsoulis et al. 1998).

$$\Delta P = \Delta P_e + \Delta P_{cap} + \Delta P_{exit} = \Delta P_{cap} + \Delta P_{End} \qquad \text{Equation 6-4}$$

The exit pressure drop can be neglected for Newtonian and low elasticity fluids. In contrast for non-Newtonian fluids with a high amount of elastic components, the exit pressure drop needs to be included. A highly elastic material shows noticeable die swell at the end of the die. The exit effect seems to be get weaker with increased shear rate. This results in a lower fluctuation of P_{exit} and consequently the measurement precision increases (Han et al. 1973). Miller (1963) reported that the scale of die swell using polyethylenes is more pronounced at zero die than at longer die. A step further was made by predicting the die swell ratio through a mathematically formula for a high density polyethylene melt. The outcome of the theoretical results is obtained by the Equation

$$B = \left[1 + \left(\frac{3\Delta P_{exit}}{\sigma_w}\right)^2\right]^{\frac{1}{4}} \qquad \text{Equation 6-5}$$

where B is the die swell ratio and shear stress, σ_w, (Liang 2000).

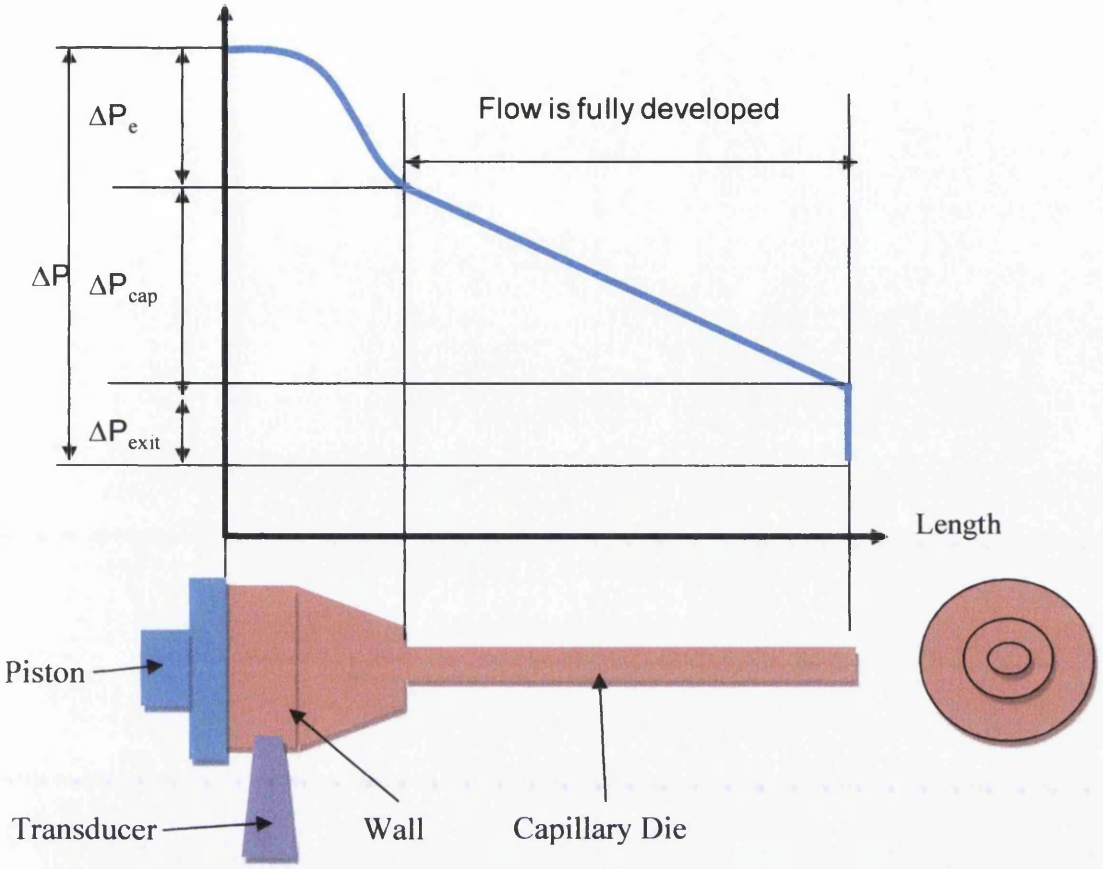

Figure 6-3: A simplified illustration of pressure losses within an extrusion rheometer. (Mitsoulis et al. 1998)

6.6 Determination of shear stress and shear rate

The determination of both parameters stress and strain from the raw data is crucial to the determination of the extensional and shear viscosities. Special procedures including the Bagley Method and the Mooney Method (1931) need to be carried out to obtain the true extensional and shear viscosity. Before going into the details, general information are provided in terms of the maximum shear stress, σ_{21}, and shear rate, $\dot{\gamma}$, which will be illustrated Figure 6-4. It shows that the maximum values of shear stress and shear rate can be found at the wall of the tube where the flow velocity is zero. Shear stress and shear rate tends to be zero towards the middle axis of the tube while the velocity achieves its maximum.

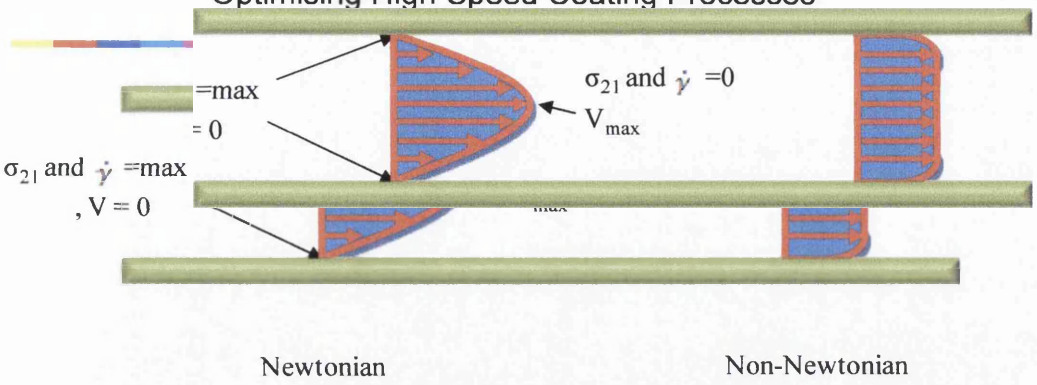

Figure 6-4: Schematic presentation about velocity profiles from a Newtonian liquid (parabolic profile) (Kulicke and Clasen 2004) and a non Newtonian fluid (plug profile).

By using the total pressure drop, ΔP, the apparent shear stress, $\sigma_{A,u}$, at the wall within the capillary can be determined as:

$$\sigma_{A,u} = \frac{\Delta P R}{2L} \qquad \text{Equation 6-6}$$

Where R is the radius of the die and L is the die length.

Equation 6.6 was made with the assumption that the pressure gradient along the entire flow channel is constant, which can normally be found with high viscosity fluids (Barroso et al 2009). As mentioned in section 6.5, the total pressure is made up with several sub pressure drops that consequently do not give the true shear stress in the die. The Bagley Method provides a method to separate the pressure drop in the die from the entrance pressure drop (see section 6.6.1).

In terms of apparent shear rate, $\dot{\gamma}_a$, fluid flowing through a capillary can be determined in a very simple way by using volumetric flow rate, Q ($=\pi R^2 V$), and geometric parameter, die radius, R, (Cogswell 1972) (see Equation 6.7).

$$\dot{\gamma}_a = \frac{4Q}{\pi R^3} \qquad \text{Equation 6-7}$$

6.6.1 Stress correction according to Bagley

The reason for applying the Bagley method is to determine the entrance pressure drop from the raw data, which will then be subtracted from the total pressure drop (see equation 6.9). With this stress correction, the true shear stress can be calculated. The use of at least three dies with constant inner radius but varying lengths is one of the approaches to obtain the magnitude of the excessive entrance pressure, P_e,. The purpose of using different length dies is to obtain various total pressure drops under constant shear rate (see equation 6.7). The resulting total pressures are then plotted against the ratio of length to constant radius, L/R_{const},. In an ideal case, a linear relationship between total pressure drop and L/R_{const} exists. Hence, a straight line can be drawn through the data and can be extrapolated to the ordinate whose intersection provides the excessive entrance pressure drop, ΔP_e, (see Figure 6-5).

However, such a linear relationship does not always take place due to the pressure dependence of viscosity and viscous heating effects. An upward curvature on the Bagley plot indicates that the viscosity is dependent on pressure. In circumstances where viscous heating is significant, the Bagley plot is concave. Viscous heating effects mainly occur in highly viscous systems such as polymer melts. To get a good model fit for an upward curvature, a second order polynomial is used to obtain the magnitude of ΔP_e (Laun 1983, Laun and Schuch 1989).

To overcome the unwanted effects, a zero or orifice die ($L/R \cong 0$) is employed. However, there are three major disadvantages of using this method. Firstly, the experimental error is extremely high because only a small amount of material will be tested within a very small length scale. Secondly, the low pressure which exits at zero die might provide a different result than the longer die due to higher distortion of noise. Thirdly, the possibility of a vortex appearing will be neglected. Without this additional information, a false conclusion can be drawn (Mitsoulis et. al 1998). In despite of the disadvantages, Binding et al (1998) used this method to finally conclude that the extensional viscosity of polymers depends on pressure. The pressure drops between a zero and long die gives crucial information for the processing of polymer because it highlights the presence of compression effects (Sunder and Goettfert 2001).

Slip is another factor which changes the Bagley plot into a convex curve (Hatzikiriakos and Dealy 1992) or depresses the slope of the linear curve. However, the magnitude of intersection is the same magnitude which is derived by data without slip using a constant diameter (Shaun 1989) (see Figure 6-5). A very good example for a successful Bagley correction was published by Kang et al. (2005) and illustrates that the viscosity versus shear rate curves obtained from different L/D merge into one curve. This indicates the successful elimination of the end effects.

A power law relationship between pressure loss and shear rate was reported by Han and Kim (1971). A mutual agreement could be found that the entrance pressure will be affected by modifying shear rheology of the sample (Mitsoulis et al. 1998 and Rajagopalan 2001). Furthermore, the pressure drop is proportional to viscosity in a laminar flow with a low Reynolds number condition. Typically, this condition can be found with Newtonian fluids with high viscosity and low density. Above a critical Reynolds number, inertial effects dominate the flow and the pressure drop no longer depends on the viscosity (Della Valle et al. 2000).

A pressure drop correction according to the Equation 6.8 was undertaken for a high solid content suspension and coating colours when Re > 100 to account for the inertia effect (Ascanio et al. 2006):

$$\Delta P_{corr}=\Delta P-\frac{1}{2}\rho v_0^2 \qquad \text{Equation 6-8}$$

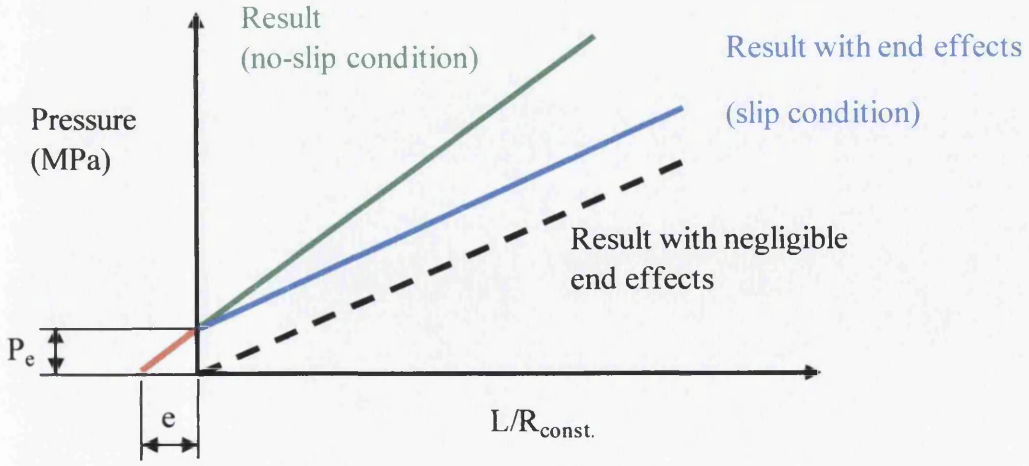

Figure 6-5: A classical Bagley plot under different conditions

To convert the apparent shear stress into the true shear stress, the excessive entrance pressure drop, P_e, needs to be subtracted from the total pressure. With P_e subtracted, Equation 6.6 will be converted to:

$$\sigma_w=\frac{(P-P_e)R}{2L}=\frac{\Delta PR}{2L}=\frac{P}{2\left(\frac{L}{R}+e\right)} \qquad \text{Equation 6-9}$$

In Figure 6-5, e is the point where the pressure curve intersects the L/R_{const} axis. Care must be taken when using the value of e because this value can only be used when no slip happens. The reason is that e will increase with the slip condition as can be deduced from Figure 6-5.

6.6.2 Determination of the shear rate including the effect of the velocity profile

Determining shear rate is more complex with non-Newtonian fluids than with Newtonian fluids. In this case, the data from Equation 6.7 can only be considered as an apparent shear rate, $\dot{\gamma}_a(=4Q/\pi R^3)$, which can be converted into the true shear rate by using the Weissenberg Rabinowitch shear correction. The Weissenberg Rabinowitsch correction takes into account the pseudoplastic (shear thinning) nature of a material. This means that it considers the actual plug like velocity profile instead of the assumed parabolic velocity profile, which is based on the shear thinning effect (see Figure 6-4). The true shear rate with a no slip boundary can be obtained by modifying Equation 6.7 to:

$$\dot{\gamma}_w=\left(\frac{3n_s+1}{4n_s}\right)\left(\frac{4Q}{\pi R^3}\right)=\left(\frac{3n_s+1}{4n_s}\right)\dot{\gamma}_a \qquad \text{Equation 6-10}$$

Where the Weissenberg Rabinowitsch correction factor, n_s, can be calculated by

$$n_s=\frac{\log\sigma_w}{\log\dot{\gamma}_a} \qquad \text{Equation 6-11}$$

For Newtonian fluids, $n_s = 1$, which leads to $\dot{\gamma}_w=\dot{\gamma}_{true}$(Grellmann & Seidler 1949).

The above equation is valid for the following assumptions. Firstly, there is no wall slip which means the velocity of the fluid at the wall is zero. Secondly, the systems will be considered as isothermal and that the flow is laminar and fully formed along

the whole length of the die. This implies that fully developed flow begins from the entrance of the capillary and ends at the exit of the capillary. However, a fully developed flow seems to be difficult to achieve. An investigation with a die of a length of 45mm came to the conclusion that a fully developed flow from a polymer melt was only achieved around 5mm below the entrance of the die (Sombatsompop and Wood 1997 and Sombatsompop 1999).

6.7 Laminar and turbulent flow

Laminar flow Turbulent flow

Figure 6-6: Differences between a laminar and turbulent flow

At present, there is not much information about the transition between laminar and turbulent flow for non Newtonian fluids. *Re* provides an indication of an onset of turbulent flow. The flow changes from laminar to turbulent when a critical disturbance velocity has been achieved and this effect can be reversed by falling below the critical disturbance velocity. The flow remains laminar when the Reynolds number is below 2300 (Baehr and Stephan 2006). However, this is only a generalised number and does not consider the different rheological flow characteristics which may affect the threshold between laminar and turbulent flow. A comparison of the flow transition between Newtonian (water) and non Newtonian (dilute polymer solutions) was made from the result that the transition Reynolds number is reduced for polymers. To date, the cause of the reduction remains unknown. However, an assumption is made in terms of the destabilisation of elasticity in the area of the entry region of the flow (Draad et al. 2010).

6.8 Wall depletion or slip effects in a capillary extrusion rheometer

The occurrence of wall slip in the die of a capillary extrusion rheometer is common for many suspensions (Barnes 1995), polymer melts (Kang et al. 2005) as well as rubber compounds (Ma et al 1985) and food materials including bread dough (Sofou et al. 2008). A statement was made by Mackey and Henson (1998) which reports that capillary rheometers are not able to accurately detect slip unless the slip is large. An appearance of wall slip can only happen when a critical stress level is exceeded (Ramamurthy 1986). For instance, a slip was detected for bread dough after exceeding the critical stress level of 5kPa (Sofou et al. 2008) and for polyethylene at around 100 kPa (Ghanta et al. 1998). The critical stress values for linear low density polyethylene (LLDPE) and high density polyethylene (HDPE) are in the region between 100 and 140 kPa (Ramamurthy 1986 and Hatzikiriakos and Dealy 1991).

There are some factors which lead to an increase of slip velocity for example through an increase in the particle concentration (Lam et al. 2007). The slip can also be promoted or inhibited by the properties of the wall (Kraynik and Schowwalter 1981 and Ramamurthy 1986). For a LLDPE, the apparent slip increased for capillary dies made out of brass whereas the slip effect is less when the die is made of stainless steel. Consequently the conclusion was drawn that capillary dies made out of brass increase the apparent slip whereas dies consisting of stainless steel reduce slip effect (Ghanta et al. 1999 and Ramamurthy 1986).

At present, an explanation for this phenomenon is not available. Surface chemistry (molecular distance) may play an important role but this is speculative (Ghanta et al. 1999). Sufficient surface energy from the inorganic solid surface allows an adsorption of the coils in polymer melt on the wall. When the wall stress is high enough, coils closer to the wall start to stretch more than the inside of the melt which leads to a layer of coil stretching. In this area, the viscosity is smaller than the bulk viscosity (Wang 1999). Different outcomes were reported such that slip velocity in stainless steel capillaries is higher than in brass capillaries (Chen et al. 1992). Furthermore, the magnitude of the slip velocity reported by Chen et al. (1992) is around 30 times higher than the value reported by Ramanarthy (1986).

The differences between the results from Ghanta et al. (1997) and the results from Chen et al. (1992) could be because of various die materials. Ghanta et al. (1997) used a stainless steel type 304 and brass CDA 464 whereas Chen et al. (1992) carried out the experiments with stainless steel type 303 and brass 3003 H14. Furthermore, a comparison of data is not possible due to the lack of information about the surface finish. To draw an explicitly and accurate conclusion about the effect of die material on slip, further investigations with different materials needs to be carried out. A rough wall surface eliminates the presence of wall slip but may lead to different effects. The surface can be roughened, for example with sand blasting or using a rough material attached to the smooth wall (Meyvis et al., 2001; Citerne et al. 2001). An increase in surface tension leads to a reduction of slip because of the work of adhesion (Chen et. al 1992).

6.9 Methods for detection of wall slip in a capillary extrusion rheometer

Several techniques are available to analyse the slip occurring on a smooth wall. One of them is the Laser Doppler Velocimetry (LDV), which measures the direction and speed of fluids through the detection of the frequency shift of a laser caused by the particles in the flow. It has been used for measuring wall slip during extrusion of a polyethylene melt (Münstedt et al. 2001). The use of LDV allowed Münstedt et al. (2000) to observer the formation of a vortex in the entrance of capillary flow of different polyolefis for the first time. Another visualisation technique is the particle image velocimetry (PIV). In this case, PIV captures two images from liquid with seeded tracer particles within a very short time to obtain the travel distance of the particle within the time. By using this data, the velocity field can be determined. Rodriguez- Gonzalesz et al. (2009) seeded solid copper sphere with a diameter less than 10 μm into high density polyethylene so that velocity profiles can be obtained with PIV. With this approach, it was detected that a slip velocity contributes 75% of the total maximum velocity at a wall stress of 0.240 MPa which occurred at a strain rate of 797 s^{-1}. Interestingly, the detection of the true plug flow was not made during the experiments due to the shear thinning effect in the melt. Further fascinating flow patterns captured and a list of flow visualisation techniques were published by Kline (1969) and explained more in details (Smits and Lim 2000). However, these devices

are expensive and not always practical to determine the wall slip. Numerical analysis methods have been developed to obtain the wall slip from experimental data. The most well known method is the Mooney analysis which had recently been used for studying the extensional behaviours of bread dough (Hicks 2010) and ink (Willenbacher 1997).

6.10 Slip analysis method

The occurrence of slip in capillary flow has been explored both theoretically and experimentally. One of the theoretical views is that a slip flow phenomenon is caused by the creation of a very thin low viscosity region near the wall. (more information see section 4.6). By considering the apparent slip, the raw data can be corrected accordingly. In this section, the well known Mooney method will be explained which quantifies the slip. Before starting with the explanation, a sketch is provided to demonstrate the difference between slip free and slip flow in a tube as illustrated in Figure 6-7.

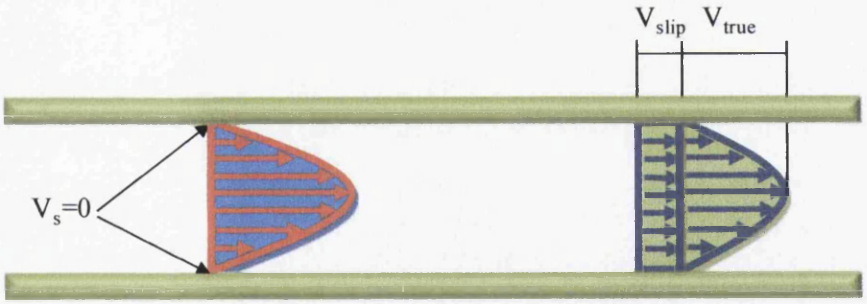

Figure 6-7: Schematic diagram of velocity profiles with presence and absence of slip

As can be seen in the Figure 6-7, the total velocity is made of the slip velocity and the true velocity. Slip effects at the tube can be quantified by the effective slip velocity, V_s, which is

$$V_s = \frac{Q_s}{\pi R^2} \qquad \text{Equation 6-12}$$

Where Q_s is the flow rate with slip appearance (Rides and Allen 2006)

6.10.1 Slip analysis according to Mooney

The fundamental idea of Mooney (1931) is based on the diameter dependency of shear viscosity which shows the degree of slip. Therefore, the determination of any slip effect can be done by using a set of different diameters. However, the ratio L/D needs to be constant so that the stress is always the same. Finally, the measured data will be plotted on a shear rate versus 1/R graph from which the slip velocity can be obtained as demonstrated in Figure 6.7.

As for many methods, there are some criteria which need to be fulfilled so that the Mooney method is valid. One of the criteria is that the ratio of die inner diameter to characteristic particle dimension should not be lower than 30 otherwise the validation of the Mooney method is doubtful (Corfield et al. 1999). Another important factor is that a linear Bagley plot exists to allow the use of the Mooney method (Mooney 1931). Furthermore, it is worth mentioning that small errors in wall shear stress have an enormous impact on the outcome of slip velocity result (Hatzikiriakos and Dealy 1992 and Arai and Aoyama 1963).

A number of researchers have used the Mooney method for some polymers (Ramamurthy 1986, Hatzikiriakos and Dealy 1992). A table with success and failure of Mooney method is provided by Martin and Wilson (2005) who also reported alternative route to obtain the slip effect.

The apparent slip shear rate, $\dot{\gamma}_{a,s}$, for a Newtonian fluid is the sum of the slip velocity, V_s, (see Equation 6.12) and the true shear rate, $\dot{\gamma}_w$, (see Equation 6.10) as:

$$\dot{\gamma}_{a,s} = \frac{4V_s}{R} + \dot{\gamma}_w \qquad \text{Equation 6-13}$$

For a non-Newtonian fluid, the apparent slip shear rate can be written as:

$$\dot{\gamma}_{a,s} = \left(\frac{4n(k+3)}{3n+1}\right)\frac{4V_s}{R} + \left(\frac{4n}{3n+1}\right)\dot{\gamma}_w. \qquad \text{Equation 6-14}$$

Where, k and n are material constants.

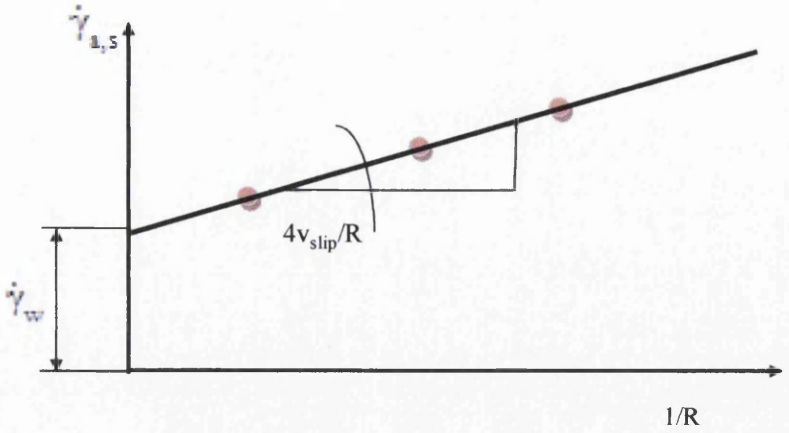

Figure 6-8: Determination of slip velocity through the use of the Mooney method

6.11 Determination of entrance viscosity and extensional viscosity

A number of approaches have been proposed such as by Cogswell (1972) and Binding (1988) to determine the extensional stress and extensional rate and so to finally obtain the extensional viscosity from pressure drop data. A good overview of additional approximate analyses can be found in Padmanabhan (1997).

6.11.1 Cogswell model

Several assumptions provide the foundation for the Cogswell model such as (Rao 2007, Cogswell 1972 and Cogswell 1972)

1) The flow is assumed to be isothermal
2) The flow speed is so slow that the inertial effects are negligible.
3) There is no elasticity effect which means that normal stress is neglected.
4) The viscosity is independent on pressure which means it behaves as an incompressible.
5) The system is considered as slip free.
6) Shear and extensional flow relate to the entrance pressure drop. During the extrusion, the elongational viscosity remains constant.
7) Cogswell considered the flow in the converging region as locally fully developed.

The following expressions are necessary to calculate the extensional viscosity (Cogswell 1972 and Cogswell 1972).

The extensional stress, σ_E, is defined as

$$\sigma_E=\frac{3}{8}(n_e+1)P_e \qquad \text{Equation 6-15}$$

where P_e is the entrance pressure drop and n_e value can be determined from:

$$n_e=\frac{d\log\left(\frac{\sigma_w}{\dot{\gamma}_a}\right)}{d\log(\dot{\gamma}_a)}-1 \qquad \text{Equation 6-16}$$

Extensional rate is determined by means of using the true shear stress, σ_w, (see Equation 6.9) and the apparent shear rate, $\dot{\gamma}_a$, (see Equation 6.7) which does not include the Weissenberg Rabinowitch correction as explained in section 6.6.2

$$\dot{\epsilon}=\frac{4}{3(n_e+1)}\sigma_w\frac{\dot{\gamma}_a}{P_e} \qquad \text{Equation 6-17}$$

Finally, the extensional viscosity can be determined according to Cogswell method.

$$\eta_E=\frac{\sigma_E}{\dot{\epsilon}} \qquad \text{Equation 6-18}$$

6.11.2 Binding model

Binding (1988) almost used the same assumptions as Cogswell (1972), however, one of the additional assumptions was that the relationship between shear viscosity and extension rate follows the power law. Furthermore, the extensional viscosity is described by a power law and the energy which is required for maintaining the vortex.

The extensional rate can be calculated as:

$$\dot{\epsilon}=\frac{(3n_e+1)(1+k)^2}{3k^2(1+n_e)^2}\frac{\sigma_w}{\Delta P_e}\dot{\gamma}_a \qquad \text{Equation 6-19}$$

and the extensional stress as:

$$\sigma_E = \frac{2^{k-1}3k(1+n_e)^2}{(2n_e+1)(1+k)^2}\frac{\Delta P_e}{I_{nk}} \qquad \text{Equation 6-20}$$

The index k comes from the power law function which belongs one of Binding's assumption and can be calculated with the Equation below:

$$k = \frac{d\ \ln\Delta P_{en}/d\ \ln\dot{\gamma}_w}{1+n_e-\left(\frac{d\ \ln P_{en}}{d\ \ln\dot{\gamma}_w}\right)}. \qquad \text{Equation 6-21}$$

and if $n \in (0,1)$, then I_{nk} can be obtained by

$$I_{nk} = \frac{n_e\left(\frac{1+n_e}{n_e}\right)^{k+1}}{2n_e+(1+n_e)(k+1)} \qquad \text{Equation 6-22}$$

Later, Binding (1991) included the first normal stress difference, N_1, which effects the pressure drop and reviewed his analysis two years later (Binding 1993). The entrance pressure drop is replaced by the modified entrance pressure drop, P_e:

$$P_e' = P_e + \frac{(3n_e-1)(3n_e+1)^{j+2}}{3n_e^{j+1}2^{2j+1}(2n_e+j+1)(3n_e+j+2)}N_1 \qquad \text{Equation 6-23}$$

and j is defined as:

$$j = \frac{d\log(N_1)}{d\log(\dot{\gamma}_a)} - 1 \qquad \text{Equation 6-24}$$

6.12 Determination of the apparent extensional viscosity and true extensional viscosity

There are two types of extensional viscosity, namely the apparent extensional viscosity, η_a, and the true extensional viscosity, η_{true}. The apparent extensional viscosity is defined by the ratio of corrected shear stress (see Equation 6.9 Bagley correction) and the apparent shear rate (see Equation 6.8)

$$\eta_a = \frac{\sigma_w}{\dot{\gamma}_a} \qquad \text{Equation 6-25}$$

Subsequently, the true viscosity of a non Newtonian fluid without any slip effect can be determined by:

$$\eta_{True} = \frac{\sigma_w}{\dot{\gamma}_w} \qquad \text{Equation 6-26}$$

6.13 The occurrence of Flow Phenomena

6.13.1 Vortex flow

A vortex flow describes an area where the motion of a fluid recirculates. This means that the streamline is closed. In relation to Capillary Extrusion Rheometers, an unwanted closed region of recirculation might appear in the corner of the bore also known as a salient corner vortex which depends on the flow rate and rheological properties of the fluid. Another flow sometimes occurs at the edge of the die hole in the reservoir known as the lip vortex. Rothstein and McKinley (2001) analysed the flow behaviour of a polystyrene Boger fluid with axisymmetric contraction device and detected an elastic lip vortex at a contraction ratio of 2 whereas no lip vortex was observed at higher contraction ratios between 4 and 8. The most common occurrence of lip vortex can be found in non-Newtonian fluids.

Münstedt et al. (2001) conducted a quantitative analysis of secondary flow patterns in a slit die using a laser Doppler velocimetry (LDV). The conclusion made from branched and linear polyethylene as well as branched and linear polypropylene was that strain hardening behaviour supports the development of vortices and elasticity only has a minor influence on the formation of vortices. This correlation was qualitatively confirmed later by Hertel and Münstedt (2008). The primary function of the vortex flow is to release stress within the fluid. When flow rate increases the shape of vortex starts to grow to compensate for the increase of stress around the contraction.

An increase in temperature may also cause an increase of the size of the vortex (e.g. viscosity decreasing) which was observed at polyethylenes (Münstedt et al. 2001). Rothstein and McKinley (2001) added another factor for vortex enhancement.

During the investigation, it was noticed that the vortex increases with growing contraction ratio. In some cases, the salient vortex will be encapsulated by the lip vortex which finally plays the most important role in vortex enhancement (Nigen 2002). As a consequence of the increases in vortex size, the pressure drop increases accordingly (Valle et al. 2000). Nigen (2002) studied the flow behaviour of viscoelastic (Boger fluid) and Newtonian material in axisymmetric and planar contraction apparatus. Vortex enhancement and pressure drop due to viscoelasticity were only detected in a Boger fluid and not in the Newtonian fluid. However, the vortex enhancement in the Boger fluid only occurred through an axisymmetric contraction. Consequently, the conclusion was drawn that axisymmetric contraction devices are more sensitive to elasticity than planar configuration (Cable and Boger 1978). Due to the occurrence of vortices, the residence time of a polymer increases in this region which has an adverse effect on polymer in terms of degradation (Hertel and Münstedt 2008).

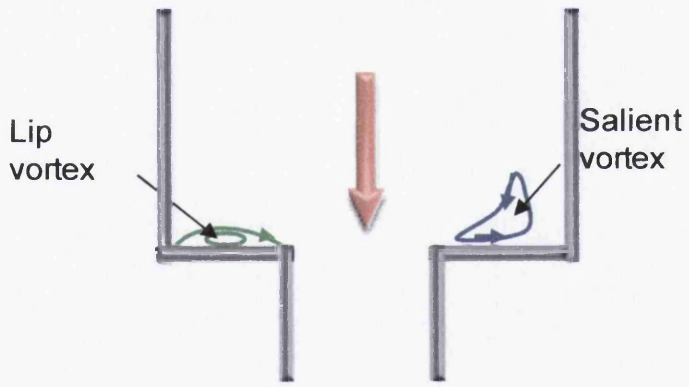

Figure 6-9: Formation of lip vortex and salient vortex

6.14 Bibliography

Abdali, S. S., Mitsoulis, E., & Markatos, N. C. (1991). Entry and exit flow of Bingham fluids. *Journal of Rheology , 36* (2), 389-407.

Aichholzer, W., & Fritz, H.-G. (1998). Rheological characterization of thermoplastic starch materials. *Starch-Starke , 50.*

Alves, M. A., Oliveira, P. J., & Pinho, F. T. (2003). Benchmark solutions for the flow of oldroyd-b and ptt fluids in planar contractions. *Journal of Non-Newtonian Fluid Mechanics , 110*, 45–75.

Alves, M. A., Oliveira, P. J., & Pinho, F. T. (2003). Numerical simulation of viscoelastic contraction flows. *2nd MIT conference on computational fluid and solid mechanics* (pp. 826-829). Elsevier, MIT, Cambridge, USA.

Alves, M. A., Pinho, F. T., & Oliveira, P. J. (2000). Effect of a high-resolution differencing scheme on finite-volume predictions of viscoelastic flows. *Journal of Non-Newtonian Fluid Mechanics , 93* (2-3), 287–314.

Arai, T., & Aoyama, H. (1963). Die Wall Restriction on Elastic Shear Deformation in Viscoelastic Flow of Polymer Melt. *Transaction of the Society of Rheology , 7*, 333-355.

Ascanio, G., & Carreau, P. J. (2002). Brito-De La Fuente E. and Tanguy P.A., Orifice Flowmeter for Measuring Extensional Rheological Properties. *The Canadian Journal of Chemical Engineering , 80*, 1189 – 1196.

Baehr, H. D., & Stephan, K. (2006). *Heat and Mass Transfer.* Berlin: Springer Verlag.

Bagley, E. B. (1957). End Corrections in the Capillary flow of Polyethylene. *Journal of Applied Physics , 28*, 624-627.

Barnes, H. A. (1995). A review of the wall slip (slip depletion) of polymer – solutions, emulsions and particle suspension in viscometers – its cause, character, and cure. *Journal of Non-Newtonian Fluid Mechanics , 56*, 221 – 251.

Barroso, E. G., Duarte, F. M., Couto, M., & Maia, J. M. (2010). High strain rate rheological charcaterizaton of low viscosity fluids. *Polymer Testing , 10* (4), 419-424.

Binding, D. M. (1988). "An Approximate Analysis for Contraction and Converging Flows. *Journal of Non-Newtonian Fluid Mechanics , 27*, 173-189.

Binding, D. M. (1993). *Contraction flows and new theories for estimating extensional viscosity. In: Collyer AA (ed) Techniques in theological measurement.* New York: Chapman & Hall.

Binding, D. M. (1991). Further considerations of axisymmetric contraction flows. *Journal of Non-Newtonian Fluid Mechanics , 41*, 27-42.

Binding, D. M., & Walters, K. (1988). On the Use of Flow through a Contraction in Estimating the Extensional Viscosity of Mobile Polymer Solutions. *Journal of Non-Newtonian Fluid Mechanics* , 291–298.

Birks, A. M., & Bagley, E. B. (1960). Flow of polyethylene into a capillary. *Journal of Applied Physics , 31*, 556-561.

Black, W. B., & Graham, M. D. (1999). Effect of wall slip on the stability of viscoelastic plane shear flow. *Physics of Fluids , 11*, 1749.

Blyler, L. L., & Hart, A. C. (1970). Capillary flow instability of ethylene polymer melts. *Polymer Engineering and Science , 10*, 193-203.

Boger, D. V., & Binnington, R. J. (1990). Circular Entry Flows of Fluid M1. *Journal of Non-Newtonian Fluid Mech. , 35*, 339–360.

Bur, A. J., Roth, S. C., & Lobo, H. (2002). Temperature Effects during Capillary Rheometry Testing. *SPE ANTEC Technical Papers , 48*, 3405 – 3409.

Cable, P., & Boger, D. V. (1978). A comprehensive experiental investigation of tubular entry flow of viscoelastic fluids; Part I. Vortex characteristics in stable flow. *AIChE Journal , 24* (5), 869–879.

Chen, Y., Kalyon, D. M., & Bayramli, E. (1992). Effects of surface roughness and chemical structure of materials of construction on wall slip behaviour of linear low

density polyethylene in capillary flow. *Journal of Applied Polymer Science , 50,* 1169-1177.

Chiba, K., Sakatani, T., & Nakamura, K. (1990). Anomalous flowpatterns in viscoelastic entry flow through a planar contraction. *Journal of Non-Newtonian Fluid Mechanics , 36,* 193–203.

Chiba, K., Tanaka, S., & Nakamura, K. (1992). The structure of anomalous entry flow patterns through a planar contraction. *Journal of Non-Newtonian Fluid Mechanics , 42,* 323–350.

Citerne, G. P., Carreau, P. J., & Moan, M. (2001). Rheological properties of peanut butter. *Rheologica Acta , 40,* 86.

Cogswell, F. N. (1978). Converging flow and stretching flow: A compilation. *Journal of Non-Newtonian Fluid Mechanics , 4,* 23-38.

Cogswell, F. N. (1972). Converging flow of polymer melts in extrusion dies. *Polymer Engineering Science , 12* (1), 64-73.

Cogswell, F. N. (1972). Measuring the extensional rheology of polymer melts. *Transaction of the Society of Rheology , 16,* 383-403.

Cogswell, F. N. (1997). *Polymer Melt Rheology, A Guide for Industrial Practice.* Cambridge: Woodhead.

Corfield, G. M., Adams, M. J., Briscoe, B. J., Fryer, P. J., & Lawrerence, C. J. (1999). A critical examination of capillary rheometry for foods (exhibiting wall slip). *Food and Bioproducts Processing , 77,* 3–10.

Cross, M. M. (1966). Analysis of Flow Data on Molten Polymers. *European Polymer Journal , 2,* 299 -307.

Cross, M. M. (1965). Rheology of Non Newtonian Fluids: A New Flow Equation for Pseudoplastic Systems. *Journal of Colloid Science , 20,* 417-437.

Dealy, J. M. (1995). Official nomenclature for material functions describing the response of a viscoelastic fluid to various shearing and extensional deformations. *Journal of Rheology , 39,* 253-265.

Evans, R., & Walters, K. (1986). Flow characteristics associated with abrupt changes in geometry in the case of highly elastic liquids. *Journal of Non-Newtonian Fluid Mechanics*, *20*, 11–29.

Evans, R., & Walters, K. (1989). Further remarks on the lip-vortex mechanism of vortex enhancement in planar-contraction flows. *Journal of Non-Newtonian Fluid Mechanics*, *32*, 95–105.

Fuller, G. G., Cathey, C. A., Hubbard, B., & Zeb, B. E. (1987). Extensional Measurements for Low-viscosity Fluids. *Journal of Rheology*, *31*, 235–249.

Genieser, L., Brown, R. A., & Armstrong, R. C. (2003). Comparison of measured centerplane stress and velocity fields with predictions of viscoelastic constitutive models. *Journal of Rheology*, *47* (6), 1331–1350.

Gevgilili, H., & Kalyon, D. M. (2001). Step strain flow: Wall slip effects and other error sources. *Journal of Rheology*, *45*, 467.

Ghanta, V. .., Riise, B. L., & Denn, M. M. (1999). Disappearance of extrusion instabilities in brass capillary dies. *Journal of Rheology*, *43*, 435.

Gibson, A. G. (1988). *Converging dies, In:Collyer AA, Clegg DW (eds) Rheological measurement.* London: Elsevier Applied Science.

Gibson, A. G. (1989). Die entry flows of reinforced polymers. *Composites*, *20*, 57-64.

Giesekus, H. (1994). *Phänomenologische Rheologie.* Springer Verlag Berling.

Halliday, P. J., & Smith, A. C. (1995). Estimation of the wall slip velocity in the capillary flow of potato granule pastes. *Journal of Rheology*.

Han, C. D., & Kim, K. U. (1971). Influence of Reservoir Diameter on the Melt Elasticity in Capillary Flow. *Polymer Engineering & Science*, *11*, 395 – 400.

Hatzikiriakos, S. G., & Deal, J. M. (1992). Wall slip of molten high density polyethylenes. II. Capillary rheometer studies. *Journal of Rheology*, *36*, 703.

Hatzikiriakos, S. G., & Dealy, J. M. (1991). Wall slip of molten high density polyethylene. I. Sliding plate rheometer studies. *Journal of Rheology*, *35*, 497.

Hay, G., Mackay, M. E., Awati, K. M., & Park, Y. (1999). Pressure and temperature effects in slit rheometry. *Journal of Rheolgy , 43*, 1099-1116.

Hay, G., Mackay, M. E., McGlashan, S. A., & Park, Y. (2000). Comparison of shear stress and wall slip measurement techniques on a linear low-density polyethylene. *Journal of Non-Newtonian Fluid Mechanics , 92*, 187.

Hertel, D., & Münstedt, H. (2008). Dependence of the secondary flow of a low-density polyethylene on processing parameters as investigated by laser-Doppler velocimetry. *Journal of Non-Newtonian Fluid Mechanics , 153*, 73-81.

Hicks, C. I., & See, H. (2010). The rheological characterisation of bread dough using capillary rheometry. *Rheologica Acta , 49*, 719-732.

Hill, D. A. (1998). Wall slip in polymer melts: A pseudo-chemical model. *Journal of Rheology , 42*, 581.

Kalyon, D. M., Yaras, P., Aral, B., & Yilmazer, U. (1993). Rheological behavior of a concentrated suspension: A solid rocket fuel simulant. *Journal of Rheology , 37*, 35.

Kang, K., Lee, L. J., & Koelling, K. W. (2005). High shear microfluidics and its application in rheological measurement. *Experiments in Fluids , 38* (2), 222–232.

Kelly, A. L., Coates, P. D., Dobbie, T. W., & Fleming, D. J. (1996). *Plast Rubb comp Proc Appl. , 25*, 313.

Kim, J. M., Kim, C., Kim, J. H., Chung, C., Ahn, K. H., & Lee, S. J. (2005). High-resolution finite element simulation of 4:1 planar contraction flowof viscoealstic fluid. *Journal of Non-Newtonian Fluid Mechanics , 129*, 23–37.

Kline, S. J. (1969). Flow Visualization, National Committee for Fluid Mechanics Films. Stanford University.

Kraynik, A. M., & Schowalter, W. R. (1981). Slip at the wall and extrudate roughness with aqueous solutions of polyvinyl alohol and sodium borate. *Journal of Rheology , 25*, 95.

Kulicke, W. M., & Clasen, C. (2004). *Viscosmetry of Polymers and Polyelectrolytes.* Berlin: Springer Verlag.

Lam, Y. C., Wang, Z. Y., Chen, X., & Joshi, S. C. (2007). Wall slip of concentrated suspension melts in capillary flows. *Powder Technology , 177*, 162-169.

Laun, H. M. (2004). Capillary rheometry for polymer melts revisited. *Rheologica Acta , 33*, 509-528.

Laun, H. M. (1983). Polymer melt rheology with a slit die. *Rheologica Acta , 22*, 171-185.

Laun, H. M., & Schuch, H. (1989). Transient elongational viscosities and drawability of polymer melts. *Journal of Rheology , 33*, 119-175.

Liang, J. Z. (2000). Estimation of die swell ratio of polymer melts from exit pressure drop data. *Polymer Testing , 20*, 29-31.

Ma, C. Y., White, J. L., Weissert, F. C., & Isayev, A. I. (1985). Flow patterns in elastomers and their carbon-black compounds during extrusion through dies. *Rubber Chemistry and Technology , 58*, 815-829.

Mackay, M. E., & Astarita, G. (1997). Analysis of entry flow to determine elongation flow to determine elongation for properties revised. *Journal of Non Newtonian Fluid Mechanics , 70*, 219.

Mackay, M. E., & Henson, D. J. (1998). The effect of molecular mass and temperature on the slip of polystyrene melts at low stress levels. *Journal of Rheology, 42*, 1505-1517.

Martin, P. J., & Wilson, D. I. (2005). A critical assessment of the Jastrzebski interface condition for the capillary flow of pastes, foams and polymers. *Chemical Engineering Science , 60*, 493-502.

Metzner, A. B., & Metzner, A. P. (1970). Stress levels in rapid extensional flows of polymeric fluid. *Rheologica Acta , 9*, 174-181.

Meyvis, T., Smedt, S. D., Stubbe, B., Hennink, W., & Demeester, J. (2001). On the release of proteins from degrading dextran methacrylate hydrogels and the correlation with the rheologic properties of the hydrogels. *Pharmaceutical Research , 18*, 1593.

Miller, J. C. (1963). Swelling behaviour in extrusion. *Polymer Engineering and Science , 3*, 134-137.

Mitsoulis, E., Hartzikiriakos, S. G., Christodoulou, K., & Vlassopoulos, D. (1998). Sensitivity Analysis of the Bagley Correction to Shear and Extensional Rheology. *Rheologica Acta , 37*, 438-448.

Mooney, M. (1931). Explicit formulas for slip and fluidity. *Journal of Rheology , 2*, 210-222.

Mourniac, P. H., Agassant, J. F., & Vergnes, B. (1992). Determination of the wall slip vrlocity in the flow of a SBR compound. *Rheologica Acta , 31*, 565-574.

Münstedt, H., Schmidt, M., & Wassner, E. (2000). Stick and slip phenomena during extrusion of polyethylene melts as investigated by laser-Doppler velocimetry. *Journal of Rheology , 44*, 413.

Münstedt, H., Schwetz, M., Heindl, M., & Schmidt, M. (2001). Influence of molecular structure on secondary flow of polyolefin melts as investigated by laser Dopppler velocimetry. *Rheologica Acta , 40*, 384-394.

Nigen, S., & Walters, K. (2002). Viscoelastic contraction flows: comparison of axisymmetric and planar configurations. *Journal of Non-Newtonian Fluid Mechanics , 102*, 343-359.

Oliveira, P. J., & Pinho, F. T. (1999). Plane contraction flows of upper-convected Maxwell and Phan-Thien-Tanner fluids as predicted by a finite-volume method. *Journal of Non-Newtonian Fluid Mechanics , 88*, 63–88.

Padmanabhan, M., & Macosko, C. W. (1997). Extensional Viscosity from Entrance Pressure Drop Measurements. *Rheologica Acta , 36*, 144–151.

Phillips, T. N., & Williams, A. J. (2002). Comparison of creeping and inertial flow of an Oldroyd-B fluid through planar and axisymmetric contractions. *Journal of Non-Newtonian Fluid Mechanics , 108* (1–3), 25–47.

Plastics - Determination of the fluidity of plastics using capillary and slit die rheometers. (n.d.). ISO 11443 .

Raiford, W. P., Quinzani, L. M., Coates, P. J., Armstrong, R. C., & Brown, R. A. (1989). LDV mesasurements of viscoelastic flow transition in abrupt axisymmetric contractions: Interaction of inertia and elasticity. *Journal of Non-Newtonian Fluid Mechanics , 32*, 39–68.

Rajagopalan, D. (2000). Computational analysis of techniques to determine extensional viscosity from entrance flow. *Rheologica Acta , 39*, 138 – 151.

Ramamurthy, A. V. (1986). Wall slip in viscous fluids and influence of materials of construction. *Journal of Rheology , 30*, 337.

Rao, M. A. (2007). *Rheology of Fluid and Semisolid Food* (2nd Edition ed.). Springer.

Rides, M., & Allen, C. (2001). Effect of die geometry on shear viscosity and entrance pressure drop determination by capillary extrusion rheometry. NPL Report MATC(A) 56.

Rides, M., & Allen, C. (1999, March). Extensional flow properties of polymer melts using converging flow methods, Measurement Good Practice Guide No. 16. National Physical Laboratory.

Rides, M., & Allen, C. (2006). Slip flow measurement by capillary extrusion rheometry, Measurement Good Practice Guide No. 90. National Physical Laboratory.

Rodd, L. E., Cooper-White, J. J., Boger, D. V., & McKinley, G. H. (2007). Role of the elasticity number in the entry flow of dilute polymer solutions in micro-fabricated contraction geometries. *Journal of Non-Newtonian Fluid Mechanics , 143*, 170-191.

Rodd, L. E., Scott, T. P., Boger, D. V., Cooper-White, J., & Mckinley, G. H. (2005). The inertio-elastic planar entry flow of low-viscosity elastic fluids in microfabricated geometries. *Journal of Non-Newtonian Fluid Mechanics , 129*, 1–22.

Rodríguez-Gonzalez, F., & Pérez-González, J. (2009). Marin-Santibánez and de Vargas L., Kinematics of the stick-slip capillary flow of high-density polyethylene. *Chemical Engineering Science , 64*, 4675-4683.

Rothstein, J. P., & McKinley, G. H. (1999). Extensional flow of a polystyrene Boger fluid through a 4:1:4 asisymmetric contraction/expansion. *Journal of Non-Newtonian Fluid Mechanics*, *86*, 61-88.

Rothstein, J. P., & McKinley, G. H. (2001). The axisysmmetric contraction – expansion: the role of extensional rheology on vortex growth dynamics and the enhanced pressure drop. *Journal of Non-Newtonian Fluid Mechanics*, *98*, 33-63.

Sedláček, T., Zatloukal, M., Filip, P., Boldizar, A., & Saha, P. (2004). On the effect of pressure on the shear and elongational viscosities of polymer metls. *Polymer Engineering & Science*, *44*, 1328 – 1337.

Shaw, M. T. (1986). An Alternative Analysis of Capillary Rheomter Data. *SPE Technical Papers*, *32*, 707-710.

Shirakashi, M., Ito, H., & James, D. F. (1998). LVD measurement of the flow field in a constantextensional-rate channel. *Journal of Non-Newtonian Fluid Mechanics*, *74*, 247.

Smits, A. J., & Lim, T. T. (2000). Flow Visualisation: Techniques and Examples. Imperial College Press.

Sombatsompop, N. (1999). A survey of rheological properties of polymer melts in capillary rheomters. *Progress in Rubber and Plastics Technology*, *15* (1), 47-68.

Sombatsompop, N., & Wood, A. K. (1997). Flow analysis of natural rubber in a capillary Rheometer: Part 2. Flow patterns and die entrance velocity profile in the die. *Polymer Engineering & Science*, *37* (2), 281-290.

Townsend, P., & Walters, K. (1994). Expansion flows of non-Newtonian. *Chemical Engineering Science*, *49*, 749-763.

Tremblay, B. (1989). Estimation of the Elongational Viscosity of Polyethylene Blends at High Deformation Rates. *Journal of Non-Newtonian Fluid Mechanics*, *33*, 137–164.

Valle, D. D., Tanguy, P. A., & Carreau, P. J. (2000). Characterization of Extensional Properties Fluids Using an Orifice Flowmeter. *Journal of Non- Newtonian Fluid Mechanics , 94*, 1–13.

Walters, K. (1992). Recent Development in Rheometry. (pp. 16-23). Proceedings of 11th International Congress on Rheology.

Walters, K., & Webster, M. F. (1982). On dominating elastico-viscous response in some complex flows. *Proceedings of the Royal Society of London. Series A , 308*, 199-218.

Wang, S. Q. (1999). Molecular Transitions and Dynamics at Polymer / Wall Interfaces: Origins of Flow Instabilities and Wall Slip. *Advances in Polymer Science, 138*.

Willenbacher, N., Hanciogullari, H., & Wagner, H. G. (1997). High Shear Rheology of Paper Coating Colors – More Than Just Viscosity,. *Chemical Engineering Technology , 20*, 557 – 563.

Winter, H. H. (1977). Viscous dissipation in shear flows of molten polymers. *Advances in Heat Transfer , 13*, 205-267.

Xue, S., Phan-Thien, N., & Tanner, R. I. (1998). Numerical investigations of Lagrangian unsteady extensional flows of viscoelastic fluids in 3-D rectangular ducts with sudden contractions. *Rheologica Acta , 37*, 158–169.

Xue, S., Phan-Thien, N., & Tanner, R. I. (1998). Three dimensional numerical simulations of viscoelastic flows through planar contractions. *Journal of Non-Newtonian Fluid Mechanics , 74*, 195–245.

Yamaguchi, M. (2001). Flow instability in capillary extrusion of plasticized poly(vynl chloride). *Journal of Applied Polymer Science , 82*, 1277-1283.

Yang, A., Salminen, P., Vervoort, S., Endres, I., & Bachmann, H. (2011). Role of Extensional Viscosity in Paper Coating. *Applied Rheology , 21*, 23607.

Yoshimura, A., & Prudhomme, R. K. (1988). Wall slip corrections for couette and parallel disk viscometers. *Journal of Rheology , 32*, 53.

7 Methodology

This chapter gives a brief overview of all commercial paints and the devices that were involved in obtaining the necessary rheological parameters. The scientific background of the commercial paints and Rotational Rheometer, the Capillary Break up Rheometer and the Capillary Extrusion Rheometer has been provided in greater detail in the previous chapters 3 to 6.

7.1 Data of Commercial Paints

The samples used for this research project were based on polyester resin. The 4 colours of the paints were used to label the samples. Therefore, samples were named as white paint, green paint, red paint and dark red paint. The main paints which were compared at the end had the same resin. Furthermore, all commercial paints used the dibasic ester solvent. Also the pigment sizes used for all paints were below 5 μm. A number of pigment types were used to obtain the correct end colour of the paint. The pigment to binder ratios ranged between 49% to 60%. The Table 4-1 below provides information about the commercial paints.

Paint	Weight Solids (%)	Pigment to Binder	Solvents	Pigments	Pigment size
White	60%	1.14	Dibasic Ester	Titanium Oxide TiO_2, Iron Oxide Alpha FeOOH and Iron Oxide Fe_2O_3	<5 μm
Green	49%	0.33	Dibasic Ester	Cu-phthalocyanine $C_{32}H_{16}N_8Cu$, Titanium Oxide TiO_2 and Chromium Titanium Yellow $(Ti, Sb, Cr)O_2$	<5 μm
Red	53%	0.55	Dibasic Ester	Iron Oxide Fe_2O_3, Chromium Titanium Yellow $(Ti, Sb, Cr)O_2$ and Titanium Oxide TiO_2	<5 μm
Dark Red	54%	0.48	Dibasic Ester	Iron Oxide Fe_2O_3 , Iron Oxide Alpha FeOOH and Titanium Oxide TiO_2	<5 μm

Table 7-1: Commercial paint specifications

7.2 Experimental Methods

7.3 Strain Controlled Rotational Rheometer (ARES)

Figure 7.1 shows the strain controlled rotational rheometer, Advance Rheometric Expansion systems (ARES), and illustrates the set up from the plate, paint and cone. ARES is fitted with a force/ torque rebalance transducer, 10K STD with a range from 10 to 10000 gcm which operates at a frequency of 79.6 Hz. Temperature can be controlled in a range from -5°C to 90°C, with a fluid circulation bath using fluid consisting of 20% ethylene glycol and 80% water. A cone and plate geometry (50 mm diameter, angle 0.04 rad) was fitted with a solvent trap made of polymer to prevent loss of volatiles from the sample.

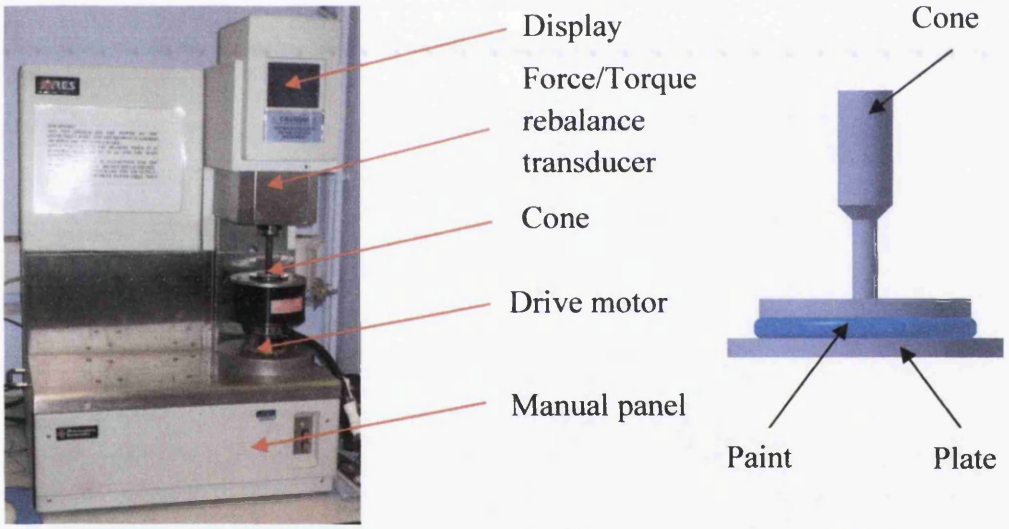

Figure 7-1 a) Strain controlled rotational rheometer ARES is depicted in operation and b) a sketch of the plate, paint and cone.

The test sample is located between the fixed cone and the moveable plate. The plate rotates at the set strain rate and whilst the cone measures the flow resistance of the sample (TA Instrument 2003).

7.3.1 Overview of experimental procedures used for ARES

Strain controlled rotational rheometer was used to undertake

- Dynamic amplitude sweep procedure,
- Frequency sweep procedure,
- Transient response controlled deformation procedures
- Steady state flow curve procedure.

7.3.1.1 Test parameters for the dynamic amplitude sweep procedure

Strain from 0.02% to 200% was applied as a sinus shaped with frequency of 1Hz. 21 data were collected over the strain range applied to determine the onset of the structure breakage. (see Figure 8-1)

7.3.1.2 Test parameters for the frequency sweep procedure

Once the linear elastic domain (LVR) was determined by the dynamic amplitude sweep procedure, a frequency sweep at a strain of 0.1% chosen in this area was applied in the angular frequency range between 0.1 s^{-1} and 100 s-1(see Figure 8-2).

7.3.1.3 Test parameters for the transient response controlled deformation procedures

A pre-shear rate of 0.5 s^{-1} was used for 210s to erase the shear history of the sample followed by a recovery time with zero shear rate for 1000s. Afterwards, data was collected under a single constant shear rate applied for 3600s. The outcome of this procedure can be seen in Figure 8-3 with 8 different shear rates of 0.5 s^{-1}, 0.7 s^{-1}, 1 s^{-1}, 2 s^{-1}, 5 s^{-1}, 7 s^{-1}, 10 s^{-1} and 20 s^{-1}. A similar test using only shorter shear rate time of 3s and 210s and applying 4 different shear rates of 0.1 s^{-1}, 1 s^{-1}, 5 s^{-1} and 10 s^{-1} was undertaken (see Figure 8-4). By varying the recovery times from 1s to 4000s

and applying the shear rate of 0.5 s^{-1} for 210s, a different rheological view could be achieved (see Figure 8-5). A time delay of 1000 s and 2000s and shear rates of 0.1 s^{-1}, 0.2 s^{-1}, 0.5 s^{-1}, 0.7 s^{-1}, 1 s^{-1}, 2 s^{-1}, 5 s^{-1}, 7 s^{-1} and 10 s^{-1} were also used as input parameters for this procedure (see Figure 8-6). Lastly the following stages pre –shear rate of 1 s^{-1} for 1000s and shear rate of 10 s^{-1} for 3s were used (see Figure 8-15 and Figure 8-18).

7.3.1.4 Steady state flow curve procedure

A pre strain rate of 0.1 s^{-1} and followed by step strain rates ranged from 0.1 s^{-1} to 100 s^{-1} were loaded to the sample for 90 s for each strain rate step (see Figure 8-8, Figure 8-14, Figure 8-16, Figure 8-17 and Figure 11-1).

7.4 Stress Controlled Rotational Rheometer (AR2000)

The Rheometer AR2000 is equipped with a ultra low inertia drag up motor, thrust bearing, radial bearing optical encoder, normal force transducer and a peltier plate. The geometries cone and plate with different sizes (4cm, 5cm and 6cm with an angle of 2°) were available as accessories. The tailored solvent trap for these devices could be used to cover the geometry.

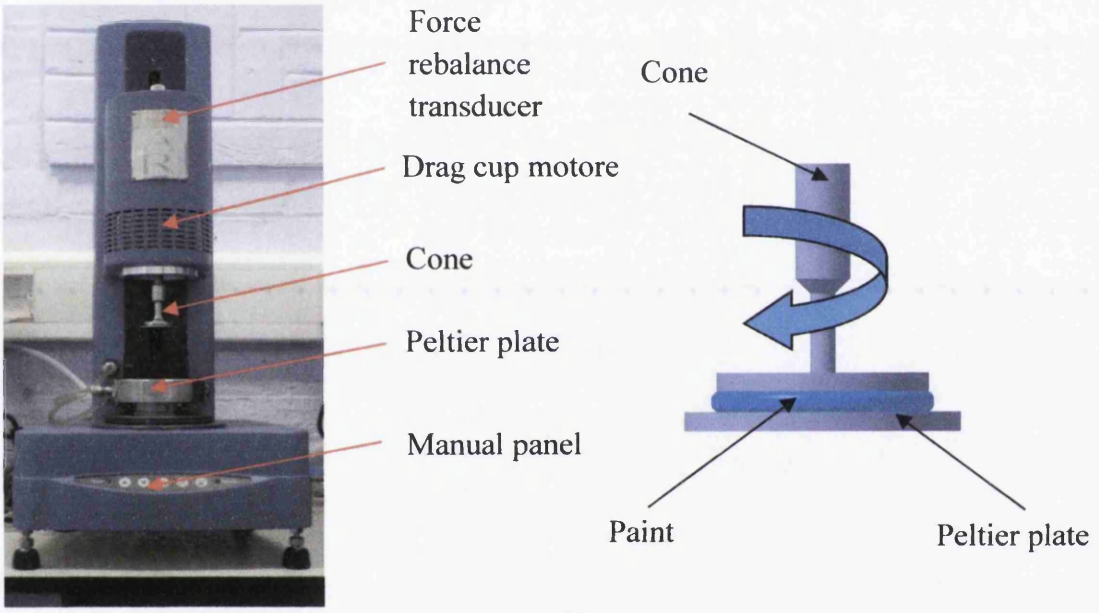

Figure 7-2 a) Stress controlled rheometer ARES 2000 and the geometry b) a sketch of the plate, paint and cone

The torque range available for the controlled stress selection was between 0.1 μN and 200 mN.m and the range for the controlled rate was between 0.03 μN and 200 mN.m. The Rheometer AR 2000 was able to apply an angular velocity in a range from 10^{-8} to 300 rad/s for a controlled stress option and from 10^{-4} rad/s to 300 rad/s for a controlled rate option. The tests were run with a displacement resolution of 0.04 μrad. Temperature could be controlled with an accuracy of +/- 0.1°C which was made possible through the peltier plate which allowed a temperature to be set between -40 °C and 200°C with a heating rate of 20°C / min (TA Instrument 2007).

7.4.1 Overview of experimental procedures used for AR2000

Strain controlled rotational rheometer was used to undertake

- Steady state flow curve procedures
- Creep procedures.

7.4.1.1 Steady state flow curve procedures

A 4cm cone was used to apply a wide range of step shear stresses (from 0.1 Pa to 300 Pa) on the samples. The time interval for each step was 90s (see Figure 8-8 and Figure 8-14). Additional investigation was carried out with the same test parameter and supplementary cone geometries of 5cm and 6cm (see Figure 8-10). Pre-shear stress of 0.5935 Pa was included with the previous test procedure which gave different outcome (see Figure 8-13).

7.4.1.2 Creep procedures

No pre-shearing and maintaining a constant stress of 0.562 Pa for 7000s was the first set up parameters (see Figure 8-10). Using a pre-stress of 0.1 Pa for method (a) and pre-sharing of 2 Pa for method (b) for 1000s followed by a recovery time of 1000s. Afterwards, a shear stress of 0.1 Pa was applied for both methods for 3500s (see Figure 8-11). Additional creep experiments were carried out with a pre-stress of 0.7 Pa for 1000s followed by rest time of 1000 Pa before applying a stress of 0.7 Pa for 3500s. Furthermore, a pre-stress of 2 Pa for 1000s was applied to the sample followed by a rest time of 1000s before the data was collected at a constant stress of 0.7 Pa (see Figure 8-12).

7.5 Surface Tensionmeter

The static surface tension of the paint was measured with a Krüss K8 static surface tension meter, using a platinum Du Noüy ring with a radius of 9.545 mm and a circumference of 59.97 mm. Surface tension could be measured with an accuracy of 0.1 mN/m .

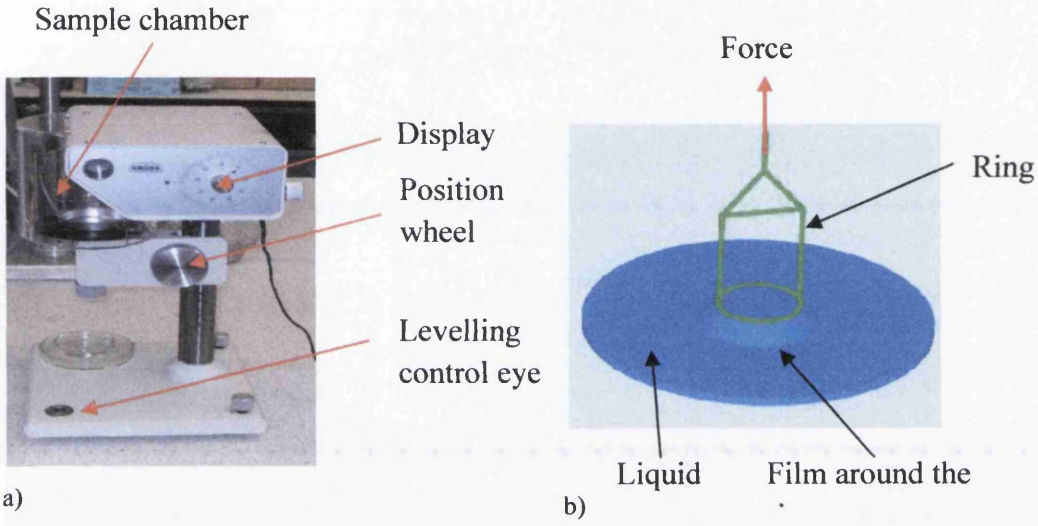

Figure 7-3 a) Surface tension meter and b) Du Noüy ring in contact with liquid

Before the surface tension was measured, the platinum ring was immersed into the liquid. This ring was then slowly moved upwards leaving a film around the ring when it was positioned above the surface of the liquid. This film would eventually break during the upwards movement of the ring under tension. Afterwards, the value of the surface tension could be read off the display (Krüss 2007).

7.6 Capillary Break Up Rheometer

Material with a shear viscosity between 10 mPas and10^6 mPas can be measured with a Capillary break up rheometer, which is able to apply a Hencky strain up to $\varepsilon = 10$. This is achieved by a linear motor with a resolution of 0.02mm. The filament decay was monitored with a Class 1 laser micrometer using a wavelength of 780nm, produced by a power of 1.7mW. Its resolution was 0.01mm. The systems response time was 10ms. The material could be heated from 0 °C to 80°C.

Photron MC1 high speed (at 1000 frames / second) with a Nikon 14 – 85 f 2.8 – 4 lens has been used to record high resolution digital videos and pictures of a filament break up. The size of the videos and pictures was cropped to 512 x 512 pixels with a pixel resolution of 26.2 μm.

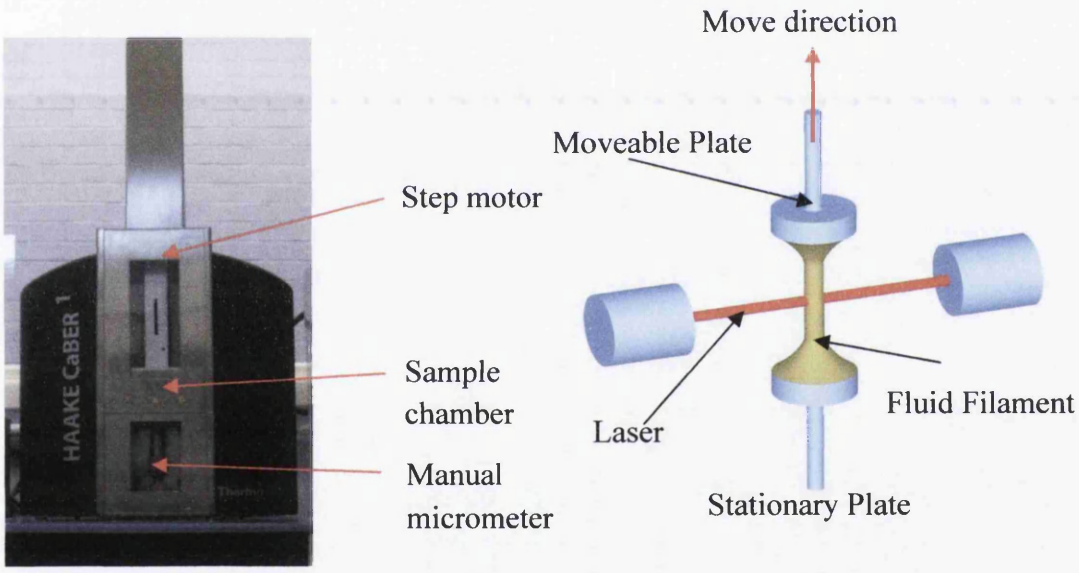

a) b)

Figure 7-4 a) Capillary break up rheometer and b) the main parts

The sample was held between the two plates see figure 7.4 b). A sudden uniaxal step strain was applied which caused the sample to stretch. Subsequently, the diameter of the filament would decay which was monitored by a laser (Caber 2002).

7.6.1 Overview of experimental procedures used for CaBER

A selection of exponential strike times of 20ms, 45ms, 90 ms with fundamental rates of 0.01 s^{-1}, 100 s^{-1} and 1000 s^{-1} as well as a linear strike times of 20ms, 50ms, 70ms, 90ms and 110ms were used for the separation of the plates whose initial distance was 2 and the final heights were either 6.98mm, 9.34mm or 11.5mm (more details can be found in chapter 8).

7.7 Capillary Extrusion Rheometer

The most important components of the capillary extrusion rheometer are the piston, transducer, capillary die and barrel made of EN40 nitrided steel which has a bore size of 15 mm. The temperature can be controlled in a range of -60°C to 500°C. The pressure transducer in a range of ~0.7 bar to ~20000 bar can be used. The maximal piston speed is 500m/min.

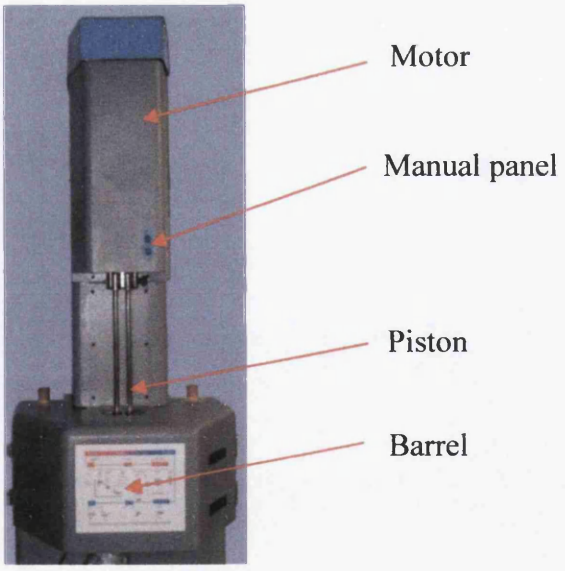

Figure 7-5: Capillary extrusion rheometer with two pistols.

The sample is confined within the bore and is pushed by the piston through the capillary die (see Figure 6-2). The maximum driving force is 150 KN with a maximum speed of 200 mm/min attainable, with an uncertainty of less than 0.1% achievable (DrRheology 2010).

7.7.1 Overview of experimental procedures used for capillary extrusion rheometer

The piston pushed the paint through dies with hole diameter of 0.5 mm and the length of either 5 mm, 20 mm and 50 mm or with hole diameter of 1 mm and the length of either 5 mm, 20 mm, 47 mm with a speed ranging from 0.471 mm/min to 333.346 mm/min.

7.8 Bibliography

A Thermo Electron Company, CaBER 1 Quantifying the extensional properties of fluids (2002), Available: http://www.campoly.com/documents/CaBER.pdf, [Access: 12 August 2008]

DRRheology P9000 Ltd, Equipment Multi rheometers, Available: http://www.drrheology.com/rheometer.htm , Access: 10 October 2008]

Krüss GmbH, "Measuring Techniques – an overview", Available: www.kruss.info/index.php?content=http%3A//www.kruss.info/techmiques/methods_overview_e.thml, [Accessed April 13, 2007]

Ta Insturment, Our Prouduct-Rheology Rheology AR 2000 http://www.tainstruments.com/product.aspx?siteid=11&id=35&n=1, Access: 15 February 2007]

TA Instruments – Walters LLC, Rheometrics Series User Manual, PN 902-30026 Rev D, 2003

8 Results of rotational rheometer

8.1 Scope of rotational experiments

Industrial paints belong to the group of very complex fluid causing a huge challenge for the rheologist to obtain trustworthy rheological data. As a consequence, the primary aim of this work was to find the optimal test procedure to characterise the rheological behaviour of the polyester resin based paints. Due to the limitation of the project time, the paint with the TiO_2 pigment was used for carrying out a thorough investigation because of its low production performance and quality in the past. Stress controlled and strain controlled rheometer were employed to get a better understanding of the behaviour of the industrial paint. The first step was to carry out an angle oscillation, one of whose values from the linear region had been used for undertaking a frequency sweep. Transient, steady state step flow and creep experiments enhanced the understanding. Once established, the test procedure that had been developed for the white paint experiments was used for all the paints systems.

8.2 Rotational Experiments on white paint

8.2.1 Experimental Design

Controlled deformation experiments to obtain flow curves and step rate were conducted on a strain controlled Rheometer ARES (TA instruments) assembled with a dual range (10/100 gcm) force balance transducer. Temperature control was maintained via a fluid circulation bath. A cone and plate geometry (50 mm diameter, angle 0.04 rad) was employed.

Further investigations running creep, dynamic amplitude sweep, amplitude oscillatory and flow curve experiments were carried out with a stress controlled rheometer, AR2000 Rheometer (TA Instruments), using different sizes of cone and

plate geometry (4cm,5cm and 6cm with an angle of 2°) at 20 ± 0.1 °C. A solvent trap was used in each experiment to prevent drying of the sample.

8.2.2 Initial rheological evaluation

Firstly, a dynamic strain amplitude sweep was carried out with a strain controlled rheometer whose results are shown in Figure 8-1. A linear response can be observed for strain amplitudes up to 0.1% strain. Above this critical strain, the storage modulus, *G'*, monotonically decreases. Applying a constant strain of 0.1, the outcome of the frequency sweep can be seen in Figure 8-2. The data collected span the elastic plateau region through to the transient region. In the plateau, G' is approximately 3 times higher than G''. The larger value of G' in comparison to G'' indicated the pronounced elastic properties off the paint. Due to experimental limitations, the terminal region was inaccessible because the data were below the range of the torque transducer (4 x 10^{-3} gcm.). Therefore, the value of relaxation time could not be determined.

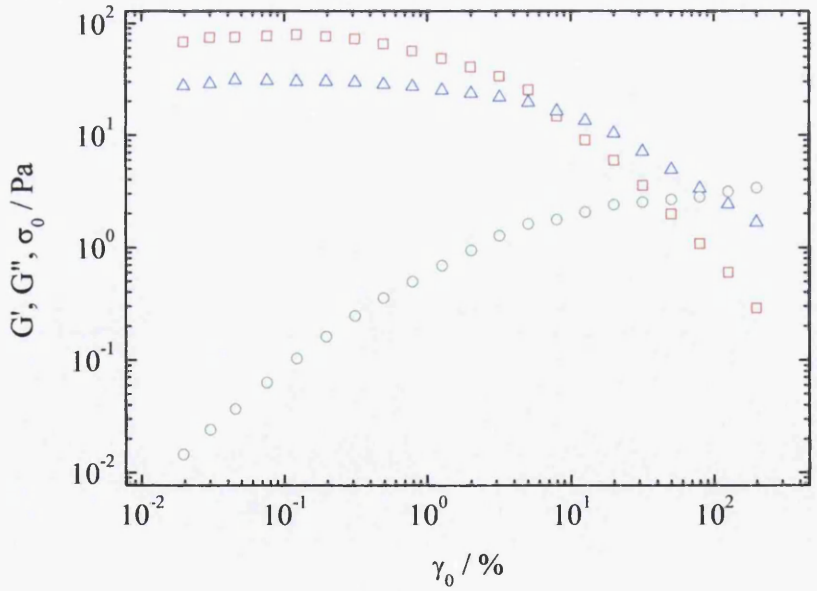

Figure 8-1: Dynamic amplitude sweep for the paint obtained using controlled deformation Rheometer. G' (□),G'' (△), σ_0 (○)

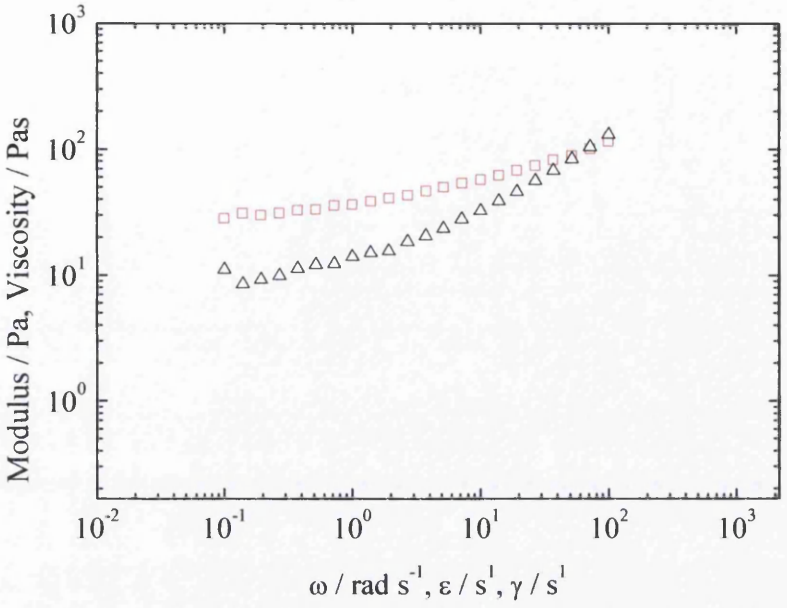

Figure 8-2: Oscillatory behaviour of white paint using controlled deformation rheometer. G' (□),G'' (△)

8.2.3 Transient response controlled deformation rate

Transient response controlled deformation rate experiments provide useful information about the elasticity and time dependent behaviour. The imposed shear rate was varied from 0.1 s^{-1} to 20 s^{-1}, the results are presented in Figure 8 3. In order to get reproducible data, pre shearing the sample was required to eliminate loading and shear histories. Each experiment involved the application of the shear rate for 3600s which was collected within a linear spaced of 350 data points (torque). These outcomes are characterised by a pronounced elastic response at short times evidenced by an overshoot in the stress growth function. However, the rate of data collection was insufficient to fully resolve the maxima in σ^{+} (t). Consequently, experiments were repeated with a faster sampling rate (200 data points within 210s and followed by fastest sampling with 350 data points collected over 3s). In all cases, a steady state shear stress was eventually attained at long times (~250s) verifying the samples stability and also indicates that evaporation of the solvent was negligible.

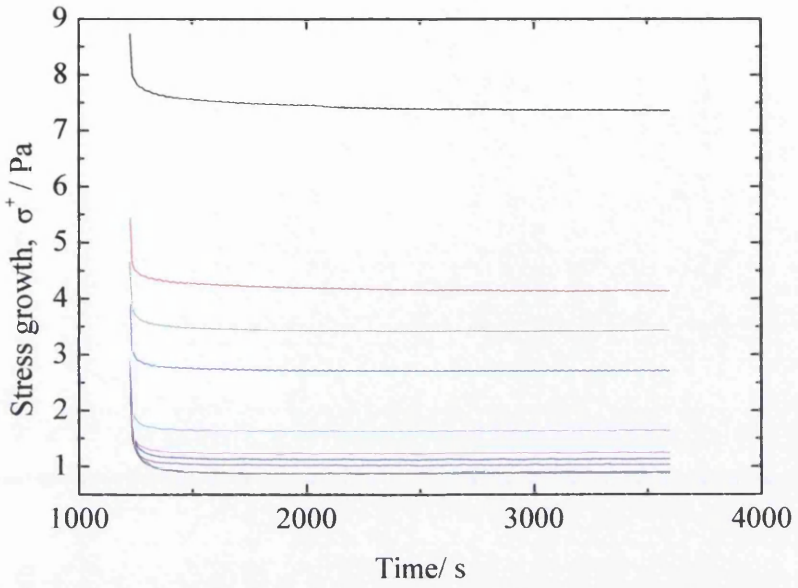

Figure 8-3: Temporal evolution of the shear stress growth function for different applied shear rates ((----) 0.5 s^{-1} , (-----) 0.7 s^{-1} , (----) 1 s^{-1}, (----) 2 s^{-1} (-----) 5 s^{-1} (-----) 7 s^{-1} , (-----) 10 s^{-1} , (-----) 20 s^{-1}), the sample was pre-sheared at 0.5 s^{-1} for 210s, followed by 1000s at rest before collecting data (350 data points collected over 3600s).

Initial consideration of the outcome from an imposed shear rate of 0.1 s^{-1} seems to suggest that the stress growth function shows simple monotonic (no overshoot) increase as seen in Figure 8-4. Further experiments with a higher deformation rate than 0.1 s^{-1} show a transition region with pronounced overshoot. This phenomenon seems to occur when the Weissenberg number $W_i = \lambda\dot{\gamma}$ exceeds a critical value of unity (Lubrecht and Dalmaz 2003). The characteristic relaxation time, λ, expressing the microstructral rearrangement, can be derived by the crosspoint from G' and G'' in the transition to flow region. The stress overshoot of entangled polymers due to sudden applied shear rate analogous to the Weissenberger number W_i >1 is reported in many published documents (Boukany and Wang 2009, Ferry 1980, Osaki et al. 2000a, 2000b, 2000c).

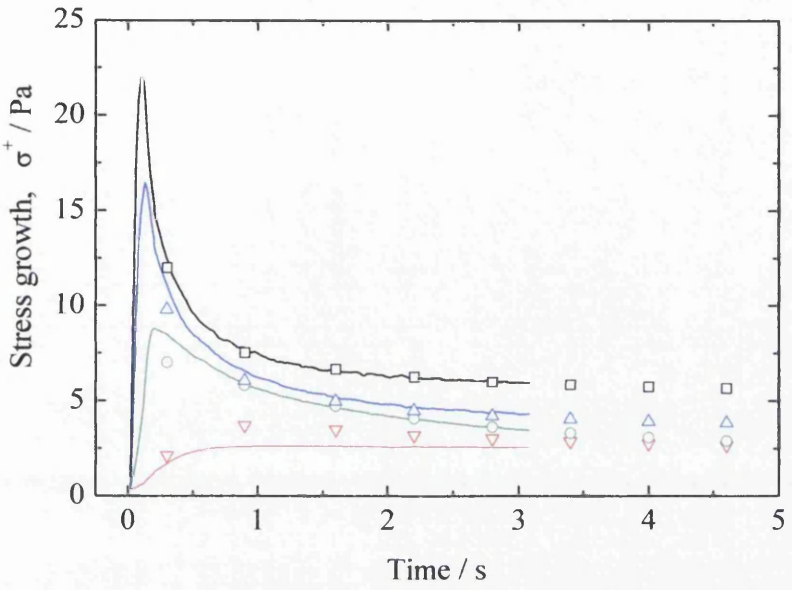

Figure 8-4 Temporal evolution of the stress growth function over a much shorter experimental duration for different imposed shear rates (350 data points collected over 3s) shown as solid lines. The open symbols are from experiments run over a much longer duration (200 data points collected over 210s). Preshearing and sample equilibration conditions as for Figure 8-3, (—▽) shear rate = 0.1 s^{-1} (— ○) = shear rate 1 s^{-1}, (—△) shear rate 5 s^{-1}, and (—□) = 10 s^{-1}.

The transient response of the paint on the sudden imposition of shearing was found to be significantly time dependent. The resulting maximum stress overshoot, σ_{max}, was highly sensitive to the previous recovery time, t_{delay}, in which the shear rate was set to 0. This thixotropic behaviour was manifested by obtaining an increase in maximal peak stress, σ_{max}, with increasing recovery time, t_{delay}. An incomplete structural recovery was detected at shorter delay times. This is illustrated in Figure 8-5a where the transient response ($\sigma^{+}(t)$) following delay times of 10s, 100s, and 1000s are compared. A series of experiments were subsequently performed to ascertain the time required for complete structural recovery, i.e. where there was no further noticeable increase in σ_{max} with t_{delay}. A similar approach was employed by Stratton and Butcher (1973) who found also out that the magnitude of the stress overshoot increased with the increased delay time. The evolution of σ_{max} with increasing t_{delay} was well described by the Equation 8-1 which encompasses a characteristic time for thixotropic recovery, τ (Stratton and Butcher 1973). The

attainment of a stress peak plateau after a critical recovery time was also detected in ink (Pangalos et al.1985). In Figure 8-5b, total structure recovery is achieved at a delay time of appr. 2000s. A good agreement between the model formula 8.1 (Stratton an Butcher 1973) was possible with the parameters of 1Pa for σ_{start} and 5.126 Pa for σ_∞ and 3000 for the relaxation time τ.

$$\sigma^{+}_{(tdelay)}(t)=\sigma_\infty-[(\frac{1}{e^{(\frac{t_{delay}}{\tau})}})(\sigma_\infty-\sigma_{start})] \qquad \text{Equation 8-1}$$

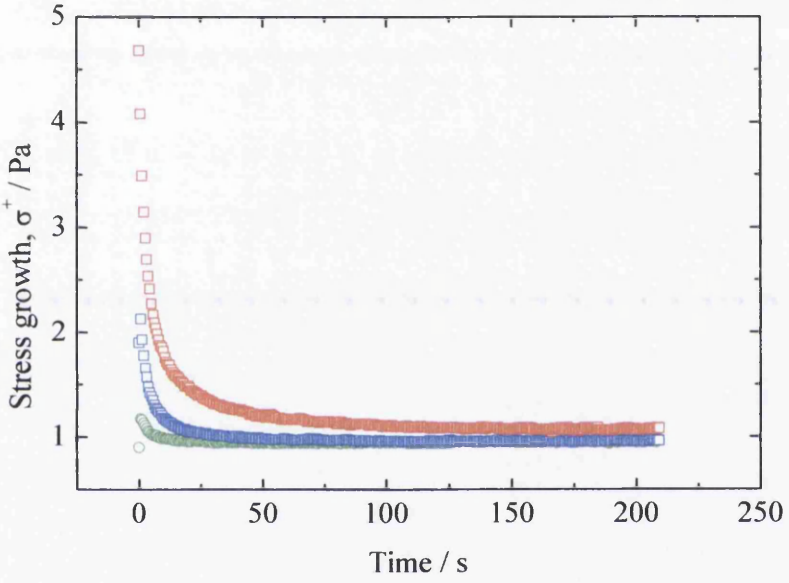

a)

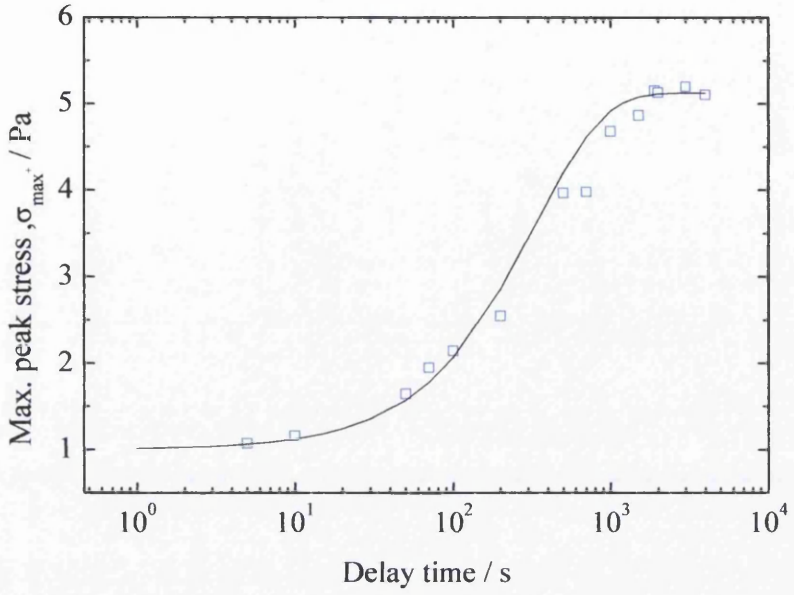

b)

Figure 8-5: a) Illustrating the dependency of stress growth on delay time. The sample was sheared for 210s at 0.5 s^{-1}, allowed to rest for times of 10s (○), 100s (□) and 1000s (□). b) Demonstration of thixotropic recovery after a commanded delay time which is highlighted by the increase in the stress overshoot. The sample was pre-sheared for 210s at 0.5 s^{-1} followed by relaxation times ($\dot{\gamma} = 0$) ranging from 1s to 4000s, the peak in the stress overshoot on re-shearing at 0.5 s^{-1} was recorded.

Once the timescale for thixotropic recovery of 2000s had been established, the effect of the magnitude of the imposed deformation rate on the transient stress growth could be re-examined. Figure 8-6 illustrates the variation in the maximum in the stress growth function, σ_{max}, on imposition of strain rates between 0.1 and 10 s^{-1}. The increase in σ_{max} with applied shear rate appeared to follow a power law, i.e.$\sigma_{max} = a\dot{\gamma}^n$. The power law curve fitted well onto the transient peak data with a rest time of 2000s when the power law constant value a = 8.33 and the exponent value n=0.45 were inserted. For the steady state data at 1000s and rest time of 2000s, the constant parameter of 1.52 and the exponent value of 0.35 were used to obtain a very good fit.

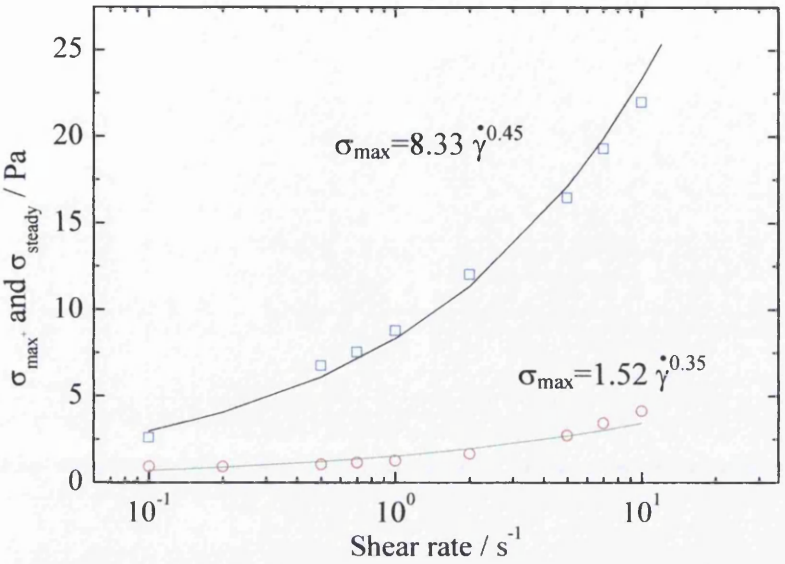

Figure 8-6: Variation in the magnitude of the peak in the stress growth, σ_{max}, and of steady state stress measured at 1000s, σ_{steady}, as function of the imposed shear rate. The samples were pre sheared for 210s followed by a time delay (2000s for σ_{max} and for σ_{steady}) before collecting the data. In both cases, the data showed a high correlation to a power law function (□ for σ_{max}, ○ for σ_{steady}).

A further comparison of the transient response can be made using dimensionless variables. This is shown in Figure 8-7 where the stress growth function, σ^+, is normalised with respect to the corresponding steady state stress, σ_{steady}, achieved after a long timescale and plotted as a function of strain, γ,.

The presence of an overshoot is now illustrated by a value of $\sigma^+/\ \sigma_{steady}$ which is greater than 1. This response even occurred at the lowest applied shear rate of 0.1 s^{-1}. Transient elastic (overshoot) behaviour of this type is usually the result of the insufficient rearrangement of micro-structure within a short time scale (Barnes 1997).

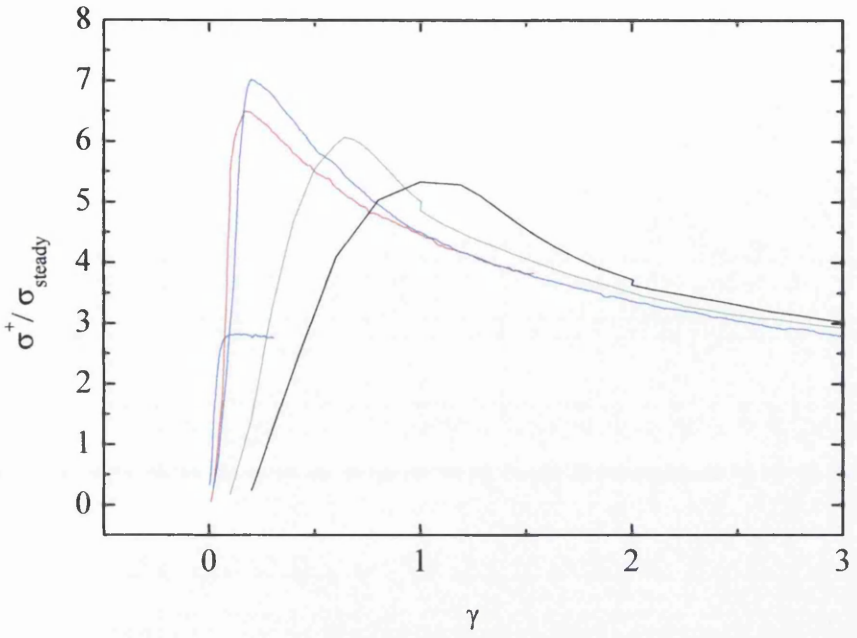

Figure 8-7: Temporal evolution of the shear stress growth function following the sudden imposition of different shear rates expressed as dimensionless variables Shear rate (—) 0.1 s^{-1}, (—) 0.5 s^{-1}, (—) 1, (—) 5 s^{-1} and (—) 10 s^{-1}

8.2.4 Transient response controlled stress

In this subchapter, the focus is chiefly on the experimental data obtained from the flow curves and creep tests. The outcome of the flow curves [$\eta(\sigma)$] generated by three different approaches – stress flow experiments using the controlled stress instrument (AR2000), shear rate flow experiments obtained using the controlled deformation and data taken from the steady state regime in transient start shear experiments (ARES, Figure 8-3) are depicted in the Figure 8-8.

In each case, the intrinsic structure of the paint breaks down from low shear rate to higher shear rate perceivable through the viscosity decrease. However, the viscosity at low applied stress and the apparent yield stress measured on the controlled stress instrument were significantly higher than that measured in controlled deformation experiments. On the other hand, the data from all test procedures was in good agreement from a critical shear stress of 300 Pa onwards.

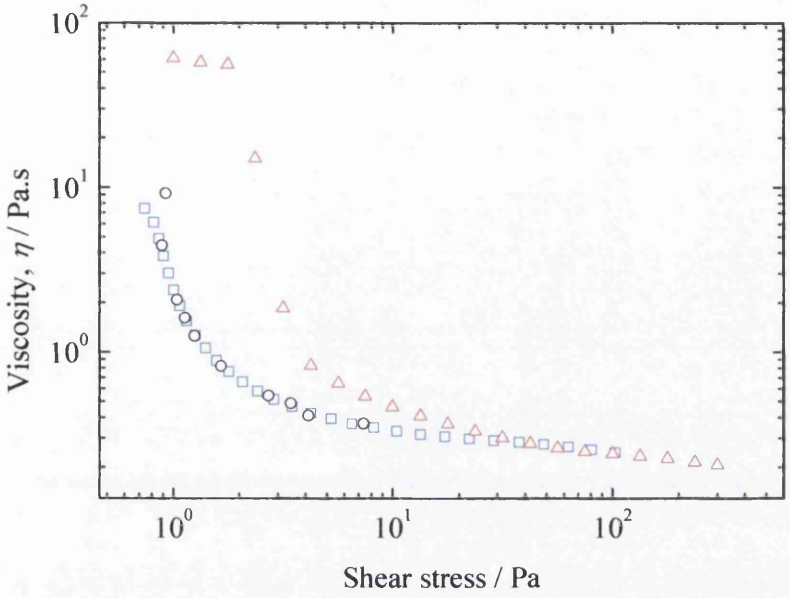

Figure 8-8: Comparison of flow curves from controlled stress and controlled deformation experiments: (△) controlled stress data (average of data in Figure 8-9) (□) controlled strain rate data; (○) steady state data (controlled rate) obtained from transient experiment (Figure 8-3).

The results from the controlled stress instrument were verified for three different geometries (40mm, 50mm, 60mm cone and plate, 2° angle), which demonstrates the absence of wall depletion effects (slip). (Figure 8-9)

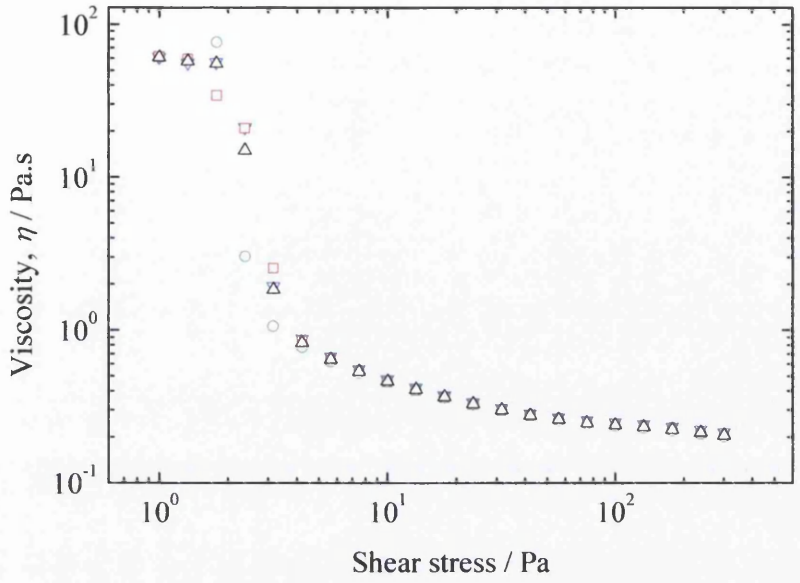

Figure 8-9: Comparison of flow curves obtained from average data points with cone diameter of (○) 4cm, (△) 5cm and (□) 6cm: (▽) represents the average value for all diameters. Coincidence of the data suggested an absence of wall depletion (slip effect)

The data from the shear rate flow experiment and the corresponding steady state values from transient experiments were in good agreement. This raised questions as to the accuracy of the viscosities measured in stepped stress experiments and suggested that the transient response to an applied stress (creep) should be investigated.

Firstly, the reproducibility of the paint's response to an applied stress was investigated (Figure 8-10). In these experiments, no pre-shearing of the sample was performed prior to the creep experiment. Figure 8-10a shows data from two separate experiments (The sample has been changed between runs) using an applied stress of 0.562 Pa. There are two features worth mentioning. Firstly, there was a clear lack of reproducibility, run-to-run. This suggested a strong influence of the samples shear history on the creep behaviour. As a result of the highly thixotropic nature of the paint, one may speculate that slight differences in loading or compression which could have led to a variety of 'non-equilibrium' microstructures. Consequently, a distinctly different response occurred after imposing a given shear stress. Secondly,

there was a pronounced structural transition from an initial viscoelastic deformation to viscous flow, associated with the attainment of a critical strain. This critical strain was again not reproducible run-to-run, in the absence of pre-shearing, and it was associated with an abrupt increase in shear rate, presumably underpinned by a loss of microstructural connectivity in the sample. Another possible reason for the different critical strain values was the effect of gravity on the sample which caused an enhancement in slip effect for long term experiments (Barnes 1995). Figure 8-10b resulted from similar experiments, with a lower applied stress (0.1 Pa) conducted over a similar duration. Again, the lack of reproducibility was noted during the run-to-run. The shapes of both curves were identical. A similar deformation rate appeared to be attained after ~ 3000s, but the absolute value of the strain varied considerably. An incipient structural transition appeared again in both sets of experience outcome at around ~6000s, characterised by an increase in the apparent strain rate.

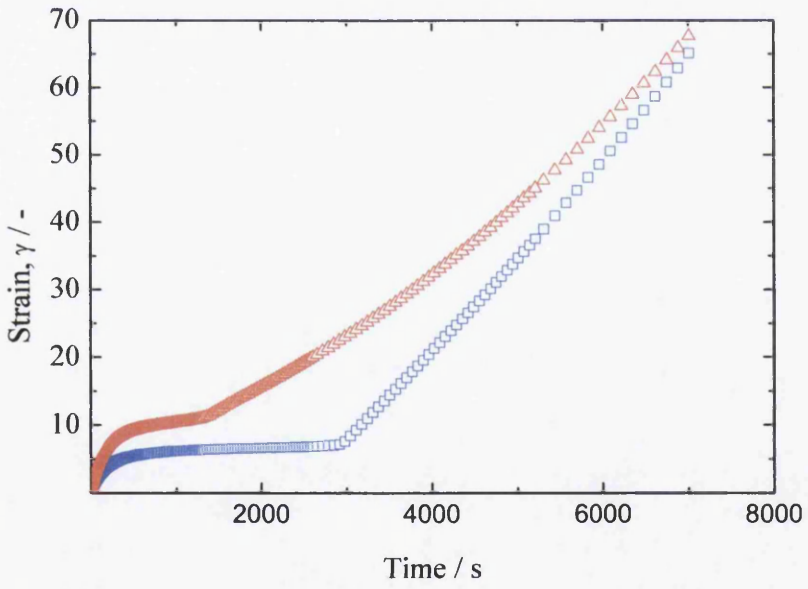

Figure 8-10a Creep data ((□) trial 1, (▽) trial 2)) showing the lack of reproducibility in the absence of preshearing following sample loading. Imposed stress = 0.5623 Pa. Note the pronounced structural breakdown and transition to viscous flow.

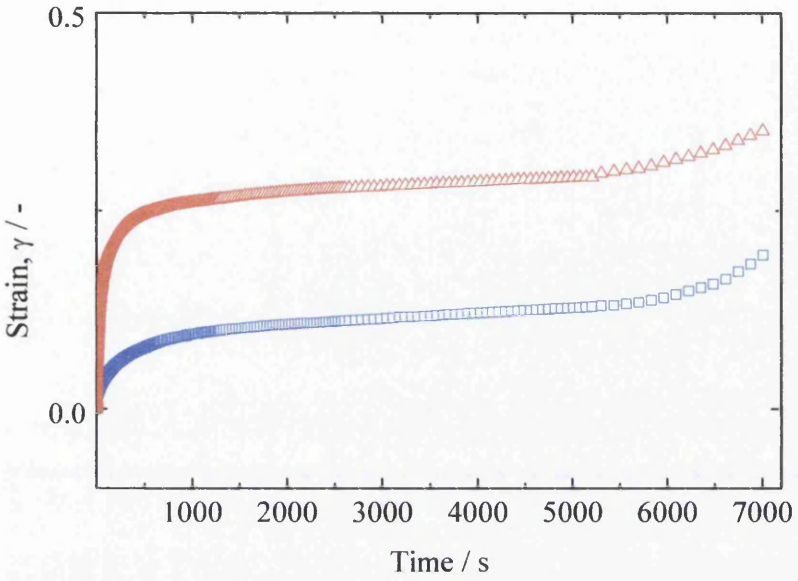

Figure 8-10 b: Creep data ((□) trial 1, (▽) trial 2)) showing the lack of reproducibility in the absence of pre-shearing the sample and allowing full structural recovery. Imposed stress = 0.1 Pa. Note the pronounced structural breakdown and transition to viscous flow.

A further series of transient experiments including pre- shearing were then conducted on samples to achieve a reproducible material response. Different magnitude of pre-shearing and a constant structural recovery time were applied prior to collecting the transient data. Figure 8-11a shows three repeat runs of the same experiment, involving the imposition of a relatively low pre-shear stress (0.1 Pa) for 1000s, followed by a recovery for a further 1000s. Most notably, there was again a lack of reproducibility between repeat experiments. In particular, the time at which structural breakdown and transition to viscous flow occurred varied from ~ 500s to ~ 2500s. The critical strain attained at this point was relatively invariant in this case. Clearly, the pre-shearing conditions applied here (stress/time) were insufficient to develop sufficient deformation in the sample to effectively 'erase' the system's shear history. Again, this was consistent on consideration of Figure 8-8, as the pre-shear stress was well below the apparent yield stress of the paint, hence clearly insufficient to cause significant structural breakdown. In contrast, Figure 8-11b, shows a similar set of experimental data in which a larger pre-shear stress was employed (2 Pa, 1000s). A recovery period of 1000s was again allowed, followed by the monitoring of the creep

in the fluid on application of a shear stress of 0.1. In this case, reproducibility of the data was very good over three repeated experiments, indicating that the sample history effects were fully 'erased' in pre-shearing. This caused a sufficient degree of breakage of the inner structure to have the same start condition for all samples. The transition from structure breakdown to viscous started at around 2500s with a critical strain of around 0.7.

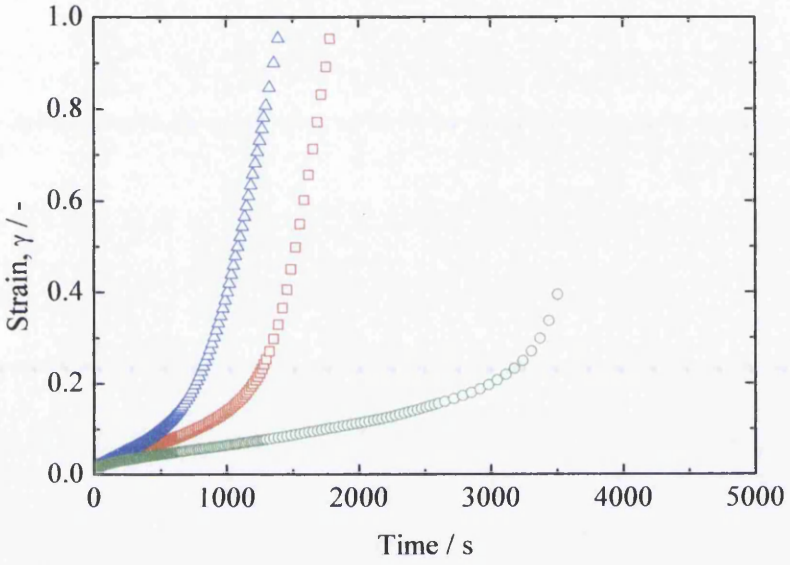

a)

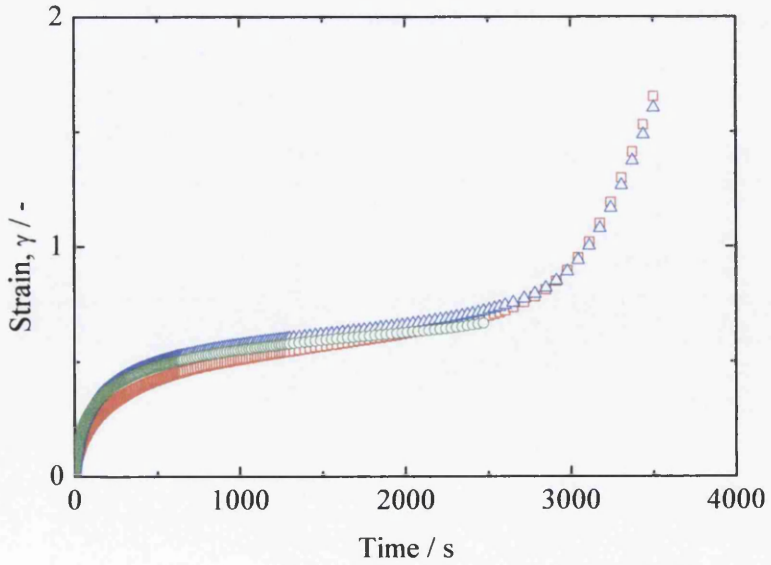

b)

Figure 8-11: Influence of preshear stress on subsequent transient (creep) response. (a) 0.1 Pa preshear for 1000s, 1000s delay time followed by creep at an imposed stress of 0.1 Pa – data from 3 separate experiments (b) 2 Pa preshear for 1000s, 1000s delay time followed by creep at an imposed stress of 0.1 Pa – data from 3 separate experiments. Note the lack of reproducibility obtained with preshearing at a lower stress.

The influence of shear history was totally eliminated in the subsequent creep experiment using a much higher shear stress. A nearly perfect overlapping of creep data from different runs with shear stress of 0.7 Pa and 2 Pa is shown in Figure 8-12a and Figure 8-12b. There was not any further sign of the structure breakdown to viscous transition in the time window from 0 to 3500s.

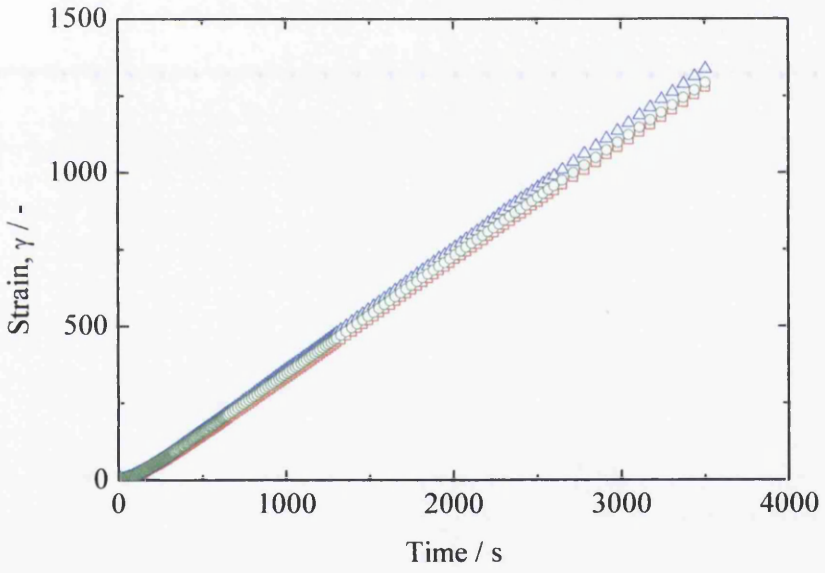

a)

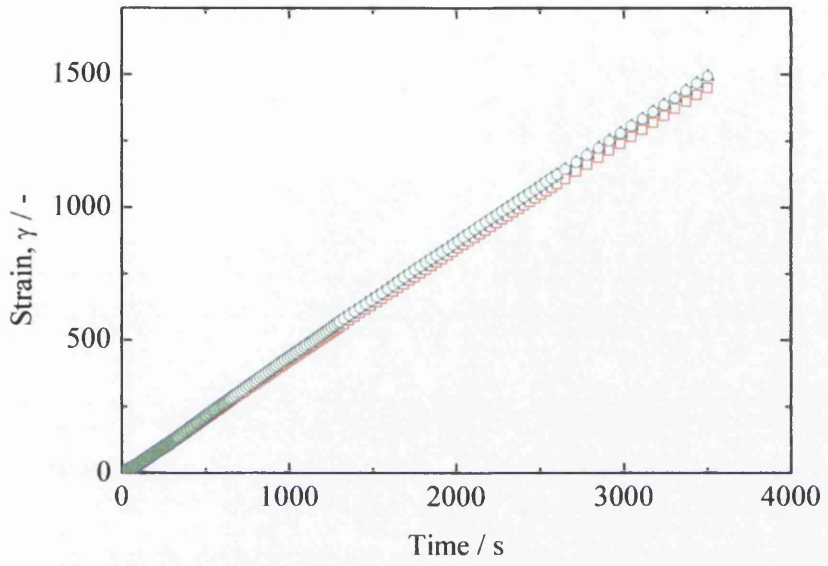

b)

Figure 8-12: Influence of preshear stress on subsequent transient (creep) response. (a) 0.7 Pa preshear for 1000s, 1000s delay time followed by creep at an imposed stress of 0.7 Pa – data from 3 separate experiments (b) 2 Pa preshear for 1000s, 1000s delay time followed by creep at an imposed stress of 0.7 Pa – data from 3 separate experiments. Note the good reproducibility obtained with preshearing

The understanding obtained from the transition experiments enabled the flow procedure to be optimised for stress controlled rheometer. By using a higher pre-shear stress of 0.5935 Pa for the stress controlled rheometer, the flow curve (Figure 8-13) which was previously obtained with a pre-shear rate by the stress controlled rheometer was now shifted upwards to a steady state which was verified by the flow curve from a strain controlled rheometer.

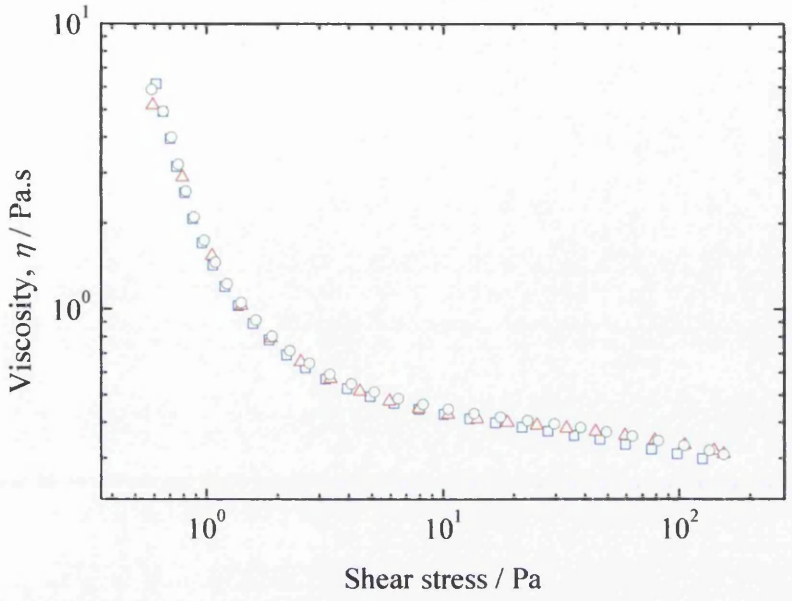

Figure 8-13: Steady state flow curves obtained under different experimental conditions: (□) stepped shear rate data (ARES) with steady state verified independently in transient experiments (○) 'stepped shear rate' experiments (AR2000) using feedback loop control (△) stepped stress experiments (AR2000) with initial pre-shearing close to apparent yield stress.

8.3 Conclusion for the white paint

A paint with TiO_2 pigments was characterised by using stress and strain controlled rheometers. Initially, a discrepancy between the flow curves was observed which prompted a deeper research activity. Additional outcomes from transient experiments indicated the complexity of the sample and its sensitivity to historical handling. By applying a pre-stress of 0.5935 Pa, the effect of history was eradicated. Surprisingly, the occurrence of slip effect was not detected with different geometries sizes techniques. Therefore it seems that the paint has a very good adhesion to steel. The main benefit from this study was that by undertaking two different experimental procedures it was possible to obtain with confidence a flow curve with greater accuracy. Otherwise an incorrect conclusion may be drawn.

8.4 Rheological investigation of different paints using rotational rheometer

In this study, two paints were chosen with respect to the production performance. One of the paints was pigmented with red pigment, which shows an extremely good performance with respect to line speed. In contrast, the paint pigmented a with dark red pigment slowed down the production line and even generated fat edges probably due to its rheological properties. A flow curve procedure and transient response controlled deformation rate experiments were used to provide useful information about the rheological parameters.

8.4.1 Experimental results

Step flow procedure was carried out with stress controlled and strain controlled rheometers. Each sample underwent either a pre-shear of 0.1 s^{-1} or pre-stress of 0.1 Pa to eliminate any loading histories. Afterwards the actual flow procedure directly started which involved applying a stress in the range from 0.1 Pa to 500 Pa or a strain rate in the range from $0.1s^{-1}$ to $500s^{-1}$. Figure 8-14a shows the viscoelastic flow behaviour of a dark red paint with yield stress. Similar to the white, there are variations between flow curve results leading to the conclusions that the paint was sensitive to shear history. The flow curve obtained by stress controlled rheometer with a pre shear rate of $0.1s^{-1}$ showed good agreement with the flow curve provided by strain controlled rheometer using shear rate of $0.1s^{-1}$. From the previous experience reported above, it can be assumed that loading history was sufficiently deleted at strain rate of $0.1s^{-1}$. In contrast to the dark red paint, the red paint behaves as a Newtonian fluid and does not have any yield stress (Figure 8-14b). Measuring approximately provided a viscosity value of 0.35 Pas for the Newtonian red and viscosity values of 0.4 Pas for yield stress red (collected from infinite – shear Newtonian Plateau).

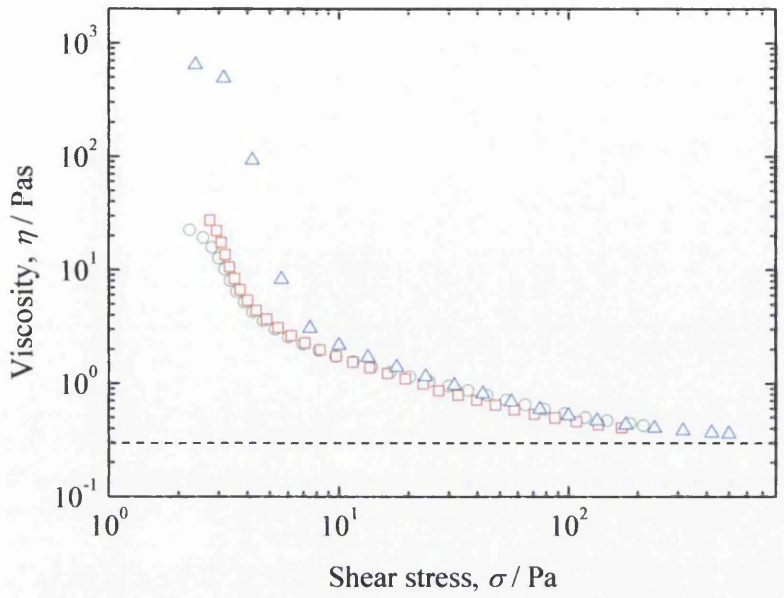

a)

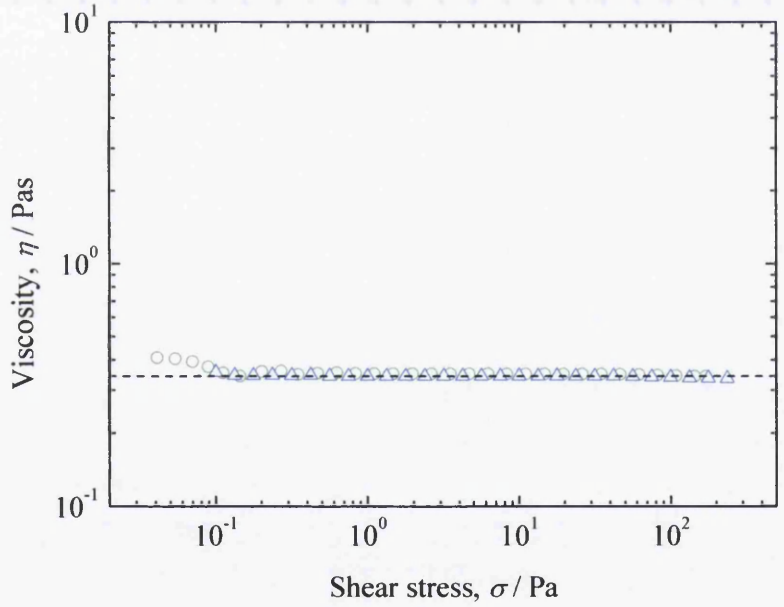

b)

Figure 8-14: Comparison of flow curves generated under different conditions and devices. a) Illustrating average data from stress controlled rheometer using pre strain rate of $0.1s^{-1}$ (○) and pre shear stress of 0.1 Pa (△) as well as average data from strain controlled rheometer (□) for dark red paint. b) Showing average data from stress controlled rheometer using pre strain rate of $0.1s^{-1}$ (○) and pre shear stress of 0.1 Pa (△).

8.4.2 Step rate

Supplementary information about the elasticity and thixotropy were delivered from the step strain rate experiments whose results are depicted in Figure 8-15a and Figure 8-15b. There were two main procedures namely break down and build up (Barnes 2000). In this research, the break down procedure was chosen only for the well performing paint (Newtonian red) and the bad performing (yield stress dark red). Before the structural underwent a break down, the influence of shear history was totally eliminated by shearing the sample at the rate of 1 s^{-1} for 1000 s. Afterwards, the structural destruction induced by an applied shear rate of 10 s^{-1} was observed in a time frame of 3s using a 350 data point resolution. The overshoot occurred at yield stress for the dark red and indicated an elastic effect, whereas the Newtonian red's response was as a classic viscous fluid which did not accumulate elastic energy and therefore the red paint might have a higher line speed performance. The structure or flocculation of the dark red paint started breaking down until its equilibrium was achieved. The red paint showed a faster respond to the sudden shear rate increase which was noticeable by reaching the equilibrium stage almost immediately.

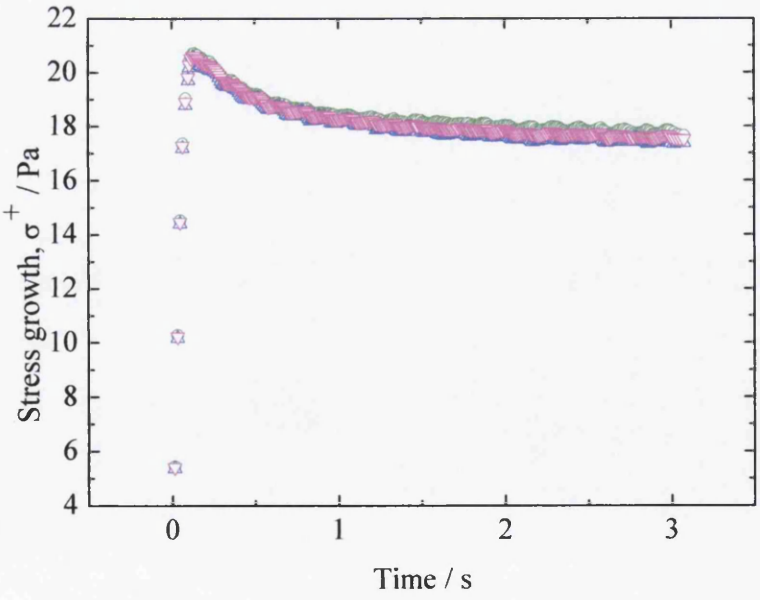

a)

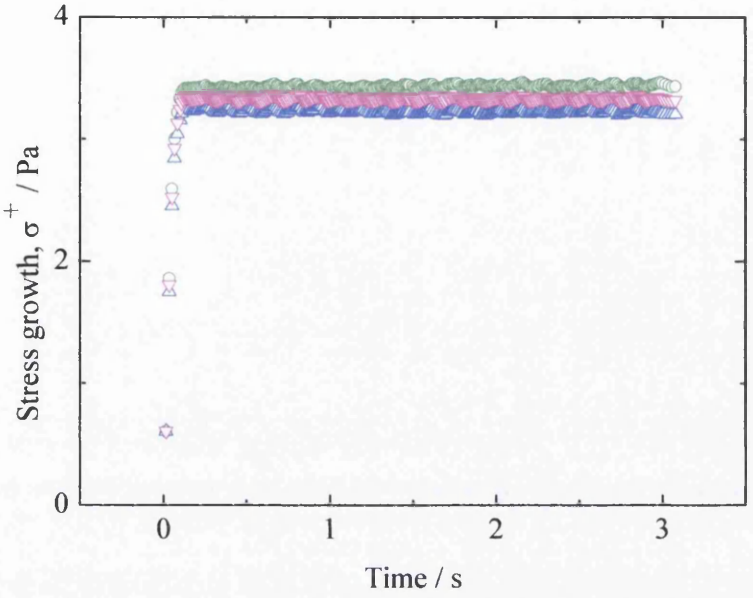

b)

Figure 8-15: Demonstration of the good repeatability of each paint ((a) yield stress red and (b) Newtonian red) imposed a shear rate of $10\ s^{-1}$.

Similar to the coil coating process, the paint undergoes a high strain rate over a very short time. After leaving the nip between the rotating rolls, the paints are nearly Newtonian at high shear rates or behave like a thixotropic yield – stress fluids. The defect which occurs between the rolls will normally be levelled out after the nip (Cohu and Magnin 1995). However, if the degree of the defect occurring in the nip is sufficiently high then the levelling process of the paint will not be able to compensate for uneven surfaces before the curing oven in the time scale. This can lead to paint defects. The type of initial flow response to the sudden strain rate (absent or present of overshoot) might dictate the degree of the defect on the substrate after the nip due to the elastic effects. Since the dark red paint seems to have a bad coating performance in terms of line speed and fat edge occurrence in comparison to the red paint, it is interesting to see the difference in their response to the step strain procedure. Two features might be the reason for the different performance. The first reason is the stress peak showing an elastic behaviour and the second reason is the thixotropic behaviour leading to a delay in the decrease in the viscosity. Looking into the microstructure, the dark red paint has iron oxide alpha

pigments whereas the red paint does not have this type of pigments. This type of pigments might help to build a more structured system with a thixotropic behaviour.

8.5 A rheological comparison of paints with different pigments

The steady–state viscosity data of paints (white, green, red and dark red) are illustrated in Figure 8-16 for a wide range of shear stresses. Three out of four tested paints were highly stress-thinning in the ranges from 0.5 Pa to 200 Pa. whereas the red paint exhibited Newtonian behaviour in the range from 0.05Pa to 200 Pa. The strong shear thinning effect of yield stress red reflected the strong intrinsic complex network of the paint. White and green exhibited shear thinning behaviours in a much milder form. The majority of the viscoelastic paints did not have a zero shear Newtonian plateau, giving a hint of yield stress and solid like behaviour (Yziquel et al. 1999 and Page et al. 2002). In these tests, the solvent based paints showed mostly shear thinning behaviour. In 1919, yield stress behaviour of paint was firstly mentioned by Bingham (1922) as shown by the dark red paint. Compared with the results from other commercial paints, the values of infinite shear viscosity of these results were very similar to the results of some of the coating paints (0.3Pas – 0.5 Pas) provided by López and Rosen (2002).

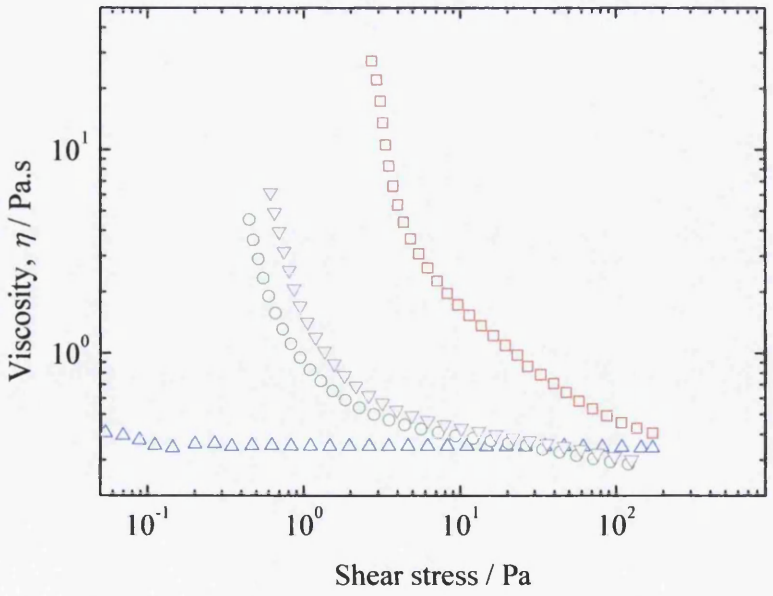

Figure 8-16: Comparison between Newtonian paint and shear thinning paints with pronounced yield stress. Paint samples are (○) green, (▽) white, (□) dark red and (△) red.

Among the test samples, the dark red had the most pronounced yield stress with a value of 2.2 Pa followed by white, 0.65 Pa and green, 0.42 Pa. The values of the yield stresses were abstracted from the Herschel Bulkley model (Figure 8-17) incorporating the Newtonian, Power law and Bingham equations and can be mathematically expressed as:

$$\sigma=\sigma_y+\eta_{HB}\dot{\gamma}^n \qquad \text{Equation 8-2}$$

Whereas σ_y is the yield stress, η_{HB} is a constant viscosity value and n stands for rate index.

The three parameter rheological model from Herschel- Bulkley was selected because it models more accurately the rheological behaviour of a yield stress fluid in comparison to the Bingham model (Hemphill et al. 1993).

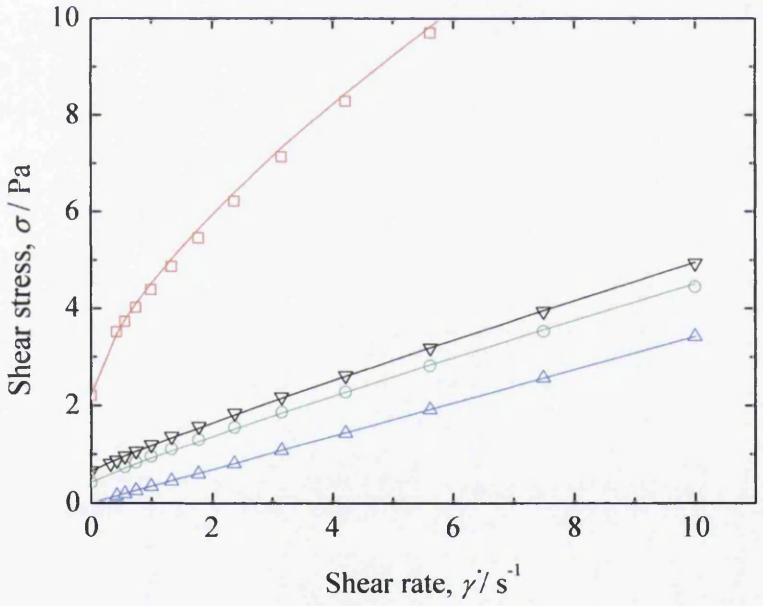

Figure 8-17: Herschel Buckley fits on all samples delivering the yield stresses for (○) green 0.42Pa, (▽) white 0.65 Pa, (□) dark red 2.2 Pa and (△) red 0 Pa.

A structure or flocculation breakage occurs in order of longest duration for dark red paint, white paint and the green paint. For the Newtonian red paint, the indication of a breakage did not appear on the graph due to the fast rearrangement of the

microstructure. By increasing the shear rate to a distinctive value, the likelihood that the red paint responds with the overshoot (indication of elasticity) would be high.

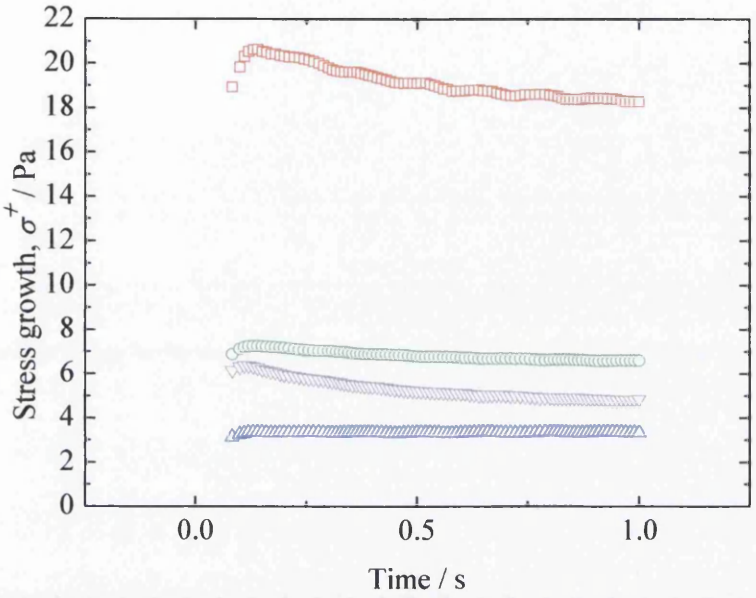

Figure 8-18: Scaling of stress growth as a function of time for paints pigmented with red (△), white (▽), green (○) and dark red (□). Using sudden imposed strain rate of 10 s^{-1}.

Samples	Solid Content
White	59%
Green	46%
Red	50%
Dark Red	50%

Table 8-1: Data of the solid content of paint in wt%

Ascanio et al. (2006) reported that with four suspensions made with kaolin clay and aqueous solution the elastic modulus obtained by strain amplitude sweep was always higher with higher solid content coatings over a wide range of strain amplitude. In these cases, this statement is not reflected in the step procedure as seen in table 8.1. Yield stress red had one of the lowest solid content and appeared to have a higher elastic overshoot than the counterpart of Newtonian red with the same solid content. The green consisting of 46 wt% of solid content had a slight overshoot whereas

Newtonian red with higher solid content had no elasticity. Therefore other ingredients must also play an important role to influence the flow behaviour.

8.6 Conclusion

The well performing red paint exhibited Newtonian behaviour whereas the worst performing dark red paint posed the highest yield stress among the paint samples and showed shear thinning behaviour. Consequently, it appears that the yield stress is a possible influencing factor for reducing the production performance by 10.4% in comparison to the red paint performance. Additionally, the degree of elasticity of the paint may also play an important role for classifying a well performing paint. A highly structured paint maintains a nearly constant flow resistance through the nip resulting in a different behaviour than a low structured paint. As a consequence, a significant defect in the nip may generate which takes more time to level out. Therefore the line speed used for the dark red is lower than the red paint to allow it more time to rectify the defect. Fat edges were only reported with dark red paint and this may be caused by high yield stress. However, more investigations need to be done to draw a final conclusion.

In terms of the relationship between rotational findings and the commercial paint specification (see Table 7-1) the following discussions can be initiated. The weight solids content does not show any relationship whether a paint is shear thinning or behaves Newtonian since the Newtonian paint posseses a weight solid content of 53% and the shear thinning green paint has a lower weight solids content of 49%. Green paint has the same type of binder. The red paint has a higher pigment to binder ratio in comparison with the dark red and green paint. The question rose whether the binder dictates the shear thinning behaviour up to a specific pigment to binder ratio. The counterargument can be shown by using the pigment to binder ratio from the white paint. However, in this case the promotion of flocculation is much higher due to the higher pigment to the binder ratio and the weight solid content. A definitive answer to this assumption can be shown when the pigment to binder ratio from dark red paint and green paint will be increased and tested afterwards. Another difference between the red paint and dark red paint is the type of pigments used. The amount of

iron oxide and titanium oxide in red paint is nearly the same as in the dark red paint. The only difference is that red paint has chromium titanium yellow pigment and the dark red paint has iron oxide alpha pigment. It would be interesting to undergo a further analysis on the basis of the both types of pigments. A subsequent question about the dependency of iron oxide alpha on flow behaviour might be answered by reducing the amount of the iron oxide alpha. If the degree of shear thinning behaviour reduced or even disappeared this would indicate that this pigment has a strong influence on the flow behaviour.

8.7 Bibliography

Ascanio, G.; Carreau, P. J.; Tanguy, P. A. (2006). High-speed roll coating with complex rheology fluids, Experiments. *Experiments in Fluid*, *40*, 1-14.

Barnes, H. A. (2000). *A Handbook of Elementary Rheology.* Aberystwyth: Institution of Non-Newtonian Fluid Mechanics University of Wales.

Barnes, H. A. (1995). A review of the slip (wall depletion) of polymer solutions, emulsions and particle suspensions in viscometers: its cause, character, and cure. *Journal of Non-Newtonian Fluid Mechanics*, *56*, 221-251.

Barnes, H. A. (1997). Thixotropy-a review. *Journal of Non-Newtonian Fluid Mechanics*, *70*, 1-33.

Bingham, E. C. (1992). *Fluidity and Plasticity.* New York: Mc Graw-Hill.

Boukany, P. E., & Wang, S.-Q. (2009). Universal scaling behaviour in startup shear of entangled linear polymer melts. *Journal of Rheology*, *53*, 1-13.

Ferry, J. D. (1980). *Viscoelastic Properties of Polymers.* New York: Willey.

Hemphill, T., Campos, W., & Pilehvari, A. (1993). Yield-Power Law Model More Accurately Predicts Mud Rheology. *Oil and Gas Journal*, *91* (34), 45-50.

Ketz, R. J., Prud'homme, R. K., & Gaessley, W. W. (1988). Rheology of concentrated mircogel solution. *Rheological Acta*, *27*, 531-539.

Lopez, F. V., & Rosen, M. (2002). Rheological effects in roll coating of paints. *Latin American Applied Research , 32* (3), 247-252.

Meechai, N., Jamieson, A. M., Blackwell, J., Carrino, D. A., & Bansal, R. (2001). Nonlinear Viscoelasticity of Concentrated Solutio of Aggrecan Aggregate. *Biomarcomelecules , 2*, 780-781.

Osaki, K., Inoue, T., & Isomura, T. (2000a). Stress overshoot of polymer solution at high rates of shear. *Journal of Polymer Science Part B: Polymer Physics , 38*, 1917-1925.

Osaki, K., Inoue, T., & Isomura, T. (2000b). Stress overshoot of polymer solutions at high rates of shear polystyrene with bimodal molecular wight distribution. *Journal of Polymer Science Part B: Polymer Physics , 38*, 2043-2050.

Osaki, K., Inoue, T., & Isomura, T. (2000). Stress overshoot of polymer solutions at high rates of shear: Semidilute polystyrene solutions with and without chain entanglement. *Journal of Polymer Science Part B: Polymer Physics , 38*, 3271-3275.

Osterhold, M. (2000). Rheological methods for characterising modern paint systems. *Process in Organic Coating , 40*, 131-137.

Page, A., Carreau, P. J., Heuzey, M. C., & Moan, M. (2002). Rheological Properties of Coating Colors: Influence of Thickener. *The Canadian Journal of Chemical Engineering* .

Pangalos, G., Dealy, J. M., & Lyne, M. B. (1985). Rheological Properties of News Inks. *Journal of Rheology , 29* (4), 471-491.

Pattamaprom, C., & Larson, R. G. (2001). Constraint release effects in monodisperse and bidisperse polystyrene in fast transient shearing flow. *Macromolecules , 34*, 5229-5237.

Stratton, R., & Butcher, A. F. (1973). Stress Relaxation upon Cessation of Steady Flow and the Overshoot Effect of Polymer Solutions. *Journal of Polymer Science , 1973*, 1747-1758.

Tapadia, P. & Wang, S.-Q. (2004). Nonlinear Flow Behaviour of Entangled Polymer Solutions:Yied like Entanglement-Disentanglement Transition. *Macromolecules* , 9083-9095.

9 Capillary breakup extensional rheometry of organic coating

This part of the research work aimed to create a reliable, repeatable experimental procedure for commercial polyester resin based paints tested by a Capillary Break up rheometer and comparing the end results. This device is one of the simplest devices for measuring extensional viscosity. In chapter 6, the operating principle was explained and therefore there is no a need to repeat it again. The first approach was to undertake experiments with both stretch conditions, namely exponential and linear strike profiles which are defined by opening time and growth constant of the plate. At the beginning of the research, experiments were conducted to gain initial experiences of a very complex fluid without any visual devices (e.g. high speed camera). In order to expose significant dynamic effects during the temporal evolution of midfilament diameter, the application of digital video imaging was needed and was then implemented in the experimental procedure. Now, the optimal work frame could be selected for polyester resin based paints accordingly. A range of dynamic effects such as central bulge, satellite drop, recoiling of the filament and unstable filament dynamic were discovered, which greatly influence the outcome. Complex filament shapes were also reported by Tuladhar and Mackley (2008).

9.1 Experimental procedure

A Photron MC1 high speed camera operating at 1000 frames / second with a Nikon 14 – 85 f 2.8 – 4 lens was employed to record the temporal evolution of midfilament thinning. The size of the videos and images were cropped to 512 x 512 pixels with a pixel resolution of 26.2 μm. A connection transferred the data to an external storage device.

The capillary break up extensional rheometer (*CaBER 1*, Thermo Haake) was used to carry out capillary break-up experiments. A syringe helped to attain an acceptable liquid bridge during the loading process. A pre-shearing was imposed when the samples went through the needle of an inner diameter, d_i , of 1mm with a volumetric flow rate, Q, of 12.6mm^3/s. Consequently, a shear rate of 16 s^{-1} ($\gamma=8Q/\pi d_i$) occurred.

A linear actuator was used to apply an axial step strain on the sample within a defined time and height. Subsequently, the middle diameter, D_{mid} , of the fluids started to decay, monitored with a resolution of 10μm by a laser sheet micrometer emitting infra red light at 780nm. The 1.4mW power infrared red laser had a laser beam of 1mm thickness. A thermostatically controlled bath kept the temperature of the plate constant at 20°C. The initial sample's aspect ratio, $\Lambda_0 = h_0/2R_0$, was 0.5, calculated with initial gap, h_0, of 2 mm and plate diameter, $2R_0$, of 4cm. The effect of sagging and bulging of the cylindrical sample can be neglected at this value. It is likely that, the initial reverse squeeze flow did not exist because the aspect ratio was in the bottom range of the free reverse squeeze flow zone ($0.5 \leq \Lambda_0 \leq 1$) (Harlen 1996, Yao and McKingley 1998).

A series of Hencky strains of 1.25, 1.54 and 1.75, $\varepsilon_f = \ln(h_f/h_0)$ were applied to the sample. The final heights, h_f, of ~ 6,95 mm, 9.3 mm and 11.45 mm respectively were below the maximum stable filament length of 12.5 mm with the 4mm plate. Plateau (1863) predicted the maximal stable length $\ell_{max} = 2\pi R_0$ for a cylindrical liquid column of volume $V_0=\pi R_0^2 L_0$ under the condition of Bo = 0. The stability decreases with increased bond number (Slobozhanin 1993). The initial axial strain might not lead to a strain hardening effect when $\varepsilon_f = \ln(\Lambda_f/\Lambda_0) \leq 2$. For small strain, $\varepsilon_f \leq 1$, the dynamic of the necking will be influenced by slumping and the quasistatic fluid reservoir (Anna and McKinley 2001). The chosen Hencky strain follows the suggestion from Ann and McKinley (2001) to keep the axial Hencky strain between 1 and 2.

Capillary break up rheometer (CaBER) provides the option to use different stretch profiles, such as exponential, linear and cushion. The exponential profile depends on the fundamental rate and time. Linear stretch profiles can be changed with the opening time.

The exponential strike performed by CaBER obeys the following formula.

$$h(t)=h_0+\frac{(h_f-h_0)\ e^{(t\,R)-1}}{e^{(t_s\,R)-1}} \qquad \text{Equation 9-1}$$

Where, h_0 is initial height in mm, h_f is final height in mm and t is time in ms, t_s stands for opening time in ms and R is the fundamental rate in 1/s.

The linear profile can be defined by:

$$h(t)=h_0+(h_f-h_0)\frac{t}{t_s} \qquad \text{Equation 9-2}$$

The time scales for achieving the final height (also called opening times) were set to 20, 50, 70, 90 or 110 ms for linear stretching. The exponential stretch profile is defined by the opening time (20, 45 or 90 ms were used in the experiment) and fundamental rate ($0.1s^{-1}$, $100\ s^{-1}$ or $1000\ s^{-1}$ used for the experiment).

An overview of the parameters set used for this research project is provided in the Table 9-1 and Table 9-2.

Stretch Profiles		
Exponential		Linear
Strike Time / ms	Fundamental Rate s^{-1}	Strike Time / ms
20	0.01	20
20	100	50
20	1000	70
45	0.01	90
45	100	110
45	1000	
90	0.01	
90	100	
90	1000	

Table 9-1: Overview of the types of stretch profiles and parameters.

Dimensional Parameters			
Hencky strain	Final Height /mm	Initial Height / mm	Plate Diameter / mm
1.25	6.98	2	4
1.54	9.34		
1.75	11.5		

Table 9-2: Shows the dimensional set up parameters

During the experiments, adhesive failures of the fluid filament at the endplates were not detected. This phenomenon is more pronounced with wormlike micelle solution (Mastrangelo 1993a and 1993b, Crossby et al. 2000 and Rothstein 2003).

Extremely volatile effects causing solidification of paints which were also not observed in contrast to the study of polymer solution from Tripathi et al. (2000).

9.2 Determination of surface tension

Filament thinning is the result of capillary pressure on the thread located between the widely separated upper and lower plate. To determine the apparent extensional viscosity (see Equation 5.3), it is imperative to know the surface tensions of each paint. A Krüss K8 static surface tensiometer measured the surface tension with a platinum Du Noüy ring which was flamed to remove any surface contaminants before using it (Shaw 1992). For every tested sample, the average value was obtained from 10 measured surface tension values at room temperature of 20° C and is listed in the Table 9-3. Clearly, it could be seen that all paints possess a similar value of surface tension.

Samples	Surface tension mN/m	Deviation %
White	34	0.9/-1.5
Green	32	1.6/-1.5
Red	31	1.1/-1.8
Dark Red	32	1.6/-1.8

Table 9-3: Lists the average surface tension values from 10 measurements

Ascanio et al. (2006) provided surface tension data of water based paint ranging from 18.6 to 23.2 mN/m with a solid content between 52 % and 62% (Ascanio et al 2006). In comparison with the solvent based paints listed in Table 9-3, the surface tensions are around 50% higher whereas the solid contents are similar to the water based paints (see solid content Table 8-1).

9.3 Possible Effects causing measurement errors

9.3.1 Sagging effects highlighted by the bond number

Bond number, *Bo*, indicates the degree of influence of gravitational forces on the unstretched fluid bridge. A high bond number normally predicts sagging of the filament bridge. When the value of *Bo* is below unity, the shape of the unstretched thread is symmetrical due to the low influence of the gravitational effects (McKinley and Tripathi 2000). For each paint, the *Bo* was determined by mathematical calculation using the formula, $Bo=\rho g R^2(t)/\sigma$, and its value is listed in Table 9-4. Unstable filament bridges due to the influence of the gravitational force were detected when using 6mm and 8mm plates because of the higher Bond number occurred. The use of a smaller sized plate helped to reduce the Bond number and, consequently, an improvement in the initial shape of the liquid bridge was noticeable.

Samples	Density kg / m^3	Bond Number		
		4mm	6mm	8mm
White	1330	1.5	3.5	6.2
Green	1180	1.4	3.3	5.8
Red	1170	1.5	3.3	5.9
Dark Red	1300	1.6	3.6	6.4

Table 9-4: Variation of Bond number with different plate diameters

Digital images were taken of the filament bridge which was built between 4mm plates at the start of the experiments. Surprisingly, the degree of sagging or slumping was smaller despite the fact that Bo >1 which illustrates that the theory is material dependent.

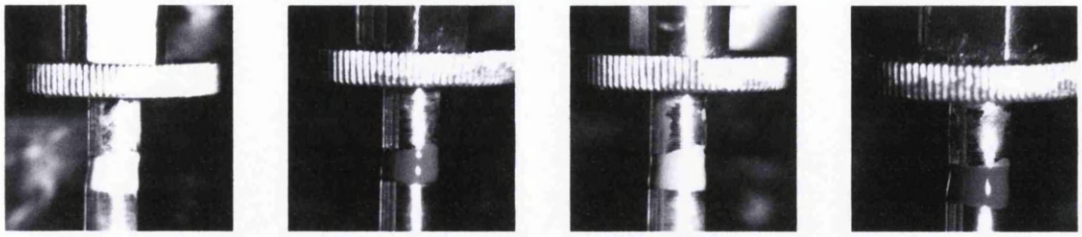

White Green Red Dark Red

Figure 9-1: Digital images of filament bridges at experiment start, using 4mm plates.

A study of liquid bridge stability was carried out by using a liquid bridge in an immiscible liquid bath. Yield stress fluids were still able to achieve stable bridge conditions when the distance between the plates becomes equal to $2\pi r$, where r is the cylinder radius (Lowry and Steen 1995 , Mahajan et al. 1999). At a stretch position, a flow between the two plates can only occur when the capillary pressure overcomes the magnitude of the yield stress (Goldin 1972). In the case of polyester resin based paint, the capillary pressure was high enough to cause filament thinning.

9.4 Occurrence of instability defects

Whilst testing the samples, interesting instability set up processes during the elasto - capillary thinning were revealed by the high speed camera. One of them was the evolution of the bulge in the centre of the filaments, which was also noticeable on the diameter versus time graph through an increase in the filament diameter in the Newtonian region (see section 9.5.1)

Another reason for the diameter increase at the end of the test is the recoiling effect which is illustrated in

Figure 9-3. The occurrence of a satellite droplet after filament breaking also leads to a diameter increase. Periodic movement of the filament created a peak in the linear region of the filament diameter decay curve. (see section 9.4.4)

At the beginning of the experiment, the diameter was partially axially uniform around the midplane of the filament. The effect of a non slip condition on the

endplates prevents the filament from having constant diameter between two plates and causes the hemispherical fluid droplets. This can be seen on all digital images.

9.4.1 Evolution of central bulge

The result below illustrates the effect of a central bulge akin to a bead on a string (Goldin et al 1969, Clasen et al 2006a and b, Wagner et al. 2005). Material was built up at the dimensionless filament diameter (D/D_0) of about 0.1 mm which occurred after around 60ms. Oliveira et al. (2006) used an aqueous solution of high molecular weight polyethylene oxide which is a low elastic material with low viscosity. During the investigation with this material, a similar phenomenon of central bulge was detected. This defect is influenced by inertia, capillary and viscous forces and can only occur for fluids with low viscosity, low elasticity and high aspect ratio (Rodd et al. 2004). The occurrence of central bulge in white paint with a viscosity of 189mPas happened at a final aspect ratio of 1.75 (see Figure 9-2). Before the central bulge could be seen, the filament exponentially decayed from point 1 to point 2, afterwards the diameter started to increase. At point 3 a central bulge, situated just above the centre interconnected by long thin fluid ligaments to hemispherical fluid droplets attached to the end plates started to build up. Simultaneously, this bulge moved downwards until it achieved its maximum value (point 4 in Figure 9-2). Surface tension dominates in the spheres where the molecules are relaxed. However, in the ligaments or axially uniform thread, the dominant viscoelastic stresses cause an extreme stretching in the molecules. A similar observation of central bulge was made with low Newtonian, polymer and inkjet fluids whose Ohnesorge number was below 1, indicating significant contribution of inertia (Tuladhar and Mackley 2008). A similar result of an increase of the midfilament diameter due to development of a central bulge has been reported by Rodd e al (2004).

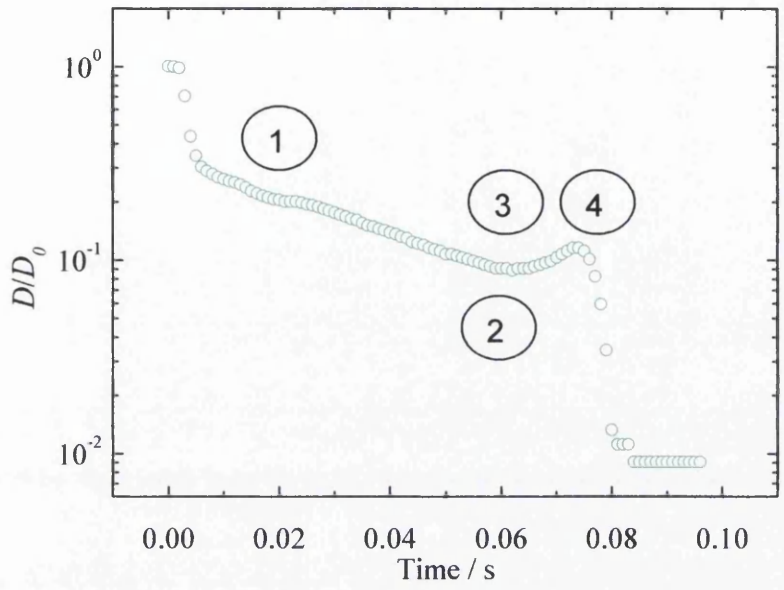

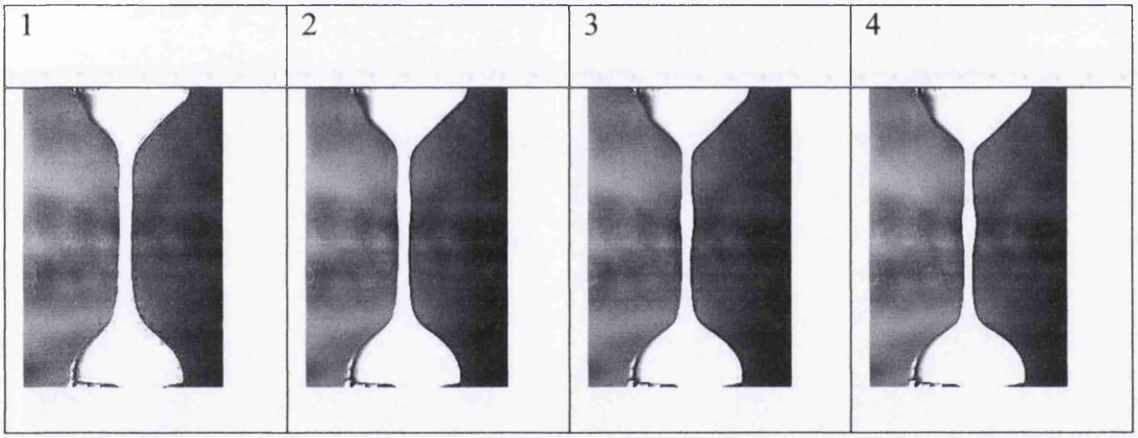

Figure 9-2 Formation of central bulge during the filament thinning of a viscoelastic fluid (white).

9.4.2 Evolution of recoiling

A clear and long exponential decay can be seen until Point 2, where normally a transition phase from elastic capillary thinning decay to viscocapillary thinning occurred. However, the decrease of the thread radius over time came in rest for around 0.003 s. During this time, a necking process just below the middle centre (point 2) of the filament started until separation of the filament. The upper mass of the string was now drawn upwards through the elasticity of the paint. The detector

recorded an increase of diameter during the elastic recoiling phase (Point 3) until the string began to move outside of the laser beam range. As a consequence, the value of the filament diameter started to decrease again (point 4).

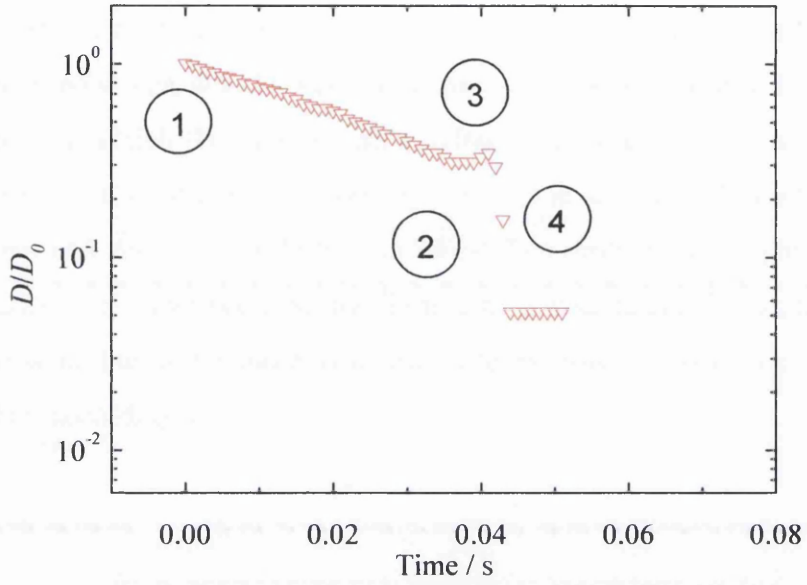

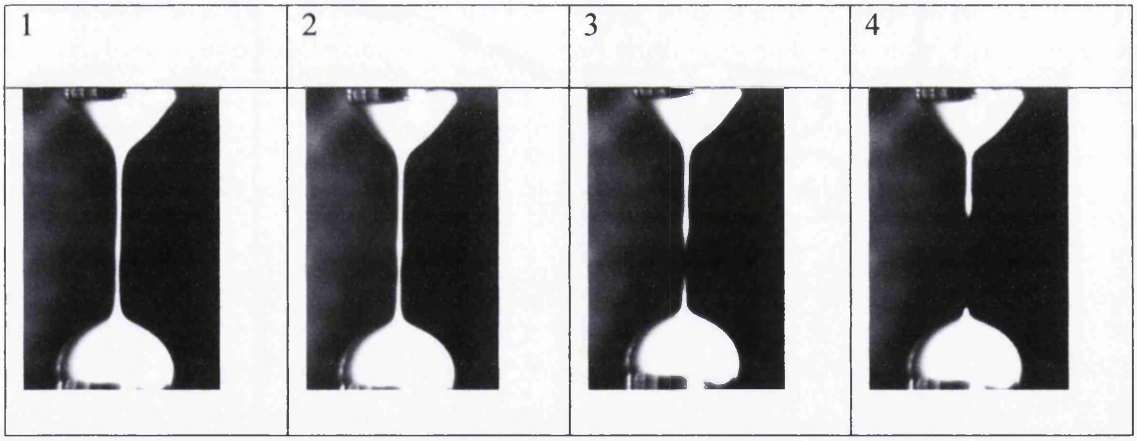

Figure 9-3: Video capture of a recoiling leading to a diameter increase at the end of the test

9.4.3 Evolution of satellite drop

The first picture in Figure 9-6 shows an almost axisymmetric filament apart from the region near the end plates, which is caused by the no slip condition on the surface of the plates. Without any initial sign of instability defects, the exponential decay of the

filament diameter (point 1) stopped (point 2) after ~ 70 ms. For about 10 ms the diameter was unchanged. The thin fluid ligaments which connected the central bulge with the hemispherical fluid droplets attached to the end plates started to thin faster around the central bulge until its disconnection (point 3). The resulting satellite drop of material maintained its position for a fraction of a second until gravitational force overcame the inertial force and the ball moved towards the lower plate (point 4). The same phenomenon can also be seen in a very low viscous sample (50% glycerol/ 50%. Water) in which the inertial and capillary forces act (Tritaatmadja 2006). A thorough study with different concentration of PEO in solutions shows that increased elastic stress can suppress the formation of satellite drops in a dripping experiment (Tritaatmadja 2006). Derived from the finding by Tritaatmadja (2006), the maximum elastic stress of the white paint still seems to be low to avoid the formation of satellite drop accordingly.

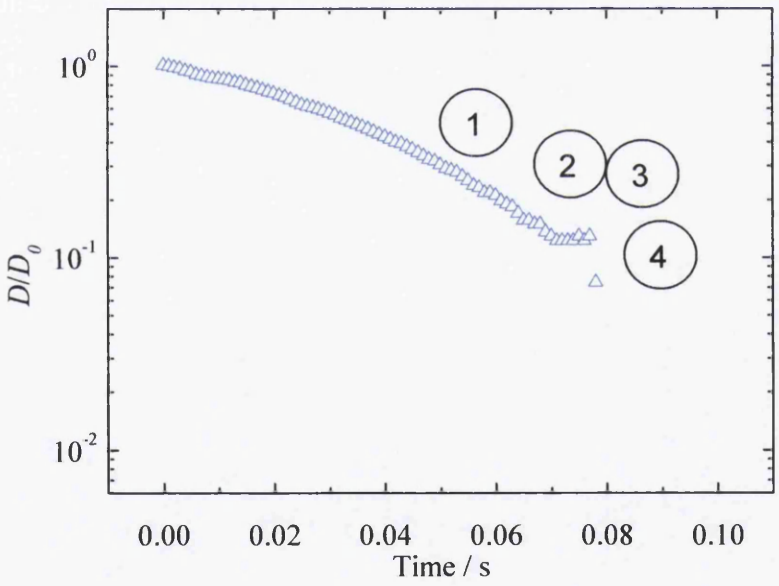

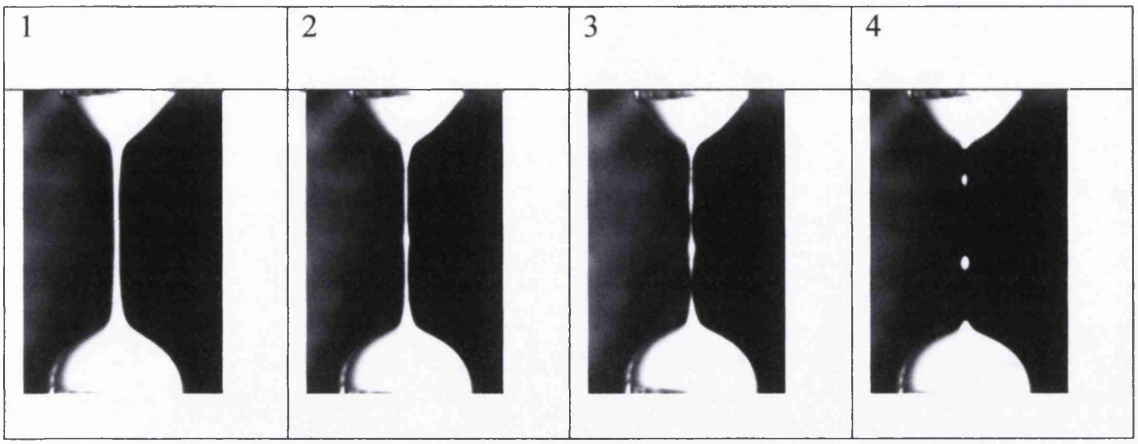

Figure 9-4 a) indicates a defect during the evolution of midfilament, b) provides optically the reason for the occurrence of a constant diameter

9.4.4 The effect of oscillatory filament movement

After the upper plate had achieved its final height, a sudden normalised diameter drop from 1 mm to around 0.5 mm was recorded within a fraction of a second. Furthermore, gravitational drainage becomes important during the opening process, noticeable by material accumulation below the midplane of the fluid filament (Kolte and Szabo 1999) as seen in Figure 9-5. The bottom mass dragged the upper mass downwards (from point 1 to point 2) due to the gravitational force. From point 2, an exponential thinning started until inertial capillary oscillations of the filament occurred whereby a diameter increase was detected. Shortly afterwards, the oscillation movement came to a halt and the filament decay progressed as usual.

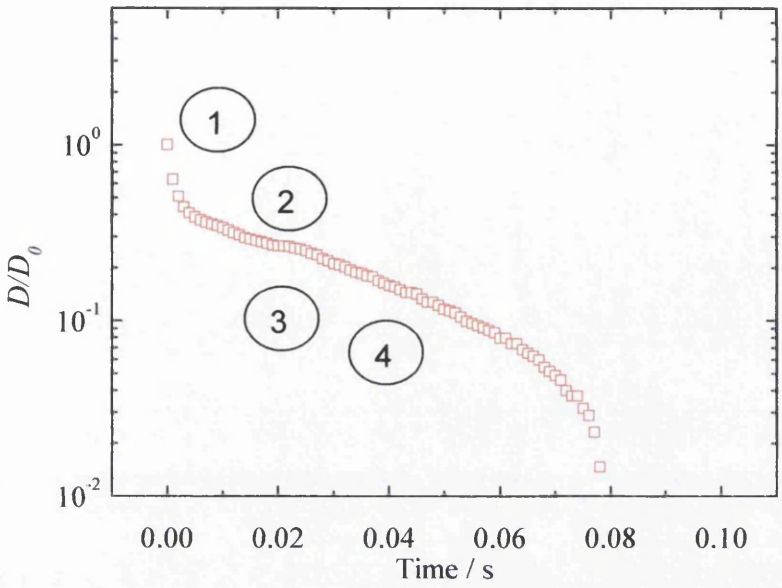

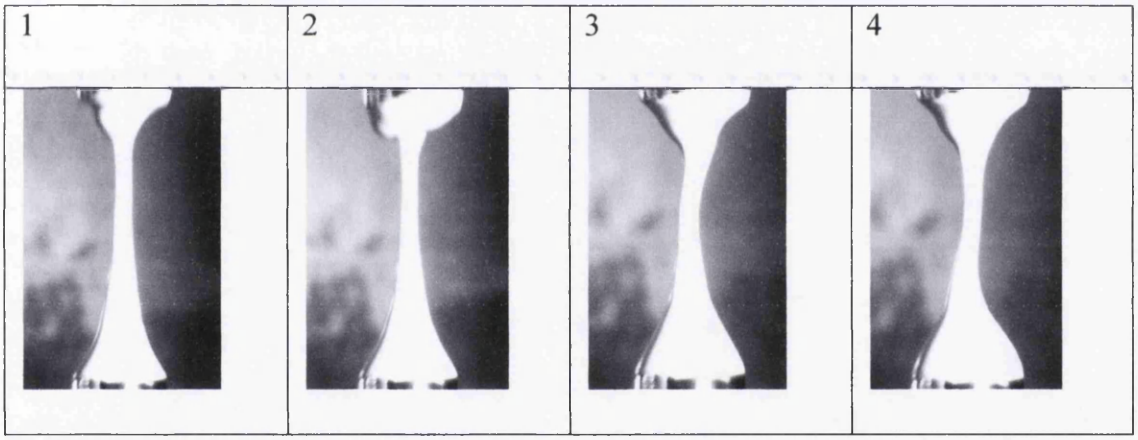

Figure 9-5: Shows two phenomena of defects: from step 1 to 2 the midfilament diameter rapidly decreases due to the downwards movement of the upper plate. The sudden increase in the filament diameter between point 3 and point 4 occurs due to the strongly periodical movement. Afterwards, the weakly periodical movements are not detectable by the laser.

9.5 Repeatability of the filament decays

The optimal operation window was assessed by collection of a matrix of data from tests in which test material and parameters were varied. To quantify the repeatability, filament break up time was used instead of considering the whole curve of filament decay for the sake of simplicity. Based on the average filament life time calculated from 10 runs, the minimum and maximum life time values were converted into percentages with Equation 9-3 and entered into Table 9-5.

$$\text{deviation in \%} = \frac{\text{filament break up time}_{\text{min or max}}}{\text{average break up time out of 10 runs}} \times 100\% \qquad \text{Equation 9-3}$$

Two sets of raw data results from green paint have been selected to demonstrate variations in repeatability as a function of experimental parameters. Using a linear opening time of 110 ms as an example for bad repeatability (see Figure 9-6 a), the calculated deviations were +14.8 % and–11.5 % reflecting widely scattered break up points within a time scale ranging from 0.062 ms and 0.082 ms. A much better repeatability can be seen in Figure 9-6 b. which has a deviation of +/- 2.2. The degrees of repeatability in percentages for all used Hencky strain and stretch profiles are presented in Table 9-5. Areas coloured green were chosen to mark any deviation below +/- 3%, orange indicates a deviation of below +/- 5%, repeatability above +/- 5% is marked as red. The table with the results obtained with a Hencky strain of 1.75 are chiefly coloured red which indicates that high variations were common for these experimental procedures. The best mutual agreements were obtained by a linear stretch profile with an opening time of 20ms. However, the recorded filament decay with the high speed camera divulged that the plate massively overshoots the final height and introduced an unwanted effect. Figure 9-7 and Figure 9-8 illustrate the overshoot in a sequence of pictures. To avoid this extreme effect, the linear profile with an opening time of 50 ms seemed to be the best alternative. The effect of gravitation is more pronounced at higher opening time and higher Hencky strains which may be the reason for the higher deviations. A filament break up before the upper end plate reaches its final position occurred under the test condition with a Hencky strain of 1.75 and opening time 90 ms or 110 ms for some samples.

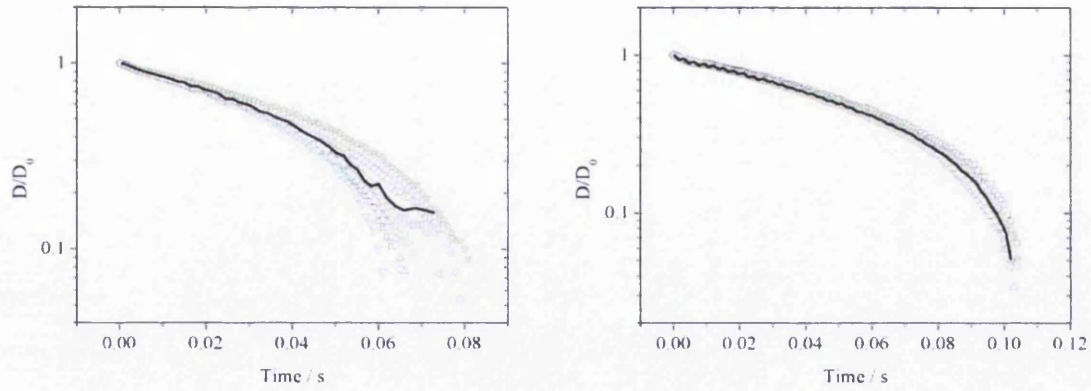

a) Green linear opening time of 110ms

b) Green linear opening time of 20ms

Figure 9-6: Evolution of filament decay of green paint under two different test conditions. The first graph a) shows a wide scattering of data points in the range from +14.8 % to -11.5 % (linear strike profile with an opening time of 110 ms) and the second graph b) a narrow scattering of data points in the range of +/-2.2% (linear opening time with a opening time of 20 ms). Solid lines correspond to an average fit of 10 runs.

Hencky strain 1.25								
	White		Green		Dark Red		Red	
Stretch Profile	max. / %	min. / %	max. / %	min. / %	max. / %	min. / %	max. / %	min. / %
Exp. F=100, S=45	2.3	-1.9	5.4	-6.9	4.8	-3.9	4.7	-4.4
Exp. F=100, S=90	7.9	-7.7	9.1	-9.9	9.2	-10.9	7.4	-6.9
Exp. F=1000, S=90	4.7	-4.3	7.8	-8.0	5.4	-6.2	4.5	-5.3
L20	3.8	-5.4	5.6	-8.1	4.4	-4.3	5.6	-3.7
L50	4.3	-4.3	6.7	-6.4	3.7	-3.6	5.3	-5.6
L70	5.6	-6.9	6.8	-6.0	3.3	-3.9	2.8	-2.4
L90	3.8	-2.8	10.3	-9.6	3.2	-4.7	3.8	-2.5
L110	19.5	-17.1	8.5	-6.6	3.6	-5.1	1.8	-3.3

a)

Hencky strain 1.54								
	White		Green		Dark Red		Red	
Stretch Profile	max. / %	min. / %	max. / %	min. / %	max. / %	min. / %	max. / %	min. / %
Exp. F=100, S=45	1.9	-2.2	4.2	-3.5	4.6	-6.7	4.7	-3.9
Exp. F=1000, S=45	6.5	-5.8	4.6	-4.1	9.2	-9.5	2.4	-3.9
Exp. F=1000, S=20	6.6	-4.9	3.1	-2.9	3.1	-3.0	1.8	-2.2
Exp. F=100, S=20	3.3	-5.6	2.9	-2.6	3.7	-4.0	2.1	-2.5
Exp. F=100, S=90	9.4	-13.2	4.4	-5.7	5.0	-5.1	10.5	-11.9
Exp. F=1000, S=90	2.7	-2.5	2.9	-1.5	3.9	-3.4	2.1	-2.4
Exp. F=0.01, S=90	12.2	-9.1	4.4	-6.2	4.8	-5.4	6.0	-8.3
Exp. F=0.01, S=45	2.8	-2.8	3.6	-4.4	4.5	-6.3	1.9	-2.4
Exp. F=0.01, S=20	5.5	-4.8	3.7	-2.9	14.2	-17.1	1.4	-2.1
Lin. S=20	3.3	-2.6	2.3	-2.2	3.6	-4.1	2.3	-2.5
Lin. S=50	4.4	-4.1	4.0	-3.2	3.8	-2.6	3.3	-3.7
Lin. S=70	4.5	-5.5	8.5	-7.0	3.0	-3.2	11.1	-7.8
Lin. S=90	7.4	-7.5	6.3	-6.3	4.1	-5.2	8.5	-8.5
Lin. S=110	6.1	-8.5	14.8	-11.5	9.0	-7.5	11.9	-16.1

b)

Hencky strain 1.75								
	White		Green		Dark Red		Red	
Stretch Profile	max. / %	min. / %	max. / %	min. / %	max. / %	min. / %	max. / %	min. / %
Exp. F=100, S=45	10.2	-11.5	6.6	-6.3	6.5	-7.7	4.6	-7.7
Exp. F=100, S=90	7.9	-10.1	24.1	-13.1	16.0	-14.9	8.3	-12.1
Exp. F=1000, S=90	4.4	-5.3	4.8	-5.2	4.6	-5.0	7.9	-6.6
L20	2.6	-2.6	4.4	-6.4	2.8	-3.9	10.9	-9.4
L50	5.6	-6.7	5.5	-6.9	12.0	-10.8	12.5	-12.1
L70	5.2	-5.2	4.8	-8.1	36.5	-21.5	8.7	-11.7
L90	12.1	-13.5	19.1	-11.7	49.1	-50.3	4.5	-5.1
L110	2083.4	-950.6	32.5	-32.1	46.8	-43.5	9.4	-8.8

c)

Table 9-5: Deviation values in % for each set of run, a) using Hencky strain of 1.25 b) using Hencky strain of 1.54 and c) using Hencky strain of 1.75; (F= fundamental rate in 1/s , S = strike time in ms and L = linear profile)

9.6 The effect of overshoot

While analysing the data of the digital images and videos, an artefact was noticed. The upper plate moves upwards and did not stop in the correct location. Eventually, the plate rebounds to its corrected location. This bouncing effect manipulates the true results and therefore cannot be used for further investigation. Two sets of sequences of pictures demonstrate the overshoots that occurred at an exponential stretch profile with a fundamental rate of 100 s^{-1} and opening time of 90 ms (Figure 9-7) and exponential stretch profile with opening time of 20 ms.

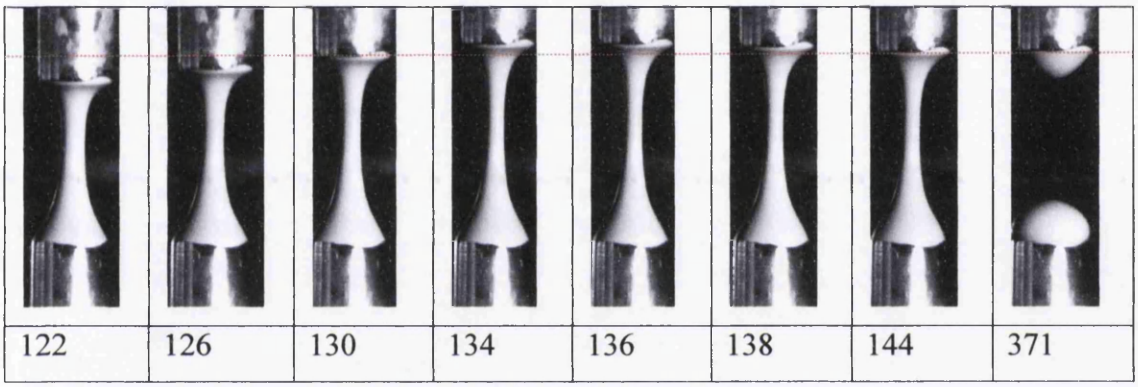

Figure 9-7: Digital images of the overshoot of the upper plate in a CaBER experiment with an exponential stretch profiles using fundamental rate 100 s^{-1} and opening time of 90ms. The target height throughout the sequence of the picture is marked with the red dotted line.

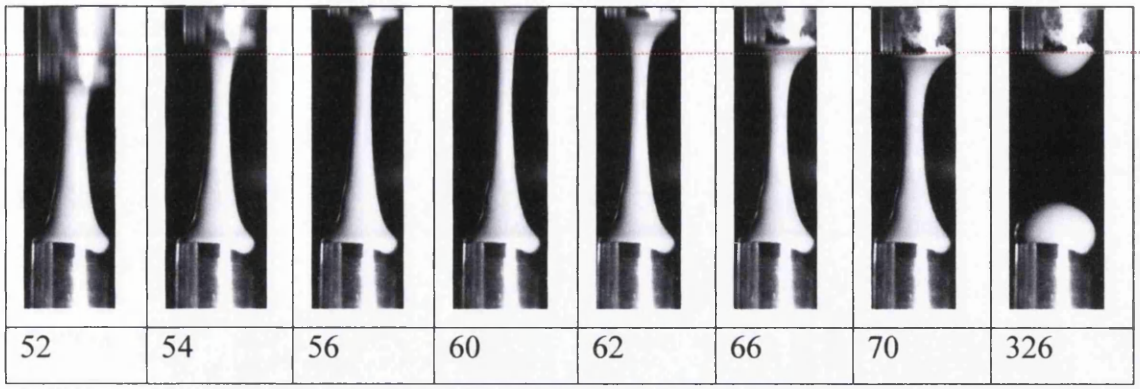

Figure 9-8: A sequence of digital images that captures an overshoot of the upper plate in a CaBER experiment with a exponential stretch profile using an opening time of 20ms. The final height throughout the sequence of the pictures is marked with the red dotted line.

9.7 Results

9.7.1 Data of evolution of midfilament diameter

A linear strike profile was employed with various opening times, δt, ranging from 20 to 110 ms to understand its effect. The sample was stretched from the initial height of 2 mm to the final height of 9.34 mm corresponding to a Hencky strain of 1.54. The evolutions of midfilament diameter from different paint samples are plotted by normalised diameter versus time graphs (see Figure 9-9 a to d) including the elastic and Papageorgiou fits.

The rapid initial viscous dominated phase was absent from all tested material at the start of measuring. Each paint starts with the exponential filament thinning obeying $R_{mid}(t)=R_1 \exp(-t/3\lambda_c)$ (λ_c = characteristic relaxation) at an intermediate time scale which can been seen in Figure 9-9. During this time scale, the drainage is controlled by a local force balance between surface tension and elasticity. It was not possible to obtain the longest relaxation time, λ_1, from oscillatory experiments and therefore a comparison with the characteristic relaxation, λ_c, was not possible. A comparison of these two fluid parameters has been done with PIB/PB Boger fluid showing that λ_c is similar to λ_1 by Kolte and Szabo (1999). The amount of discrepancy between the

values of λ_c and λ_1 indicates the degree of radial inhomogeneity in the stretched material (Kolte and Szabo 1999). Liang and Mackley (1994) used polyisobutylene solutions and found out that the relaxation time λ_c was nearly three times higher than the longest relaxation time λ_1. In this case, it was not possible to apply the concept of Kolten and Szabo (1999) because of the unknown data of longest relaxation time.

A clear and fast crossover from elastic to viscous stress which tries to counteract the capillary stress driving the flow is shown in Figure 9-9. Interestingly, the time scale of the exponential filament decays increases with decreasing opening time for all paints. This implies that it takes longer to achieve the finite extension limits of the polymers. Accordingly, the magnitude of characteristic relaxation time increases. An almost pure, viscous capillary behaviour always occurs at an opening time of 110ms after stretching. This implies that the finite extension limit is achieved before the measurement begins. Unsurprisingly, the lifetime of a filament strongly depends on the opening time. The following statement can be made without any doubt: the longer the opening time the shorter is the lifetime. A possible explanation for this phenomenon is that the longer opening time allows gravitational force to act longer on the sample filament before the actual measurement starts.

Dark red paint possesses the highest yield stress among the samples, reflected in the longest lifetime. Quite the contrary was observed for red paint without a yield stress, its lifetime being the shortest (see Figure 9-11). The build up of capillary pressure σ/R_{min} to exceed the yield stress might take longer and might explain this outcome. In the step rate test experiment, it was detected that the red paint does not have any elasticity which normally extends the life time. However the dark red paint possesses the highest elasticity which can be confirmed with the outcome of the step strain experiments (see Figure 8-15).

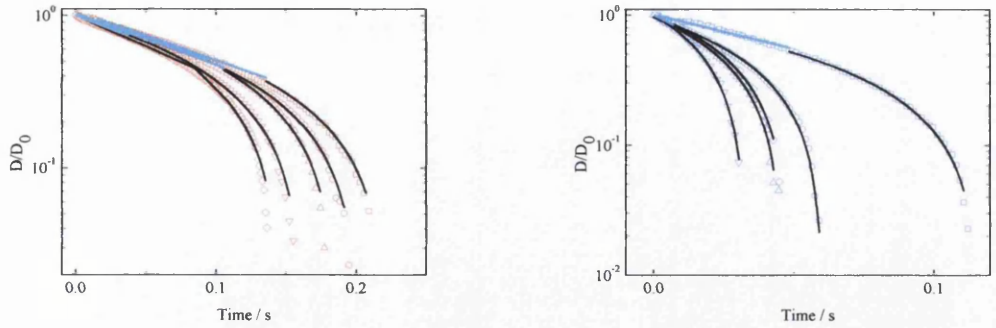

a) dark red b) red

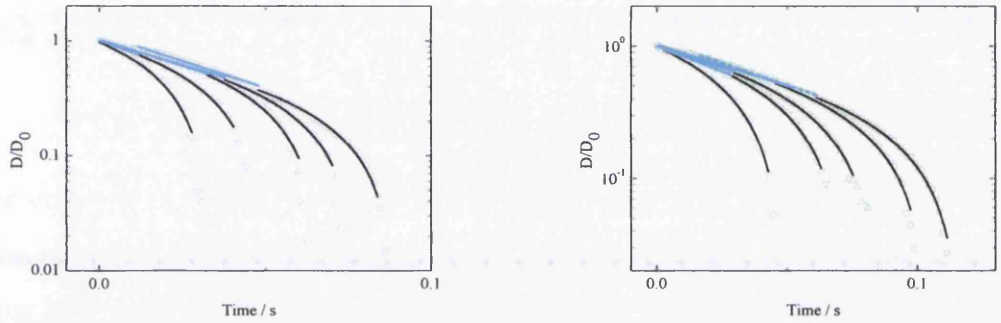

c) white d) green

Figure 9-9: Comparison of transient midfilament diameter curves as a function of time for a) dark red, b) red, c) white and d) green paints for linear opening times of (□) 20, (○) 50, (△) 70, (▽) 90 and (◇) 110 ms. Papageorgiou and elastic fits are represented by black and blue lines respectively

Data for each single filament decay curve were analysed by fitting with the Papageorgiou model to obtain extensional viscosities. The average value of extensional viscosity was determined from the average filament decay curve calculated from 10 single runs. Eventually, a graph could be created with the derived extensional viscosity as a function of opening time (Figure 9-14). At a first glance, it is noticeable that the repeatability becomes worse at higher Hencky strains. Due to filament breakage before the end plate achieved its end position, some experiments were invalid, highlighted by missing data points at a Hencky strain of 1.75 (see Figure 9-14 b, Figure 9-14 c and Figure 9-14 d). This implies that the elastic time and viscous time scale were shorter than the opening time scale for this condition. In Table 9-6, the viscosity ranges are listed from measurements which were undertaken with Hencky strains of 1.25, 1.54 and 1.75 and strike times of 20, 50, 70, 90 and

110ms. The well performing red paint possesses the lowest apparent extensional viscosity, followed by white, green and then dark red.

Paint Sample	Extensional Viscosity Pas
White	1.05-1.75
Green	1.2-1.75
Red	0.75-1.25
Dark Red	2.5-2.75

Table 9-6: Range of viscosities from polyester paints

9.7.2 Comparing data obtained with the linear profile and opening time of 50ms

For comparison purposes for each paint, the linear stretch profile with an opening time of 50 ms was used. The deviation of each test has been made visible by using error bars. The extracted information from the various paints was compared in terms of extensional viscosity versus opening time (for Hencky strains 1.25. 1.54 and 1.75), filament life time versus opening time and normalised diameter versus time. Filament life time versus opening time was plotted in Figure 9-10. Dark red paint has consistently the highest life time over all measurements whereas the shortest life time was exhibited by the red paint. The maximum life time of the dark red paint occurred at a linear opening time of 20 ms and was 0.208s whilst the shortest life time of the red paint was 0.0143s occurring under a linear opening time of 110 ms. A linear decrease in filament life time was observed with increased opening time. This linear behaviour might be able to be controlled by the initial opening condition.

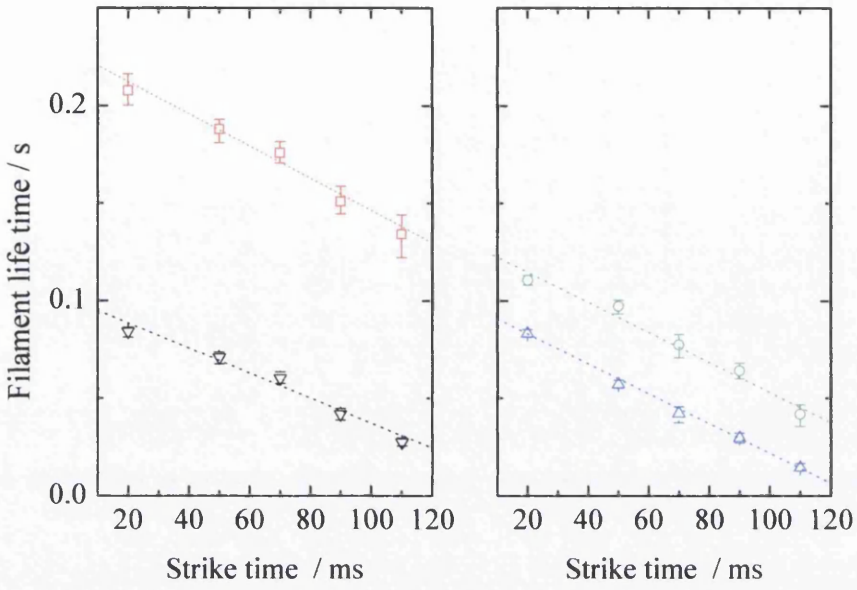

Figure 9-10: Linear fits to the filament data of lifetime versus strike time: (□) dark red, (○) green, (△) red, (▽) white paints; Hencky strain 1.54

A simple linear regression was fitted to the data providing slope and an intercept point. The following relationship between filament break up time and opening time could be found.

Samples	Linear Regression Fit	R^2 value
White	=-0.0006408811x +0.100509918	0.98
Green	=-0.0007650492x+0.1301893443	0.98
Red	=-0.0007545902x+0.0965723112	1.00
Dark Red	=-0.0008301148x+0.2276518033	0.98

Table 9-7: Statistical data relating to linear fits to filament lifetime versus opening time plots

9.7.3 Diameter versus time

The evolution of midfilament diameter of all paints used is illustrated with a Hencky strain of 1.54 in Figure 9-11 and the sequence of digital images during the evolution of filament thinning can be seen in Figure 9-12. The red paint that exhibits

Newtonian behaviour when it is subjected to shear underwent a more rapid filament breakup than the non–Newtonian fluid. One of the reasons for the shorter life time may be due to the low polymer concentration in the paint. Normally, the lifetime of a filament increases with higher polymer concentration (Kheirandish et al. 2008). The capillary velocity, $v = \sigma_s/\eta_0$, decreases with increased life time. In this respect, the red paint with the shortest life time thins with the fastest capillary speed of 0.094 m/s, the white paint with 0.072 m/s, green paint with 0.065 m/s and the lowest capillary velocity occurs at dark red paint 0.037 m/s. Furthermore, the dark red paint possesses the longest time scale in the elastic capillary region (see Table 9-8).

Figure 9-13 illustrates the evolution of extensional rate over time. For the dark red paint the extensional rate slowly increases until 0.17s after which the gradient of the extensional rate grows rapidly. Whereas for red paint, the gradient is steep from the beginning.

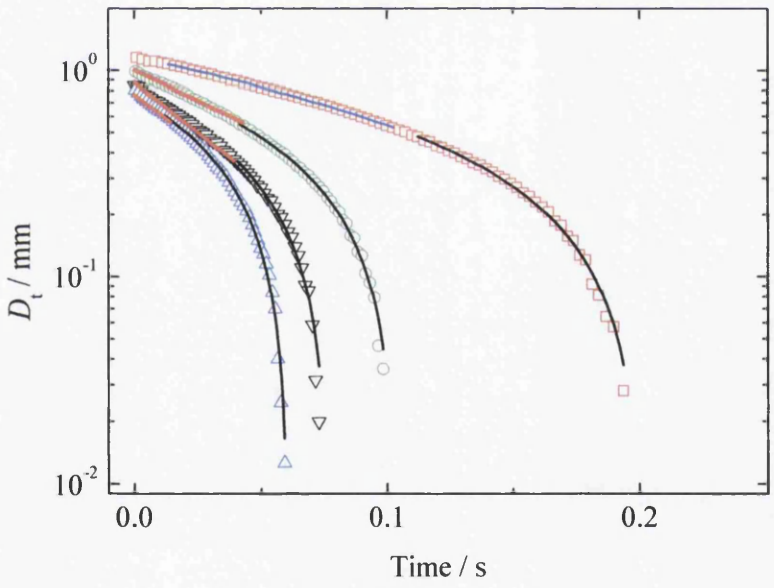

Figure 9-11: Evolution of filament diameter at a Hencky strain of 1.54 with a linear opening time of 50 ms. The symbols , △, ▽, ○, □ represent the red, white, green and dark red paints.

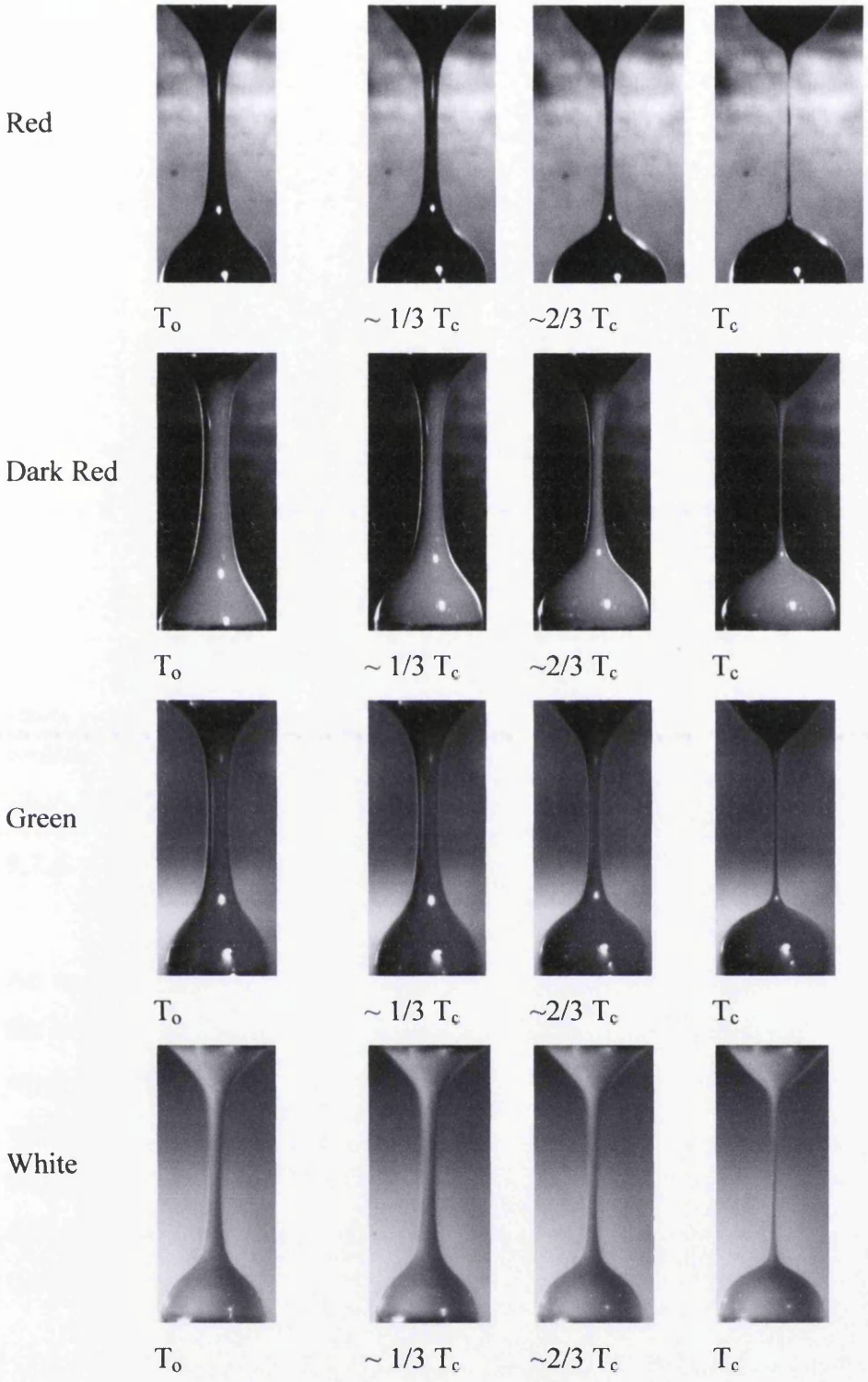

Figure 9-12: Sequence of digital images during the evolution of filament thinning.

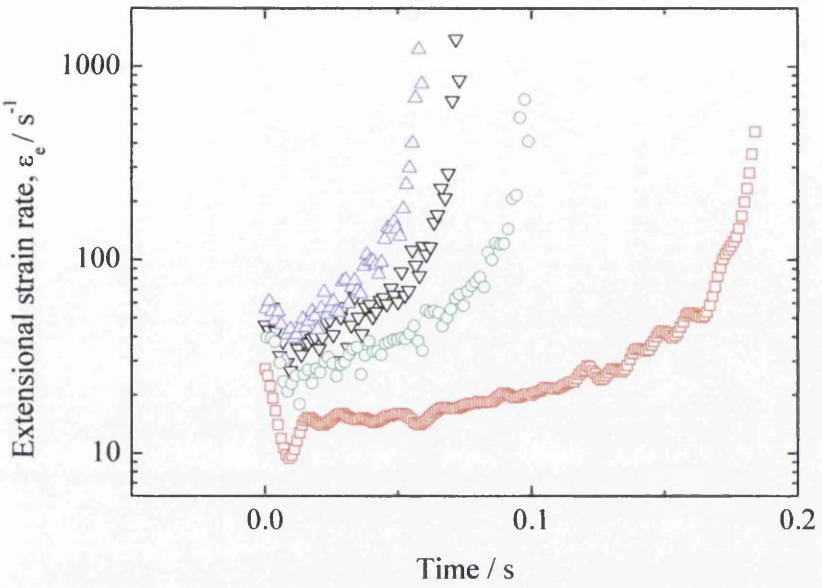

Figure 9-13: Illustrating the different extensional strain rates as a function of time for each paint. The symbols , △, ▽, ○, □ represent the red, white, green and dark red paints.

9.7.4 Extensional viscosity versus opening time

An opening time dependency of extensional viscosity could not be detected during the experiments. Error bars indicate the range of deviation that occurs within a single experiment procedure. From the error bars, it can be seen that the repeatability of the whole data set worsened at higher the Hencky strains due to the occurrences of flow instability. Some filament decays could not be monitored at Hencky strain of 1.75 and higher opening time (depending on the samples) because filament break up occurs before the end plate achieved its final height.

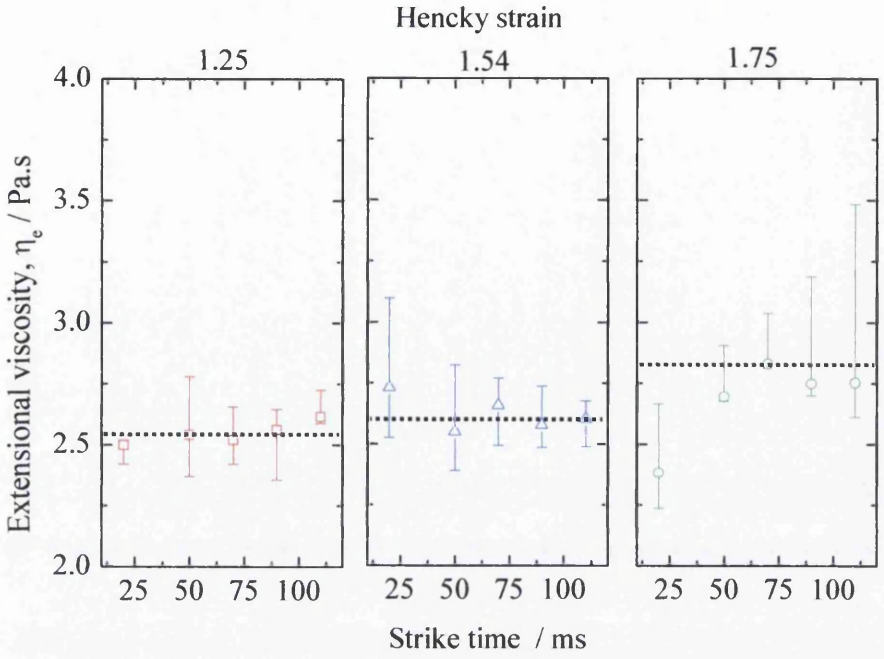

a) dark red

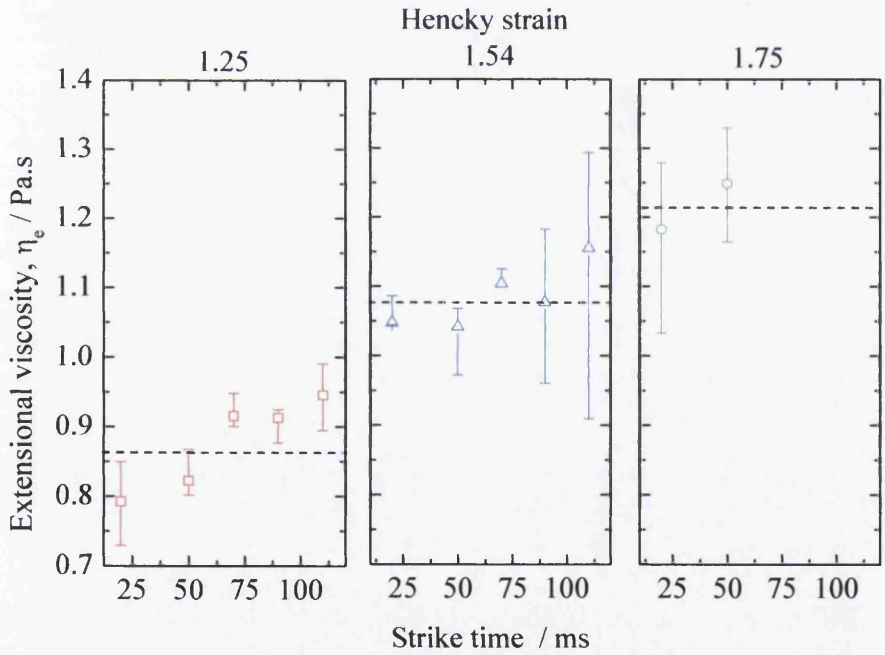

b) red

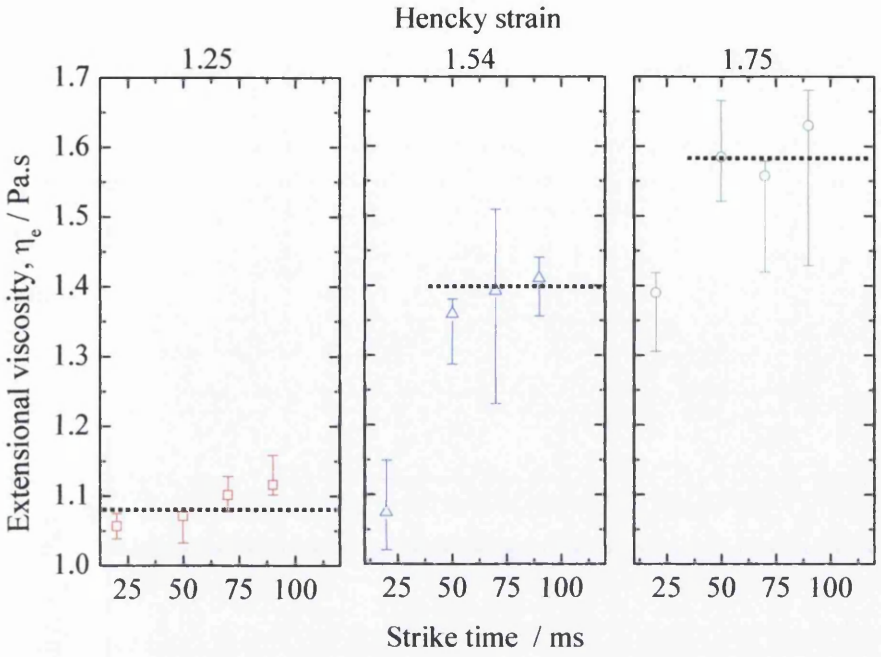

c) white

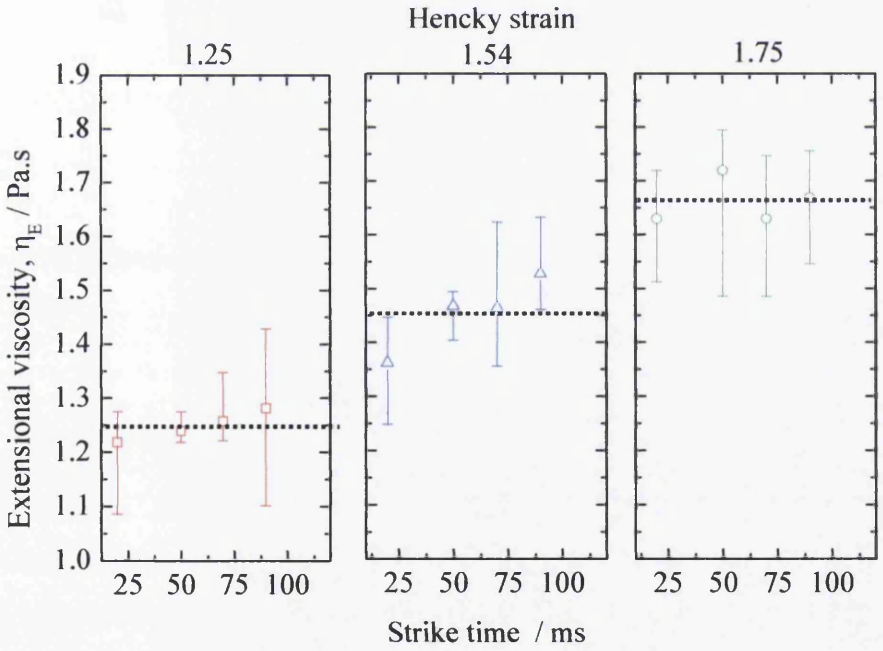

d) green

Figure 9-14: Graphs for extensional viscosity versus strike time for a) dark red, b) red, c) white and d) green paint

In Figure 9-15, the extensional viscosity is plotted for various strike times. The dark red paint has the highest viscosity of around 2.6 Pas and red paint the lowest viscosity of approximate 1.05 Pas. Use of error bars demonstrates the degree of repeatability of the outcome. The extensional viscosities of the paints in decreasing order are dark red (2.6 Pas), green (1.5 Pas) white (1.4 Pas) and red (1.05 Pas) at Hencky strain of 1.54 and opening time of 50ms.

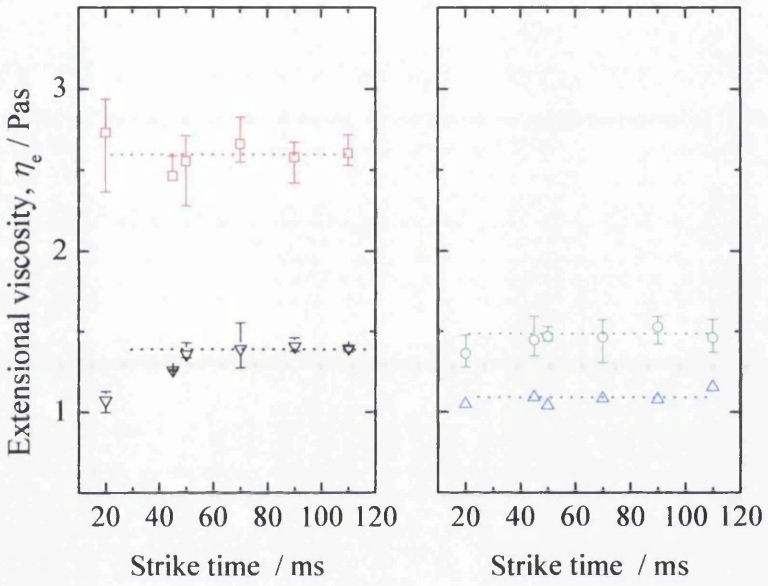

Figure 9-15: Extensional viscosity at various strike time for red (△), white(▽), green (○), dark red(□) paints.

9.7.5 Evaluation of dimensional number

Sufficient viscous stress is needed to stabilise the thread during the filament decay which can be related to the Ohnesorgen Number (Oh) (see Equation 5.11). A highly viscous fluid will be defined when Oh > 1, whose values were calculated for all paints listed in Table 9-8. The Oh number of the white paint is below 1 indicating for a low viscous fluid. Digital pictures show also an additional evidence of the stability of the thread for the paints which has Oh < 1. Since the red paint possesses the lowest relaxation time, λ, and the lowest surface tension among the samples, consequently the Deborah number (see equation 5.14) is also the lowest whereas the

dark red paint has the highest. The Weissenberg number is 2/3 in the relaxation scale (Entov and Hinch 1997) (see section 5.4.2).

	White	Green	Red	Dark Red
Density, ρ / kg m^{-3}	1332	1181	1172	1299
Surface tension, σ / N m^{-1}	0.034	0.032	0.031	0.032
Viscosity, η / Pa s	0.24	0.32	0.34	0.42
Length scale, r / m	0.002	0.002	0.002	0.002
λ / s	0.017	0.023	0.014	0.045
$Wi = \lambda\dot{\varepsilon}$	2/3	2/3	2/3	2/3
$De = \lambda / \sqrt{(\rho r^3 / \sigma)}$	0.96	1.34	0.81	2.50
$Oh = \eta / \sqrt{(\rho r \sigma)}$	0.8	1.2	1.3	1.5

Table 9-8: Dimensionless numbers, material properties and values obtained by the model fits for the paints

9.8 Conclusion

Caber is a useful device to characterise paint in terms of extensional viscosity and elastic components quantified with relaxation time. However, care must be taken when interpreting the data because there are plenty of unwanted effects which can distort the results. A very good approach is to use the filament life time for comparing the repeatability. Despite the good reproducibility from an exponential profile with the fundamental rate of 1000 s^{-1} and strike time of 90ms, it is not ideal because of the dynamic process imposed by the instrument.

The best condition in consideration of the overshoot seems to be the linear strike profile with an opening time of 50 ms because exponential strike profiles are more prone to overshoot. Interestingly, the filament life time was linearly dependent on the opening time. The dark red paint possessed a pronounced yield stress and the highest infinite shear viscosity, it has the highest filament life time and relaxation time. The fastest filament decay was detected at the Newtonian red paint which has the lowest infinite shear viscosity, furthermore, the extensional viscosity of dark red is 2.5 times higher than the red and this may be the reason for the different production performances within the coil coating process. The higher extensional viscosity might not allow levelling out of the paint in a short time. As a consequence, the line speed

compared to the red paint's line speed is reduced by 10.4% to increase the travel time from application roll to the curing oven.

The detection of instability defects during the filament break up experiments at a specific set up parameter might relates to paint defects such as misting /spatter defect. It would be interesting to discover a possible correlation between instability defects and the paint defects.

9.9 Bibliography

Anna, S. L., & McKinley, G. H. (2001). Elasto capillary Thinning and Breakup of Model Elastic Liquids. *Journel of Rheology , 45* (1), 115-138.

Ascanio, G.; Carreau, P. J.; Tanguy, P. A. (2006). High-speed roll coating with complex rheology fluids, Experiments. *Experiments in Fluid , 40*, 1-14.

Clasen, C., Eggers, J., Fontelos, M. A., & McKinley, G. H. (2006a). The beads-on-string structure of viscoelastic threads. *Journal of Fluid Mechanics , 556*, 283-308.

Clasen, C., Plog, J. P., Kulicke, W. M., Owens, M., Macosko, C., Scriven, L. E., et al. (2006b). How dilute are dilute solutions in extensional flow? *50*, 849-881.

Clasen, C., Verani, M., Plog, J. P., McKinley, G. H., & Kulicke, W. M. (2004). Effects of Polymer Concentration and Molecular Weight on the Dynamic of Visco-Elastic-Capillary Breakup. *Proceeding of the XIVth International Congress on Rheology.* Seoul.

Cossby, A. J., Shull, K. R., Lakrout, H., & Creton, C. (2000). Deformation and failure modes of adhesively bonded elastic layers. *Journal of Applied Physics , 88*, 2956-2966.

Entov, V. M., & Hinch, E. J. (1997). Effect of a Spectrum of Relaxation Times on the Capillary Thinning of a Filament of Elastic Liquid. *Journal of Non-Newtonian Fluid Mechanics , 72* (1), 31-54.

Goldin, M., & Pfeffer, R. (1972). Break-up of a capillary jet of a Non-Newtonian fluid having a yield stress. *Chemical Engineering Journal , 4*, 8-20.

Goldin, M., Yerushalmi, H., & Pfeffer, R. (1969). Breakup of a Laminar Capillary Jet of a Viscoelastic Fluid. *The Journal of Fluid Mechanics , 38*, 689-711.

Kheirandish, S., Guybaidullin, I., Wohlleben, W., & Willenbacher, N. (2008). Shear and elongational flow behaviour of acrylic thickener solutions Part I: Effect of intermolecular aggregation. *Rheologica Acta , 47*, 999-1013.

Kheirandish, S., Guybaidullin, I., Wohlleben, W., & Willenbacher, N. (2009). Shear and elongational flow behaviour of acrylic thickener solutions, Part II: effect of gel content. *Rheologica Acta , 48*, 397-407.

Kolte, M. I., & Szabo, P. (1999). Capillary thinning of polymeric filaments. *Journal of Rheology , 43*, 609-625.

Liang, R. F., & Mackley, M. R. (1994). Rheological characterisationof the time and strain dependence of polyisobythlene solution. *Journal of Non-Newtonian Fluid Mechanics , 52*, 387-404.

Lowry, B. J., & Steen, P. H. (1995). Capillary Surfaces: Stability from Families of Equilibria with Application to the Liquid Bridge. *Proceedings of the Royal Society A , 449*, 411-439.

Mahajan, M. P., Tsige, M., Taylor, P. L., & Rosenblatt, C. (1999). Stability of liquid crystalline bridge. *Physics of Fluid , 11*, 491-493.

Mastrangelo, C. H. (1993b). Mechanical stability and adhesion of microstructures udner capillary forces - Part II: Experiments. *Journal of Microelectromechanical Systems , 2*, 44-45.

Matrongelo, C. H. (1993a). Mechanical stability and adhesionof microstructures under capillary forces-Part I: Basic theory. *Journal of Microelectromechanical Systems , 2*, 33-43.

McKinley, G. H., & Sridhar, T. (2002). Filament-Stretching Rheometry of complex Fluids. *Annual Review of Fluid Mechanics , 34*, 375-415.

McKinley, G. H., & Tripathi, A. (2000). How to Extract the Newtonian Viscosity from Capillary Breakup Measurements in a Filament Rheomter. *Journal of Rheology , 44* (3), 653-671.

Oliveira, M. S., Yeh, R., & McKenley, G. H. (2006). Iterated stretching, extensional rheology and formation of beads-on-a-string structures in polymer solutions. *Journal of Non-Newtonian Fluid Mechanics , 137*, 137-148.

Rodd, L. E., Scott, T. P., Cooper-White, J. J., & McKinley, G. H. (2004). Capillary Break-Up Rheomtry of low viscosity elastic fluids. Department of Chemical and Biomolecular Engineering, Australia: The University of Melborne.

Rothstein, J. P. (2003). Transient extensional rheolgy of wormlike micelle solutions. *Journal of Rheology , 47*, 1227-1247.

Shaw, D. J. (1992). Introduction to colloid and surface chemestry. Oxford, Boston.

Slobozhanin, L. A., & Perales, J. M. (1993). Stability of liquid bridges between equal disks in an axial gravity field. *Physics of Fluids A , 5* (6), 1305-1314.

Tripathi, A., Whitingstall, P., & McKinley, G. H. Using filament stretching rheometry to predict stand formations and processablility in adhesives and other non Newtonian fluids. *Rheologica Acta , 39* (4), 321-337.

Tuladhar, T. R., & Mackley, M. R. (2008). Filament stretching rheometry and break-up behaviour of low viscosity polymer solutions and in. *Journal of Non-Newtonian Fluid Mechanics , 148*, 97-108.

Wagner, C., Amarouchene, Y., Bonn, D., & Eggers, J. (2005). Droplet detachment and satellite bead formation invisco-elastic fluids. *Physical Review Letters , 95*, 164504.

10 Experimental Outcome of the Capillary Extrusion Rheometer

10.1 Aim of the experiments

The main focus of this study was to obtain reproducible extensional rheological parameters from a commercial paint using the capillary extrusion rheometer. In our case, the dark red paint was chosen and because of its apparent yield behaviour, an interesting result was expected. A twin bore capillary extrusion rheometer was employed to measure the pressure in the barrel which was finally used to extract the extensional viscosity under the consideration of Bagley and Rabinowitsch corrections.

10.2 Experimental protocol

A pressure transducer made by Dynisco was subject to calibration before commencing the experiments. The calibration instrument from Fisher consisted of weight disc, weight holder, transducer and voltage meter as illustrated in Figure 10-1. The weight holder and the transducer were directly connected to the instrument. By placing additional weights on the weight holder the inner pressure within the fluid board linearly increased accordingly to a known value. The transducer detected the increased pressure which was converted into a voltage that was displayed on the voltage reader. This value was compared to the nominal value and, if needed, the transducer was calibrated to the accurate value.

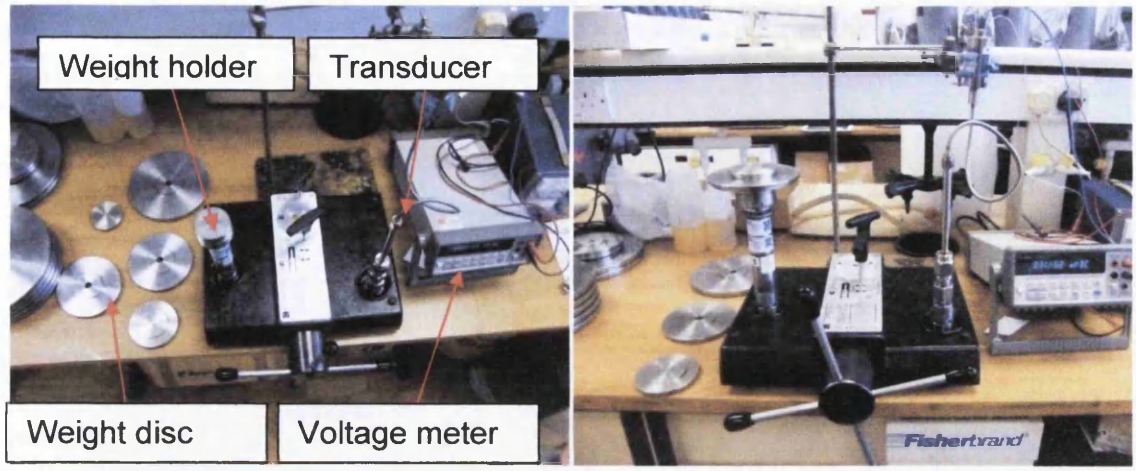

a) b)

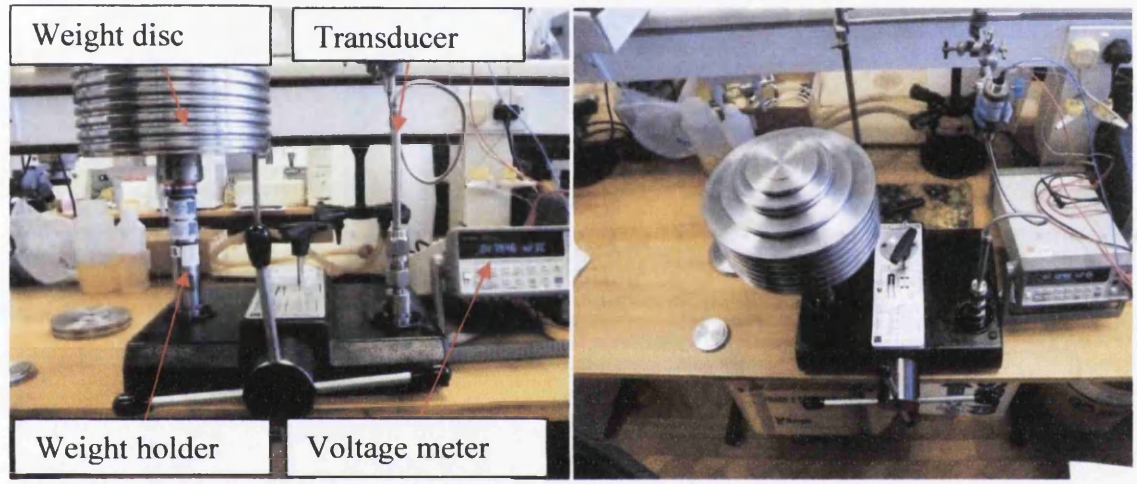

c) d)

Figure 10-1: Calibration instruments and their accessories

10.3 Principle of capillary rheometer

The capillary rheometer (DRRheology P9000) was employed to study the extensional flow behaviour in a contraction flow. It is equipped with twin bore barrels whose inner diameter of 15 mm and a length of 210 mm allow approximately 350 ml of material in total to be extruded through two different die sizes during a single run. A piston pressed the sample confined in the bore through a die with speed controlled by digital motor driver. The occurrence of any pressure loses due to leakage was eliminated by fitting a high pressure seal (viton rubber o – ring, able to withstand the corrosive nature of some of the paint formulations) on the piston to

close the gap around the interface between transducer and bore. As a consequence of the high rate of wear and tear that occurred on the o - ring, it was crucial to regularly replace the pressure seal to avoid any "noise effects", in particular, pressure drop caused by leakage.

The magnitude of the pressure occurring in the bore dictates the type of pressure transducer selected and that transducer was located just above the orifice via the small hole of 8 mm bored in the reservoir. Initially, a number of various melt pressure transducers from the Dynisco with an output of 3.33mV/m were employed to measure the pressure generated in the bore. The three pressure transducers used were capable of measuring pressures in the range of 0 - 50 psi (3.45 bar / 0.35 MPa), 0 - 500 psi (34.5 bar / 3.45MPa) and 0 - 1500 psi (103.42 bar / 10.3 MPa) and were connected to a PC which recorded the pressure drop. As a precaution, the initial test sequence was performed with the highest pressure transducer ranging from 0 psi to 1500 psi (103.42 bar / 10.3 MPa) to avoid damaging the sensor in the case that high pressure occurred. However, the drawback for using this type of transducer was its insufficient sensitivity at lower pressures, which also occurred during this experiment. At the end, only two pressure transducers which covered the range of 0 - 50 psi (3.45 bar / 0.35 MPa) and 0 - 500 psi (34.5 bar / 3.45MPa) were deemed sufficient to measure the data. Using a relative large membrane diameter of 8mm provides the ability to measure low pressure. Repeatability of a data set could be achieved with fresh samples.

10.4 Pressure flow rate accuracy

The quality of the results strongly depends on accuracy and choice of the pressure transducer used. The first pressure transducer used for measuring low pressure up to 3.45 bar had an accuracy of ± 0.125% and the second could measure pressure up to 34.5 bar with a tolerance of ± 1.25%. Both transducers may be adversely affected by viscous dissipation around the membrane which leads to an incorrect measurement of pressures. Therefore, a heat exchanger was integrated into the capillary extrusion rheometer to control the temperature and consequently, minimise the effect of the viscous dissipation.

Vortex enhancement and pressure drop due to viscoelasticity were detected at Boger fluid which flowed through an axisymmetric contraction (Nigen 2002). In this case, the occurrence of the vortex cannot be excluded from the experiments with the fluid of interest since Non-Newtonian fluids are prone to vortex development (Münsted et. al. 2001) (see section 6.13). Currently, there is no research about the absence of vortices in polyester resin based paints.

10.5 Experimental Method

A strict set of test procedures were followed to ensure that the initial conditions were kept constant which provided a good repeatability and accuracy of the data. Whenever the bore were filled with the sample, it was necessary to avoid or minimise air entrapment, which was achieved by using a syringe. All samples were kept within a heat exchanger at a constant temperature of 20°C. Under this isothermal condition, the viscous heating effect is minimised and does not affect the mobile systems. Different die set ups were used to obtain different pressure drops and also to detect any possible slip effects. The chosen lengths of the die for these experiments utilised the findings of Sunder and Goettfert (2001) who advised the use of die lengths that are not so close together to avoid the accumulation of measured errors. The longest dies of 50 mm and 47mm were chosen to allow high pressures to be obtained within the sample.

The danger of compression effects as mentioned by Sunder and Goettfert (2001) (see section 6.6.1 for more explanation) with LDPE is not given in our case since the paint has a more characteristic liquid behaviour (low viscosity). For a high viscous material PP, Sunder and Goettfert (2001) used an L/D ratio of 30 and could not detect any compression effect.

The dimensions of dies used for this research are listed in Table 10-1 resulting in contraction ratios of 15:1 and 30:1 and L/D ratios between 5 and 100. Due to experimental limitations, in relation to amount of sample in the bore, the range of piston speed from 0.417 mm/min to 333.346 mm/min could not be used in a single experiment. Consequently, a whole bore filling was needed to obtain 2 or 4 data

points at higher piston speeds. Before measuring the actual data, the sample underwent a pre-run to provide the same starting condition for all experiments. In this case, a piston speed of 0.417 mm/min (corresponding to a shear rate of 12.5 s^{-1}, for a die diameter of 1mm or 100 s^{-1} for a die diameter of 0.5mm, where $\dot{\gamma} = \frac{4Q}{\pi R^3}$,) was sufficient to eliminate the loading and pre shear history resulting in good repeatability of the data. Different pressure transducers were employed to cover a wide range of pressure drops, which occurred during these experiments.

Die systems	
Length / mm	hole diameter / mm
5	0.5
20	0.5
50	0.5
5	1
20	1
47	1

Table 10-1: Provides an overview of all dies used

Turbulent flows with Reynolds numbers ($Re = \rho \bullet v \bullet d/\eta_\infty$) higher than 100 would additionally affect the resulting pressure drop. As a result of the additional effect, further correction is needed with the formula ($\Delta P_{corr} = \Delta P - 0.5\rho v^2$) (Ascanio et al. 2002). In this case, the Reynolds numbers ranges from 0.014 to 7 which are very low, therefore, the pressure drop correction due to the absence of turbulent flow was not necessary. Low Reynolds numbers indicated that viscous force dominates the inertial flow in the contraction flow. Generally speaking, the flow could be considered laminar, incompressible and axisymmetric.

10.6 Results

10.6.1 Pressure versus speed

The software from the extrusion rheometer usually supports data collection of the pressure drop measured with the pressure transducer positioned just above the entrance. Several runs were undertaken to determine the repeatability of the results with different die diameters and lengths. Each data point was measured under equilibrium conditions, indicated by the constant pressure in the barrel at the constant flow speed. The results of the raw data illustrated in Figure 10-2 showed an excellent repeatability and encouraged an analysis of the values. More confidence was provided due to the fact that the pressure increased with increased die length and smaller die diameter. Data around the dotted line coloured with red occurred at die lengths of 47 mm (1 mm die diameter) or 50mm (0.5 mm die diameter), blue at 20mm and green at 5mm.

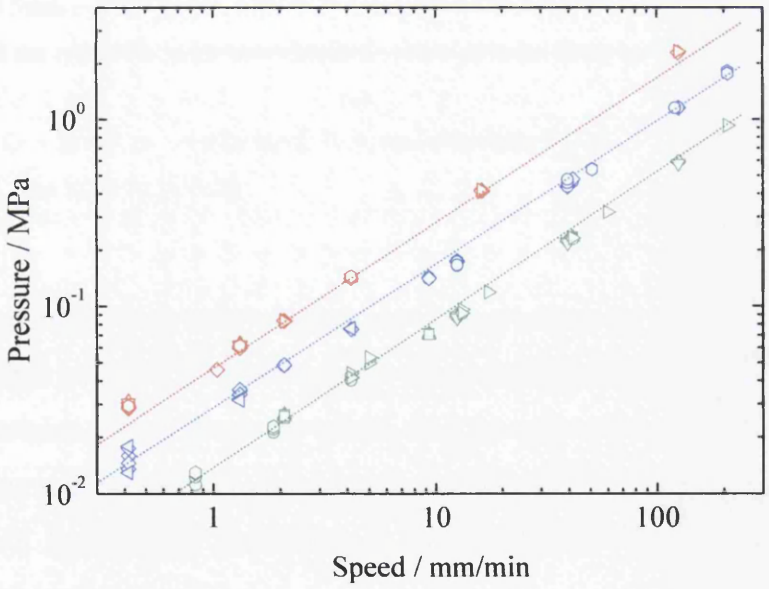

a) dark red, diameter 0.5 mm

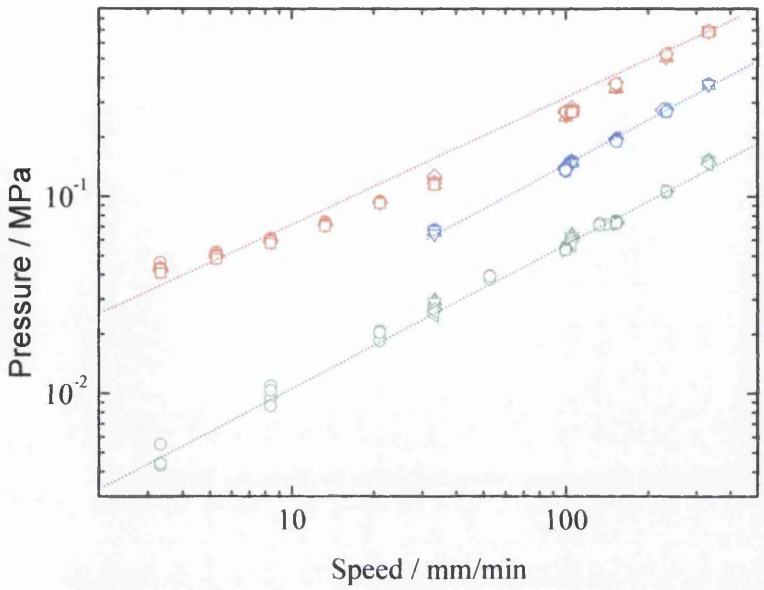

b) dark red diameter 1 mm

Figure 10-2: Illustrates the raw data in a pressure versus speed plot. a) red mark data obtained by using a die with a diameter of 0.5 mm and a die lengths of 50 mm (red: △= 1. run, ▽ = 2. run, ◇ = 3. run, □ = 4. run and ▷ = 5. run), 20 mm (blue: △= 1. run, ▽ = 2. run, ◇ = 3. run, □ = 4. run and ▷ = 5. run) and 5mm (green: △= 1. run, ▽ = 2. run, ◇ = 3. run, □ = 4. run and ▷ = 5. run) b) Data points around the red dotted line were obtained with a constant diameter of 1mm and a die length of 47mm (red: △= 1. run, ▽ = 2. run, ◇ = 3. run, □ = 4. run and ▷ = 5. run), 20 mm (blue: △= 1. run, ▽ = 2. run, ◇ = 3. run, □ = 4. run and ▷ = 5. run) and 5mm (green: △= 1. Run, ▽ = 2. Run, ◇ = 3. Run, □ = 4. Run and ▷ = 5. run).

The mathematical linear relationships between pressure and speed for the dark red paint are listed in Table 10-2. Very good agreements between the linear fits and raw data were attained throughout the whole data set with a tolerance below ±10%. At lower pressure, the degree of scattering is more visible due to the fact that the lower measurement limit of the transducer is reached and also any noise had a higher impact at the lower pressure.

Die Sizes		Linear regression fit	R^2
Diameter / mm	Lenght / mm		
0.5	5	y = 0.00429x + 0.039	0.998
0.5	20	y = 0.00836x + 0.0884	0.996
0.5	50	y = 0.01796x + 0.05226	0.998
1	5	y = 0.00041x + 0.01287	0.993
1	20	y = 0.00101x + 0.0386	0.997
1	47	y = 0.00198x + 0.05064	0.996

Table 10-2: Results of the linear regression fits on the relationship of pressure versus speed and the degree of accuracy.

10.6.2 Bagley correction

The design concept of Bagley (1957) was used to determine the P_e. To obtain the P_e, the resulting raw pressures were plotted against L (where D was kept constant) as illustrated in Figure 10-3 followed by extrapolation to the pressure axis (L = 0) whose intersection value gives the entrance pressure drop P_e at zero length die. This entrance pressure drop was subtracted from the total raw pressure drop measured by the transducer. The entire data set is listed in the Table 10-3. At this point, it is worth mentioning that the influence of the vortex on the pressure drop cannot be ruled out during this analysis, which normally increased the magnitude of the entrance pressure drop.

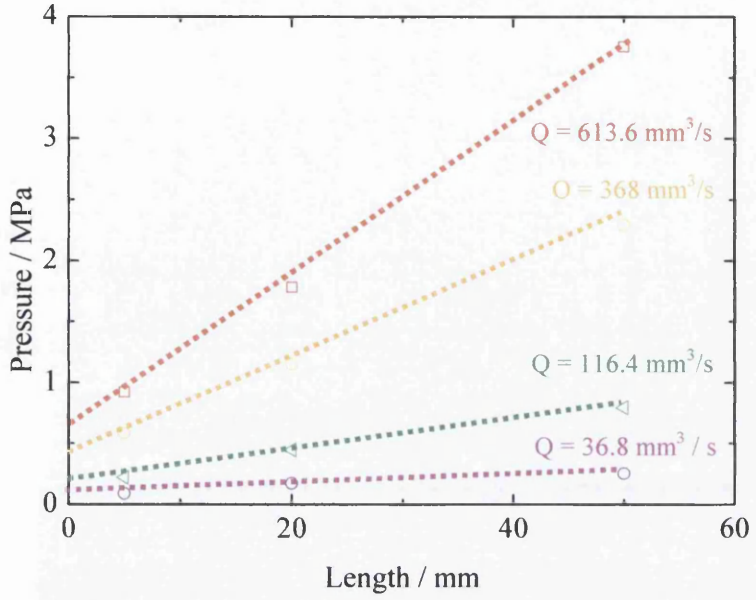

Diameter 0.5mm

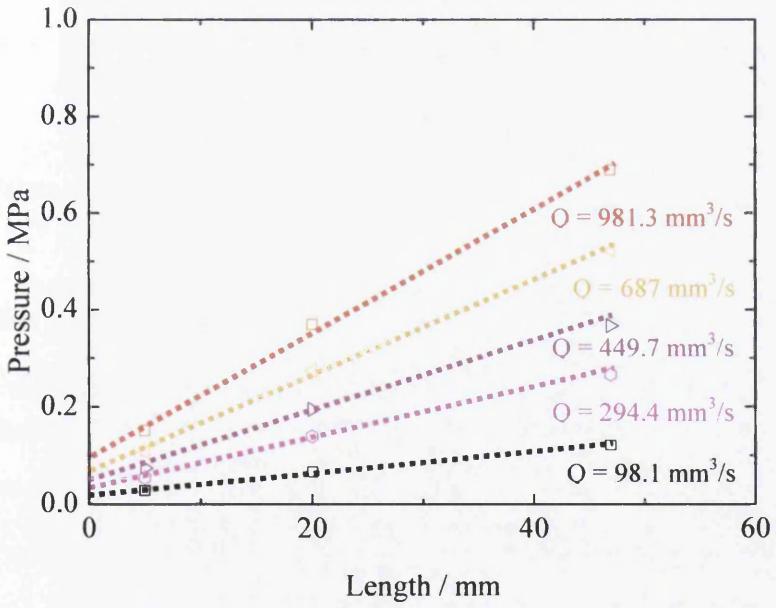

Diameter 1mm

Figure 10-3: End pressure corrections of dark red paint through a Bagley plot for a different volumetric flow and for a capillary die with a diameter of 0.5mm and 1mm whose entrance angle was 180 ° at a temperature of 20°C. Linear regression analysis of data delivered straight lines with R^2 of 0.99 for all curves

For the dark red paint, the Bagley curve obtained with different volumetric flow rates and various lengths to diameter ratios seemed to be almost linear over the entire range which indicated that the pressure has minimum or no effect on the viscosity of paint (see Figure 10-3). A non linear upward curve is the result of a pressure dependence of viscosity (Laun 1983, Laun and Schuch 1989). The effect of viscous heating is suppressed by the use of the temperature controlled device and the absence of a concave Bagley plot provides evidence that this effect is eliminated (Hatzikiriakos and Dealy 1992).

Dark Red			
D= 0.5mm		D= 1mm	
P_e / kPa	Q / mm^3/s	P_e / kPa	Q / mm^3/s
518.4	613.6	85.7	981.3
357.1	368	52.8	687
151.18	116.4	32.9	449.7
37.8	36.8	20.5	294.4
		6.4	98.1

Table 10-3: Values of P_e extracted from Bagley plot used for wall stress calculation.

So far, all this data processing has been necessary to calculate the shear stress, $\sigma_w = (P-P_e)\ R\ /\ 2L$ in the capillary die. According to Han (1976), the Bagley end correction factor (in this case P_e) will increase with increased shear rate; the dark red paint follows this trend.

10.6.3 Shear stress versus shear rate average

In a flow curve plotted as stress versus strain rate, the occurrence of slip effect can be simply detected through comparing the data obtained with different die diameters. In the absence of slip, a good agreement between data exists whereas slip effects cause a lack of correlation between the data. A good example of slip and no slip effect

within one flow curve is given for low density polyethylenes where slip starts above a critical stress of 0.09MPa (Hatzikiriakos 1994).

Figure 10-4 displays the flow curve of shear stress versus shear rate for dark red paint with different diameters. A linear increase of shear stress with increased shear rate can be seen at a constant temperature. Interestingly, all data (after Bagley correction) seemed to agree over a wide range of shear rates. This implies that a slip correction was not needed for red dark paint. In contrast to this study, the ink samples used by Willenbacher (1997) developed slip condition during the experiments, which caused a reduction in runnability performance. As expected, there are no upstream instabilities, also named melt fraction, at higher shear rate which was reported with high density polyethylenes since there is no change in the slope of the stress – shear rate curve at high shear rate (Hatzikiriakos and Dealy 1992).

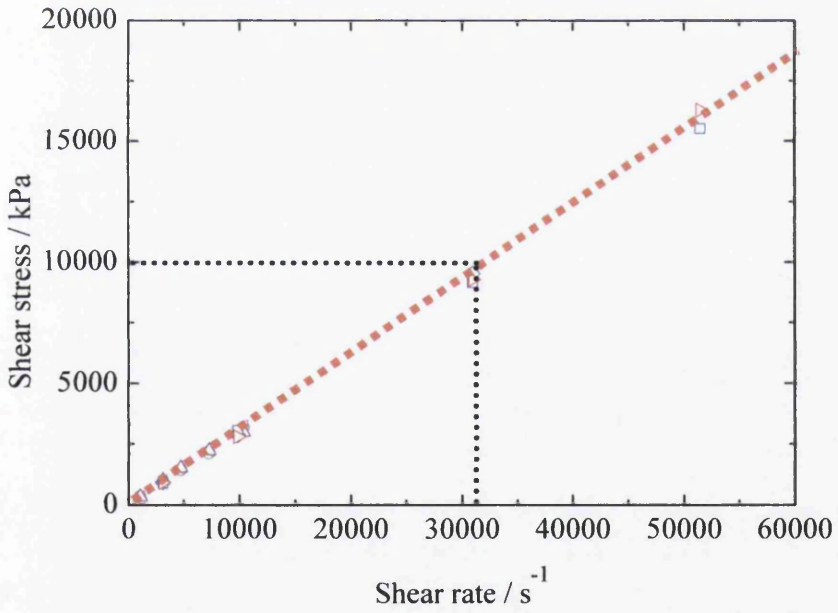

Figure 10-4: Flow curve of dark red paint at 20°C after stress correction. Dark red paint was extruded through dies with ◇ 5x 0.5, □ 20 x 0.5, ▷ 50 x 0.5, ○ 5x1, ◁ 20 x1 and △ 47 x1. The result indicates a no slip boundary since nearly all the data from the same diameter and different lengths agree with each other.

10.6.4 Determination of shear viscosity and extensional viscosity

Before the shear viscosity can be determined, the shear rate needs to undergo the Weissenberg Rabinowitsch correction (see equation 6.10) to consider the actual plug like fluid behaviour. As can be seen from equation 6.10, n_s needs to be calculated from the equation 6.11. Table 10-4 provides the results of these calculations.

Die Diameter 0.5mm			
Q [mm^3/s]	Log (σ_w)	Log($\dot{\gamma}_a$)	n_s
36.8	6.82	8.01	0.85
116.4	7.98	9.16	0.87
368	9.14	10.31	0.89
613.6	9.67	10.8	0.89

a)

Die Diameter 1 mm			
Q [mm^3/s]	Log (σ_w)	Log($\dot{\gamma}_a$)	n_s
98.13	5.78	6.91	0.84
294.45	6.87	8.01	0.86
449.45	7.29	8.43	0.87
687.04	7.69	8.85	0.87
981.29	8.04	9.21	0.87

b)

Table 10-4: Lists of n_s for each volumetric flow. a) for a die diameter of 0.5mm and b) for a die diameter of 1mm

For the determination of extensional viscosity, the Cogswell model has been chosen for simplicity. The temperature was kept constant so that assumption 1 in section 6.11 was fulfilled. Furthermore, pressure dependence could not be detected and there is no slip effect, therefore, assumptions 4 and 5 were also fulfilled. The Reynolds number is below 8 and therefore the inertial effect can be neglected. Assumption 7

cannot be confirmed since it is not known whether the flow in the converging region is fully developed. However, at this stage, it was considered that a fully developed flow existed. In order to calculate the extension viscosity according to Cogswell, the equations 6.15, 6.16, 6.17 and 6.18 are needed. The outcome is illustrated in Figure 10-5. The last data point may indicate an extensional thinning behaviour or a measurement error which needs to be investigated in the next project phase. The shear viscosity seems to be constant over a very high shear rate ($10^3 s^{-1} < \dot{\gamma} < 50^4 s^{-1}$) and has a value of 0.3 Pas.

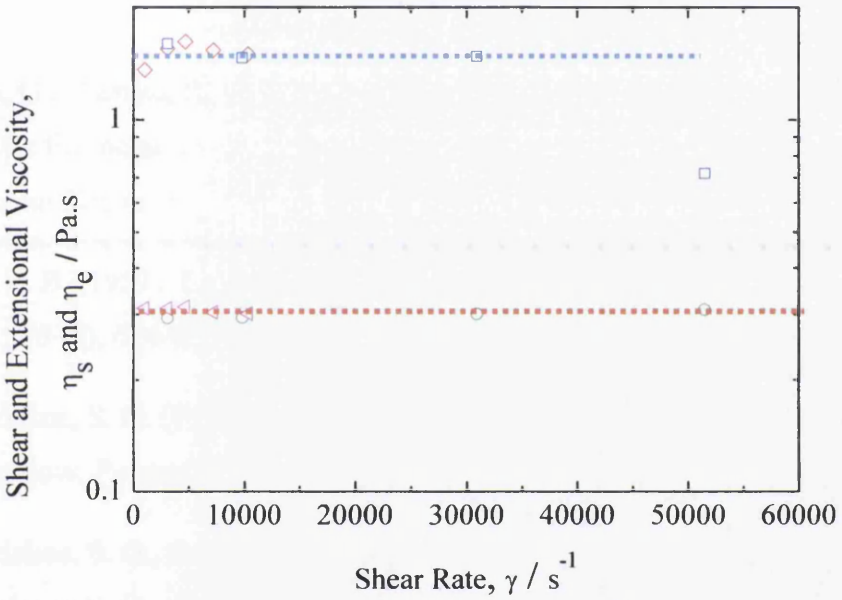

Figure 10-5: Shear and extensional viscosity functions of the commercial paint (dark red) with the capillary extrusion rheometer: true shear viscosity (◁ 1mm ,○ 0.5mm) and extensional viscosity (◇ 0.5mm,□ 1mm) after using Bagley and Rabinowitsch corrections versus shear rate

10.7 Conclusion for the capillary extrusion rheometer

The extrusion capillary rheometer provided an additional source of information of rheological features for commercial dark red paint. As expected, the pressure increased with increased piston speed. The full linear Bagley plot over a wide range suggests the absence of pressure dependence of viscosity or viscous heating. As a result, an action of correcting the data was not needed. The absence of slip effects

was a surprise for a high flocculated structure system, however, slip effects did not occur during rotational experiments and therefore supports the credibility of the results gained by the extrusion capillary rheometer. Overall, more commercial paints need to be tested to allow a comprehensive understanding of the flow behaviour in such a contraction device. A comparison with the red paint is not possible at this stage. Therefore the effect of the weight solid content, pigment to binder ratio and the types of pigments on the capillary extrusion flow cannot be related.

10.8 Bibliography

Ascanio, G., Carreau, P. J., Fuente, E. B., & Tanguy, P. A. (2002). Orifice Flowmeter for measuring extensional rheological properties. *The Canadian Journal of Chemical Engineering*, *80*, 1189-1196.

Bagley, E. B. (1957). End correction in capillary flow of polyethylene. *Journal of Physics*, *28* (5), 624-627.

Hatzikiriakos, S. G. (1994). The onset of wall slip and shaskin melt fracture in capillary flow. *Polymer Engineering Science*, *34* (19), 1441-1449.

Hatzikiriakos, S. G., & Deal, J. M. (1992). Wall slip of molten highdensity polyethylenes II. Capillary rheometer studies. *Journal of Rheology*, *36*, 703-707.

Laun, H. M. (2004). Capillary rheometer for polymer melts revisited. *Rheologica Acta*, *43*, 509-528.

Laun, H. M., & Schluch, H. (1899). Transient elongational viscosity and drawability of polymer melts. *Journal of Rheology*, *33*, 119-176.

Liang, J.-Z. (2007). Die swell behaviour during the short tube flow of rubber compounds. *Journal of Applied Polymer Science*, *104*, 70-74.

Nigen, S., & Walters, K. (2002). Viscoelastic contraction flows: comparison of axisymmetric and planar configurations. *Journal of Non-Newtonian Fluid Mechanics*, *102*, 343-359.

Shaw, M. T. (1896). An alternative analysis of capillary rheometer Data. *SPE Technical Papers , 32*, 707-710.

Walter, K. (1992). Recent Development in Rheometry. *Proceedings XIth International, Conference on Rheology*, (pp. 16-23).

Willenbacher, N., Hanciogullari, H., & Wagner, H. G. (1997). High shear rheology of paper coating colors - more than just viscosity. *Chemical Enginneering and Technology , 20*, 557-563.

11 Conclusion

The work presented in this thesis has contributed to the knowledge enhancement of commercial mobile systems through rheological characterisation with particular emphasis on those used in the coil coating process. Various rheometers such as rotational (see chapter 8), capillary break up (see chapter 9) and capillary extrusion rheometer (see chapter 10) were employed to obtain a thorough understanding of the flow behaviours.

Some interesting and very detailed outcomes of experiments on polyester based paint pigmented with titanium dioxide (TiO_2) are presented in Chapter 8 and highlight the repeatability of the rheological data produced. Creep experiments highlighted that the main cause for the lack of repeatability in results is primarily due to shear history. Using a test procedure with an adequate magnitude of pre-shearing provided a good agreement between the flow curves obtained from a stress controlled and a deformation controlled rheometer. These findings were used and applied to perform experiments on additional samples such as dark red, red and green paints. Despite the fact that all the paints had the identical resin content, their rheological properties seemed to differ. Green, dark red and white paints possess high structures within the mobile fluid, recognisable through the overshoot in a response to a sudden applied shear rate and subsequent shear thinning. Additionally, apparent yield stress and thixotropy were detected on these samples. Also the duration of the structure breakage until equilibrium was provided with this type of experiments. It showed that dark red paint is more resistant to structure breakage when compared to the other paints. A possible conclusion can be made by stating that the defects occurred in the nip might have been caused by the resistance to the structure breakage leading to a higher flow resistance within the nip. The contrast could not be greater with the red paint, which exhibited Newtonian behaviour and did not show any elasticity. Apparently, the red paint appears to have the best coating performance although this statement requires more evidence by comparing the process parameters with the rheological data. By the current knowledge, the coil coating line speed difference between red paint and dark red paint is 10.4%. The reason for the reduction in the line speed may be needed to allow the levelling out process more time. By only comparing the pigment to binder ratio (see Table 7-1), the binder might dictate the

degree of resistance for structure breakage and line speed performance accordingly. Another factor which might play a role is the usage of iron oxide alpha pigment instead of chromium titanium yellow.

In Chapter 9, the systematic approach that was used to obtain an ideal operation window for CaBER when used with polyester resin based paints is presented. To the author's knowledge, work of this kind has not been published elsewhere. During the experimental work, a video camera was used to capture the effect of an undesired machine dynamic causing an overshoot of the moving plate beyond the defined separation height. This phenomenon presented itself with a test set up consisting of a separation time of 20ms. To eliminate the influence of the machine dynamic on the outcome, the opening time needed to be increased, thus, all experiments were carried out with an optimal opening time of 50ms. As a result, the shortest filament life time occurred for the Newtonian red paint which has the lowest infinite shear viscosity. In contrast, the yield stress for dark red paint possessed the longest filament life time and also had the highest infinitive shear viscosity. The pigment to binder ratio for the dark red paint is lower than the pigment to binder ratio for the red paint. Furthermore, the iron oxide alpha pigment was added into the dark red paint whereas the red paint does not have this type of paint. These differences might be the factors which determines the life time of the filament and the relaxation time. Whilst observing the filament decays, interesting filament thinning defects such as the evolution of central bulge, recoiling and satellite drop were captured. Without the support of a digital high speed camera, it would not have been possible to highlight such defects. Therefore, a good approach is to use a digital high speed camera for samples which have not been previously tested with a capillary break up rheometer to allow finding an ideal operation window which is not influenced by unknown defects. The onset of the occurrence of instability effects under a specific condition might provide a hint for the appearance of the coating defects .

The work presented in Chapter 10 focused on an abrupt contraction flow within a capillary extrusion rheometer. The dark red paint provided the initial experimental data, by using the capillary extrusion rheometer. Surprisingly, the slip effect did not occur due to the good adhesion of dark red paint to steel and the absence of particle depletion and therefore a slip analysis was not needed. However, this result was

representational of only one type of paint and therefore, a final conclusion cannot be drawn.

The comparison of the data of dark red paint measured by different rheological devices can be seen in Figure 11-1. Furthermore, the shear viscosity curve obtained by the rotational rheomter continuously followed the shear viscosity from the capillary extrusion rheometer. The extensional viscosity showed a Newtonian behaviour which is measured by both capillary break up rheometer and capillary extrusion rheometers.

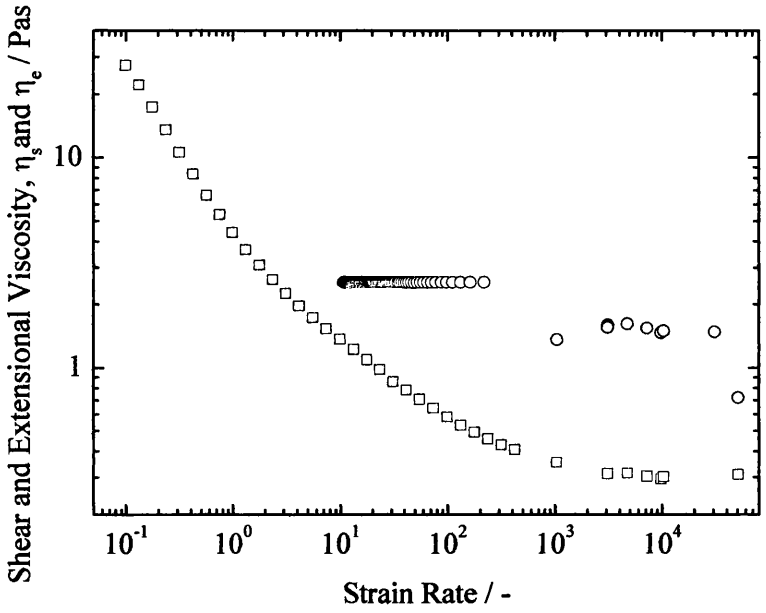

Figure 11-1: Comparison of data measured by different devices shear viscosity (□) from deformation controlled rheometer, shear viscosity (□) and extensional viscosity (O) from capillary extrusion rheometer and extensional viscosity (O) from capillary break up rheometer

Currently, it can be said that rheological properties of polyester resin based paint can be measured with the mentioned rheometers using the previously defined experimental procedures.

Since the solvent and the pigment size were all the same for the paints used, the influence factors for changing the flow behaviour can only be the weight of solid content, pigment to binder ratio and the types of pigments. It is more likely that, the

pigment to binder ratio and the types of pigments play an important role for the flow behaviour. The white paint seems to be a special case due to the high amount of titanium oxide and the high pigment to binder ratio.

12 Future research

Looking to the future, additional, interesting research activities could be expected from the outcomes of this project, in particular, by making use of the knowledge gained during the research activities which were undertaken, including:

The rheological characterisation of commercial complex polyester resin based paints enabled a thorough distinction and classification of these products in a scientific manner. The result from this project also provided evidence of the feasibility of capturing rheological data using both rotation and capillary break up rheometers. However, further experimental investigations on polyester resin based paints using a capillary extrusion rheometer are required to fully complete the feasibility study of capturing rheological data with different rheometers used in this project. In addition, an observation of the contraction flow within the barrel of the capillary extrusion rheometer could increase the understanding of the flow characteristics of different paints.

Commercial, solvent based paints which are used for the coil coating process are not only produced from polyester resins. Therefore, the scope of rotational and extensional experimental work could be extended to different "paint families" (i.e. paints manufactured from polyurethane resin or epoxy resin) using a similar methodology to that employed for this project. Additionally, the trend to reduce volatile, organic compounds (VOCs) which is driven by environmental regulations has led to a 'new' generation of water based paints being developed. This new generation of paint will also require in depth rheological assessment.

For both scientific and commercial interests, effort could be made to develop an empirical model, capable of predicting the production performance of a paint in the coating process by using its fundamental rheological properties. However, a significant amount of both process and rheological data would be required to create, validate and finalise a suitable empirical model. Therefore, in order to achieve this, the next step for future research should be the simultaneous collection of rheological and process data.

In terms of future paint development, finding a relationship between a paint's components and the rheological data presented in this project would provide a more detailed understanding of the impact of material's properties on its flow behaviour. Once the "ideal flow" behaviour for the coil coating process has been established, paints could be modified to achieve this ideal flow behaviour by using knowledge regarding the influence of a particular paint's components.

Additionally, an investigation into the effects of temperature on the rheological behaviour of commercial paints could produce interesting data which could be used to further optimise the coil coating process.

Further to this, the critical slip effect of polyester based paint, which may occur in other samples would also provide a very interesting area of research as it may occur undertake which might happen on both application roll and pressure roll. Willenbacher et al. (1997) found out that poor runnability occurred with increased viscosity, pressure losses and wall slip effect.

By undertaking some or all of these suggestions for further research, it may be possible to improve the coil coating production, in particular productivity and quality, which was the main goal of this research project.

12.1 Bibliography

Willenbacher, N., Hanciogullari, H., & Wagner, H. G. (1997). High shear rheology of paper coating colors-more than just viscosity. *Chemical Enginneering and Technology*, *20*, 557-563.